Doctoral theses at NTNU, 2015:335

Elena Vidal Sarmiento

Flowable fibre-reinforced concrete for structural applications

A modelling approach that can take anisotropic and inhomogeneous fibre configuration into account

NTNU
Norwegian University of
Science and Technology

Doctoral thesis

Elena Vidal Sarmiento

ISBN 978-82-326-1324-3 (printed ver.)
ISBN 978-82-326-1325-0 (electronic ver.)
ISSN 1503-8181

Doctoral theses at NTNU, 2015:335

NTNU
Norwegian University of
Science and Technology

Elena Vidal Sarmiento

NTNU
Norwegian University of
Science and Technology
Thesis for the Degree of
Philosophiae Doctor
Faculty of Engineering Science and Technology
Department of Structural Engineering

NTNU

Elena Vidal Sarmiento

Flowable fibre-reinforced concrete for structural applications

A modelling approach that can take anisotropic and inhomogeneous fibre configuration into account

Thesis for the Degree of Philosophiae Doctor

Trondheim, December 2015

Norwegian University of Science and Technology
Faculty of Engineering Science and Technology
Department of Structural Engineering

NTNU
Norwegian University of
Science and Technology

NTNU
Norwegian University of Science and Technology

Thesis for the Degree of Philosophiae Doctor

Faculty of Engineering Science and Technology
Department of Structural Engineering

ISBN 978-82-326-1324-3 (printed ver.)
ISBN 978-82-326-1325-0 (electronic ver.)
ISSN 1503-8181

Doctoral theses at NTNU, 2015:335

Printed by NTNU Grafisk senter

Preface

The doctoral thesis is submitted to the Norwegian University of Science and Technology (NTNU) for the degree of *Philosophiae Doctor* (PhD). The research was carried out at the Department of Structural Engineering, Faculty of Engineering Science and Technology at NTNU in Trondheim, Norway. The main supervisor was Professor Dr Terje Kanstad (NTNU, Norway); the co-supervisors were Professor Dr Mette R. Geiker (NTNU, Norway) and Professor Dr Max A.N. Hendriks (NTNU, Norway, and Delft University of Technology, the Netherlands).

The PhD project was initiated and funded through the Concrete Innovation Centre (COIN, www.coinweb.no), a centre for research-based innovation, which was established in 2006 by the Research Council of Norway for an eight-year period. COIN was divided into three focus areas: environmentally friendly concrete structures, competitive construction, and technical performance. The research for this thesis was a part of the second focus area under the sub-project High tensile strength all-round concrete, one of whose aims was to design concrete without traditional reinforcement.

The PhD project started in August 2011 and the thesis was submitted in October 2015. The PhD position included one year of teaching assistance at the Department of Structural Engineering, NTNU.

The thesis consists of an extended introduction and five scientific papers included in the main body of the thesis. Three of the scientific papers were submitted to international scientific journals and two were published in international conference proceedings.

The author, Elena Vidal Sarmiento, declares that the thesis and the work presented in it are her own. The thesis contains no material that has previously been submitted for a degree at this university or any other institution.

Elena Vidal Sarmiento

Trondheim, October 2015

Acknowledgements

Undertaking this PhD would not have been possible without the support and guidance that I received from many people.

First and foremost I want to thank my main supervisor, Prof. Terje Kanstad. I really appreciate all his contributions of time, ideas and support during my research. He has been a constant source of inspiration and enthusiasm. Many thanks also to my co-supervisors, Prof. Mette R. Geiker and Prof. Max A.N. Hendriks. I am really grateful for their scientific advice, and many insightful discussions and suggestions. Without their encouragement and positive feedback this PhD project would not have been achievable.

My grateful thanks are extended to all the technicians working in the laboratory. It would have taken forever to carry out all my experimental work without their help, which is really appreciated.

My time at NTNU has been very enjoyable, in large part due to the many colleagues that became a part of my everyday life. Thanks for all the good conversation during lunch and coffee breaks. The last few years would not have been the same without all the great times that we have shared.

I also gratefully acknowledge the funding that made my PhD work possible. This came from the Concrete Innovation Centre (COIN), funded by the Norwegian Research Council and its industrial partners. The most recent industrial partners included: Aker Solutions, Norcem, Norwegian Public Roads Administration, Rescon Mapei, Skanska, Unicon, Veidekke and Weber Saint Gobain.

Lastly, I would like to thank my family and friends for all their love and encouragement. Thanks to my parents and sister who supported me in all my pursuits. And thanks to Xavi whose faithful support during the final stages of this PhD is so very much appreciated. Thank you.

Abstract

The fibre orientation and distribution in a structural element cast with flowable fibre-reinforced concrete (FRC) is affected by the concrete flow, which can enhance its non-uniform and anisotropic fibre configuration. The structural behaviour may deviate substantially, in favourable or unfavourable ways, from behaviour corresponding to a uniform and isotropic fibre configuration, or from behaviour measured in a material characterization test.

The aim of this research project was to evaluate the impact of the fibre configuration on the mechanical behaviour of elements cast with flowable FRC and to provide a methodology for predicting this effect in their structural behaviour. The experimental investigation focused on characterizing the fibre volume content and orientation to make it possible to explain the structural behaviour. The examination was done at two levels of application: at the full-scale level using structural beams, and at a small-scale level using test specimens for material characterization.

The analysis of the fibre configuration at the full-scale level confirmed that casting under full-scale conditions can lead to non-uniform fibre configurations which may be difficult to foresee in the production stage and may not occur in standard test specimens. The observed non-uniform fibre configuration in the full-scale beams had a direct consequence on their mechanical response; the areas with unfavourable orientation and low fibre content played a decisive role in the crack propagation and reduced the load-carrying capacity. These observations suggest that procedures for estimating the structural performance of flowable FRC need to consider determinations or predictions of its fibre configuration.

From a design-oriented perspective, one possible approach is to characterize the material using small-scale standard tests and correct these results for favourable or unfavourable variations in fibre content and fibre orientation in the full-scale element. As a more advanced solution, a numerical modelling approach was developed to predict the mechanical response of a structural element taking its actual fibre configuration into account. This approach was found to capture the large differences in the loading capacity of the beams tested, which can only be attributed to the differences in their fibre configurations.

Incorporating the effect of fibre configuration in the prediction of structural behaviour will contribute to more reliable and effective use of flowable FRC. In combination with simulations of casting and non-destructive methods of characterizing the fibre configuration, this will encourage the use of this material in structural applications.

Notation and terms

Latin symbols

$\mathbf{A}$	Fibre orientation tensor
A_s	Area of reinforcement
A_f	Area of fibre cross-section
$\mathbf{a}_i$	Eigenvector of $\mathbf{A}$, i = 1, 2 or 3
d	Effective depth of a concrete cross-section
d_f	Fibre equivalent diameter
E_c	Young's modulus of concrete
F_n	Weighting fibre function
f_{R1}	Residual flexural tensile strength at CMOD = 0.5 mm
f_{R2}	Residual flexural tensile strength at CMOD = 1.5 mm
f_{R3}	Residual flexural tensile strength at CMOD = 2.5 mm
f_{R4}	Residual flexural tensile strength at CMOD = 3.5 mm
f_{Fts}	Residual tensile strength significant for SLS (MC 2010)
f_{Ftsd}	Design value for the residual tensile strength significant for SLS
$f_{Ftsd,mod}$	Modified design value of f_{Ftsd}
f_{Ftu}	Uniaxial residual tensile strength significant for ULS (MC 2010)
$f_{Ftu,norm}$	Uniaxial residual tensile strength for normalized conditions
$f_{Ftu,str}$	Uniaxial residual tensile strength for a structural element
f_{Ftud}	Design value for the residual strength significant for ULS
$f_{Ftud,mod}$	Modified design value of f_{Ftud}
f_{cm}	Mean value of cylinder compressive strength
f_{ctm}	Mean value of uniaxial tensile strength
$f_{fctm,fl}$	Mean value of flexural tensile strength
$f_{t,res}$	Analytical residual tensile strength based on Thorenfeldt's equation
$f^f_{ct,L}$	Limit of proportionality
G_F	Fracture energy
h	Height of a concrete cross-section; equivalent length of a finite element
K	Correcting factor for the residual tensile strength
K_{str}	Correcting factor for the residual tensile strength in a structural element
L	Beam span
L_i	Length of the fibre i (or the fibre segment i)
l_{cs}	Structural characteristic length
l_{el}	Length of a finite element

l_f	Fibre length
M	Bending moment
N	Axial force; number of fibres in the analysed volume
N_f	Total number of fibres crossing a plane
n	Unit vector normal to the crack plane
n_f	Number of fibres per surface unit
p	Unit vector in the direction of a fibre
$\mathbf{p}_i$	Unit vector in the direction of the fibre i
p_x, p_y, p_z	Components of vector **p**
R^2	Coefficient of determination
T_{40}	Flow time measured in the L-box test
t500	Flow time measured in the slump-flow test
V_c	Concrete volume
v_f	Fibre volume fraction
$\bar{v}_f$	Fibre volume fraction in the analysed element or in the concrete mix
$v_{f,local}$	Local fibre volume fraction
$v_{f,nom}$	Nominal fibre volume fraction
w/b	Water-binder ratio
w_1	Weighting for the orientation component for calculation of μ
w_2	Weighting for the volume fraction component for calculation of μ
w_{ult}	Ultimate crack opening
w_u	Crack opening corresponding to ULS
Ø	Diameter

Greek symbols

α	Orientation factor
α_{local}	Local orientation factor
δ	Beam deflection
ε	Strain
ε_c	Concrete strain
ε_s	Steel strain
ε_{ult}	Ultimate strain
η_0	Capacity factor for fibres
η_θ	Orientation number
θ	Fibre out-of-plane angle
κ_h	Size factor
λ_i	Eigenvalue of **A**, i = 1, 2 or 3

μ	Fibre efficiency variable
σ	Stress
σ_c	Concrete stress
σ_s	Steel stress
σ_{fm}	Mean value of stress in all the fibres crossing a crack
ϕ	Fibre in-plane angle

Abbreviations

2D	Two-dimensional
3D	Three-dimensional
ASTM	The American Society for Testing and Materials
CV	Coefficient of variation
CMOD	Crack mouth opening displacement
COIN	Concrete Innovation Centre
CT	Computed Tomography
FE	Finite element
FRC	Fibre-reinforced concrete
MC 2010	*fib* Model Code 2010
NTNU	Norwegian University of Science and Technology
SCC	Self-compacting concrete
SFRC	Steel fibre-reinforced concrete
SLS	Service Limit State
ULS	Ultimate Limit State
VSI	Visual Stability Index

Subscripts

c	Concrete
el	Element
f	Fibre
local	Local
mod	Modified
nom	Nominal
norm	Normalized
res	Residual
s.beam	Standard beams
str	Structural element
ult	Ultimate

List of definitions

Aspect ratio	Ratio of the length of a fibre to its diameter (or equivalent diameter).
Balling effect	The effect of a bunch of fibres sticking together during concrete mixing or casting.
Consistence	A measure of the ease by which fresh concrete can be placed.
Dynamic segregation	Downward settling of coarse aggregate or fibres due to the movement of the fresh concrete.
Fibre structure	The structure of all the fibres that together constitute the fibre reinforcement in a hardened element.
Fibre configuration	The way fibres are arranged in a hardened element.
Flow length	Distance that the concrete flows to fill the formwork.
Filling ability	The ability of fresh concrete to flow under its own weight and completely fill all the spaces in the formwork.
Flowability	The flow of fresh concrete when not restricted by formwork or reinforcement.
Flowable concrete	Concrete that is able to flow under its own weight and consolidate without the need for vibrating compaction.
Matrix	The fraction of cement paste plus the aggregates less than 0.125 mm.
Ordinary concrete	Concrete characterized by the need to be vibrated to achieve full compaction.
Packing density	The volume of the solid particles in a unit volume of concrete.
Passing ability	The ability of a concrete to flow through tight spaces, like congested steel reinforcing bars or narrow spots in the formwork.
Plug-flow	Flow of concrete at low shear rates (below the yield stress) in which concrete moves as a rigid body.
Robustness (material)	The capacity of concrete to retain its fresh properties when small variations in the properties or quantities of the constituent materials occur.

Robustness (structural)	The ability of a structure to perform adequately in an accidental situation.
Segregation resistance	The ability of a concrete to remain homogeneous while in its fresh state; during transport and placing, i.e. in dynamic conditions, and after placing, i.e. in static conditions. Also called stability.
Self-compacting concrete	Concrete that is able to flow under its own weight and completely fill the formwork, while maintaining homogeneity even in the presence of congested reinforcement, and then consolidate without the need for vibrating compaction.
Static segregation	Downward settling of the coarse aggregate or fibres when concrete is at rest.
Wall effect	Tendency of fibres to align along a boundary as a result of the interaction of the fibre with the boundary.
Workability	The property of fresh concrete which is indicated by the amount of work done to overcome the internal friction between individual particles in the concrete necessary to produce full compaction.

List of papers

The thesis comprises the following papers, which are included in Chapters 4-8.

I. Influence of fibre distribution and orientation on the flexural behaviour of beams cast from flowable hybrid polymer-steel FRC
E.V. Sarmiento, M.R. Geiker & T. Kanstad
Submitted to an international scientific journal in September 2015

II. Influence of fibre configuration on the mechanical behaviour of standard test specimens and full-scale beams made of flowable FRC
E.V. Sarmiento, M.R. Geiker & T. Kanstad
Submitted to an international scientific journal in August 2015

III. Impact of the combined effect of fibre orientation and volume fraction on the mechanical properties of fibre reinforced concrete
E.V. Sarmiento, T. Kanstad, M.R. Geiker & M.A.N. Hendriks
In: *Proceedings of the XXII Nordic Concrete Research Symposium, Reykjavik, Iceland.* Norsk betongforening, Oslo, Norway; 2014. p. 141-144.

IV. Accounting for the fibre orientation on the structural performance of flowable fibre reinforced concrete
E.V. Sarmiento, M.A.N. Hendriks, T. Kanstad
In: *Computational Modelling of Concrete Structures, Volume 2*. N. Bícanić N, H. Mang, G. Meschke, R. de Borst R, editors. CRC Press, Leiden, The Netherlands; 2014. p. 609-618.

V. Modelling the influence of the fibre structure on the structural behaviour of flowable fibre-reinforced concrete
E.V. Sarmiento, M.A.N. Hendriks, M.R. Geiker & T. Kanstad
Submitted to an international scientific journal in September 2015

Declaration of authorship

The author of the thesis, Elena Vidal Sarmiento, planned and conducted most of the experiments, evaluated the results, and wrote the major part of all the papers included in the thesis. The co-authors of the papers contributed in planning the experiments, discussing and evaluating the results, and by assisting in writing the papers. Part of the experimental work presented in Paper I was conducted within a master project (students: Ø.S. Nordhus, E. Steinnes & T. Simpson). Likewise, the experimental work

in Paper II was carried out in collaboration with the master student H. Røer. For papers II and V, language support was provided by the Language Support Centre Denmark (Lawrence White).

Other publications

In addition to the papers included in the thesis, the author of this thesis has contributed to the following works.

Journal papers

Žirgulis, Giedrius; Švec, Oldřich; Sarmiento, Elena V.; Geiker, Mette R.; Cwirzen, Andrzej; Kanstad, Terje. (2015) "Importance of quantification of steel fibre orientation for residual flexural tensile strength in FRC". *Submitted to Materials and Structures*.

Spangenberg, Jon; Roussel, Nicolas; Hattel, Jesper; Sarmiento, Elena V.; Žirgulis, Giedrius; Geiker, Mette R. (2012) "Patterns of gravity induced aggregate migration during casting of fluid concretes". *Cement and Concrete Research* **42**(12): 1571-1579.

Conference papers

Hisdal, Jorun-Marie; Žirgulis, Giedrius; Sarmiento, Elena V.; Kanstad, Terje. (2013) "Strut and tie models for disturbed regions: Steel fibre reinforced concrete dapped end beams". *Proceedings of the 5th International Conference on Structural Engineering, Mechanics and Computation, SEMC 2013*. Cape Town, South Africa.

Sarmiento, Elena V.; Žirgulis, Giedrius; Sandbakk, Sindre; Geiker, Mette R.; Kanstad, Terje. (2012) "Influence of concrete flow on fibre distribution, orientation and mechanical properties of fibre reinforced concrete". *8th RILEM International Symposium on Fiber Reinforced Concrete: challenges and opportunities (BEFIB 2012)*. Guimaraes, Portugal.

Kanstad, Terje; Geiker, Mette R.; Žirgulis, Giedrius; Sarmiento, Elena V. (2012) "Flowable fibre reinforced concrete: Materials development, fibre distribution and structural properties". *Conference Proceedings of fib Symposium 2012: Concrete Structures for Sustainable Community*. Stockholm, Sweden.

Master thesis

Sarmiento, Elena V. (2011) "Influence of concrete flow on the mechanical properties of ordinary and fibre reinforced concrete". Norwegian University of Science and Technology. Trondheim, Norway.

Scientific lectures

Sarmiento, Elena V. (2015) "Accounting for the fibre orientation on the structural performance of flowable fibre reinforced concrete". *10th International DIANA Users Meetings*. Barcelona, Spain.

Sarmiento, Elena V. (2015) "Utfordringer med fiberfordeling og orientering i selvkomprimerende fiberarmert betong". *Norsk Betongdag og SINTEF-NTNU Betonginformasjonsdag*. Trondheim, Norway.

Sarmiento, Elena V. (2013) "Fibre reinforced concrete in dapped-end beams". *8th International DIANA Users Meetings*. Gothenburg, Sweden.

Table of contents

Chapter 1

Introduction

1.1 Background and motivation

The major development of fibres as a reinforcement technology to improve the mechanical properties of concrete started in the 1960s. Since then, a substantial amount of research has led to the development and commercialization of fibres with various compositions and geometrical configurations to enhance concrete properties, see e.g. ACI Committee 544 (2002) or Löfgren (2005).

The greatest benefit from the introduction of fibres into the concrete is the enhanced post-cracking response. Fibres bridge the cracks and transfer load across them through frictional or mechanical bond action. This changes the mode of fracture from brittle for unreinforced concrete, to ductile. The improved ductility has the potential to increase impact resistance, flexural fatigue strength, load-carrying capacity, and consequently reduce the need for traditional reinforcement. This last aspect is especially relevant for complex geometries with highly congested reinforcement solutions, where the use of fibres can lead to substantial reductions in time and labour effort.

a) b)

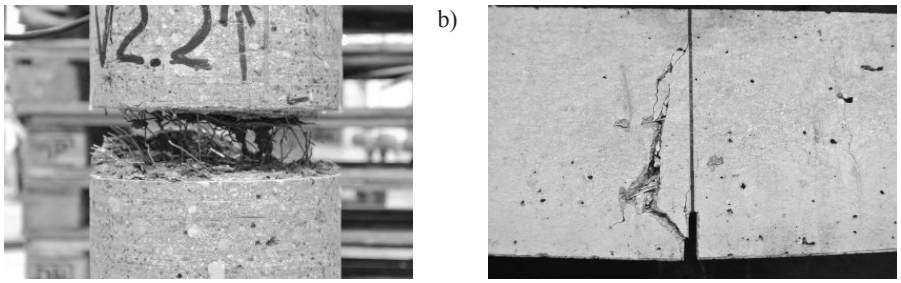

Fig. 1.1. Crack-bridging effect: a) fibres across two crack faces in uniaxial tension testing, and b) fibres bridging a bending crack.

Another benefit of the use of fibres is related to crack control. The reduction in crack width and in some cases the number of cracks can improve the quality of the structure and limit the penetration of harmful agents that cause deterioration. As a result, the use of fibre-reinforced concrete (FRC) can lead to a reduction in long-term costs related to repair and maintenance.

It can therefore be concluded that enhanced flexural performance, ductility, durability and economic aspects are the fundamental factors driving the development of FRC into an industrially competitive material.

Nowadays fibres are used in multiple engineering applications. Pavements, industrial floors and bridge decks often use micro fibres for thermal and shrinkage crack control, and macro fibres as structural reinforcement to reduce their thickness or to improve the impact resistance and the flexural performance. Fibres can partially or totally replace traditional forms of reinforcement for example in curved structures such as tunnel segments (Fig. 1.2a) and water tanks and pipes, in elements with complicated geometric shapes, or in elements with high reinforcement concentrations (Fig. 1.2b). Other civil engineering applications include shotcrete, geotechnical slope stabilization, and in the repair and restoration of existing structures.

a) b)

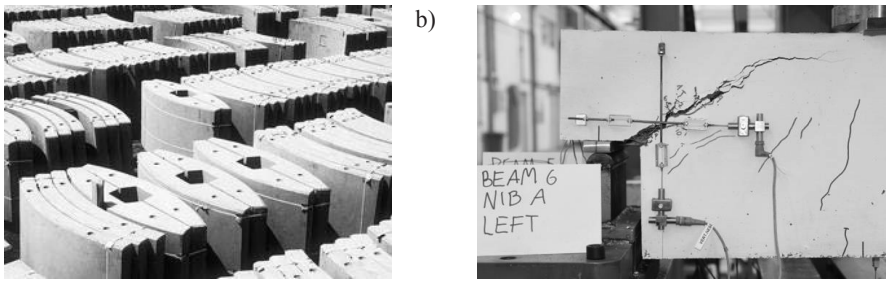

Fig. 1.2. Examples of applications of steel FRC: a) industrial manufacture of precast tunnel segments[1], and b) investigation on the use of FRC in dapped-end beams to simplify the highly congested traditional reinforcement layout (Nedrelid and Kanstad, 2014a).

The use of fibres in flowable or self-compacting concrete (SCC) has the potential to optimize both technologies. Self-compacting concrete spreads homogeneously without any need for compaction. Numerous benefits are associated with this, such as increased productivity due to reduced casting time, improved working environment, high concrete quality under difficult casting conditions, and improved surface quality. Moreover, the application of SCC with fibre reinforcement has revealed several potential synergistic effects (Ferrara, 2014, Grünewald, 2004), including the following:

[1] http://tunnelbuilder.com/suppliers/bekaert_profile.htm

- A more uniform distribution of fibres due to the elimination of compaction methods and high stability in the SCC matrix (Ferrara and Meda, 2006, Ozyurt et al., 2007).
- Enhanced structural performance in cases where fibres orient in the direction of the tensile stresses for certain load conditions.
- Improved efficiency in the construction and transportation processes.

The advances in material development in the field of FRC, including flowable and self-compacting FRC, and its potential for new applications mean that test methods and design rules are required for the specific characteristics of this material to enable reliable engineering design. Differences in fibre distribution and orientation between structural elements and test specimens have been reported in several investigations (Blanco, 2013, Montaignac et al., 2012, Di Prisco et al., 2009). If the fibre configuration in the test specimens is unrepresentative, this can lead to unreliable prediction of the structural performance. This is why some of the recently developed guidelines (SFRC Consortium, 2014, Swedish Standards Institute, 2014, DAfStb, 2012, RILEM, 2003, *fib*, 2010, Kanstad et al., 2011) include corrections to the design material properties to take into account the fact that the fibre orientation in the structural elements may be different than in the reference test specimen.

Usually, uniform distribution of fibres is examined as part of the quality control of the fresh concrete during production. With flowable FRC, however, the casting process and the fresh concrete behaviour may induce a preferred orientation and/or an uneven distribution of the fibres in the structural element. Research on the development of the final fibre configuration and its influence on mechanical performance in various applications is still necessary to improve our understanding of structural behaviour and reduce the uncertainty of material properties in industrial applications.

1.2 Objectives

The overall objective of this thesis was to do research work that could stimulate and prepare the ground for the increased use of fibres in load-carrying structures.

The more specific objectives were to:

- Document the structural behaviour of flowable FRC in full-scale beams.
- Identify potential differences in structural behaviour between full-scale beams and small-scale test specimens.
- Characterize the fibre distribution and orientation patterns in full-scale beams in order to explain the impact of the fibre configuration on the structural behaviour.

- Characterize the fibre distribution and orientation in small-scale test specimens, and identify potential causes of differences in structural behaviour between full-scale beams and small-scale test specimens.
- Provide a methodology for predicting the effect of fibre configuration on the structural behaviour of flowable FRC.

1.3 Research strategy

To achieve the objectives of this research project, the following strategy was developed.

With regard to the experimental research, the material was investigated at two levels of application: at the full-scale level using structural beams, and at the small-scale level using test specimens for material characterization.

For the full-scale beams, the fibre configuration at various locations in the beams was characterized to identify variations in fibre orientation and distribution over the thickness and along the length. The flexural response of the beams was also tested.

For the small-scale specimens, the fibre configuration was examined to study the representativeness of the fibres in the test specimens, and the main variations in the fibre orientation and distribution between them. The post-cracking response was determined and evaluated in relation to variations in both fibre orientation and volume fraction.

The investigation led naturally to a comparison of the performance at the two levels, which made it possible to evaluate the limitations of using results from small-scale test specimens for the prediction of structural behaviour. Once the differences in the fibre configuration at both levels were known, it was possible to identify the main causes that limit the translation of results. The outcome of the study made it necessary to address the discussion of the need for a correcting factor in design assumptions.

A modelling approach was therefore developed to take into account the fibre configuration in finite element analysis of structural elements of FRC. Two fibre configuration parameters were defined volume-wise in accordance with a chosen discretization of the element in volumes: the orientation tensor and the local volume fraction. These parameters were incorporated in a numerical model, which uses a single-phase material definition for each discrete volume based on the fibre configuration parameters. This modelling approach was validated using two case studies. The first included analysis of three small-scale beams loaded with three-point bending, while the second included analysis of two full-scale beams in four-point bending.

1.4 Research limitations

The research topics covered in this thesis are:

- The application of flowable FRC concrete in load-carrying structural elements and the characterization of the fibre configuration in these elements.
- The influence of the distribution and orientation of fibres on mechanical behaviour.
- Description of the structural performance of full-scale elements based on the characterization of the fibre configuration.

The main experimental research focused on two flowable concrete mixes: a hybrid FRC with 1% vol. of polymer and steel fibres, and an FRC with 2% vol. of steel fibres. The development of the mixes was not a part of this thesis. They were developed during research activity on high tensile strength all-round concrete, which was a sub-project included in COIN's focus area 2[2].

To limit the scope of this thesis, the following limitations were made:

- The full-scale application of the mixes to structural elements was limited to the study of beams. The experimental research described in this thesis was carried out on a limited set of specimens.
- The characterization of the fibre distribution and orientation using manual methods, such as fibre counting and separation of fibres from the hardened matrix, was comprehensive but laborious (Chapter 4). A more exhaustive characterization including more specimens was therefore excluded by limits on the amount of laboratory work considered reasonable.
- The characterization of fibre distribution and orientation using Computed Tomography scanning (Chapter 5) allowed complete analysis of test specimens. The analysis of full-scale beams, however, was limited by the capacity of the equipment. The examination was therefore limited to the critical parts of the beams.
- The experimental evaluation of the structural performance was limited to bending tests, and discussion of the flexural behaviour mainly focused on load-carrying capacity, ductility and crack patterns. The influence of the fibres on crack widths was not investigated for the full-scale elements.
- The numerical approach presented in Part III of this thesis was verified on a limited number of examples and only covered flexural behaviour.
- The numerical analysis of a wall element presented in Chapter 9 was not verified experimentally.

[2] www.coinweb.no

1.5 Outline of the thesis

This PhD thesis is comprised of four parts.

Part I (Chapters 2 and 3) introduces the research topic and methods relevant for this thesis. Chapter 2 covers the main features of flowable FRC, both in the fresh state and in the hardened condition. In addition to establishing a general background, the focus is on the various mechanisms of fibre orientation and distribution and the identification of their main effects on post-cracking tensile behaviour. Chapter 3 provides a brief introduction to the materials and methods used in this thesis.

Parts II and III comprise the main body of the thesis and include five papers that are organized in Chapters 4-8.

Part II (Chapters 4-6) includes the main experimental investigations. Chapters 4 and 5 describe the flexural behaviour and fibre configuration in full-scale beams and standard test specimens. The limitations involved in using results from test specimens to predict structural behaviour are discussed in relation to differences in their fibre configurations. Chapter 4 is devoted to elements made of flowable hybrid polymer-steel FRC, while Chapter 5 deals with elements of flowable FRC with 2% vol. of fibres.

Chapter 6 discusses the need to incorporate the contributions of both the local fibre orientation and the local volume fraction in relationship to the post-cracking response of FRC and, in particular, its residual flexural tensile strength.

Part III (Chapters 7-9) deals with the modelling approach that was developed to take fibre structure into account when simulating the mechanical behaviour of structural elements cast with flowable FRC.

Chapter 7 introduces the methodology of the approach and describes the numerical framework. The model incorporates spatial variations in the fibre content and fibre orientation in finite element modelling. This chapter shows the ability of the numerical framework to properly simulate the flexural response of notched beams with different fibre configurations. The modelling approach, as described in Chapter 7, constitutes the first phase of development.

A significant refinement of the modelling approach is introduced in Chapter 8. While the model in Chapter 7 considers fibre orientation with respect to a given plane, the approach in Chapter 8 considers fibre orientation with respect to the direction of the principal strains. This enables the model to take into account both the inhomogeneities of the fibre structure and the anisotropic behaviour of the material. The overall

modelling approach is validated against experimental results from four-point bending tests on full-scale beams.

In Chapter 9, the modelling approach is applied to analyse a structural element whose fibre configuration is obtained using a simulation of the concrete flow. This chapter demonstrates the coupling between the two simulation approaches.

Part IV contains the final chapter of the thesis. This chapter puts the research undertaken in Parts II and III into a perspective of research, development and practical applications of FRC and gives the main conclusions and future perspectives of this research project.

Part I

Research motivations and applied methods

Chapter 2

The research topic: Flowable fibre-reinforced concrete

2.1 Introduction

Fibres bridge cracks and retard their propagation, improving the post-cracking response of hardened concrete. The post-cracking response, however, appears to strongly depend on the distribution and orientation of the fibres, which typically distribute and orient during the casting process, governed by the casting conditions and the fresh concrete properties. In flowable or self-compacting concrete, such effects can result in uneven fibre configuration, which can make it difficult to characterize the post-cracking response of the material.

This chapter introduces the research topics relevant for this thesis. First, the main effects of including fibres in the fresh state of flowable concrete are described. Second, reference is made to the mechanisms that determine the distribution and orientation, and to the characterization methods and predictive tools that are available. The main effect of fibres in the hardened state and the characterization methods most commonly used are then briefly introduced. And finally, focus is given to the effect of the fibre configuration on the post-cracking tensile behaviour.

2.2 Fresh concrete performance of flowable FRC

The addition of fibres affects the fresh concrete properties by considerably stiffening and reducing the workability of the concrete. This effect depends on the fibre type and limits the content of fibres that can be uniformly distributed throughout a mix. Considering that improved mechanical behaviour strongly depends on the addition of

fibres, the choice of fibre type and content is usually based on the balance between ease of handling of the fresh concrete and maximum efficiency in the hardened state.

2.2.1 Effect of fibres on fresh state behaviour

According to Grünewald (2004) and Ferrara (2014), the main reasons why fibres affect the fresh state performance of a concrete mix are related to the large surface area of fibres, which increases the demand of fluid phase, and their elongated shape, which affects the packing density and promotes interlocking among the fibres and between fibres and aggregates (Bayasi and Soroushian, 1992, Martinie et al., 2010). High fibre content creates a stiff internal structure in which fibres tend to ball-up in the mix, causing workability problems (Grünewald, 2004, Swamy and Mangat, 1974). This occurs because the packing density of the particles decreases with increasing fibre content. Considering a given fibre content, the degree to which packing density and workability decrease depends on the mix composition and on fibre properties such as the aspect ratio[3], the rigidity, the shape and the material of the fibres (Swamy, 1975).

Martinie et al. (2010) have reported that reducing the aspect ratio is one way to increase the fibre content in a mix. Fig. 2.1 illustrates the effect of increasing the fibre factor, defined as the product $v_f \cdot l_f / d_f$, on the consistency of a cement paste.

Fig. 2.1. Effect of increasing the fibre factor ($v_f \cdot l_f / d_f$) on the consistency of a cement paste mixed with fibres (Martinie et al., 2010).

It is also possible to increase the fibre content without excessive loss of workability by optimizing the packing density with respect to the aggregates (Rossi and Harrouche, 1990, Berg and Jacobsen, 2007). Reducing the coarse aggregate volume fraction allows the fine aggregate and the paste volume fraction to increase, which facilitates the accommodation of fibres (Johnston, 1996, Martinie et al., 2010). The maximum coarse

[3] Ratio of fibre length to equivalent diameter, l_f / d_f.

aggregate size is also an important factor, because the number of fibres within a unit volume decreases with increasing aggregate size (Fig. 2.2).

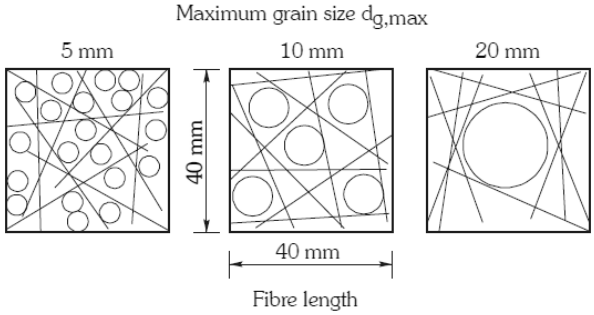

Fig. 2.2. Effect of aggregate size on packing density in a mix (Johnston, 1996, Grünewald, 2004).

2.2.2 Fresh state performance of flowable FRC

In studies of the properties of fresh concrete, SCC is often understood as a suspension of solid particles in a fluid phase (cement paste), in which the particle size distribution and fluid phase are usually optimized to meet the three key characteristics of SCC in the fresh state: filling ability, passing ability, and segregation resistance, see e.g. Geiker (2008). The effect of fibres on the fresh state of SCC is usually also discussed in terms of these three key characteristics. Before presenting some of the investigations on fresh self-compacting FRC, a brief introduction to common test methods is given.

Numerous attempts have been made to correlate fresh concrete properties with convenient measurements. One test widely used for describing filling ability is the slump-flow test (European Standard, 2010a, ASTM International, 2014), which provides a measure of the consistency and unconfined flow potential (slump-flow) and a measure of the flow rate (t500), which is considered as an indication of viscosity. The same test also provides visual rating criteria to classify ability to resist segregation.

There are numerous other methods that refer to the aforementioned key properties of SCC. In addition to the slump-flow test, the V-funnel test (European Standard, 2010b) is widely used to characterize viscosity and filling ability. The J-ring test (European Standard, 2010c) and the L-box test (European Standard, 2010d) provide a measure of passing ability. The sieve segregation test (European Standard, 2010e) is used to assess segregation resistance. The methods mentioned here do not represent a complete list, but are among the most commonly used today.

These methods were designed for SCC, but are extensively applied to self-compacting FRC in their standard form or with small modifications. Grünewald (2004) adapted several test methods to investigate how fresh properties are affected by the presence of fibres, depending on their type and content. The fibre funnel, for instance, was proposed as an alternative to the V-funnel to avoid long fibres blocking during the test. The rebar spacing was modified to assess the passing ability of fibres in the J-ring test. The sieve segregation test was also adapted for the presence of fibres.

In the same investigation, Grünewald (2004) reported on the effect of the fibre factor on slump-flow, concluding that the greater the fibre content and the larger the aspect ratio, the lower the slump-flow. A decrease in the flow rate was also observed with the addition of fibres. Similar results were previously found by Groth (2000a) (Fig. 2.3), who characterized the flow rate using the L-box flow time at 40 cm (T_{40}) in a test performed without reinforcing bars. According to Groth, obtaining T_{40} is better than the measurement of t500, because in a slump-flow test the spread of concrete is not always symmetrical, which makes it difficult to obtain t500.

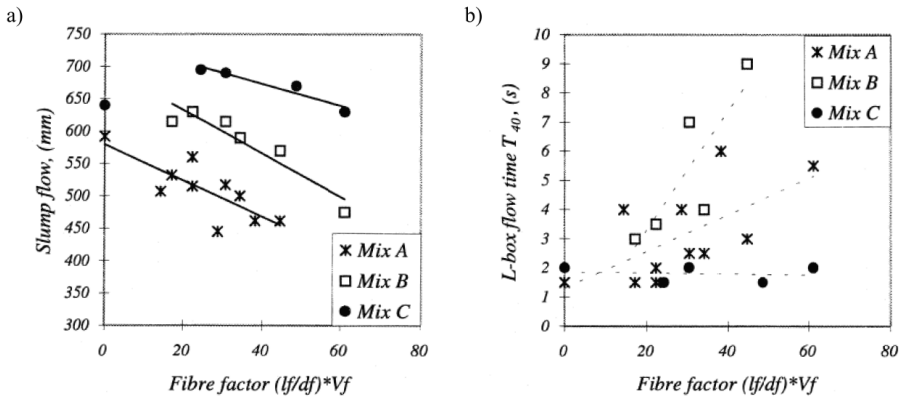

Fig. 2.3. Influence of fibre factor on the workability expressed as: a) slump-flow, and b) L-box flow time T_{40} (Groth, 2000a).

With reference to the passing ability of flowable FRC, Grünewald (2004) studied the bar spacing required to avoid blocking, and observed a dependence of this spacing on the rheological properties of the mix. Groth (2000b) documented that the minimum gap distance that the concrete should be able to flow through depends on the fibre content and the fibre aspect ratio. The same author suggested that the minimum gap distance should be determined for each case depending on the intended application.

Several studies describe the tendency of fibres to separate from the matrix or distribute unevenly (Groth, 2000a, Grünewald, 2004, Døssland, 2008). This is often related to the

maximum fibre content being exceeded or the packing density not being appropriately optimized for that fibre content. Martinie et al. (2010) described the existence of a critical packing density at which contacts between fibres and aggregates strongly reduce the ability to flow. Beyond this critical value, fibres tend to ball. For mix design purposes, Grünewald (2004) established acceptance criteria to evaluate the balance between filling ability and stability based on the flow pattern of the slump-flow test.

The ability of the material to distribute the fibres is recognized as one of the key features of flowable and self-compacting FRC that has a strong impact on the properties of the hardened FRC. This issue is therefore further described in the following section.

2.3 Distribution of fibres in flowable FRC

Like any other composite material, FRC needs to have low variation in the distribution of its components to be considered as a reliable material for engineering design (Chiachio et al., 2012). Fibres need to provide consistent 3D reinforcement based on a homogeneous and random distribution. However, homogeneous flowable FRC is often difficult to achieve, because the inclusion of fibres creates an internal structure that counteracts the flow, affecting the desired compromise between fluidity and stability.

This can hinder the uniform distribution of the fibres within structural elements. As Ferrara et al. (2012a) point out, areas with a reduced fibre dosage or no fibres act as flaws triggering early failures and activating unforeseen mechanisms that affect load-carrying capacity and structural performance.

The type of mixer and mixing procedure are also important for achieving complete and uniform distribution of fibres throughout the concrete mix. Furthermore, an inappropriate method for the fibre addition may prolong the mixing time needed, which can lead to overmixing and increase the tendency of fibres to ball-up (Johnston, 1996).

2.3.1 Mechanisms of fibre distribution

The ability of a flowable FRC to distribute the fibres uniformly is strongly related to the stability or segregation resistance of the mix. A distinction is often made between resistance to dynamic segregation and resistance to static segregation (Şanal and Özyurt Zihnioğlu, 2013).

Static segregation refers to the downward settling of particles such as coarse aggregates or fibres when the concrete is at rest, before or after casting. It is related to the density difference between the particles and the suspending phase (cement paste) (Roussel, 2006).

Dynamic segregation refers to flow-induced particle migration. Spangenberg et al. (2012b) identified three physical phenomena which can lead to flow-induced particle migration: (i) shear-induced particle migration, (ii) gravity-induced particle migration, and (iii) particle blocking. They concluded that, in industrial casting, gravity-induced particle migration dominates all other sources of heterogeneity during flow. Internal friction and cohesive forces between the particles and the suspending phase tend to decrease with the casting flow; after a certain flow length, they may become too low to counteract the effect of gravitational forces. This can lead to segregation of the particles with highest density, usually coarse aggregates and fibres.

The stability of a mix is usually checked at the production stage, using tests that characterize the segregation resistance of a concrete sample at rest or under limited flow conditions. A stable mix implies that the tested concrete did not exhibit downward settlement of fibres or aggregates. However, this is not sufficient to ensure a uniform distribution of these components under full-scale casting conditions. Spangenberg et al. (2012a) demonstrated that a concrete which is stable at rest can be unstable during flow leading to non-uniform aggregate distribution (Fig. 2.4). The same can be expected for fibres.

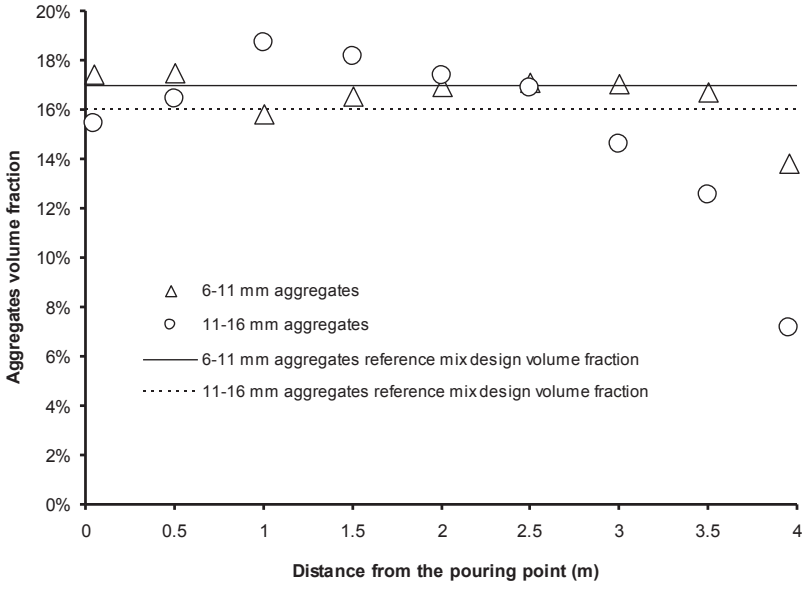

Fig. 2.4 Aggregate volume fraction measured in the fresh state as a function of the distance from the casting point (Spangenberg et al., 2012a).

Under full-scale casting conditions, the reduction of segregation resistance might lead to a non-uniform distribution of fibres:

- Over the element height. Fibres may settle at the bottom of the formwork and be sparsely present at the top (Fig. 2.5a).
- Over the element length or width. A higher content of fibres may be found closer to the casting point than further away from that point (Fig. 2.5b).
- Close to areas that disturb or obstruct the concrete flow during casting (Fig. 2.6).

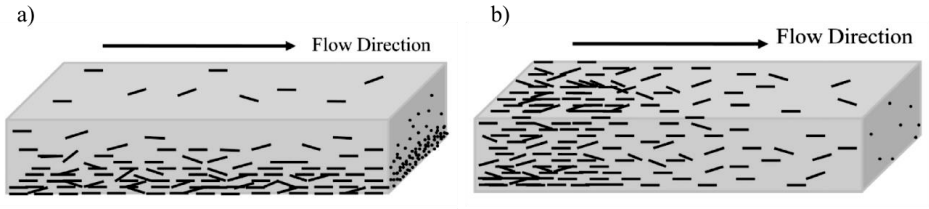

Fig. 2.5. Representation of: a) downward settlement of fibres caused by static segregation, and b) uneven fibre distribution caused by dynamic segregation (Şanal and Özyurt Zihnioğlu, 2013).

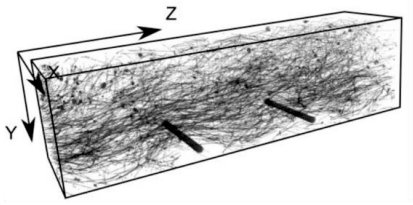

Fig. 2.6. Computed Tomography image of the fibre distribution in a beam sawn from a reinforced slab. Low fibre content is detected under the reinforcing bars (Žirgulis et al., 2015a).

2.3.2 Characterization of fibre distribution

Various methods have been proposed to evaluate the ability of an FRC to distribute its fibres, based on the resistance of the mix to static and dynamic segregation. Often, the characterization of this property is assessed by visual observations, for instance, in slump-flow tests. Common quantitative evaluation methods obtain the fibre volume fraction using either washing-out, in which the fibres are separated from the fresh concrete matrix, or by crushing a hardened sample and separating the fibres (Fig. 2.7). In both cases, the weight of fibres and the volume of the tested sample are measured to provide the result of the fibre volume fraction.

Fig. 2.7. Determination of the fibre content in a hardened concrete sample (Sarmiento, 2011).

Specific ways to characterize the degree of static segregation include the washing-out of a fresh concrete sample as depicted in Fig. 2.8a (Grünewald, 2004) and the column test used by Ferrara et al. (2012a), which is performed using hardened cylinders (Fig. 2.8b).

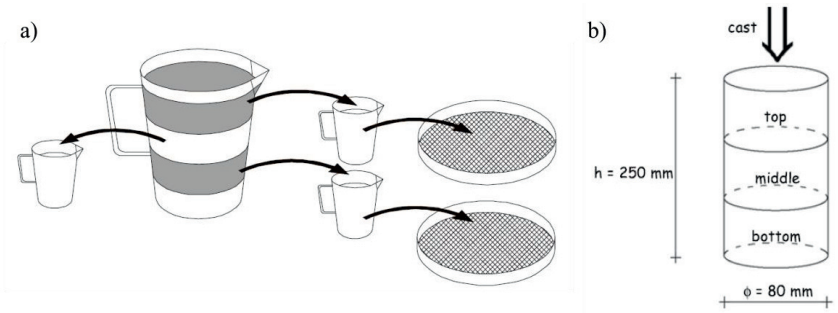

Fig. 2.8. Testing the static resistance to fibre segregation by comparing the fibre volume fraction in each third of a) a fresh concrete sample (Grünewald, 2004), and b) a hardened cylinder (Ferrara et al., 2012a).

With regard to dynamic segregation, concentric regions of the slump-flow test patty can be washed-out to characterize the fibre distribution in unconstrained flow conditions (Ferrara et al., 2012a, Ferrara et al., 2011). On a larger scale, the channel flow test (Ferrara et al., 2012a, Ferrara et al., 2011) can be performed to investigate the matrix ability to drive the fibres along a constrained flow by determining the fibre content at various distances from the casting point. Other investigations (Ferrara and Meda, 2006) report fibre content determined from cores drilled from structural elements.

Sawing of specimens along the directions of interest and counting fibres on the sawn surfaces is often used to evaluate the homogeneity of the fibres in a cast specimen or to examine the tendency of the fibres to segregate (Gettu et al., 2005, Ferrara et al., 2011). Methods such as X-ray imaging (Ferrara and Meda, 2006, Vandewalle et al., 2008) and Computed Tomography scanning (Stähli et al., 2008, Şanal and Özyurt Zihnioğlu, 2013, Suuronen et al., 2013) have also been used to characterize the fibre distribution, because they provide an actual visualization of the fibres in 2D or 3D, respectively.

Recently, significant advances have been achieved with regard to non-destructive methods for the assessment of the fibre distribution. Some examples of these methods include the use of alternate current impedance spectroscopy (Ferrara et al., 2008, Woo et al., 2005, Ozyurt et al., 2006a), magnetic induction tests (Ferrara et al., 2012c, Faifer et al., 2010, Torrents et al., 2012), and microwave imaging (Roqueta et al., 2011, Van Damme et al., 2004, Torrents et al., 2009).

The fibre content of the fresh mix is an important parameter of uniformity for purposes of quality control in the production of FRC. For this reason, some of the recently published guidelines on FRC (DAfStb, 2012, SFRC Consortium, 2014, Swedish Standards Institute, 2014) incorporate conformity requirements for the uniformity of the fibre content of fresh and hardened concrete based on fibre-matrix separation, e.g. EN 14721 (European Standard, 2007) or EN 14488-7 (European Standard, 2006), or on magnetic induction tests, e.g. DAfStb (2012).

2.4 Orientation of fibres in flowable FRC

The orientation of fibres in a cast element often differs from the random orientation in a mixer. The material behaviour, the production and casting conditions, and the flow of concrete can influence the orientation of the fibres, and this strongly affects the mechanical properties of the cast element in the hardened state (Soroushian and Lee, 1990, Kooiman, 2000, Markovic, 2006, Stähli and van Mier, 2007).

The loss of random orientation of the fibres may, in principle, jeopardize the use of the concrete because it makes the characterization and prediction of the structural behaviour more complex (Grünewald et al., 2012). However, a non-isotropic 3D structure in the fibre reinforcement could also be used to optimize the performance of the material, for instance, by tailoring the predominant fibre orientation to meet the principal tensile stress direction. Several authors (Ferrara et al. 2011; Martinie and Roussel 2011) have stated the basic principles for a tailored orientation of fibres: controlling the casting conditions and ensuring appropriate rheological properties. The effective orientation of the fibres may improve the mechanical behaviour of the FRC (Ferrara et al., 2011, Barnett et al., 2010, Boulekbache et al., 2010) and lead to the more efficient design of a structural element.

2.4.1 Mechanisms of fibre orientation

Fibres orient in flowable FRC mainly for two reasons: due to the wall effect, or due to shear rates related to variations in the flow velocity profile (Martinie and Roussel, 2011).

The flow of concrete during casting is influenced by shear stresses that depend on the geometry of the element to be cast, the rheological behaviour of the material, and the casting method. These shear stresses determine the flow velocity profile. According to Stähli et al. (2008), variations in flow velocities affect the fibres and may cause their orientation. In the case of a channel, the flow velocity is greatest in the centre, while it is reduced close to the walls of the formwork due to the frictional restraint of the walls. As depicted in Fig. 2.9a, such a velocity profile may induce rotation of the fibres towards an ideal equilibrium position orientated in the direction of the sheared flow (Stähli et al., 2008, Boulekbache et al., 2010).

The flow velocity profile that occurs when casting slabs usually differs significantly from a channel flow, which best represents the casting of a beam. Typically for slabs, concrete spreads radially from the casting point. As it diffuses uniformly outwards in all directions, the flow velocity declines. This creates extensional stresses that orient the fibres perpendicular to the flow direction (Martinie and Roussel, 2011, Abrishambaf et al., 2013, Švec, 2013, Boulekbache et al., 2010), as illustrated in Fig. 2.9b.

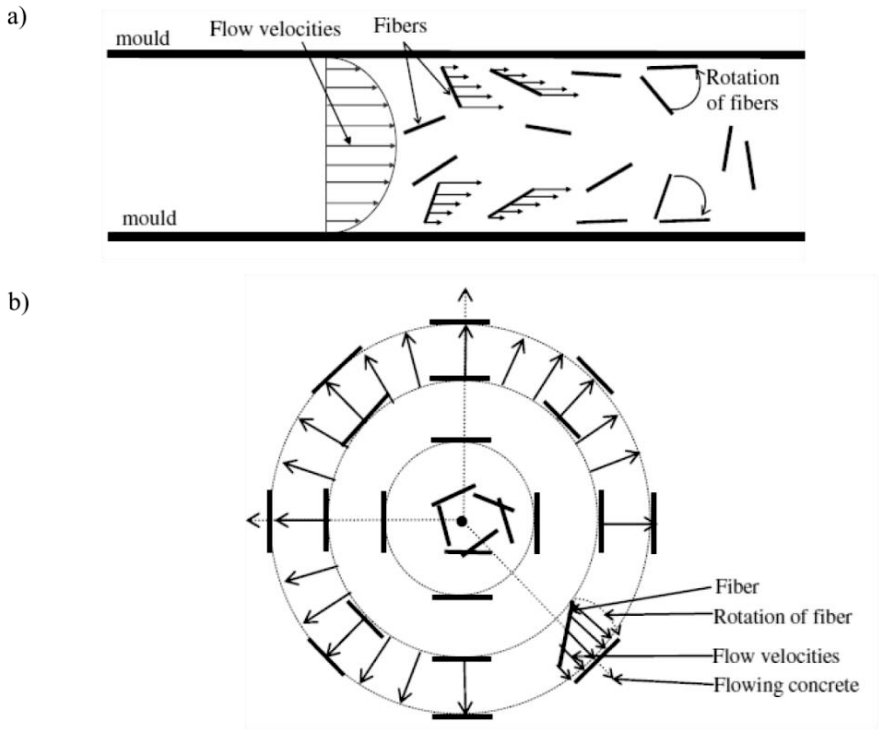

Fig. 2.9. Fibre orientation caused by the flow velocity profile. Representation of a top view of fibres oriented: a) in a channel flow, and b) in a radial flow (Boulekbache et al., 2010).

The wall effect refers to the tendency of fibres to align along a boundary, such as the walls of a formwork or ordinary reinforcing bars. It is explained by the interaction of a fibre with the boundary, which restricts its orientation (Soroushian and Lee, 1990, Dupont and Vandewalle, 2005). It is, for instance, impossible to find a rigid fibre perpendicular to a wall with its centre at a distance less than half the length of the fibre (Dupont and Vandewalle, 2005, Martinie and Roussel, 2011), see Fig. 2.10a.

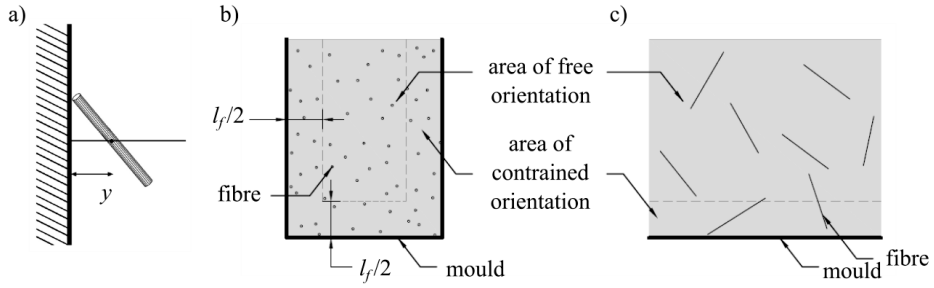

Fig. 2.10. a) Wall effect for a fibre of length l_f at a distance of the wall $y < l_f/2$ (Martinie and Roussel, 2011). Areas of free and constrained orientation caused by the wall effect: b) in a cross-section of a cast beam, and c) along its length.

The wall effect depends mainly on the geometry of the element to be cast and on the fibre length. Although it does not depend on the flow or the casting process, the wall effect can affect the flow-induced rotation of the fibres described earlier. This leads to the areas of possible free rotation and constrained rotation depicted in Fig. 2.10b and c in the case of a beam.

Boulekbache et al. (2010) argued that flow-induced orientation can be stronger at higher flow velocity or when shear rates can affect the fibre for a long time. This is related to the distance that the concrete travels to fill the formwork, usually referred to as the flow length or the flow distance (Ferrara et al., 2011, Martinie and Roussel, 2011, Vandewalle et al., 2008). It is also related to the rheological behaviour of the material, and in particular to its plastic viscosity. This property is connected with the velocity at which a given concrete will flow once the material begins to flow.

The yield stress, which is the minimum stress to be overcome for flow to occur, is recognized as one of the main rheological properties governing fibre orientation (Ozyurt et al., 2007, Boulekbache et al., 2010, Martinie et al., 2010). In the highly sheared areas close to the formwork, the flow-induced effects contribute to orient the fibres. With increasing distance from the wall, the shear stress may decrease until reaching the yield stress value. This delimits the area defined as the plug-flow area, where deformations do not occur and the material is just transported. In consequence, a fibre inside the plug-

flow area maintains its orientation unchanged (Martinie and Roussel, 2010). The low yield stress values of SCC mean that most of the material will be affected by flow-induced orientation, which explains why a higher degree of anisotropic orientation is generally observed for SCC than for ordinary concrete (Fig. 2.11).

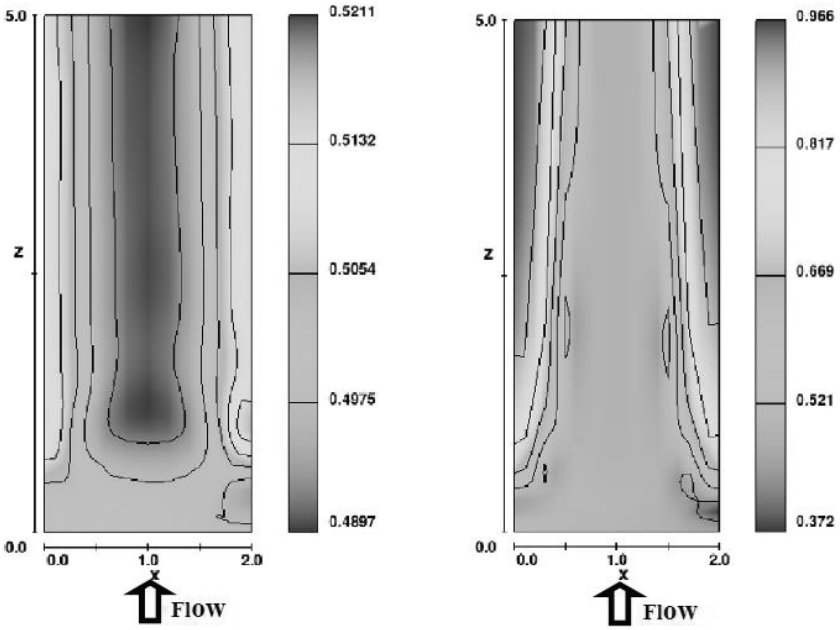

Fig. 2.11. Orientation factor relative to the flow direction calculated from a system with two individual fibres immersed in an ordinary concrete with a yield stress of 800 Pa (left), and an SCC with yield stress of 50 Pa (right) (Martinie and Roussel, 2010).

2.4.2 Characterization of fibre orientation: data acquisition methods

Several techniques have been developed for characterizing the fibre orientation in hardened concrete. These techniques are usually grouped into destructive or non-destructive, and into direct or indirect methods, based on the measuring principles. An overview of the methods is presented in Table 2.1.

In Section 2.3.2, reference was already made to some of the methods in Table 2.1, which means that the data obtained from most of them is well correlated with both fibre orientation and fibre content. Correlations based on indirect measurements, such as impedance or magnetic permeability, are only feasible for conductive fibres (Žirgulis, 2015).

Table 2.1. Data acquisition techniques for fibre orientation (Žirgulis, 2015, Blanco, 2013).

Method / Measurement		Technique	References
Destructive	Indirect	Manual counting	(Soroushian and Lee, 1990, Gettu et al., 2005, Dupont and Vandewalle, 2005)
		Mechanical testing	(Kooiman, 2000, Pujadas et al., 2014c, Grünewald, 2004)
	Direct	Image analysis	(Grünewald, 2004, Wuest et al., 2009)
		X-ray imaging (Fig. 2.12a)	(Robins et al., 2003, Vandewalle et al., 2008, Ferrara and Meda, 2006)
		X-ray Computed Tomography (Fig. 2.12b)	(Stähli et al., 2008, Şanal and Özyurt Zihnioğlu, 2013, Suuronen et al., 2013)
Non-destructive	Indirect	Alternate current impedance spectroscopy	(Ferrara et al., 2008, Woo et al., 2005, Ozyurt et al., 2006a)
		Magnetic induction	(Ferrara et al., 2012c, Faifer et al., 2010, Torrents et al., 2012)
		Microwave imaging	(Roqueta et al., 2011, Van Damme et al., 2004, Torrents et al., 2009)

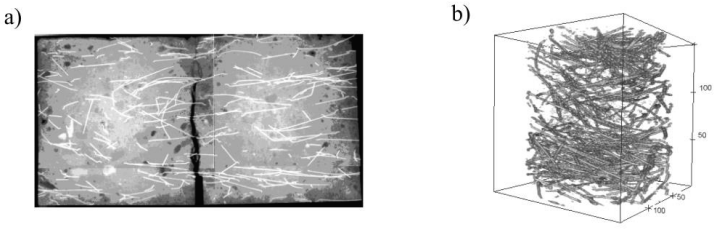

Fig. 2.12. a) X-ray image of self-compacting FRC with 0.38% vol. of 60 mm steel fibres (Vandewalle et al., 2008). b) CT visualization of self-compacting FRC with 0.5% vol. of 60 mm steel fibres.

Fibre orientation has also been studied using a viscous transparent fluid instead of self-compacting concrete matrix (Boulekbache et al., 2010, Švec et al., 2012a, Zhou and Uchida, 2013). The main advantage of this method is that the evolution of the fibre distribution and orientation can be observed during the "casting" process (Fig. 2.13).

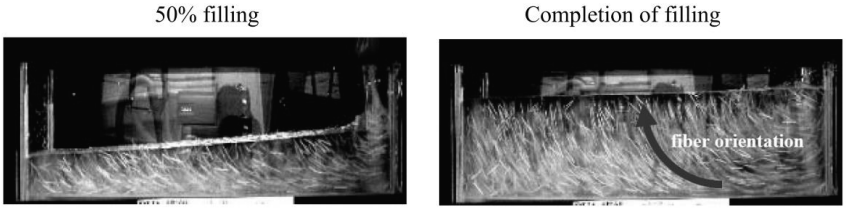

Fig. 2.13. Filling process of 0.5% vol. polyvinyl alcohol fibres immersed in a transparent fluid (Zhou and Uchida, 2013).

2.4.3 Characterization of fibre orientation: orientation factor and other formulations

Several parameters have been proposed in the literature to express fibre orientation quantitatively. Some of the most commonly used parameters are described here.

Fibre orientation factor (α)

A number of early studies found in the literature were carried out to evaluate the average spacing or the number of fibres in a plane considering orientation effects (Krenchel, 1975, Romualdi and Mandel, 1964, Aveston and Kelly, 1973, Soroushian and Lee, 1990). The orientation factor α, as formulated in these studies, has become a widely used parameter to evaluate the main orientation of fibres crossing a given plane. This orientation factor is defined as:

$$\alpha = n_f A_f / v_f \tag{2.1}$$

in which n_f refers to the number of fibres per surface unit, v_f to the fibre volume fraction, and A_f to the fibre cross-section area. The orientation factor ranges from 0 to 1, with its limits describing the situations where fibres align either parallel or perpendicular to the given plane.

Its value is commonly computed by determining n_f using any fibre counting method. Under the condition of a perfectly uniform distribution of fibres in a specimen, it is possible to state that the larger the proportion of fibres counted in a plane, the greater is the perpendicular alignment of the fibres in respect to this plane.

Fibre in-plane angle (ϕ) and fibre out-of-plane angle (θ)

These parameters represent the Eulerian angles that describe fibre orientation with respect to a given plane (Fig. 2.14a). The out-of-plane angle is the angle that the fibre forms with the direction perpendicular to that plane. A common way of expressing this

angle is by its cosine (cosθ), which can be physically interpreted as the projection of the fibre in the direction perpendicular to the plane.

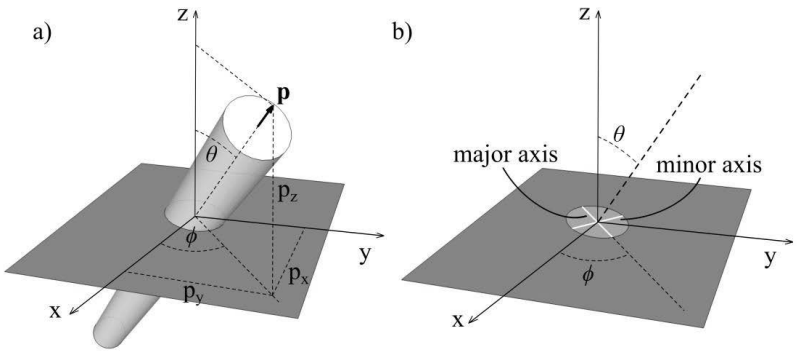

Fig. 2.14. a) Spatial description of a fibre with respect to the plane of interest. b) Elliptical intersection between the fibre and the plane.

The orientation number η_θ, defined as the average out-of-plane angle in Eq. 2.2, is often used to characterize the orientation of fibres over a cross-section of a hardened element (Schönlin, 1988, Laranjeira de Oliveira, 2010, Deeb et al., 2014, Wille et al., 2014, Grünewald et al., 2012, Žirgulis et al., 2015c). In Eq. 2.2, N_f is the number of fibres in the cross-section.

$$\eta_\theta = \frac{1}{N_f} \sum_{i=1}^{N_f} \cos\theta_i \tag{2.2}$$

The out-of-plane angle of every fibre can be directly evaluated if the fibre direction is known, i.e. the components p_x, p_y and p_z in Fig. 2.14a. Usually, the cosθ of a fibre with circular cross-section is estimated as the ratio between the major and the minor axes of the elliptical intersection between the fibre and the plane of interest (Fig. 2.14b). One limitation of this approach is that the elliptical intersection does not allow differentiation between two fibres oriented at (ϕ, θ) and at (ϕ+π, θ) because their cross-sections are identical (Bay and Tucker, 1992). Image analysis of polished cross-sections is an efficient method to compute the out-of-plane angles of all the fibres in the cross-section (Fig. 2.15).

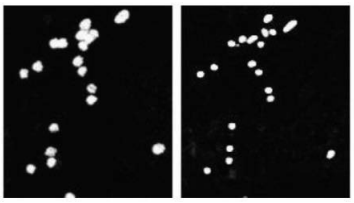

Fig. 2.15. Image analysis of a sawn section before (left) and after polishing (right) for characterizing the elliptical intersections of the fibres with the cross-section (Žirgulis, 2015).

The limits of the orientation number η_θ coincide in range and meaning with those of the orientation factor α, i.e. $\eta_\theta = 0$ refers to fibre orientation parallel to the cross-section, and $\eta_\theta = 1$ refers to fibre orientation perpendicular to the cross-section; however, the results of α and $\cos\theta$ are in general not comparable (Žirgulis et al., 2015c).

The fibre orientation over the cross-section can also be described by a distribution function expressing the relative number of fibres that are orientated with a certain out-of-plane angle (Laranjeira de Oliveira, 2010, Grünewald et al., 2012, Žirgulis et al., 2015c, Kang et al., 2011). These functions require a more complex analysis, but they allow the average orientation and the distribution of orientations over the cross-section to be characterized.

*Second-order orientation tensor (**A**)*

The orientation of a group of fibres can be described using a second-order orientation tensor (Švec et al., 2014, Advani and Tucker, 1987, Ferrara et al., 2011, Şanal and Özyurt Zihnioğlu, 2013, Ozyurt et al., 2006b), defined as:

$$\mathbf{A} = \frac{\sum_n F_n \mathbf{p}_n \mathbf{p}_n^{\mathrm{T}}}{\sum_n F_n} \tag{2.3}$$

In Eq. 2.3, **A** stands for the orientation tensor. The vector $\mathbf{p}_n$ is the unit vector in the direction of the fibre n (Fig. 2.14a), which may be either known or computed from the in-plane (ϕ) and out-of-plane (θ) angles in accordance with:

$$p_x = \sin\theta \cos\phi, \quad p_y = \sin\theta \sin\phi, \quad p_z = \cos\theta \tag{2.4}$$

If the orientation tensor is assessed from the angles ϕ and θ obtained in the analysis of a cross-section, a weighting function F_n should be considered to take into account the effect of fibre orientation on the probability of a fibre being intercepted by the cross-section under consideration, see e.g. Ozyurt et al. (2006b). If the vectors $\mathbf{p}_n$ are known, the fibre length should replace the function F_n (Švec et al., 2014).

By definition, the orientation tensor has the properties of being symmetric and having normalized components. Symmetric second-order tensors can be visualized using 3D

ellipsoids, where the eigenvectors and eigenvalues give the direction and half-length of the principal axes of the ellipsoids. In this way, ellipsoids are used as a visual tool to identify the dominant direction of the group of fibres (Fig. 2.16).

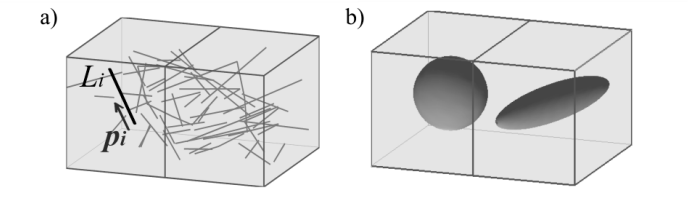

Fig. 2.16. a) Group of fibres oriented in two volumes. b) Ellipsoids represent the orientation tensors of the fibres in each volume. The leftmost ellipsoid (a sphere) characterizes an isotropic orientation, while the rightmost ellipsoid depicts a preferred fibre orientation.

2.4.4 Numerical prediction

The investigation of fibre orientation has been carried out mostly from an experimental perspective. However, the development of tools to predict fibre orientation based on the geometry of the element to be cast, the rheological behaviour of the material, and the casting method, provides the opportunity to integrate this latter aspect into the design of FRC elements. By anticipating the orientation of fibres with the direction of principal tensile stresses for the element when in service, a step towards a more efficient design of FRC can be achieved (Laranjeira et al., 2012).

Reviews of methods for the computational modelling of concrete flow and its applications were presented by Roussel et al. (2007) and Gram and Silfwerbrand (2011). These methods have been extensively used for modelling the flow of SCC to investigate formwork filling effects, for instance blocking or migration of aggregates (Spangenberg et al., 2012b). Recently, some of these methods have been applied to model SCC flow with fibre suspensions. Some examples are the computational fluid dynamics simulations using the lattice Boltzmann technique presented by Švec et al. (Švec et al., 2012b, Švec and Skoček, 2013) (Fig. 2.17), or the flow simulations used by Deeb et al. (2014) based on Lagrangian smooth particle hydrodynamics. Some authors have investigated the use of distinct element methods, which are based on the interaction between two neighbouring particles, for simulating fresh FRC by modelling fibres as clusters of solid spheres (Mechtcherine and Shyshko, 2007, Ferrara et al., 2012d).

Martinie and Roussel (2010) applied the classical Jeffery orbits (Jeffery, 1922), which describe the rotation of ellipsoids immersed in an incompressible fluid, to investigate

the evolution of the orientation of a group of fibres induced by the flow. The aim of this study was to investigate the effect of matrix rheology, as previously seen in Fig. 2.11.

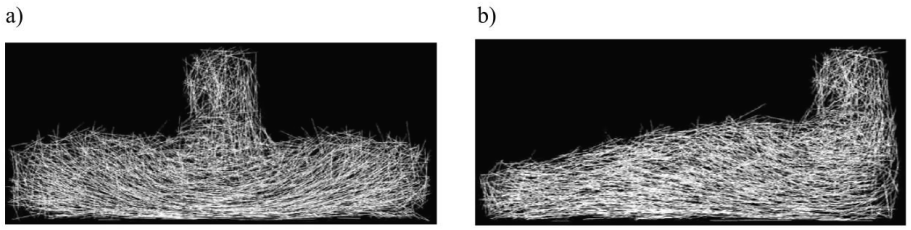

Fig. 2.17. Numerical simulation of beam casting with self-compacting FRC. Side view of two different casting methods: a) casting from centre, and b) casting from one side (Švec, 2013).

The same authors (Martinie and Roussel, 2011) also presented a semi-empirical equation allowing for the prediction of the fibre orientation factor over a cross-section perpendicular to the casting flow. A comprehensive approach was proposed by Laranjeira et al. (2012) to predict the fibre orientation in practical applications by means of a step-wise calculation of the fibre orientation factor that takes into account fresh-concrete properties, casting methods, dynamic effects that take place during casting, and the wall effect induced by the formwork.

2.5 Hardened concrete performance of flowable FRC

Fibres in cementitious materials usually have a positive influence on the mechanical properties of the material in its hardened state. This influence depends on various factors such as the geometry of the fibres, the strength of the filament, the strength of the matrix, the fibre-matrix bond, the fibre content, the fibre distribution, and the fibre orientation with respect to the applied stress.

Up to the point of cracking, stresses are carried by both the matrix and the fibres. Once cracking initiates and propagates in the matrix, fibres transfer the stresses through the cracks until the fibre-matrix interaction is exhausted due any of the following mechanisms: fibre rupture, fibre pull-out, or concrete failure (Sandbakk, 2011). Thus, although fibres make a contribution under all types of loading, some FRC properties do not differ widely from those of plain concrete, e.g. compressive strength, while others, such as the post-cracking tensile behaviour, are governed by the presence of fibres.

2.5.1 Effect of fibres on hardened state behaviour

Generally, fibres have negligible influence on compressive strength, but they may substantially increase post-peak behaviour in compression (Fanella and Naaman, 1985). This is mainly because fibres provide a small level of internal confinement during failure as internal cracks are held together.

Fibres improve the tensile and flexural behaviour of concrete due to their crack-bridging effect by changing the failure mode from brittle to ductile. For many practical applications, first-crack strength is not increased and the enhancement from fibres mainly affects the post-cracking response. Tensile and flexural toughness, which are measures of the ductility of the material and its ability to absorb energy, are recognised as the foremost enhanced properties.

Fibres generally increase shear strength. According to ACI Committee 544 (2002), fibres have several potential advantages when used to replace vertical stirrups in beams: (i) random fibre distribution throughout the material can lead to distributed cracking and reduced crack widths; (ii) shear-friction strength can be increased by fibres bridging the cracks; and (iii) the residual tensile strength of the material is increased.

One of the greatest enhancements from the use of fibres is cracking control. Fibres can prevent the occurrence of large crack widths, which makes a substantial significance in durability and structural safety. Incorporating fibres is generally recognised as effective in controlling and mitigating shrinkage cracking. Fibres can reduce early-age cracking by increasing early-age tensile strength, and they can allow multiple cracking to occur, transfer tensile stresses across the cracks, and reduce their progressive opening.

Several studies have set out to investigate the contribution of fibres to long-term behaviour under sustained load, although according to Buratti and Mazzotti (2012a) this behaviour has not yet been fully understood. Fibres can be expected to have only a small effect on concrete creep because creep does not generally involve cracking (Mangat and Motamedi Azari, 1985). However, several investigations of post-cracking creep behaviour (see e.g. Buratti and Mazzotti, 2012b, Kanstad and Žirgulis, 2012, Blanco, 2013) point out the importance of creep deformations affecting the bond between fibres and concrete, time-dependent bond failure, or creep deformations in the fibre material. A new RILEM Technical Committee (261-CCF) has recently started activity to coordinate studies on the creep response of cracked FRC, and to unify test methods to quantify creep in FRC.

Improvements from the inclusion of fibres have furthermore been reported for other mechanical properties such as torsion, fatigue, impact resistance, and abrasion and erosion resistance (see e.g. Bentur and Mindess, 2006, ACI Committee 544, 2002).

2.5.2 Characterization of post-cracking behaviour

Characterization of the mechanical properties of FRC is of major importance for the effective and economical structural design of elements using this material. This section deals with the characterization of its tensile or flexural behaviour.

Strength and toughness are the parameters best suited for establishing design criteria for FRC. Most recent guidelines (e.g. *fib*, 2010, DAfStb, 2012, SFRC Consortium, 2014, Swedish Standards Institute, 2014) use measurements of post-cracking residual strength to characterize material performance. This recognizes that using FRC generally has little influence on the tensile strength at the cracking event, but offers a measure of the post-cracking effect of the fibre reinforcement which is useful for design and analysis for the use of FRC.

Several standard test methods have been proposed to determine the tensile behaviour of FRC (RILEM, 2001, RILEM, 2002b, European Standard, 2005, ASTM International, 2012b, ASTM International, 2010, DAfStb, 2012, ASTM International, 2012a). These methods are generally based on either direct assessment, i.e. uniaxial tension tests, or indirect approaches, like bending tests of beams and panels. More recently, other indirect tension tests have also been proposed, including the Brazilian splitting test (Carmona and Aguado, 2012, Ozyurt et al., 2007), the wedge splitting test (Löfgren et al., 2008, Meda and Plizzari, 2001), the double-edge wedge splitting test (Di Prisco et al., 2013b, Ferrara et al., 2012b), and the multidirectional double punch test (Pujadas et al., 2014c). Some of these tests were developed to evaluate the behaviour of FRC on test specimens from existing structures. This is especially relevant with flowable FRC, because it makes it possible to characterize the behaviour of the material in specimens where flow-induced fibre orientation occurred in a relevant part of the structure.

Various difficulties in performing direct tension tests, such as labour costs, dedicated equipment, and laborious specimen manufacturing, hinder the use of these test methods. From a design-oriented perspective, the most widely used test methods for assessing post-cracking behaviour are bending tests on beam specimens (RILEM, 2002b, European Standard, 2005, DAfStb, 2012, ASTM International, 2012b, ASTM International, 2010). Among the different standards and proposals, differences can be found in the size of specimens, the presence or absence of a notch, and the configuration in three-point or four-point bending.

As an alternative to these methods, several investigations have aimed at predicting the mechanical response of FRCs from the pull-out behaviour of individual fibres and information on fibre distribution (Armelin and Banthia, 1997, Jones et al., 2008, Sandbakk, 2011, Laranjeira de Oliveira, 2010, Cunha et al., 2011).

2.5.3 Effect of fibre distribution and orientation on post-cracking behaviour

The ability of fibres to transfer tensile forces depends on their distribution and orientation relative to the crack plane. If the amount or direction of fibres varies, then the ability to transfer tensile forces varies too.

As already mentioned, a non-uniform fibre distribution may lead to areas with a reduced fibre dosage that have an impact on structural behaviour. An interesting investigation on the impact of fibre distribution on structural behaviour was presented by Ozyurt et al. (2007). In this study, the fibre segregation in ordinary and self-compacting mixes was investigated in cylinders with dimensions Ø150 mm × 300 mm. A close correlation was found between the fibre content and the splitting tensile strength determined for 75 mm thick disks sawn along the height of the cylinders (Fig. 2.18).

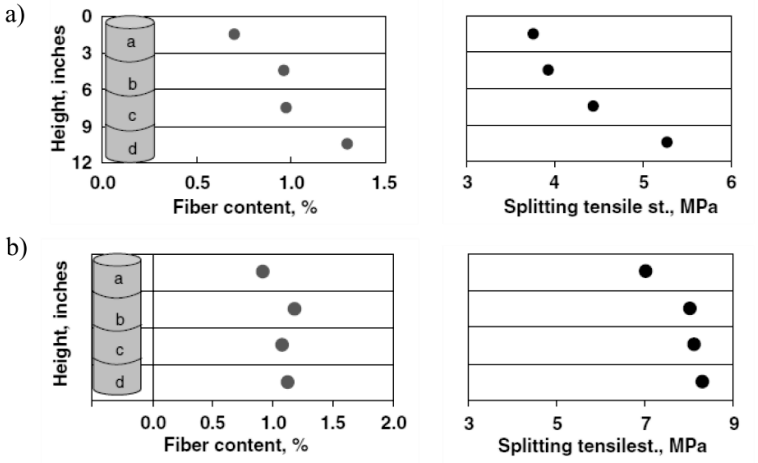

Fig. 2.18. Variation in fibre content and splitting tensile strength along the height of cylinders cast from a) ordinary FRC, and b) self-compacting FRC, both containing 1% vol. of 40 mm steel fibres (Ozyurt et al., 2007).

According to Ferrara et al. (2012a), the casting method and the maximum distance that the fluid has to travel from the casting point should be explicitly considered when deciding acceptable levels of spatial variation in material properties. This would avoid undesired effects on structural performance due to the lack of homogeneity within structural elements.

Numerous investigations have reported the strong effects of fibre orientation on the mechanical properties of FRC in the hardened state (e.g. Soroushian and Lee, 1990, Kooiman, 2000, Markovic, 2006, Stähli and van Mier, 2007), which emphasizes the

importance of taking fibre orientation into account in relation to the intended application of the material.

Fibres can be effectively aligned in the flow direction of the element in question (Ozyurt et al., 2007, Stähli and van Mier, 2007, Stähli et al., 2008, Ferrara et al., 2008, Ferrara et al., 2011, Boulekbache et al., 2010, Barnett et al., 2010) as a result of the mechanisms described in Section 2.4.1. Whenever the fibre orientation pattern aligns with the principal tensile stress field in the structural element under service loads, a beneficial effect of the fibre orientation on structural performance is to be expected (Ferrara et al., 2011, Barnett et al., 2010, Boulekbache et al., 2010).

Sections 2.3 and 2.4 discussed how fibre distribution and orientation are the results of the fresh-state behaviour of the material; in fact, they are the key properties of flowable FRC, and the link between its fresh and hardened state performance (Ferrara et al., 2012a). For this reason, a thorough understanding of the mechanisms underlying the connection between the fresh-state material, fibre distribution and fibre orientation is needed to accurately predict the mechanical behaviour of the hardened material.

2.5.4 Fibre orientation correction factors

For design purposes, the effects of fibre distribution and orientation described above need to be carefully considered when the identification of the tensile behaviour of flowable or self-compacting FRC is experimentally addressed using test specimens. Fibre distribution and orientation should also be considered for the intended application of the structure cast from this material. Although a certain degree of standardization has been achieved in the test methods for characterizing FRC, at the present time it is still not clear how these aspects should be addressed.

Several approaches can be found in the design recommendations for FRC, usually based on correcting the basic residual tensile strength parameters to take fibre orientation into account.

The approach to the identification of the constitutive behaviour of ordinary FRC is based on the assumption of a random orientation of fibres. For instance, the German guidelines for steel FRC (DAfStb, 2012), which are devised for ordinary FRC, still propose a correction factor of 0.5, except for slabs, floors and beams with tensile stresses in their lengthwise direction, for which the factor should be set equal to 1. Other guidelines, such as the Swedish Standard (Swedish Standards Institute, 2014), which is also valid for flowable FRC, recommend considering element dimensions, fibre length and casting procedure to determine a correction factor between the same limits, i.e. 0.5 and 1. A two-step correction is proposed by the Danish design guidelines (SFRC

Consortium, 2014) and the proposal for Norwegian guidelines (Kanstad et al., 2011). First, residual strength values from test specimens must be converted to strength values for the reference fibre orientation; second, the reference strength must be corrected for the actual structural application.

The correction factors for the guidelines mentioned here are generally formulated to take into account the effect of orientation; only the Norwegian guideline is devised to incorporate variations in fibre content in relation to the fibre distribution.

The design approach proposed in the recently issued Model Code 2010 (*fib*, 2010) also provides a correction factor (K) to be applied to the design values:

$$f_{Ftsd,mod}=f_{Ftsd}/K \tag{2.5}$$

$$f_{Ftud,mod}=f_{Ftud}/K \tag{2.6}$$

where f_{Ftsd} and f_{Ftud} are two reference residual tensile strength values, and $f_{Ftsd,mod}$ and $f_{Ftud,mod}$ are their corresponding corrected values. In the general case, an isotropic fibre distribution is assumed, for which $K = 1$ should be adopted. If the behaviour in the standard tests deviates substantially from the behaviour in the structural element, K must be verified experimentally to take account of a possible favourable ($K < 1$) or unfavourable ($K > 1$) structural effect.

These correction factors aim at taking into account the representativeness of the specimen used for the identification of the tensile behaviour of the structure. It is argued by several authors (Di Prisco et al., 2009, Di Prisco et al., 2013a) that the representativeness of a standard notched beam is questionable for certain applications. To reproduce as close as possible the orientation of the fibres with respect to the applied tensile stress in the structural application, these authors propose the use of specimens extracted from larger elements or cast by reproducing the full-scale casting method.

2.5.5 Structural modelling

Various methodologies can be found in the literature for analysing the structural performance of FRC elements. For both research and practical design purposes, sectional analyses are used to determine the structural response of a critical part of a structure, for which the assumptions for conventional reinforced concrete are usually adopted. Sectional analyses can be carried out using the so-called multi-layer method, see e.g. Hordijk (1991). This modelling method assumes that the structural element is divided into two parts connected by springs, each spring representing the behaviour of a layer of the fracture zone. This modelling procedure has been extensively used to simulate the flexural response of FRC beams (Kooiman, 2000, Grünewald, 2004,

Døssland, 2008, Blanco, 2013). Sectional analyses can also be carried out modelling the fracture area as a non-linear hinge at the point where the main non-linear behaviour due to cracking is concentrated (RILEM, 2002a, Pedersen, 1996, Olesen, 2001, Casanova and Rossi, 1996).

For research and development purposes, the analysis of the global structural behaviour of FRC elements is usually addressed with nonlinear finite element methods, for which either the discrete crack approach or the smeared crack concept are typically adopted. Some investigations (Døssland, 2008, de Montaignac et al., 2012, Löfgren et al., 2008) compare the results using sectional analysis with those using finite element analysis.

The common practice for modelling FRC elements is to consider the material as a continuum, based on the tensile behaviour identified using the characterization tests described in Section 2.5.2. This means that the heterogeneity of the tested material is only implicitly taken into account.

A number of approaches have been developed to take the fibre structure explicitly into account. Modelling every individual fibre in a specimen is probably the most direct way of representing the influence of the fibre orientation and distribution on the mechanical properties. Some examples of such models are the embedded fibre model proposed by Cunha et al. (Cunha et al., 2012, Cunha et al., 2011), the approach based on the partition of unit method of Radtke (2012), and the micromorphic model of Oliver, Huespe et al. (Oliver et al., 2012, Huespe et al., 2013). Rigid particle models or lattice models have also been used to model FRC elements (Bolander et al., 2008, Li et al., 2006).

For practical design purposes, the structural analysis is usually based on either elastic, or yield line theory.

Chapter 3

Materials and methods used in the present investigation

3.1 Mixes

The main experimental research presented in this thesis concerned two flowable FRC mixes: a hybrid FRC with 1% vol. of polymer and steel fibres, and an FRC with 2% vol. of steel fibres. The design and optimization of these mixes was not a part of this thesis. They were developed during a research project included in COIN's focus area 2, whose main goal was to develop robust and highly flowable FRC mixes with high tensile strength and ductility. The activity of this project was initiated by Vikan et al. (2011) and Sandbakk (2011), and included mixes in three strength classes:

- Ductile low tensile strength concretes with compressive strength in the range 25-30 MPa.
- Ductile medium tensile strength concretes with compressive strength in the range 45-50 MPa.
- Ductile high tensile strength concretes with compressive strength in the range 70-75 MPa.

The hybrid FRC with 1% fibres is a low tensile strength concrete with high ductility, conceived for use in combination with traditional reinforcement. In contrast, the steel FRC with 2% fibres is a ductile high tensile strength concrete, developed to investigate its capacity for use without traditional reinforcement. Both mixes seemed to have a potential for application in load-carrying structures. For this reason, they were investigated under full-scale conditions within the scope of this thesis.

3.1.1 1% Hybrid polymer-steel FRC

The mix proportioning of the flowable hybrid FRC was developed during research work by Vikan et al. (2011) considering ordinary strength concrete. This mix contains 1% vol. fibre dosage, with equal volumes of polymer and steel fibres. The main properties of the fibres are listed in Table 3.1. The mix design, given in Table 3.2, was optimized in accordance with the particle-matrix model (Mørtsell, 1996) to achieve a satisfactory level of stability and flowability.

Table 3.1. Properties of polymer and steel fibres.

Properties	Polymer fibres	Steel fibres
Material	Polyolefin (98% polypropylene)	Cold drawn steel wire
Specific gravity [-]	0.90 – 0.92	7.85
Length, l_f [mm]	48	60
Equivalent diameter, d_f [mm]	0.90 – 0.91	0.90
Aspect ratio, l_f/d_f	53	67
Tensile strength [N/mm^2]	550	1160
Elastic modulus [N/mm^2]	10000	210000
Configuration	Continuously embossed surface	Smooth surface, hooked-ends

Table 3.2. Mix design for hybrid polymer-steel FRC.

Component	Dosage
Cement [kg/m^3]	286.8
Limestone [kg/m^3]	71.7
Total free water [kg/m^3]	226.6
Aggregate 0-2 mm [kg/m^3]	250.5
Aggregate 0-8 mm [kg/m^3]	1419.8
Super-plasticizer [kg/m^3]	2.4-3.7
Stabilizer [kg/m^3]	4.0
Polymer fibres [kg/m^3, (% vol.)]	4.6, (0.5)
Steel fibres [kg/m^3, (% vol.)]	39.0, (0.5)
w/b ratio [-]	0.79
Matrix volume (< 0.125 mm) [l/m^3]	393

The main characteristics of the mix proportioning were the limitation of the maximum aggregate size to 8 mm and the replacement of 20% vol. of cement by limestone powder. The main properties of the fresh and hardened state performance were:

- Slump-flow in the range 550-650 mm.
- Adequate stability based on visual examination.

- Residual flexural tensile strengths f_{R1} and f_{R3} (*fib*, 2010) of approximately 3.5 MPa and 4.0 MPa, respectively.
- Compressive strength in the range 25-30 MPa.

As mentioned above, the full-scale application of this mix was conceived as in combination with traditional reinforcement.

3.1.2 2% Steel FRC

The mix proportioning of the flowable FRC with high steel fibre content was developed during research work by Kjellmark et al. (2014) on the optimization of flowable FRC mixes with high tensile strength and ductility. This mix contains 2% vol. of steel fibres with the properties listed in Table 3.1. The mix design, given in Table 3.3, was developed using the EMMA concrete mix particle packing program developed by Elkem AS[4], which is based on optimization of the particle packing density. The mix has reasonably good casting properties, with adequate flowability and compactability.

Table 3.3. Mix design for steel FRC with 2% vol. fibres.

Component	Dosage
Cement [kg/m^3]	492.2
Silica fume [kg/m^3]	24.6
Total free water [kg/m^3]	197.5
Aggregate 0-8 mm [kg/m^3]	1594
Super-plasticizer [kg/m^3]	7.4-9.8
Stabilizer [kg/m^3]	0.5
Steel fibres [kg/m^3, (% vol.)]	156, (2)
w/b ratio [-]	0.35
Matrix volume (< 0.125 mm) [l/m^3]	400

The main characteristics of the mix proportioning were the limitation of the maximum aggregate size to 8 mm and the high content of cement. The main properties of the fresh and hardened state performance were:

- Slump-flow in the range 500-600 mm.
- Adequate stability based on visual examination.
- Residual flexural tensile strengths f_{R1} and f_{R3} of approximately 15.4 MPa and 18.8 MPa, respectively.
- Compressive strength in the range 80-90 MPa.

[4] www.elkem.com

In view of the high performance of this mix attained during the mix development process, the full-scale application of this mix was planned to be without or with only a small amount of traditional reinforcement.

3.2 Experimental methods

3.2.1 Fresh concrete properties

Density and air content

Density and air content were tested in accordance with EN 12350-6 and EN 12350-7 (European Standard, 2009a, European Standard, 2009b), respectively.

The tests were performed using an air entrainment meter, which consists of a container of known volume and mass, and a pressure gauge fitted to a cover assembly. The principle of the air entrainment meter is based on Boyle's law, which states that the volume occupied by air is proportional to the applied pressure. At the end of the test, the pressure gauge indicates the apparent percentage of air.

The container was filled with the fresh concrete in one operation; no mechanical or hand compaction was applied. The container was then weighed to obtain the density. Subsequently, the cover assembly was clamped in place ensuring a good seal, and the procedure described in EN 12350-7 was followed to obtain the air content.

Slump-flow test

Flowing ability in the absence of obstructions was tested in accordance with the slump-flow test described in EN 12350-8 (European Standard, 2010a) and C1611 (ASTM International, 2014). The test was used to determine: the slump-flow, which is an indication of flowability; the t500 time, which is a measure of speed of flow; and the Visual Stability Index (VSI), which characterizes ability to resist segregation.

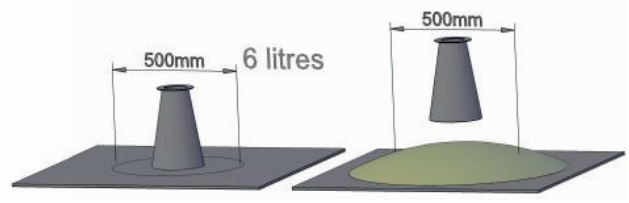

Fig. 3.1. Slump-flow test.

The test was performed using a standard cone and a baseplate with scribed circles of 210 mm and 500 mm. The cone was centrally placed within the 210 mm circle on the

baseplate and filled in one operation. The cone was removed from the concrete by a steady upward lift (Fig. 3.1). The t500 time was recorded as the time in seconds taken for the concrete to reach the 500 mm circle. After the concrete flow had stopped, the diameter of the largest circular spread of concrete was measured. A second diameter was measured at an angle approximately perpendicular to the first diameter. The slump-flow was obtained as the average of the two measurements.

The concrete spread was visually inspected by observing the distribution of fibres and coarse aggregates. The VSI was assigned using the range 0-3, where 0 stands for highly stable concrete and 3 stands for highly unstable concrete (ASTM International, 2014).

LCPC box test

Another way to characterize the filling ability of flowable concrete is the LCPC-box test presented by Roussel (2007). In contrast to the slump-flow test, this test reproduces the unidirectional flow of concrete.

The test was performed using a channel of fixed dimensions, the LCPC-box (Fig. 3.2). A concrete sample of 6 litres was poured slowly into one end of the box using a plastic bucket. The emptying of the bucket took about 30 s. After the concrete flow had stopped, the longitudinal spread and the thickness of the concrete at the "casting" end of the box were measured. The analytical expressions in Roussel (2007) can be used to assess the yield stress value with the parameters measured in this test.

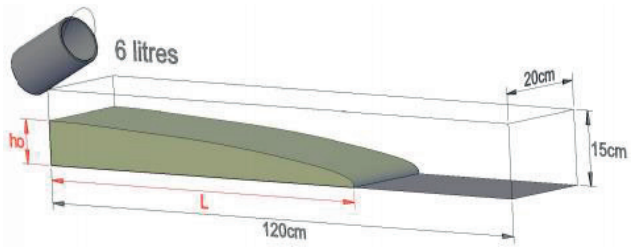

Fig. 3.2. LCPC-box test.

3.2.2 Flexural and tensile properties

Three-point bending test

Three-point bending tests were performed to determine the load-deflection response of FRC test beams. The standard test EN 14651 (European Standard, 2005) was adopted as the reference test. This test enables the determination of the limit of proportionality ($f^{f}_{ct,L}$) and the typical values of residual flexural tensile strength f_{R1}, f_{R2}, f_{R3} and f_{R4} which correspond to crack mouth opening displacements (CMODs) of 0.5 mm, 1.5 mm, 2.5 mm and 3.5 mm, respectively.

The test specimens consisted of notched prisms with dimensions of 150 mm × 150 mm × 550 mm or 150 mm × 150 mm × 600 mm (Fig. 3.3). Two types of specimens were investigated:

- Standard beams
  Three specimens were cast for each batch considered in this thesis using the layered casting method described in EN 14651. No mechanical or hand compaction was applied. These test specimens were rotated 90º around their longitudinal axis and notched through the width of the lowest edge at midspan. The testing direction was then perpendicular to the casting direction.
- Sawn beams
  These specimens were sawn from full-scale elements and notched through the width of the lowest edge of their position within the existing element.

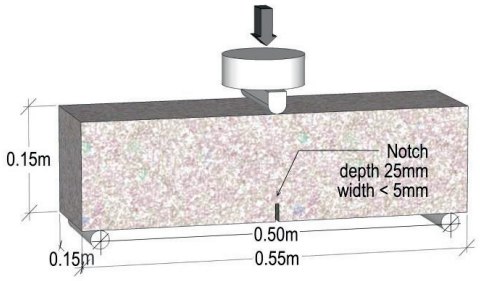

Fig. 3.3. Dimensions of specimens for three-point bending testing.

The test setup and testing procedure were in accordance with EN 14651 (Fig. 3.4). Two displacement transducers, one on each side, measured the deflection at midspan. The load was applied at a constant rate of deflection of 2 mm/min. This is a slight deviation from the standard procedure, which specifies a lower loading rate during the initial phase of the test.

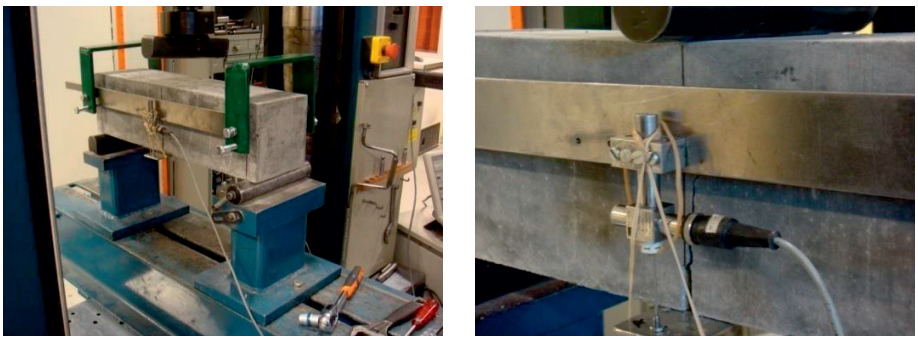

Fig. 3.4. Setup for three-point bending testing.

Uniaxial tension test

Uniaxial tension tests were performed to characterize the uniaxial tensile response of FRC on test specimens. The test described in the RILEM recommendations (RILEM, 2001) was adopted as the reference test. This test enables the determination of the stress-crack opening relationship.

The test specimens consisted of notched cylinders with dimensions of Ø150 mm × 150 mm (Fig. 3.5). Two types of specimens were investigated:

- Cast cylinders
  Six cylinders were cast for each batch. Cylindrical moulds (Ø150 mm × 300 mm) were filled in one operation up to a height of approximately 250 mm. No mechanical or hand compaction was applied. The cylinders were sawn to a height of 160 mm removing parts at both top and bottom.
- Drilled cores
  Cores with dimensions of Ø150 mm × 160 mm were drilled from full-scale elements.

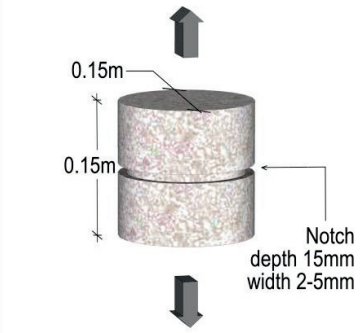

Fig. 3.5. Dimensions of specimens for uniaxial tension testing.

The sawn surfaces were ground to the final height (150 mm). The notches were sawn along the centreline to a depth of 15 mm. Grinding and notching were executed with care to ensure that the top and bottom surfaces and the notched sections were perpendicular to the axis of the cylinder. The specimens were glued “in situ” to metal plates, which were fixed to the testing machine with rigid bolted connections. They were tested after the glue had hardened for approximately 24 hours. Three extensometers measured the strain across the notch with a gauge length of 35 mm (Fig. 3.6).

The test was conducted with an electromechanical testing machine with a capacity of 100 kN (Instron 5982). The machine was not able to perform the test with closed-loop

control, so the test was controlled using the rate of extension of the upper crosshead of the machine. The following displacement rates were adopted: 50 μm/min up to an average displacement in the notch of 0.1 mm, and 100 μm/min until the completion of the test (displacement in the notch > 2 mm). The system was not able to avoid sudden opening at the onset of cracking. Nevertheless, the average displacement rates in the notch before and after the sudden crack were recorded as ~1 μm/min and ~100 μm/min, respectively, which are values within the limits recommended in RILEM (2001). Throughout the test, data was logged with a frequency of 0.5 Hz.

Fig. 3.6. Setup for uniaxial tension testing.

3.2.3 Characterization of fibre distribution and orientation

Fibre counting on sawn cross-sections

Fibre counting consists of quantifying the number of fibres crossing a certain plane. Usually, it requires sawing the element in question along the plane of interest. If the contrast between fibres and the other components is sufficient, images of the cross-section can be subjected to a thresholding operation using image analysis software. This identifies the fibres without the need for manual counting.

The fibre counting was performed over cross-sections of full-scale and standard beams cast with the hybrid polymer-steel FRC. There was poor contrast between the polymer fibres and other components, so the fibres were hand-dotted on a transparent paper and then counted. The red and black dots in Fig. 3.7 represent the polymer and steel fibres, respectively, recognized over the cross-section of a full-scale beam. The results were expressed in terms of the number of fibres per surface unit.

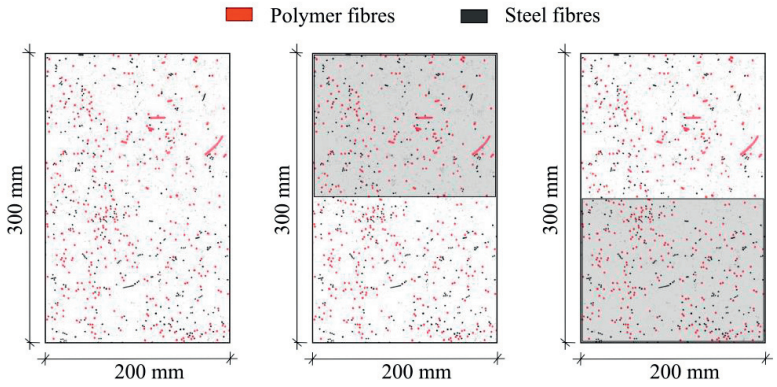

Fig. 3.7. Hand-dotting of fibres over the cross-section of a full-scale beam, and counting across the top and bottom halves.

Fibre volume fraction

The fibre volume fraction was determined for sawn slices of full-scale beams and standard beams cast with the hybrid polymer-steel FRC. A hardened slice was crushed in a compression test machine (Fig. 2.7) and the fibres were separated from the crushed matrix. The weight of the fibres and the volume of the tested sample were measured to determine the fibre volume fraction. Fig. 3.8 depicts one of the examined slices from a standard beam.

Fig. 3.8. Polymer and steel fibres contained in a slice of standard beam.

Analysis of a CT-scanned volume

X-ray Computed Tomography (CT) scanning is used as a method for qualitative and quantitative evaluation of the orientation and distribution of steel fibres in FRC. Scanning of an element produces a large number of radiographic projections, which are captured with the rotation of an X-ray source. Digital analysis enables reconstruction of the projections into a sequence of images, which can be post-processed to produce 3D visualizations of the structure of fibres in the element, as shown in Fig. 3.9.

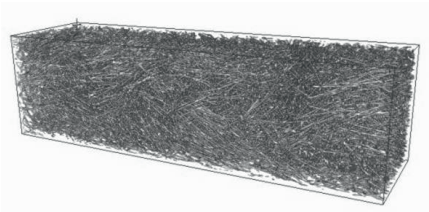

Fig. 3.9. 3D visualization of the fibre structure in a specimen obtained using CT scanning.

The CT scanning was performed using a Siemens Sensation 4 CT Scanner, which is presently available at NTNU for research purposes (Fig. 3.10). Scanning was performed producing an image of the sample every 1 mm, and using the maximum working voltage, which was limited to 120-140 kV.

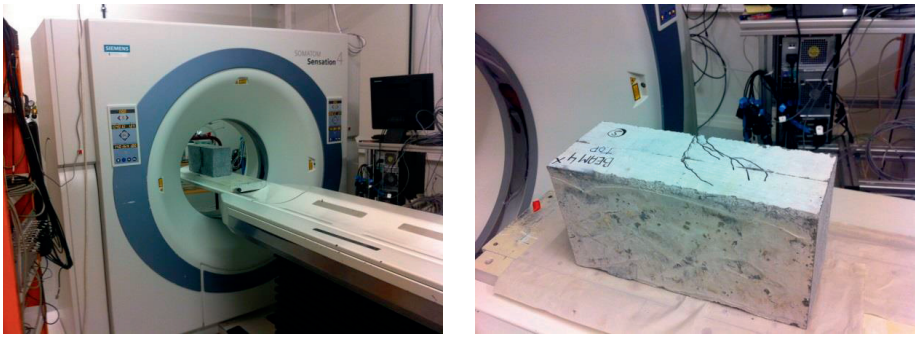

Fig. 3.10. An FRC element positioned for CT scanning.

The open-source software FIJI was used for image analysis of the CT scans. The scans consisted of a sequence of images of the scanned element. To separate the fibres, a thresholding operation was applied to the entire sequence. Post-processing the images to a "skeleton" converted fibres to 3D segments located in the volume. Fig. 3.11 illustrates the various steps of the analysis for a cross-section image of the element: (i) image reconstruction, (ii) thresholding of fibres, and (iii) conversion to skeleton.

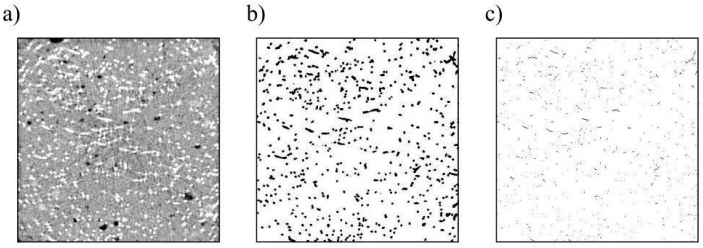

Fig. 3.11. A cross-section image produced using CT scanning: a) reconstruction of the image, b) thresholding of fibres, and c) conversion to skeleton.

The digital analysis of the skeleton produced a complete list of 3D coordinates of fibre ends, from which fibre lengths and vectors of the fibre orientation were computed. Given the complete description of the fibre structure in the element, it was possible to characterize the fibre volume fraction, the orientation factor (Eq. 2.1), the orientation number (Eq. 2.2), and the fibre orientation tensor (Eq. 2.3), with respect to any given plane or volume.

3.3 Analytical methods and modelling

3.3.1 Correction method for the residual tensile strength

Thorenfeldt (2003) proposed the simplified analytical model in Eq. 3.1 for determining residual tensile strength of FRC based on fibre volume, fibre orientations with respect to the crack plane and the average fibre stress representing all the fibres crossing the plane.

$$f_{t,res} = \eta_0 \, v_f \, \sigma_{fm} \tag{3.1}$$

In Eq. 3.1, η_0 denotes the capacity factor, v_f is the fibre volume fraction, and σ_{fm} represents the average stress in the fibres crossing the crack plane. The capacity factor η_0 indicates to what extent the fibre forces are effective, i.e. normal to the crack plane. This parameter can be related to the orientation factor α (Eq. 2.1) by means of the following expressions:

$$\eta_0 = 4/3 \; \alpha - 1/3 \qquad \text{when} \quad 0.5 < \alpha < 0.8 \tag{3.2}$$

$$\eta_0 = 2/3 \; \alpha \qquad \text{when} \quad 0.3 < \alpha < 0.5 \tag{3.3}$$

As a general method, the Norwegian guideline proposal (Kanstad et al., 2011) recommends three-point bending testing in accordance with EN 14651 (European Standard, 2005) to characterize the residual tensile strength of FRC. If α and v_f can be quantified, the residual tensile strength derived from the standard test can be normalized

using the factor $(v_f/v_{f,nom})(4\alpha\text{-}1)$, which is based on the analytical expressions in Eq. 3.1 and 3.2. Within the framework of the guideline, this factor can be applied to correct for the actual fibre orientation and fibre content in the structure, or to estimate the residual tensile strength for an FRC with a different fibre dosage.

In Chapter 4 of this thesis, the principles of the correction factor described above are applied to estimate the residual tensile strength for a structural element ($f_{Ftu,str}$) from the residual flexural tensile strength (f_{R3}) determined in a standard specimen. This was done in accordance with the following sequence:

- without correction for fibre configuration,

$$f_{Ftu}=\frac{f_{R3}}{3} \tag{3.4}$$

- normalized to isotropic conditions,

$$f_{Ftu,norm}=\frac{1}{\left[\left(\frac{v_f}{v_{f,nom}}\right)(4\alpha\text{-}1)\right]_{s.beam}}f_{Ftu} \tag{3.5}$$

- including the fibre configuration of the structure,

$$f_{Ftu,str}=\left[\left(\frac{v_f}{v_{f,nom}}\right)(4\alpha\text{-}1)\right]_{str}f_{Ftu,norm} \tag{3.6}$$

where the index "*s.beam*" refers to standard beams, and "*str*" refers to structural elements. If $\alpha < 0.5$, the correcting factor in Eq. 3.6 and 3.7 should be determined as $(v_{f,local}/v_{f,nom})(2\alpha_{local})$ (Eq. 3.3). Substituting Eq. 3.6 into 3.7 leads to:

$$f_{Ftu,str}=\frac{\left[\left(\frac{v_{f,local}}{v_{f,nom}}\right)(4\alpha_{local}\text{-}1)\right]_{str}}{\left[\left(\frac{v_{f,local}}{v_{f,nom}}\right)(4\alpha_{local}\text{-}1)\right]_{s.beam}}f_{Ftu}\overset{def}{=}\frac{f_{Ftu}}{K_{str}} \tag{3.7}$$

where K_{str} therefore becomes an indicator of the representativeness of the fibre properties of the standard beams for the structural application.

3.3.2 Sectional analysis

Chapters 4 and 5 show how the flexural behaviour was modelled using sectional analyses based on the principles of the so-called multi-layer method (Hordijk, 1991, Kooiman, 2000, Grünewald, 2004, Døssland, 2008, Blanco, 2013). As briefly described in Section 2.5.5, this method assumes that the sectional behaviour is described by a series of springs. Each spring represents a small layer of the concrete cross-section, and behaves (in terms of stress and strain) in accordance with the chosen constitutive law (Fig. 3.12). The internal forces are thus taken as the sum of the behaviour of all springs.

At any given compressive strain, the tensile strain was varied in a sequential iterative process until force equilibrium in the cross-section was satisfied. The corresponding bending moment was computed from the internal forces. Successively increasing the compressive strain enabled the simulation of the entire moment-curvature relationship. Such an analytical model was implemented in a MATLAB subroutine, considering a discretization of the cross-section in one thousand layers and successively applying compressive strain increments of 0.01‰.

Reinforced cross-sections were analysed by introducing the corresponding axial force at the location of the reinforcement, and by adopting the additional assumption of perfect bond between the steel bars and the surrounding concrete.

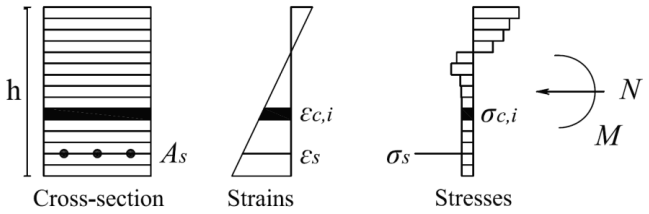

Fig. 3.12. Distribution of strains and stresses over a cross-section.

In order to transfer cross-sectional results to global response, the relationship between the moment-curvature results and the load-deflection response was established using the unit-load method for the test configuration considered.

With regard to the material models, a strain hardening behaviour was assumed for the reinforcement. The compressive behaviour of concrete was assumed to be in accordance with the parabola-rectangle diagram given in the Eurocode 2 (European Standard, 2004). The three models in Fig. 3.13 were considered to characterize the tensile behaviour of FRC. The parameters for the Elasto-plastic model and the Linear model are defined in the Model Code 2010 (*fib*, 2010), while the parameters for the RILEM σ-ε model are given in RILEM (2003). Before application to the structural beams, all these material parameters were calibrated with the results from the standard three-point bending tests.

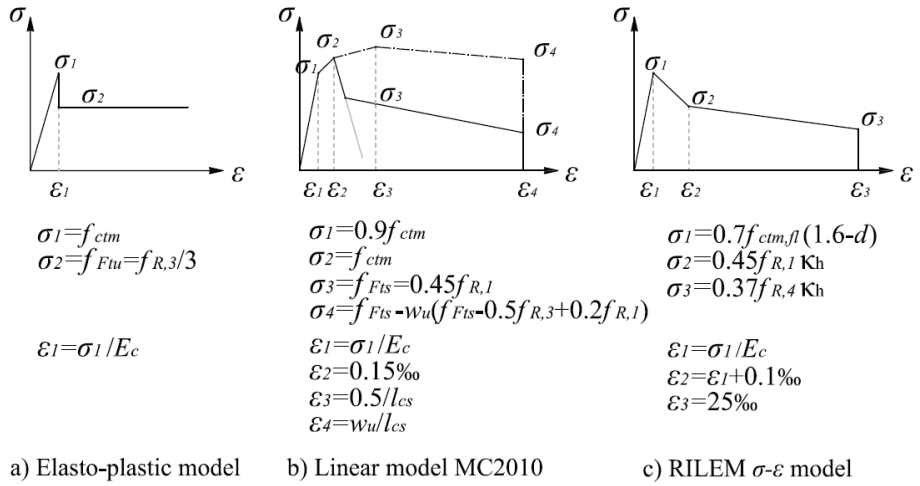

Fig. 3.13. Constitutive models considered for the σ-ε tensile relationship of FRC in the sectional analysis.

3.3.3 Nonlinear finite element modelling

The performance of nonlinear finite element analyses of FRC elements is described in Part III of this thesis. A description of the whole modelling approach that includes these analyses is, in fact, the aim of Chapters 7 and 8; this section therefore describes just some of the general aspects related to their implementation.

The nonlinear finite element analyses were performed using the commercially available program package DIANA. All the analyses presented in this thesis considered eight-node quadrilateral plane stress elements with 2 × 2 Gauss integration. The nonlinear behaviour of the material was described using a rotating smeared crack model based on a total strain concept, for which the definition of the shear retention factor after cracking was not needed, see e.g. Rots (1988).

The compressive behaviour of FRC was defined using an ideal elasto-plastic model. The tensile behaviour, however, was defined as dependent on the fibre parameters. As will be seen in Chapter 7 and 8, two main fibre parameters need to be incorporated in each element of the FE model: the fibre volume fraction and the unit vector that defines the dominant orientation of the fibres.

The uniaxial tensile stress-strain behaviour was defined using a user-supplied subroutine, for which the dependence on fibre volume fraction and dominant fibre orientation was established.

Part II

Experimental investigation and characterization of fibre configuration

Chapter 4

Fibre configuration in beams of flowable hybrid polymer-steel FRC

Paper I

Influence of fibre distribution and orientation on the flexural behaviour of beams cast from flowable hybrid polymer-steel FRC

E.V. Sarmiento, M.R. Geiker & T. Kanstad

Submitted to an international scientific journal in September 2015

Abstract

The structural performance of hybrid polymer-steel fibre-reinforced concrete is strongly influenced by the fibre distribution and preferred orientation induced during casting. This effect is pronounced for elements cast from highly flowable concrete. To detect possible fibre configurations that differ from those of standard specimens, the fibre distribution and orientation in full-scale elements was investigated. The objective was to reduce uncertainty at the structural design stage, when tensile behaviour is generally derived from standard specimens. The research showed that an uneven fibre configuration can occur in full-scale beams. Steel fibres were prone to segregate after a certain flow length, while polymer fibres distributed evenly. A higher degree of preferred orientation was detected in the bottom half of the beams, especially for polymer fibres. The results confirmed that disregarding the fibre configuration for the modelling of the full-scale beams on the basis of results from standard specimens led to an overestimation of their flexural response. Such overestimation was considerably reduced if the tensile response from standard tests was corrected to account for the actual fibre configuration in both standard specimens and full-scale beams.

Keywords

Flowable concrete, Hybrid polymer-steel fibre-reinforced concrete, Fibre volume distribution, Fibre orientation, Residual tensile strength, Correction factor

4.1 Introduction

Hybrid fibre systems have proven successful in improving the mechanical behaviour of concrete with fibres working at various stages of the cracking process (Stähli and van Mier, 2007, Rossi et al., 1987, Rossi, 1997). So far, most research has focused on the use of multi-scale or multi-geometry fibre systems (Rossi, 1997, Markovic, 2006, Vandewalle, 2007, Park et al., 2012, Stähli and van Mier, 2007, Akcay and Tasdemir, 2012). The development of polymer macro-fibres has led to the study of polymer fibre-reinforced concrete (FRC) as an alternative to steel FRC for structural applications (Pujadas et al., 2014a, Buratti et al., 2011, Alberti et al., 2014a, Soutsos et al., 2012) and also to the recent development of hybrid polymer-steel FRC (Qian and Stroeven, 2000b, Qian and Stroeven, 2000a, Ding et al., 2009, Dawood and Ramli, 2012, Alberti et al., 2014b). The combination of polymer and steel fibres has the potential to optimize the crack-bridging effect of FRC due to the synergistic effect described by Banthia and Gupta (2004), in which a strong and stiff type of fibre improves the cracking response at low deformations, and a more flexible and ductile type of fibre leads to improved toughness in the latter cracking stage.

Only few investigations report the use of polymer-steel fibres in flowable or self-compacting concrete (SCC) (Alberti et al., 2014b, Ding et al., 2009, Ding et al., 2008, Dawood and Ramli, 2012). At the present time, there is limited experience on how this combined fibre system affects the desired compromise between fluidity and stability of fresh concrete and how steel and polymer fibres, when combined, distribute and orient in full-scale elements cast with flowable concrete. A concrete which is stable at rest implies that the material has sufficient segregation resistance to avoid downward settlement of fibres and aggregates (Fig. 4.1a). However, this is not sufficient to ensure a uniform distribution of fibres after casting. In a study of plain self-compacting concrete, Spangenberg et al. (2012a) demonstrated that a concrete which is stable at rest can be unstable during flow leading to non-uniform aggregate distribution. The same may be expected for fibres (Fig. 4.1b). Moreover, fibre orientation also occurs during casting (Boulekbache et al., 2010, Ferrara et al., 2011, Abrishambaf et al., 2012, Martinie and Roussel, 2010), with the fibres reorienting due to physical contact with the constraints, the so-called wall effect (Fig. 4.1c), or due to shear rates related to variations in the flow velocity profile (Fig. 4.1d). If the downward settlement and the orientation of the fibres are affected by stress gradients, different behaviour may be expected for different types of fibres. So it remains uncertain how a combined fibre system, with polymer fibres having a density which is one eighth compared with steel fibres, will distribute and orient under full-scale conditions.

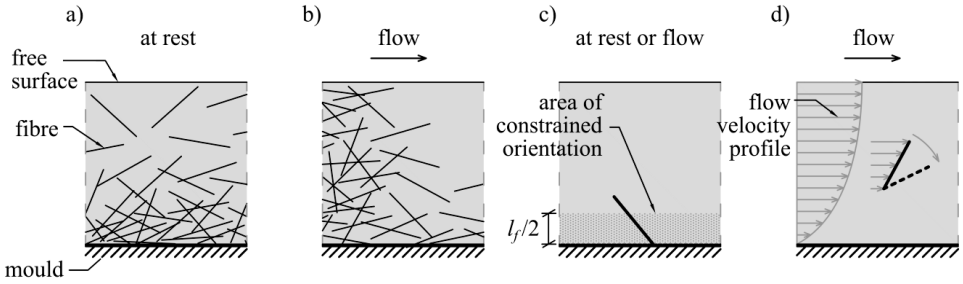

Fig. 4.1. a) Downward settlement of fibres at rest, b) uneven fibre distribution occurring during flow, c) fibre orientation constrained by the wall effect, and d) orientation induced by shear rates during flow.

The structural application of (flowable) hybrid FRC requires the development of recommendations that cover its design and execution practice. During the last decade, several guidelines have been developed and contributed to establish the basis for a structural use of FRC (SFRC Consortium, 2014, Swedish Standards Institute, 2014, DAfStb, 2012, RILEM, 2003, *fib*, 2010, Kanstad et al., 2011) and simple methods for the material characterization. For this, load-deflection responses from indirect tests, such as bending tests of notched beams (European Standard, 2005), are often used. However, large differences in fibre distribution and orientation between structural elements and test specimens have been reported in several investigations (Blanco, 2013, Montaignac et al., 2012, Di Prisco et al., 2009), as a consequence of the influence of the casting conditions. If the fibre configuration in the test specimens is not representative, this can lead to an unreliable prediction of the structural performance of the FRC element. Given that the crack-bridging action of fibres is strongly influenced by their distribution and orientation in a certain element, some of these guidelines propose the consideration of the fibre orientation to correct the tensile behaviour derived from test specimens with regard to the application at the structural level. However, some of the correcting methods proposed in the guidelines are not specifically defined for SCC, for which usually an improved flexural behaviour of test specimens with less scatter is observed in comparison to ordinary concrete (Kooiman, 2000, Grünewald, 2004). Further investigation appears to be needed to extend the scientific basis of correction methods to flowable or SCC and to fibre types and systems other than steel fibres.

Within this context, the main objectives of this research were:

- To characterize the fibre distribution and orientation patterns along the length of full-scale beams cast from flowable concrete with a polymer-steel fibre system.
- To identify major differences in the fibre configuration (i.e. distribution and orientation) between full-scale beams and standard specimens with regard to the representativeness of standard specimens for structural design purposes.

- Finally, to consider the need to correct the tensile behaviour derived from standard tests to reflect the actual fibre configuration in a full-scale beam, and evaluate approaches for this.

The principles discussed in this paper relate primarily to flowable hybrid polymer-steel FRC, but some of the research findings can also be extended to flowable concretes with polymer or steel fibres only.

4.2 Materials and experimental methods

4.2.1 Materials

The mix proportioning of the flowable hybrid FRC used in the present study was developed during the research work by Vikan et al. (2011) considering ordinary strength concrete. A 1% vol. fibre dosage, with equal volume of polymer and steel fibre, was used. The mix (Table 4.1) was optimized in accordance with the particle-matrix model (Mørtsell, 1996) to reach a satisfactory level of stability and flowability.

Table 4.1. Mix design.

Cement [kg/m^3]	286.8
Limestone [kg/m^3]	71.7
Total free water [kg/m^3]	226.6
Aggregate 0-2 mm [kg/m^3]	250.5
Aggregate 0-8 mm [kg/m^3]	1419.8
Super-plasticizer [kg/m^3]	2.4-3.7
Stabilizer [kg/m^3]	4.0
Polymer fibres [kg/m^3, (% vol.)]	4.6, (0.5)
Steel fibres [kg/m^3, (% vol.)]	39.0, (0.5)
w/b ratio [-]	0.79
Matrix volume (< 0.125 mm) [l/m^3]	393

The polymer fibres had a composition of 98% polypropylene, a continuously embossed surface, a length of 48 mm and an aspect ratio of 53. The minimum tensile strength and elastic modulus were 550 and 10000 MPa, respectively, according to the manufacturer. The steel fibres were ordinary hooked-end fibres with a length of 60 mm and an aspect ratio of 67. The minimum tensile strength and elastic modulus were 1160 MPa and 210000 MPa.

4.2.2 Specimens

The studied specimens are a part of a larger experimental series on the application of flowable hybrid FRC to load-carrying structures with a reduced amount of ordinary reinforcement, which comprises elements designed for flexural and shear failure (Nedrelid and Kanstad, 2014b). Due to the large concrete volume required, the casting was carried out in four batches of the same mix (denoted Batch 1-4). The elements investigated in the current paper include:

- 12 small-scale beams with dimensions of 150 mm × 150 mm × 550 mm, three cast from each batch, notched at midspan in accordance with EN 14651 (European Standard, 2005). Hereinafter referred to as the standard beams.
- two full-scale beams with dimensions of 200 mm × 300 mm × 4000 mm, cast with Batch 1 and 2, which were reinforced with 1Ø20 mm rebar in addition to the fibres.

The full-scale beams were cast from one end of the mould, allowing the concrete to flow along the length of the mould, *i.e.* 4 m. In contrast, the standard beams were cast using the layered method described in EN 14651 (European Standard, 2005).

4.2.3 Fresh concrete tests

Slump-flow tests in accordance with EN 12350-8 (European Standard, 2010a) were carried out to characterize the consistency and flow potential of each batch. The amount of super-plasticizer was adjusted during the mixing process to achieve a target slump-flow ranging from 550 to 650 mm. For Batch 1, 2, 3 and 4, the percentage of super-plasticizer (expressed as % of cement) was 0.99, 0.85, 1.11 and 0.92, respectively, while the slump-flow was 642, 585, 560 and 570 mm, respectively. The stability was visually examined and qualitatively evaluated based on the Visual Stability Index (VSI) (ASTM International, 2014). All batches had a satisfactory flowable and non-segregating consistency with a VSI of either highly stable or stable.

4.2.4 Hardened concrete tests

To determine the compressive strength, six 100 mm cubes (European Standard, 2009c) were tested for each batch. To characterize the residual flexural tensile strength, three-point bending tests of the standard beams were conducted in accordance with EN 14651 (European Standard, 2005).

The two full-scale beams were tested under the bending conditions illustrated in Fig. 4.2. The load was applied using a hydraulic jack acting on a steel profile that transferred the load to the loading points. A constant displacement rate of 1 mm/min was applied. The deflection at midspan was measured with displacement transducers attached to the

bottom face of the specimens. The age of the beams at testing was 33 and 34 days, and accompanying standard beams and cubes were tested on the same day as the full-scale beams.

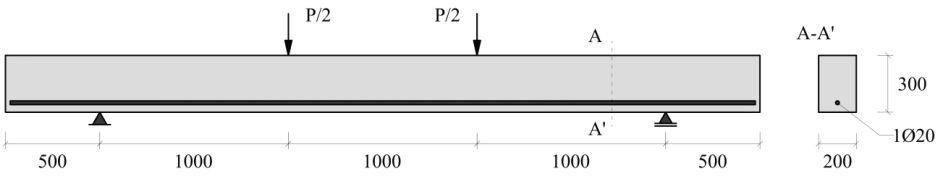

Fig. 4.2. Test setup and cross-section of the full-scale beams. Dimensions in mm.

4.3 Evaluation methods

4.3.1 Determination of fibre distribution and orientation

Various parameters have been proposed to quantitatively express the dominant orientation of fibres in a certain volume, including: the second-order orientation tensor (Advani and Tucker, 1987, Ferrara et al., 2011, Sarmiento et al., 2014a, Şanal and Özyurt Zihnioğlu, 2013, Švec et al., 2014), the average out-of-plane angle (Bay and Tucker, 1992, Deeb et al., 2014, Ferrara et al., 2011), or the fibre orientation factor (Krenchel, 1964, Aveston and Kelly, 1973, Stroeven, 1978, Stroeven, 1979, Soroushian and Lee, 1990, Krenchel, 1975). Several methods can be used to assess such parameters; an overview of these can be found in Žirgulis et al. (2013) and Laranjeira de Oliveira (2010). Computed Tomography (CT) scanning is recognized as an effective method to produce 3D images of the fibre distribution in a specimen. Such images allow the posterior assessment of any of the mentioned orientation parameters. While CT has been successfully used for steel FRC (Stähli et al., 2008, Švec et al., 2014, Sarmiento et al., 2014a), medical scanners like the one used by Švec et al. (2014) cannot detect polymer fibres due to their low density. Pujadas et al. (2014b) recently reported the successful use of an industrial CT scanner to investigate polymer fibres in small samples.

The out-of-plane angle can be assessed by studying plane sections using microscopy or high-resolution images. The angle is often determined from the elliptical intersections between fibres and the cross-section (Bay and Tucker, 1992, Deeb et al., 2014, Ferrara et al., 2011). However, this method is limited to fibres with a uniform cross-section, so it is not applicable to fibres with an embossed surface like the polymer fibres used in

this research. Simpler approaches can be used to compute the orientation factor α based on the analytical expression:

$$\alpha = n_f A_f / v_f \tag{4.1}$$

in which n_f refers to the number of fibres per surface unit, v_f to the fibre volume fraction, and A_f to the fibre cross-section area. α ranges from 0 to 1, with its limits describing the situations where fibres align either parallel or perpendicular to the plane studied. α is commonly computed by merely determining n_f in a plane section using any fibre counting method. Under the condition of perfectly uniform distribution of fibres in a specimen (i.e. v_f constant and equal to the fibre dosage), it is possible to state that the larger the number of fibres in a plane, the greater the perpendicular alignment of the fibres in respect to this plane. However, if the distribution of the fibres is not uniform, a large number of fibres in a plane might be caused either by a favourable alignment of the fibres, by a high fibre content, or by both phenomena occurring simultaneously. This means that computing α without including the locally determined volume fraction ($v_{f,local}$) is simply an alternative way of expressing n_f, and not a method to strictly describe the orientation.

In the current investigation, the mechanisms of fibre distribution and fibre orientation were separately studied by determining local volume fractions and local orientation factors α_{local}. Note that a distinction is made with the previously described α to explicitly indicate the inclusion of the local volume fraction: $\alpha_{local} = n_f A_f / v_{f,local}$. Although the number of fibres should not be directly used to conclude about the orientation and distribution phenomena, it is still recognised as a valuable factor for correlating the fibre parameters with the measured mechanical properties of the material (Ferrara et al., 2011, Švec et al., 2014), mainly due to its advantageous simplicity. Consequently, this investigation only discusses its eligibility for this particular application.

For the standard beams, the number of fibres was counted in the cross-sections indicated in Fig. 4.3a. The volume of fibres within the slice delimited by the two cross-sections was determined by first crushing the slice and then separating polymer and steel fibres from the crushed matrix (European Standard, 2007, European Standard, 2006). The fibre volume fraction $v_{f,local}$ and the orientation factor α_{local} were then computed from these results.

Fibre distribution and orientation were likewise studied in the full-scale beams after their mechanical test. The local fibre volume fractions and orientation factors of sawn slices were determined at the locations indicated in Fig. 4.3b, in the same way as described for the standard beams. In this case, however, the two parameters were determined for both the upper and lower half of each slice.

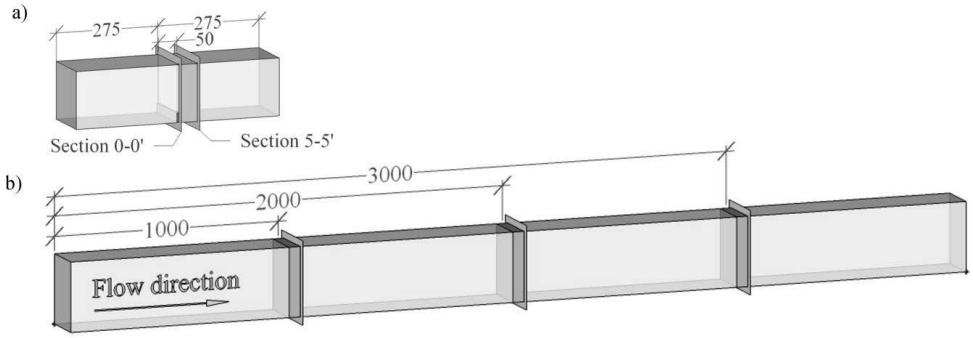

Fig. 4.3. Cross-sections and slices to determine fibre content and number of fibres for a) standard beams, and b) full-scale beams. Dimensions in mm.

4.3.2 Flexural analysis of FRC beams

The tensile properties needed to establish the constitutive material model of FRC are often derived from the flexural response of notched specimens. Transferring these results to tensile stress-crack width or stress-strain (σ-ε) relationships requires analytical expressions (Laranjeira de Oliveira, 2010) or inverse analyses of experimental results (Tlemat et al., 2006, Tailhan et al., 2012). Recommendations for FRC offer design-oriented simplified approaches based on the straightforward application of predefined models. This paper discusses three simplified constitutive models proposed in international guidelines, calibrated with the results from three-point bending tests of notched specimens (Fig. 4.4).

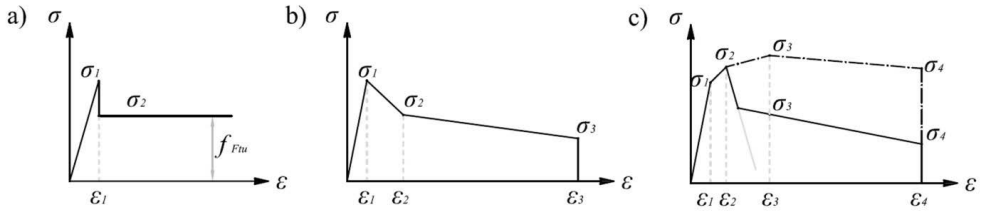

Fig. 4.4. Constitutive models for the σ-ε tensile relationship: a) Elasto-plastic model, b) RILEM σ-ε model, and c) Linear model from Model Code 2010 (MC2010).

The Elasto-plastic model is the simplest and is characterized by a brittle drop after the initial elastic phase and perfect plastic behaviour for the post-cracking state. Its simplicity represents a practical advantage for the ULS design, for which the initial elastic phase can be disregarded (*fib*, 2010). Both the RILEM σ-ε method (RILEM, 2003) and the Linear model from MC2010 (*fib*, 2010) consider two stresses at different

levels of deformation to characterize the post-cracking behaviour. In addition, the Linear model from MC2010 is also defined for materials with hardening behaviour.

Sectional analyses are commonly applied for predicting the flexural behaviour of FRC members (RILEM, 2002a, Montaignac et al., 2012, Kooiman, 2000, Grünewald, 2004). The methods used are based on numerical integration of stresses over the cross-section, or on the principles of the so-called multi-layer method, see e.g. Hordijk (1991). In this paper, the multi-layer method was applied to analyse the full-scale beams experimentally tested with the tensile constitutive models for FRC presented above. In order to transfer cross-sectional results to global response, the relationship between the moment-curvature results and the load-deflection response was established using the unit-load method for the test configuration considered. For more accurate calculations, finite element analyses should be considered.

4.4 Results and discussion

4.4.1 Fibre distribution and orientation in standard beams

The average values of orientation factors and fibre contents for the standard beams are presented in Table 4.2. The fibre content is expressed by the normalized volume fraction, referring to the local fibre volume fraction within the concrete volume studied ($v_{f,local}$) normalized by the fibre dosage (0.5% vol. for each fibre type), here called the nominal volume fraction ($v_{f,nom}$).

Table 4.2. Fibre volume fraction and orientation factor of standard beams, average of all batches.

	Average value	CV
Normalized volume fraction ($v_{f,local}/v_{f,nom}$) [-]		
Polymer	1.08	14.0%
Steel	1.02	31.8%
Total	1.05	20.0%
Orientation factor α_{local} [-]		
Polymer	0.63	5.4%
Steel	0.66	10.7%
Total	0.64	6.1%

With an average orientation factor of 0.64, the fibre orientation factor did not widely differ between the two fibre types. A low variation was also observed among the specimens. In contrast, the measured volume fractions exhibited a large scatter. When macro-fibres are used, a relatively low number of fibres can be found in any cross-

section. Minor variations in the number of fibres in small-sized cross-sections can cause a significant scatter in the results of $v_{f,local}$ and have a great impact on the flexural response (Di Prisco et al., 2009, Buratti et al., 2011). As can be seen in Table 4.2, the longest fibres, in this case the steel fibres (60 mm), show a greater variation than the polymer ones (48 mm), which supports the idea that the scatter is related to the size of the fibres.

4.4.2 Fibre distribution and orientation in full-scale beams

Results from the two full-scale beams, cast from two different batches, are presented separately. Although they were cast under comparable casting conditions, the study revealed that the variation between different batches was not negligible.

Volume fraction distribution

The tendency of each fibre type to segregate was evaluated by comparing the fibre contents of the upper and lower halves of the slice located at a distance of one meter from the casting point. This slice was assumed to be located sufficiently far from the casting area, where the discharge of concrete can locally affect the material, and sufficiently close to be least exposed to possible flow-induced effects. Fig. 4.5 shows that the polymer fibres did not suffer any symptom of downward settlement; they distributed uniformly over the height. In contrast, a significant downward settlement of the steel fibres, quantified by a normalized fibre volume of 1.4, was observed for the beam cast from Batch 2 (Fig. 4.5b), characterized as least stable.

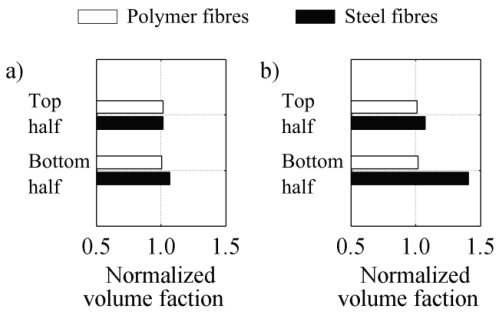

Fig. 4.5. Distribution of the fibre volume fraction over the height of the full-scale beams at a distance of one meter from the casting point: a) beam cast from Batch 1, and b) beam cast from batch 2. The normalized volume fraction is determined as $v_{f,local}/v_{f,nom}$.

The measurements of the fibre volume fraction distribution are presented in Fig. 4.6a-b and Fig. 4.6c-d for the beams cast from Batch 1 and 2, respectively. These figures reveal a non-uniform distribution of the steel fibre volume fraction along the length of

the beams, which indicates that fibre migration or segregation occurred during casting. Internal friction and cohesive forces between fibres and matrix tend to decrease during flow and they may become too low to counteract the effect of gravity forces. This can potentially lead to segregation of the constituents with highest density, the steel fibres in this case.

It is clear from Fig. 4.6b and d that the two batches differ in their rates of segregation, presumably due to different rheological properties. For the beam cast from Batch 1, the dotted line in Fig. 4.6b shows that the total steel fibre content remains constant, but that there is a certain tendency for steel fibres to migrate from the upper half towards the lower half after a flow length ranging between 2 and 3 m. For the beam cast from Batch 2, the steel fibre content is significantly reduced at the further end of the beam (Fig. 4.6d), which indicates that the matrix of this concrete had difficulty in dragging the steel fibres along the specimen.

It is worth noting that the content of polymer fibres remains uniform along the two beams (Fig. 4.6a and c), also for the least stable batch. The low tendency to segregate of these fibres, probably due to their low density, appears to add robustness to the mix. Although it is not possible to evaluate whether interactions between polymer and steel fibres helped mitigate the downward settlement of steel fibres, it is straightforward to conclude that this effect, if any, was insufficient.

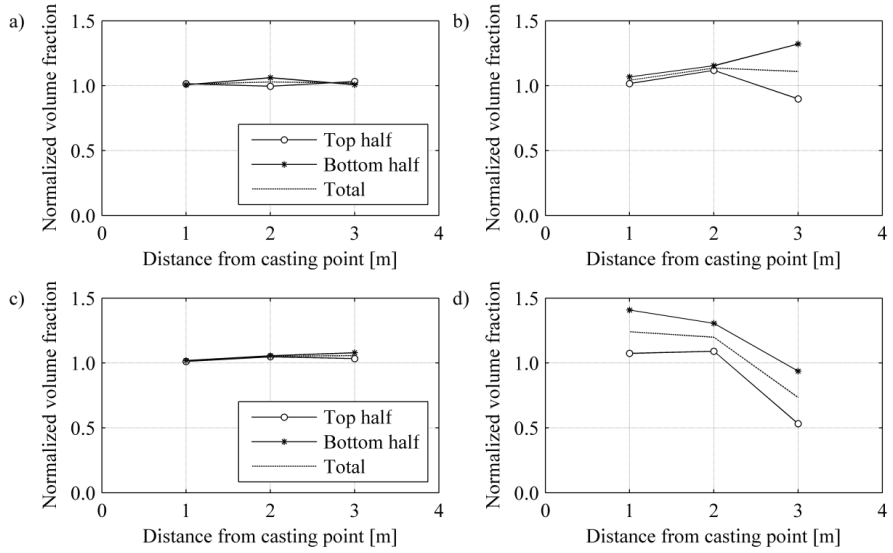

Fig. 4.6. Distribution of the fibre volume fraction along the length of the full-scale beams: a) polymer and b) steel fibres for the beam cast from Batch 1; and c) polymer and d) steel fibres for the beam cast from Batch 2. The normalized volume fraction is determined as $v_{f,local}/v_{f,nom}$.

Orientation

The results of the local orientation factors determined along the length of the beams are presented in Fig. 4.7. Comparing Fig. 4.7a-b with Fig. 4.7c-d reveals a higher degree of fibre orientation for the beam cast from Batch 2. This could be related to the rheological behaviour of this batch; previous studies report that rheological properties strongly influence the orientation of fibres with the flow, see e.g. Martinie and Roussel (2010). For this batch, however, the orientation factor does not change along the beam. Only Batch 1 shows a slight tendency to more pronounced orientation with increasing distance from the casting point.

Wall effect and high shear rates cause orientation of fibres in the area close to constraints (Martinie and Roussel, 2011). Assuming these effects to occur over a zone along the formwork with a breadth of half the fibre length, the area affected by wall effect and high shear rates is 46% larger for the bottom half than for the top half of the beam. The results in Fig. 4.7a-d show that fibre orientation factor is higher in the bottom half, and that this is valid irrespective of batch stability and fibre type. Moreover, both batches show significantly higher orientation factor for polymer fibres than for steel fibres, especially for the bottom half. This indicates a higher tendency of the polymer fibres to orient due to high shear rates.

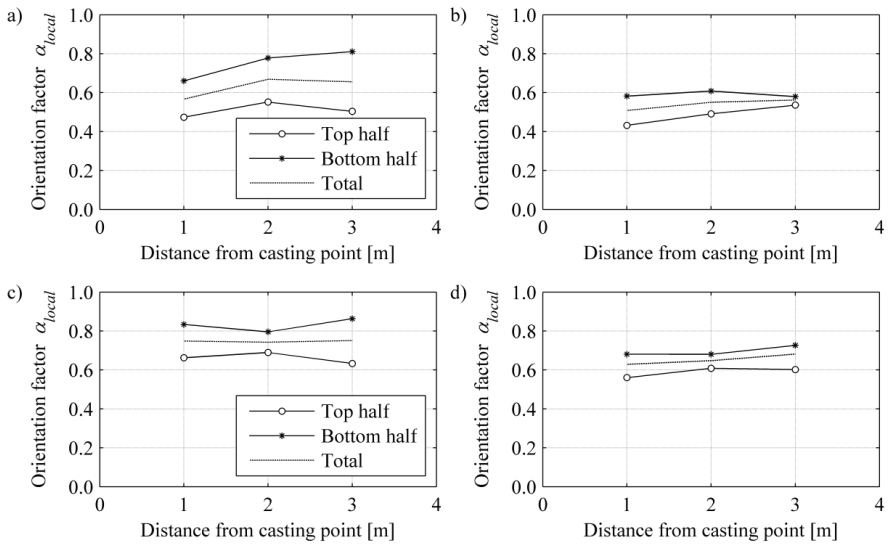

Fig. 4.7. Orientation factors along the length of the full-scale beams: a) polymer and b) steel fibres for the beam cast from Batch 1; and c) polymer and d) steel fibres for the beam cast from Batch 2.

The common practice of computing the orientation factor assuming uniform fibre distribution leads to the results presented in Fig. 4.8. With this assumption, the orientation factor of the steel fibres for the beam cast from Batch 2 would decrease severely with increasing distance from the casting point. Comparing Fig. 4.8 with Fig. 4.7d, in which the local fibre volume content is included in the assessment of the orientation factor, shows that the assumption of constant fibre content can lead to an unsound interpretation of the orientation.

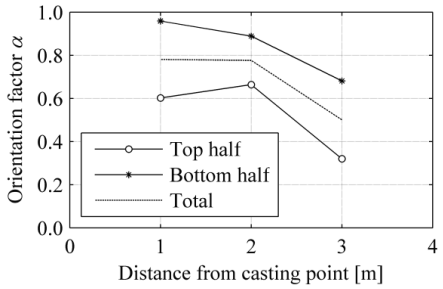

Fig. 4.8. Orientation factor of steel fibres along the length of the full-scale beam cast from Batch 2 assuming $v_f = v_{f,nom}$ (0.5% vol.) when determining α.

4.4.3 Comparison of standard to full-scale beams

Since the aim of the standard beam test is to characterize the mechanical behaviour of the material, the fibre configuration in these specimens should be representative for multiple structural solutions and casting conditions. To identify possible differences in the fibre configuration, the fibre parameters of the standard beams and the full-scale beams are compared in Table 4.3 for each batch.

Table 4.3. Comparison of fibre volume fraction and orientation factor between standard and full-scale beams.

	Standard beams	Full-scale beams			
	Average (CV)	Average (CV)	1 m	2 m	3 m
			from casting point		
Normalized volume fraction ($v_{f,local}/v_{f,nom}$) [-]					
Batch 1	1.24 (7.2%)	1.06 (2.7%)	**1.03**	1.08	1.06
Batch 2	1.15 (36.4%)	1.05 (12.7%)	1.13	1.13	0.90
Average	1.19 (18.6%)	1.05 (8.21%)			
Orientation factor α_{local} [-]					
Batch 1	0.64 (3.6%)	0.58 (6.9%)	**0.54**	0.61	0.61
Batch 2	0.65 (8.1%)	0.70 (3.0%)	0.68	0.69	0.72
Average	0.65 (4.9%)	0.64 (10.8%)			

The fibre distribution and orientation in the standard beams hardly differed from the average values of the full-scale beams. This suggests that standard beams could be representative for the material with regard to the application at the structural level. However, for design purposes, it should be kept in mind that fibres did not distribute uniformly along the full-scale beams. This aspect is further discussed in Section 4.4.6.

4.4.4 Bending test of standard beams

Fig. 4.9a depicts the average curves of the three standard beams tested for each batch in terms of flexural stress versus crack mouth opening displacement (CMOD). The figure also includes the average compressive strength (f_{cm}) and the residual flexural tensile strength f_{R3}, which corresponds to a CMOD of 2.5 mm. A deflection-hardening response characterized the post-cracking phase for all the batches, fulfilling the targets of the mix design. The shaded area in Fig. 4.9a represents the envelope of the complete family of curves, which clearly demonstrates the large scatter related to the average curves.

The flexural responses of the three specimens from the batch that registered the largest scatter are represented in Fig. 4.9b. The maximum scatter was recorded for a residual flexural tensile stress corresponding to a CMOD of 0.5 mm, which ranged from 5.1 to 2.8 MPa. This large scatter was consistent with the number of fibres counted in the notched sections, which ranged from 1.21 to 0.66 fib/cm^2. This confirms the well-known fact that large scatter of the flexural results is related to the number of fibres in the fracture area.

However, while a good correlation between n_f and the residual flexural strengths generally applies to FRCs with a deflection-softening behaviour, concretes with a deflection-hardening response require closer analysis. Specimen 1 in Fig. 4.9c suffered an abrupt drop in flexural stress at a crack width of approximately 2 mm, which was related to the development of a secondary crack. Normally, the reduction of the cross-section at the notch and the symmetric loading condition should favour a single crack growing vertically, but a strong fibre-bridging effect may cause the stress to redistribute, resulting in new weak paths that lead to multiple cracking. For this particular specimen, the notched section (section 0-0' in Fig. 4.3a) was highly reinforced with 1.42 fib/cm^2 and, although the first crack appeared in this section, a new crack grew towards a weaker section with 0.97 fib/cm^2. The results presented in Table 4.4 reveal a reduction in the number of the steel fibres of this specimen from 0.85 fib/cm^2 in the notched section to 0.44 fib/cm^2 in a section 5 cm away (section 5-5' in Fig. 4.3a).

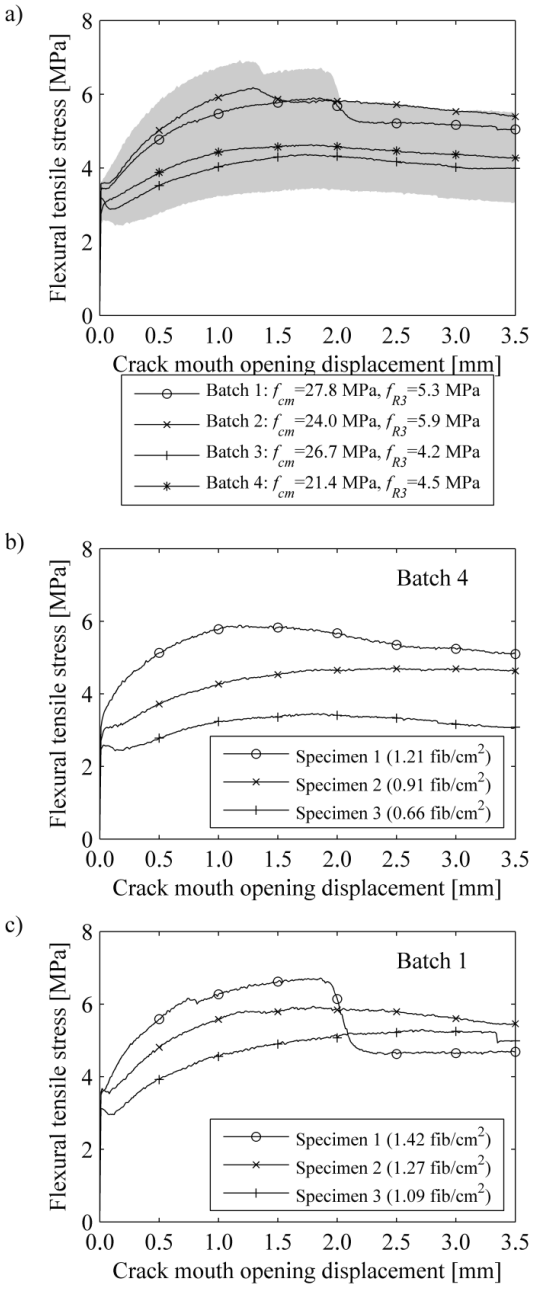

Fig. 4.9. a) Results of three-point bending and compressive tests, average of batches (only two specimens were successfully tested for Batch 3). Results of three-point bending tests and number of fibres in notched sections for: b) Batch 4 and c) Batch 1.

Table 4.4. Number of fibres in cross-sections of standard beams from Batch 1. The sections considered are depicted in Fig. 4.3a.

	Total number of fibres (Polymer/Steel) [fib/cm^2]		
	Specimen 1	Specimen 2	Specimen 3
Section 0-0'	1.42 (0.57/0.85)	1.09 (0.58/0.51)	1.27 (0.71/0.55)
Section 5-5'	0.97 (0.53/0.44)	1.50 (0.74/0.76)	1.52 (0.88/0.64)

Fig. 4.10 depicts the relationship between the residual flexural tensile strength and the number of fibres in the notched cross-section. A good linear correlation between both parameters is found for a crack developed to a width of 1 mm. However, the correlation worsens for a crack width of 2.5 mm, which seems to be related to a redistribution of stress towards less reinforced sections and the appearance of diffuse cracks. This demonstrates the difficulties of interpreting results from standard bending tests with deflection-hardening materials, as well as the shortcomings of considering the number of fibres in a cross-section as the only parameter needed to correlate the fibre configuration with the residual flexural strength.

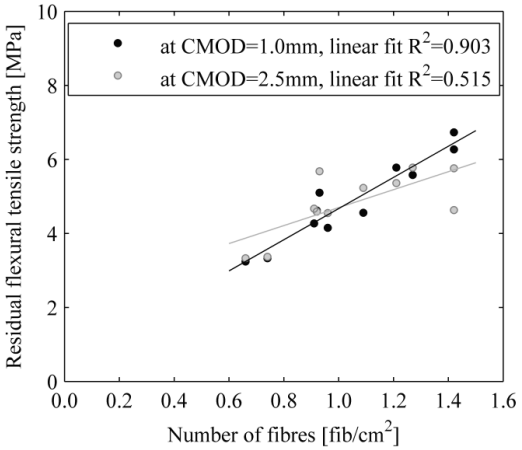

Fig. 4.10. Correlation between residual flexural strength at different CMODs and number of fibres in the notched section.

4.4.5 Bending test of full-scale beams

The experimental load-deflection curves of the full-scale beams are presented in Fig. 4.11a. The beams reached the maximum load and yielding at a deflection corresponding to δ/L (deflection-span ratio) of 1/150, and they were able to sustain this load for subsequent deflections. Both specimens exhibited a densely distributed cracking.

The structural effect of the fibre reinforcement was deducted by comparing FRC beams with reference beams without fibres. The flexural behaviour of the latter was predicted with the sectional analyses of their ordinary reinforced section according to the principles described in Section 4.3.2. For the reinforcement, the yield stress was tested to be 566 MPa, the elastic modulus was assumed as 200 GPa, and a hardening coefficient of 1.04 was to represent the strain-hardening post-yield behaviour. According to the cross-sectional analysis, 1% vol. polymer-steel fibre content increased the load capacity of the beams by 20%, 15% and 12% for deflections at midspan of 10 mm, 20 mm and 35 mm, respectively (Fig. 4.11a). These results hardly vary between the two beams, which indicate that the differences in fibre distribution and orientation observed in Section 4.4.2 did not lead to a deviation of the flexural response between the two beams.

4.4.6 Modelled flexural behaviour of full-scale beams

The three tensile constitutive models presented in Section 4.3.2 were implemented in the sectional analysis to estimate the flexural behaviour of the full-scale FRC beams (Fig. 4.11a). The applied models, which were calibrated with the results from the three-point bending tests, are presented in Fig. 4.11b.

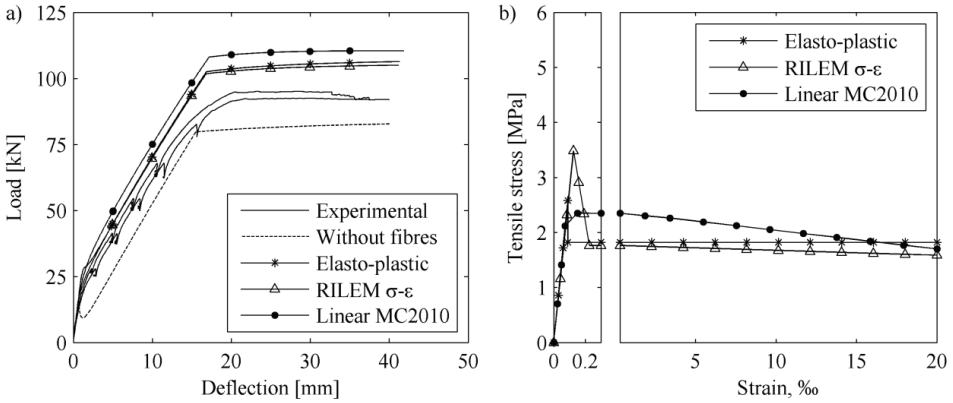

Fig. 4.11. a) Experimental and modelled load-deflection curves for full-scale beams, and b) constitutive σ-ε relationships derived from the results of standard beams.

The RILEM model predicts a significantly higher tensile strength than the other models, as previously reported by others (Barros et al., 2005, Blanco, 2013). This high tensile strength leads to cracking loads greater than those observed in the experiments.

There are only small differences in the residual tensile stresses at large deformations between the three models. However, at small deformations, the Linear model in

MC2010 results in a higher residual stress than the Elasto-plastic model. This gives rise to a significant difference in the load-deflection response between the two models. The prediction of the RILEM model depends on the structural geometry. The size factor κ_h (RILEM, 2003), which only depends on the cross-section height, reduces the residual strength by a factor of 0.78. As a consequence, the RILEM model provides a similar approximation compared to the Elasto-plastic model (Fig. 4.11a).

The most prominent is that all the results, irrespective of the model selected, significantly overestimate the actual flexural response. This suggests that for this specific flowable hybrid FRC the tensile properties derived from standard beams might lead to unsafe predictions when applied to structural beams. As mentioned in the introduction, some of the recently published guidelines (DAfStb, 2012, SFRC Consortium, 2014, Swedish Standards Institute, 2014, *fib*, 2010) for the design of FRC propose corrections of the basic residual tensile strength parameters to take account of anisotropic fibre orientation. The corrections apply when the standard specimens do not represent the actual fibre orientation of the structure. This aspect was already discussed in Section 4.4.3; however, due to the non-uniform distribution of the fibres in the full-scale beams and the large scatter of the fibre content in the standard beams, the authors consider that an accurate correction of the post-cracking response should take the variations of the fibre content into account. In this regard, the Norwegian guideline proposal (Kanstad et al., 2011) recommends normalizing the residual tensile strength from standard beams to the ideal isotropic condition, and then again correcting this value to meet the actual structural case.

The residual tensile strength f_{Ftu} that approximates the post-cracking response of the Elasto-plastic model (Fig. 4.4a) can thus be determined in accordance with the following sequence:

- without correction for fibre configuration,

$$f_{Ftu}=\frac{f_{R3}}{3} \tag{4.2}$$

- normalized to isotropic conditions,

$$f_{Ftu,norm}=\frac{1}{\left[\left(\frac{v_{f,local}}{v_{f,nom}}\right)(4\alpha_{local}-1)\right]_{s.beam}} f_{Ftu} \tag{4.3}$$

- including the fibre configuration of the structure,

$$f_{Ftu,str}=\left[\left(\frac{v_{f,local}}{v_{f,nom}}\right)(4\alpha_{local}-1)\right]_{str} f_{Ftu,norm} \tag{4.4}$$

where $(v_{f,local} / v_{f,nom})(4\alpha_{local} -1)$ is the correcting factor for the fibre properties, indexed as "*s.beam*" when referred to standard beams, or "*str*" when referred to structural elements. Thorenfeldt (2003) described the main principles of this correcting factor

based on a theoretical linear relationship of the residual tensile strength to the fibre volume, the fibre directions with respect to the crack plane and the average fibre stress representing all the fibres crossing this plane. It should be mentioned that in the case of markedly unfavourable orientation in which $\alpha_{local} < 0.5$, the correcting factor in Eq. 4.3 and 4.4 should be determined as $(v_{f,local} / v_{f,nom})(2\alpha_{local})$ (Thorenfeldt, 2003). Substituting Eq. 4.3 into 4.4 leads to

$$f_{Ftu,str} = \frac{\left[\left(\frac{v_{f,local}}{v_{f,nom}}\right)(4\alpha_{local}-1)\right]_{str}}{\left[\left(\frac{v_{f,local}}{v_{f,nom}}\right)(4\alpha_{local}-1)\right]_{s.beam}} f_{Ftu} \overset{def}{=} \frac{f_{Ftu}}{K_{str}} \tag{4.5}$$

where K_{str} therefore becomes an indicator of the representativeness of the fibre properties of the standard beams for the structural scale, which can be directly used, for instance, in MC2010.

If the fibre configuration of the full-scale beams is considered using the average α_{local} and $v_{f,local}$ from the three sections studied along each beam (Table 4.3), K_{str} takes the value 1.15. In this case, $f_{Ftu} = 1.8$ MPa from the standard test is corrected to $f_{Ftu,str} = 1.6$ MPa. However, when the fibre configuration of the most unfavourable section (bold type in Table 4.3) is considered, K_{str} has the value 1.60 and $f_{Ftu,str}$ is reduced to 1.1 MPa. The impact of such a reduction on the flexural strength can be seen in Fig. 4.12. In the latter case, the analysis gives a prediction close to the experimental results, though the capacity is still somewhat overestimated.

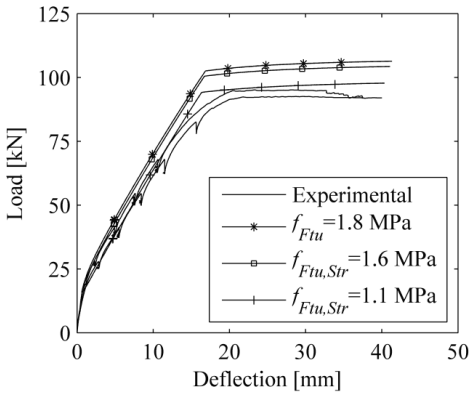

Fig. 4.12. Experimental and modelled load-deflection curves for full-scale beams using the Elasto-plastic σ-ε model with: f_{Ftu} = 1.8 MPa from standard tests, f_{Ftu} = 1.6 MPa for K_{str} = 1.15, and f_{Ftu} = 1.1 MPa for K_{str} = 1.60.

It appears therefore that, since fibres did not distribute uniformly along the full-scale beams, the correction of the tensile behaviour in accordance with the fibre parameters led to a better approximation only if the most unfavourable configuration of the fibres was considered. Moreover, it seems likely that the presence of the notch in the standard beams could have an impact when results are transferred from standard tests to structural analysis.

4.5 Conclusions

In this paper, the application of flowable hybrid polymer-steel FRC to structural beams is discussed. The study includes a comparison between the performance of standard specimens and full-scale beams with regard to fibre distribution and orientation and the influence thereof on flexural behaviour and design assumptions.

The characterization of the fibre distribution and orientation in full-scale beams led to the following conclusions:

- Polymer fibres distributed uniformly over the height and length of the beams. Because their low tendency to downward settlement, their presence appeared to add robustness to the mix.
- In contrast, steel fibres were prone to segregate depending on the consistency of the fresh concrete. For the two studied beams, non-uniform fibre distribution was observed after a certain flow length.
- Significant changes of the orientation over the length of the beams were not detected. However, fibres had typically a more pronounced orientation in the bottom half of the beams, probably due to a combination of wall effect and high shear rates in the fresh concrete. Of the two fibre types, polymer fibres exhibited a higher degree of orientation in this region, which suggests that they are more affected by these effects.
- The determination of orientation factors without considering the actual volume fraction may lead to unsound interpretation of the results if a non-uniform distribution of the fibres in the elements occurs.

The comparison of full-scale and standard beams showed that the fibre content and the orientation factor of the standard beams hardly differed from the average values of the full-scale beams. This suggests that standard beams could be representative of the material in structural beams for design purposes. Nonetheless, the tensile constitutive models directly derived from the results of the standard beams led to an overestimation of the structural performance at the structural scale. This overestimation was significantly reduced when a correction of the tensile behaviour was made in

accordance with the most unfavourable fibre configuration observed in the full-scale beams.

The fact that the uneven fibre distribution could not be foreseen at the production stage suggests that, for design purposes of elements cast from highly flowable FRC, the fibre configuration in the intended application should be characterized. In so doing, correction methods should take into account any possible unfavourable fibre configuration. In view of the large variations of the fibre content identified both in the standard test beams and the full-scale beams, it is suggested that correction factors include potential variations in the fibre content in addition to the orientation, similarly as the investigated model proposed by Thorenfeldt (2003) does.

Acknowledgements

The authors acknowledge support from COIN – the Concrete Innovation Centre (www.coinweb.no) – which is a centre for research-based innovation, initiated by the Research Council of Norway (RCN) in 2006. The Centre is directed by SINTEF, with NTNU as a research partner, and its current industrial partners are: Aker Solutions, Norcem, Norwegian Public Roads Administration, Rescon Mapei, Skanska, Unicon, Veidekke, and Weber Saint Gobain.

Chapter 5

Fibre configuration in beams of flowable FRC with high fibre content

Paper II

Influence of fibre configuration on the mechanical behaviour of standard test specimens and full-scale beams made of flowable FRC

E.V. Sarmiento, M.R. Geiker & T. Kanstad

Submitted to an international scientific journal in August 2015

Abstract

Variation in the performance of flowable fibre-reinforced concrete limits its use in structural applications. The experimental programme presented in this paper was aimed at evaluating the influence of fibre configuration (orientation and distribution) on the flexural behaviour of full-scale structural beams. The investigation focused on fibre-reinforced concrete with high ductility provided by 2% vol. steel fibres with a length of 60 mm. Computed Tomography scanning of the fibre configuration revealed large variations in fibre orientation and volume content. These inhomogeneities explained the flexural behaviour. The activation of cracks in locally weak areas proved to be decisive in the crack propagation and the load-carrying capacity of the beams.

Three-point bending and uniaxial tension test methods used on notched specimens were assessed. The unrepresentative configuration of the fibres and the predetermined location of the crack were identified as the main causes of the overestimation of structural behaviour using these standard test methods.

Keywords

Flowable fibre-reinforced concrete, High fibre content, Fibre configuration, Computed Tomography, Structural behaviour

5.1 Introduction

The use of fibres for structural purposes has led to continuous improvements with regard to crack control, post-cracking strength and fracture toughness. This enhanced structural performance has the potential to improve ductility, increase load-carrying capacity, or reduce the need for traditional reinforcement. This last aspect is especially relevant for structures with complex geometries and highly congested reinforcement solutions (Nedrelid and Kanstad, 2014a, Randl and Mészöly, 2014), where the use of fibres can lead to substantial reductions in costs and labour effort.

Extensive work has been carried out in the development of guidelines and engineering standards to help the use of fibres gain acceptance in the concrete industry (ASTM International, 2010, ASTM International, 2012b, *fib*, 2010, RILEM, 2002b, RILEM, 2001). These guidelines typically evaluate the mechanical behaviour of fibre-reinforced concrete (FRC) using standard bending tests or uniaxial tension tests.

Efforts have also focused on developing FRC into an industrially competitive material (Löfgren, 2005). The use of fibres in flowable or self-compacting concretes (SCC) has revealed potential synergistic effects: improved distribution of fibres due to the elimination of vibration, increased stability of the SCC matrix, and enhanced structural performance. See e.g. Ferrara (2014) for a comprehensive literature review of this topic.

An adequate mix design should potentially provide a homogeneous 3D distribution of fibre reinforcement that ensures a reliable engineering design. The distribution of fibres is often visually examined as part of the quality control of the fresh concrete during production. However, the casting method (Grünewald and Walraven, 2002), the concrete casting location, the direction of casting (Døssland, 2008), the flow length (Abrishambaf et al., 2013, Pujadas et al., 2014b), and the formwork surface conditions (Švec et al., 2014) are just some of the numerous factors that may induce a preferred orientation or an uneven distribution of the fibres in a structural element. Inhomogeneities arising from such factors can be almost impossible to foresee at the production stage and may not necessarily occur in standard test specimens, which have different casting conditions. The translation of standard test results to structural behaviour is therefore not straightforward (Blanco, 2013, Grünewald et al., 2014). For this reason, some recently published guidelines for the design of FRC (DAfStb, 2012, SFRC Consortium, 2014, Swedish Standards Institute, 2014, Kanstad et al., 2011) propose corrections to the residual tensile strength parameters to take account of anisotropic fibre orientation.

Interest in the use of fibres as a partial or complete substitute for traditional reinforcement has grown with the recent development of high ductility concretes.

However, advances at the material level require increased understanding of the mechanisms that affect the fibre configuration (i.e. fibre distribution and orientation) in the specific casting conditions. This is of crucial importance for predictions of the structural performance that can serve as a reliable basis for the design of robust structures.

In this paper, the structural performance and load-carrying capacity of a flowable FRC mix containing 2% vol. steel fibres was investigated. The material was examined at two levels of application: at the full-scale level with structural beams, and at the small-scale level with material test specimens. With respect to the full-scale level, the aim was not only to evaluate the structural performance, but also to understand the structural impact of fibre inhomogeneities having their origin in the casting process. At the small-scale level, the purpose was to assess standard test methods when used for flowable concrete containing a high content of fibres. The paper focusses on the suitability of these methods in the case of FRC that exhibits hardening in the post-peak regime. This investigation led us naturally to compare the performance at both levels, detecting the limitations with regard to the interpretation of results from small-scale test specimens for the prediction of full-scale structural behaviour.

5.2 Experimental programme

The overall performance of a flowable and highly ductile FRC was investigated experimentally. Fresh concrete properties were examined to describe the workability and flow limitations of the mix. The mechanical behaviour was investigated of both small-scale test specimens and full-scale structural beams. The fibre reinforcement configuration was determined to identify variations in fibre orientation and distribution that could influence the mechanical behaviour.

5.2.1 Materials and mixing procedure

The mix proportioning of the FRC used in the present study was developed during research work by Kjellmark et al. (2014) on the optimization of flowable FRC mixes with high ductility. This mix has reasonably good casting properties, with adequate flowability and compactability, and does not require vibration. In the hardened state, the mix shows a clear deflection-hardening behaviour in three-point bending of notched beams, with an average residual flexural strength at a crack width of 2.5 mm of 19 MPa. Table 5.1 gives the mix proportions.

The mix contained 2% vol. hooked-end steel fibres, with a length of 60 mm and an aspect ratio of 67. The minimum tensile strength reported by the manufacturer was 1160 MPa.

Table 5.1 Mix design.

Component	Dosage
Cement [kg/m^3]	492.2
Silica fume [kg/m^3]	24.6
Total free water [kg/m^3]	197.5
Aggregate 0-8 mm [kg/m^3]	1594
Super-plasticizer [kg/m^3]	7.4-9.8
Stabilizer [kg/m^3]	0.5
Steel fibres [kg/m^3, (% vol.)]	156, (2)
w/b ratio [-]	0.35
Matrix volume (< 0.125 mm) [l/m^3]	400

The total volume of concrete was mixed in two batches of 710 litres each. The concrete was mixed without fibres for 7 min, and the slump-flow was checked approximately 10 min after adding the water. A slump-flow of 720-740 mm was required before the addition of fibres. If necessary, the dosage of super-plasticizer was to be adjusted to reach this consistency. In both batches, the initial dosage of super-plasticizer, 1.5% of cement (7.4 kg/m^3), was adjusted to 2.0% (9.8 kg/m^3) to meet the required slump-flow. With this dosage, the mixes without fibres were highly flowable and stable, and a uniform distribution of aggregates was observed.

The fibres were added approximately 15 min after water addition, and the concrete was mixed for another 2 min. The fresh concrete properties of the FRC were measured approximately 20 min after water addition. The measurements included fresh concrete density in accordance with EN 12350-6 (European Standard, 2009a), and slump-flow and flow time t500 in accordance with EN 12350-8 (European Standard, 2010a), as well as LCPC box measurements (Roussel, 2007). The results of these tests are presented in Table 5.2. No results are given for slump-flow after fibre addition because of difficulties in filling the cone due to its incompatibility with the fibre size, and the concrete tested was therefore not representative.

Table 5.2 Fresh concrete properties.

Test	Batch 'a'	Batch 'b'
Before fibre addition:		
Slump-flow	730 mm	725 mm
t500 (+/-0.2 s)	2.8 s	2.8 s
After fibre addition:		
Density	2359 kg/m^3	2508 kg/m^3
Air content	3.7%	1.1%
LCPC box test		
Tested volume	6.0 l	5.7 l
Spread length in the box	55 cm	51 cm
Thickness of the sample at the extremity of the box	6.5 cm	7.5 cm
Yield stress	63 Pa	92 Pa

5.2.2 Specimens and casting procedure

The specimens from each batch (denoted 'a' and 'b') comprised casting of:

- three full-scale beams with dimensions of 200 mm × 300 mm × 3000 mm. The first was used to extract sawn prisms and drilled cores (see below and Fig. 5.1). The other two were put through bending tests; one had fibres only (FSB), and the other also had a reinforcing bar of Ø20 mm (FSRB)
- six cylinders with dimensions of Ø150 mm × 250 mm cast in moulds (CF1-CF6) for uniaxial tension testing
- six standard beams with dimensions of 150 mm × 150 mm × 550 mm in accordance with EN 14651 (European Standard, 2005), three of which were for testing at the same age as the full-scale beams (BF1-BF3), while the other three (BF4-BF6) were for testing at the same age as the cylinders and sawn beams.

From the first full-scale beam, the following specimens were obtained:

- five cores with dimensions of Ø150 mm × 160 mm, three of which were drilled horizontally (CSH1-CSH3) while the other two were drilled vertically (CSV1, CSV2), all for uniaxial tension testing
- three sawn beams with dimensions of 150 mm × 150 mm × 550 mm (BS1-BS3).

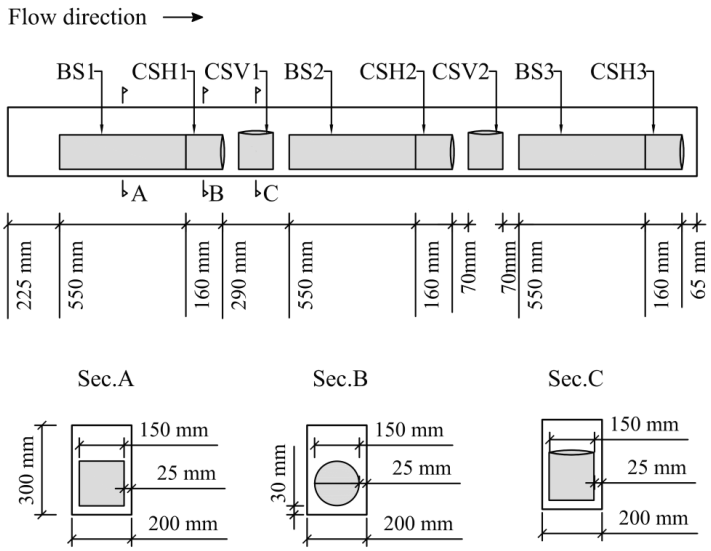

Fig. 5.1. Location of sawn beams and drilled cores.

The full-scale beams were cast with a falling stream of concrete from a single discharge, which was initially located at one end. When approximately 70% of the formwork was filled, the casting point was moved towards the centre of the beam to completely fill the formwork. Standard beams were cast using the layered method described in EN 14651 (European Standard, 2005). The cylinders for uniaxial tension testing were cast as described in EN 12390-3 (European Standard, 2009c). No mechanical compaction was applied to any of the specimens.

After casting, the specimens were covered with plastic sheets and stored at room temperature for 24 h. The formwork and moulds were then removed. Small-scale specimens were stored in a water tank, while full-scale beams were kept in moist conditions until testing.

5.2.3 Test methods

The full-scale beams were loaded using a hydraulic jack acting on a steel profile that transferred the load to two loading points spaced 800 mm apart (Fig. 5.9). A constant displacement rate of 1 mm/min was applied and the logging speed was set to 1 Hz. The deflection at midspan was measured by displacement transducers attached to the bottom face of the specimens.

Uniaxial tension tests of the cylinders were conducted based on the RILEM recommendations (RILEM, 2001). After preparation, the cylinders had dimensions of

Ø150 mm × 150 mm and a circumferential notch with a depth of 15 mm. The cast cylinders, whose original height was 250 mm, were first sawn to reduce the height to 155-160 mm. Then, both cast cylinders and drilled-core cylinders were ground down to the final height (150 mm) to ensure proper contact with the testing plates. The cylinders were glued "in situ" to metal plates connected to the testing machine with rigid bolted connections. Three extensometers measured the strain across the notch with a gauge length of 35 mm.

The testing machine was not able to adopt a closed-loop control using the extensometers at the notch. The test was therefore run with deformation control of the upper crosshead of the machine with the rates: 50 μm/min up to an average displacement in the notch of 0.1 mm and 100 μm/min until the completion of the test. The system was not able to avoid the sudden opening at the onset of cracking. Nevertheless, the average displacement rates in the notch before and after the sudden crack were recorded as ~1 μm/min and ~100 μm/min, respectively, which are values within the limits recommended in RILEM (2001).

Three-point bending tests of the standard beams and sawn beams were performed in accordance with EN 14651 (European Standard, 2005). Standard beams were rotated 90º around their longitudinal axis and then notched through the width at midspan. Beams sawn from a full-scale specimen were notched in the lowest edge in their position within the full-scale beam.

5.2.4 Determination of fibre orientation and distribution

X-ray Computed Tomography (CT) has been successfully used as a non-destructive method for the qualitative and quantitative evaluation of the orientation and distribution of steel fibres in FRC (Stähli et al., 2008, Švec et al., 2014, Sarmiento et al., 2014a, Fuentes et al., In press). CT scanning of an element produces a large number of radiographic images, and digital analysis of the sequence of images allows 3D visualization of the structure of fibres. Moreover, post-processing the images to a skeleton converts fibres to 3D segments located in the volume from which their topology, length and direction can be extracted.

Such information allows us to describe the fibre orientation pattern of the element using a set of second-order orientation tensors defined over a set of discrete volumes of the element (Advani and Tucker, 1987, Ferrara et al., 2011, Şanal and Özyurt Zihnioğlu, 2013, Švec et al., 2014). Each orientation tensor defines the fibre orientation state within the discrete volume and can be defined as:

$$\mathbf{A}=\frac{\sum_i^N L_i \mathbf{p}_i \mathbf{p}_i{}^T}{\sum_i^N L_i} \tag{5.1}$$

where **A** is the orientation tensor, N the number of fibres found in the volume, $\mathbf{p}_i$ the unit vector in the direction of the fibre i, and L_i the length of that fibre. By definition, the orientation tensor has the properties of being symmetric and having normalized components. Symmetric second-order tensors can be visualized using 3D ellipsoids, where the eigenvectors and eigenvalues give the direction and half-length of the principal axes of the ellipsoids. In this way, ellipsoids are used as a visual tool to identify the direction of the fibres in each discrete volume.

The eigenvector associated with the largest eigenvalue of each tensor represents the "dominant" direction of the fibres in each discrete volume. The orientation with respect to a plane can therefore be described with the out-of-plane angle θ, or simply with $\cos\theta$, which can be determined as:

$$\cos\theta=\mathbf{a_1}\cdot\mathbf{n}\,, \quad (\|\mathbf{a_1}\|=\|\mathbf{n}\|=1) \tag{5.2}$$

where $\mathbf{a_1}$ is the eigenvector associated with the largest eigenvalue of tensor **A**, **n** is the unit vector normal to the plane, and θ is the angle between the two unit vectors.

The fibre volume fraction (v_f) can be computed for each discrete volume as:

$$v_f=\frac{\sum_i^N L_i A_f}{V_c} \tag{5.3}$$

where A_f is the fibre cross-section area and V_c the discrete concrete volume.

The described procedure was used to represent the orientation and distribution pattern of a structural element by choosing a specific discretization of the element in volumes and defining **A** and v_f for each discrete volume.

A medical CT scanner (Siemens SOMATOM Sensation 4) was used to scan a total of 38 specimens. All small-scale specimens were scanned entirely before being tested. Full-scale beams were tested first, and then parts of the beam of 400 mm in length near the failure crack (Fig. 5.9) were sawn and scanned.

5.3 Results and discussion

This section describes the results of the experimental programme and discusses the following aspects with regard to the mechanical characterization tests: the test method, either uniaxial or three-point bending; and the type of specimen, either cast beams (cast cylinders) or sawn beams (drilled cores). With regard to structural application, the fibre

configuration results are examined to explain the difference in the response of the full-scale beams. Finally, the limitations of using test results from small-scale specimens for the prediction of structural behaviour are discussed.

In the following, the endings -a and -b in the names of parallel specimens differentiate them by batch.

5.3.1 Uniaxial tension testing of notched cylinders

The results of the uniaxial tension tests measured using the three extensometers are presented in Fig. 5.2, expressed as tensile stress versus average strain. All the curves depicted in this figure are from cylinders from batch 'a'. Cylinders from batch 'b' gave very similar responses and are omitted to avoid repetition.

All the cylinders presented linear behaviour until cracking occurred, typically after reaching 3.8 MPa. This was the average value for the 22 cylinders tested, with a coefficient of variation (CV) of 18%. At this stage, a single crack arose in the notched section. The constant displacement rates of the test procedure caused a sudden and unstable opening of the crack. However, the control of the test was regained at a small crack width. This is reflected in the abrupt drop in stress in Fig. 5.2.

Post-cracking behaviour varied greatly between the specimens. In Fig. 5.2, results are grouped in cylinders cast in a mould (Fig. 5.2a) and cores drilled from a full-scale specimen (Fig. 5.2b). The six cast cylinders in Fig. 5.2a sustained nearly constant stress up to the termination of the test. For a crack width of 2.5 mm, the average residual strength of these cylinders was as low as 1.0 MPa. This low value is as remarkable as the fact that its CV is above 66%.

As expected, large differences were observed between the responses of horizontally and vertically drilled cores. There was also large variation in the responses within the group of horizontally drilled cylinders and within the group of vertically drilled cylinders. This suggests a non-uniform fibre orientation and distribution in the full-scale specimen from which the cores were drilled. This is discussed in more detail later in the paper. For both batches, the tests of cylinders CSH2 (see Fig. 5.1 for location) were interrupted when the testing plate at the top separated from the sample. A posterior analysis showed that the failure occurred in the concrete immediately in contact with the glue, when the tensile stress of both cylinders was above 5.3 MPa.

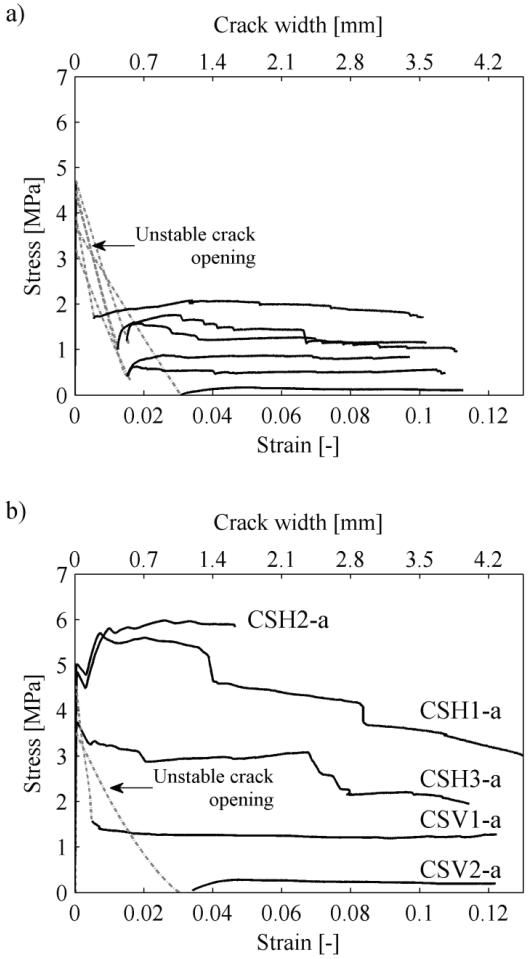

Fig. 5.2. Results of uniaxial tension tests for a) cast cylinders and b) drilled cores from batch 'a'.

The parameters that describe fibre orientation ($\cos\theta$) and distribution (v_f) in this research are listed in Table 5.3. In each sample, $\cos\theta$ and v_f represent the fibre parameters in a transverse slice located in the middle of the specimen with a thickness of the fibre length (60 mm). The out-of-plane angle θ is defined with respect to the plane that contains the notched section.

Table 5.3 Cosine of out-of-plane angle (cosθ) and fibre volume fraction (v_f) for small-scale specimens.

	cosθ	v_f [% vol.]		cosθ	v_f [%. vol.]
Cast cylinders			Horizontally drilled cores		
CF1-a	0.3	1.4	CSH1-a	1.0	2.3
CF2-a	0.0	1.5	CSH2-a	1.0	1.9
CF3-a	0.2	1.1	CSH3-a	0.8	2.3
CF4-a	0.1	1.4	CSH1-b	0.7	2.0
CF5-a	0.1	1.4	CSH2-b	1.0	2.3
CF6-a	0.2	1.5	CSh.3-b	0.9	1.7
CF1-b	0.3	1.6	Average	0.9	2.1
CF2-b	0.1	2.2	CV	11%	11%
CF3-b	0.1	1.8	Vertically drilled cores		
CF4-b	0.4	2.4	CSV1-a	0.6	2.2
CF5-b	0.2	1.8	CSV2-a	0.1	2.0
CF6-b	0.1	2.2	CSV1-b	0.0	2.5
Average	0.2	1.7	CSV2-b	0.1	2.5
CV	62%	23%	Average	0.2	2.3
			CV	103%	10%
Standard beams			Sawn beams		
BF4-a	1.0	2.2	BS1-a	0.8	2.3
BF5-a	1.0	1.8	BS2-a	0.9	1.7
BF6-a	1.0	1.9	BS3-a	1.0	1.5
BF4-b	1.0	1.6	BS1-b	1.0	1.9
BF5-b	1.0	1.9	BS2-b	1.0	2.2
BF6-b	1.0	1.8	BS3-b	1.0	1.9
Average	1.0	1.9	Average	0.9	1.9
CV	0%	9%	CV	6%	15%

Fig. 5.3 illustrates a skeleton of fibres, orientation ellipsoids, and a typical crack surface for each of the three main groups of cylinders tested. The skeleton of only half a cylinder is shown to avoid the presence of too many fibres in the image.

The low post-cracking response of the cast cylinders can be explained by their rather low fibre volume fraction and unfavourable fibre orientation. Fig. 5.3a shows that the ellipsoid in the centre approximates a horizontal disc, which indicates a random orientation of fibres in a plane parallel to the notched cross-section.

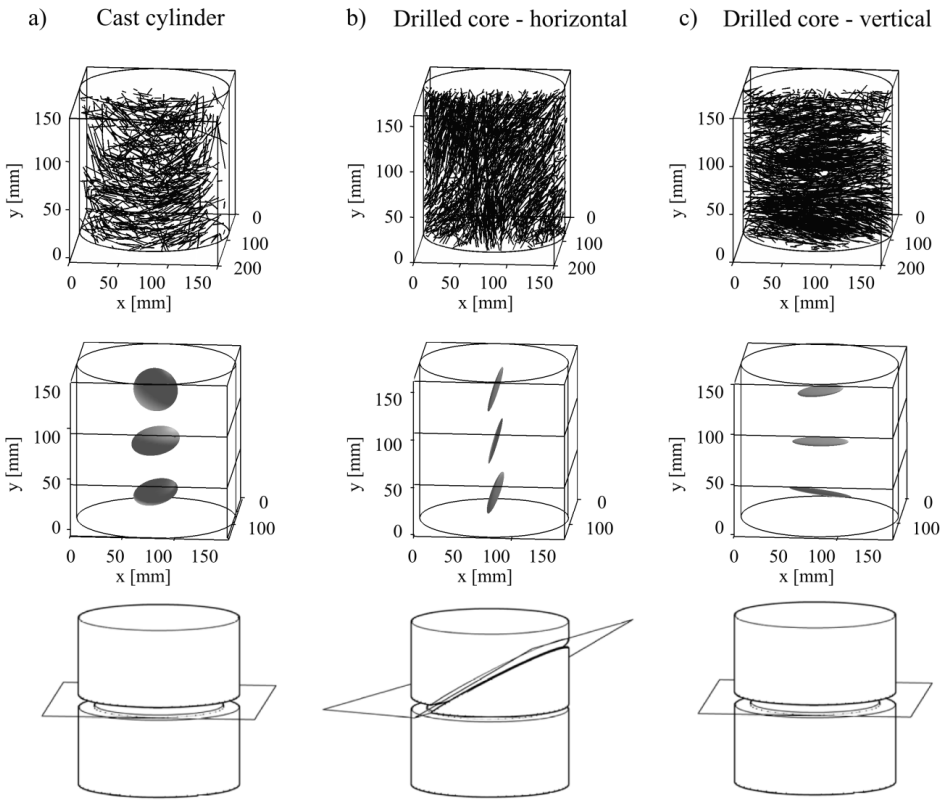

Fig. 5.3. From top to bottom: the skeleton of fibres, orientation ellipsoids, and sketch of typical fracture surface from a) a cast cylinder, b) a horizontally drilled core, and c) a vertically drilled core.

The favourable and unfavourable orientation of fibres in horizontally and vertically drilled cores is made evident in Fig. 5.3b and c, respectively. The more prolonged shape of the ellipsoids in Fig. 5.3c indicates an unidirectional orientation of fibres that differs from that of Fig. 5.3a, even though this results in low residual tensile stress in both cases.

Cores with a high post-cracking response developed multiple cracks that later localized to form a crack surface outside the notched section. In these cases, the average of the strains in Fig. 5.2 was calculated only with the extensometers crossing the dominant crack. This problem could probably be avoided by increasing the depth of the notch.

5.3.2 Three-point bending tests of notched beams

Fig. 5.4 shows the results of three-point bending tests of notched beams expressed as flexural tensile stress versus deflection at midspan. The curves for standard beams are grouped, while the curves for sawn beams BS1-BS3 (see Fig. 5.1 for locations) are depicted separately. In this case, the results of the two batches are presented (in Fig. 5.4a and b, respectively), because there were some differences between them. In the following discussion, the flexural tensile strength f_{R3} is used as a reference value for the post-cracking capacity. This stress corresponds to a crack mouth opening displacement of 2.5 mm, which compares with a deflection at midspan of 2.17 mm. Here it is assumed that the crack widths of the micro-cracks that formed in addition to the main crack were negligible.

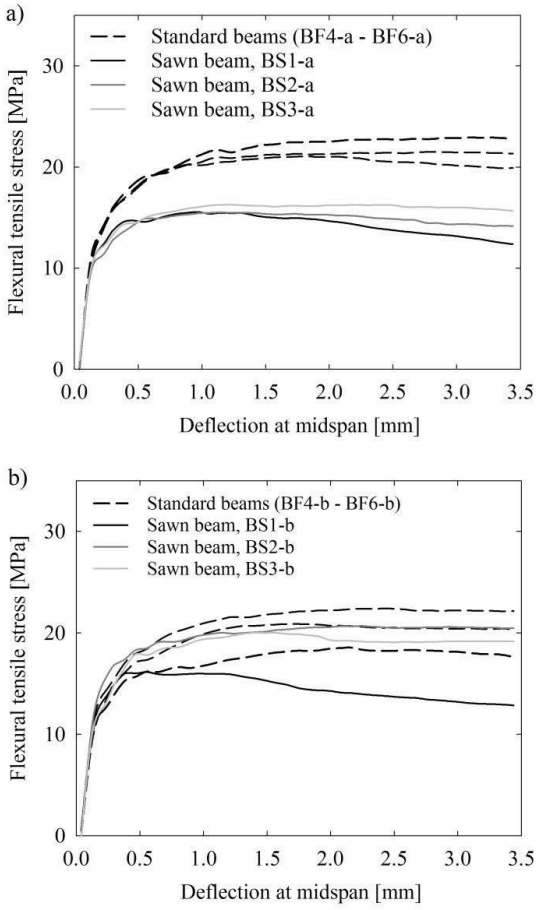

Fig. 5.4. Results of bending tests for standard beams and sawn beams from a) batch 'a' and b) batch 'b'. All the beams were tested on the same day.

In general, all test results indicate high ductility and a deflection-hardening response. The standard beams had an average flexural strength (f_{R3}) of 21 MPa with a relatively low scatter (CV = 7.3%). Usually, the use of macro fibres leads to a large scatter in the results of standard three-point bending tests. This is because the number of fibres crossing the fracture surface for small cross-sections is usually small with high statistical variation (Buratti et al., 2011). High fibre content seems to reduce this variation, which results in a reduction of the scatter despite the small size of the cross-section.

The set of sawn beams had an average f_{R3} of 17 MPa with a larger scatter than the standard beams (CV = 16.5%). The results for $\cos\theta$ and v_f in Table 5.3 cannot directly explain the differences in the post-cracking response between these beams. One possible reason for the differences may be that the fracture process in the sawn beams did not occur with a single crack growing vertically, but with multiple cracks that eventually localized in an inclined or tortuous critical crack. In many cases therefore, the fracture surface was not included in the volume for which $\cos\theta$ and v_f from Table 5.3 were assessed. The reason the critical crack inclines is discussed in the following.

The various crack patterns of the sawn beams are illustrated in Fig. 5.5 together with the skeleton of fibres. The skeleton of fibres is shown only in a longitudinal slice with a thickness of 20 mm to avoid too dense an image. At any point of the beam, the fibres seem to have a generally pronounced unidirectional orientation. However, the orientation varies greatly along the length of the beam, and the overall observation is that the fibres are aligned in full-scale beams following wavy (sinuous) flow lines. One tentative explanation for this is that the fibres may have oriented locally due to the discharge of concrete into the formwork and have been driven on mainly in plug-flow layers (Spangenberg et al., 2012a). In such layers, the material behaves like a solid and fibres keep their initial orientation. In the sheared zones close to the mould, the rotation of fibres due to shear stresses (Boulekbache et al., 2010, Ferrara et al., 2011) may have been partly hindered by direct interactions between the large number of fibres in this concrete (Martinie and Roussel, 2010).

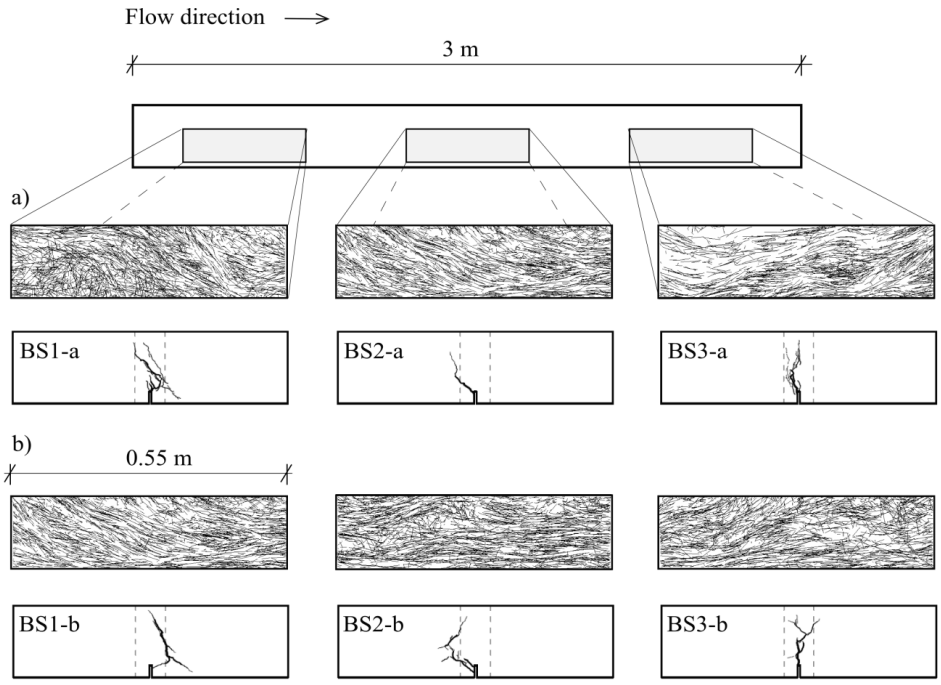

Fig. 5.5. The skeleton of fibres and the crack pattern for sawn beams from a) batch 'a' and b) batch 'b'.

The structural consequence of this particular fibre configuration can be seen in the crack pattern of the sawn beams: the fracture surface bends to find weakness paths instead of developing vertically along the ligament ahead of the notch. This is especially evident for beams BS1-a, BS2-a and BS1-b in Fig. 5.5, where the crack inclinations clearly agree with the orientation of the fibres.

Unlike the sawn beams, the standard beams generally showed vertical cracking. To investigate the reason for this, Fig. 5.6 compares the orientation and distribution patterns for two representative examples of standard and sawn beams. Ellipsoids and volume fractions were plotted in small discrete volumes to observe local changes. The figure also includes fibre skeletons and crack patterns.

The fibre content varies within reasonable limits in both types of beam (see colour maps of v_f in Fig. 5.6). The plot of the sawn beam indicates the presence of inclined bands with greater fibre density. These bands follow the inclination of the fibre skeletons, which could be related to the plug-flow layers discussed above.

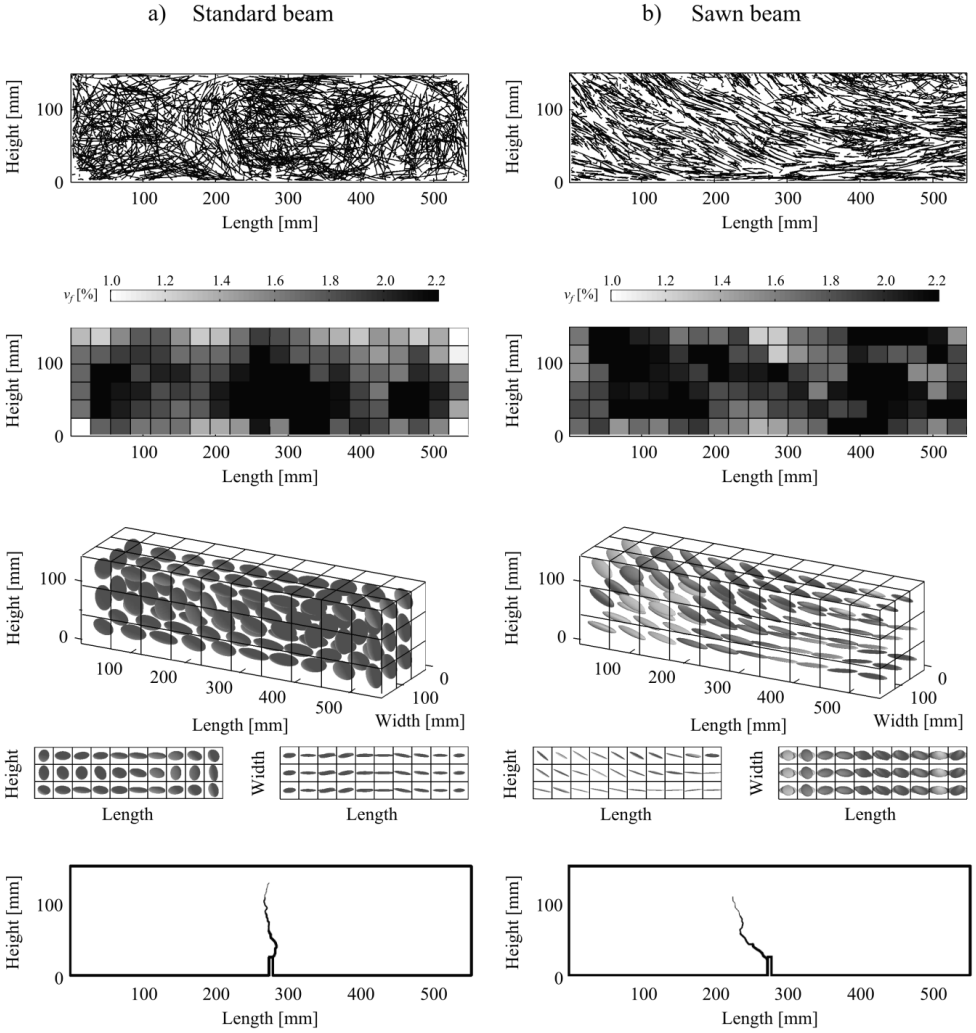

Fig. 5.6. From top to bottom: the skeleton of fibres, fibre volume fraction, orientation ellipsoids, and crack pattern from a) a standard beam, and b) a sawn beam.

The fibre skeletons reveal large differences between the two specimens. The orientation ellipsoids in Fig. 5.6a are like thick ellipses in the height-length plane, but elongated in the width-length plane. This means that fibres in standard beams are distributed in vertical planes, which are actually horizontal planes in view of the casting direction. This is represented in Fig. 5.7a for an ideal situation in which the transversal component of the direction of all fibres is zero, and the ellipsoids therefore have no thickness in that direction. Fibres adopt this orientation due to physical contacts with the mould.

In contrast, the orientation ellipsoids in the sawn beams (Fig. 5.6b) are elongated in the height-length plane, while thick in the width-length one. This means the fibres are distributed in planes that extend transversal to the beam (Fig. 5.7b). This has an impact on the bending test: cracks propagate following a weak surface parallel to the fibres, where they find low resistance because very few fibres bridge this path. This explains the differences in the crack patterns between the two groups.

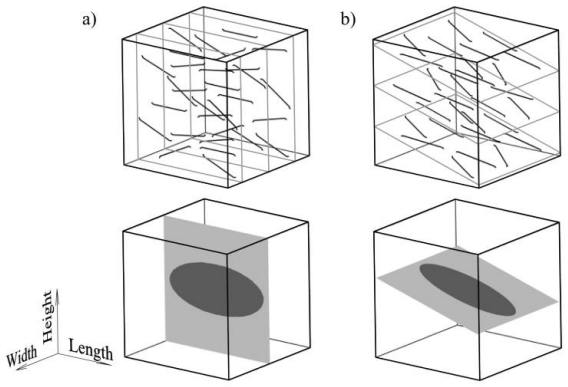

Fig. 5.7. Fibres distributed in planes that approximate the fibres a) in standard beams and b) in sawn beams.

It is worth mentioning that fibres distributed in the outermost part of the sawn beams are cut, which means not only a reduction of the length of the fibres, but also the loss of the hooked-end. This explains the lower post-cracking response of the sawn beams (Fig. 5.4), besides the fact that their cracks easily propagate following the weak transversal surfaces.

5.3.3 Full-scale beams

Fig. 5.8 shows the load-deflection relationships for the four full-scale beams. The beams from the two batches are identical, but the flexural behaviour of beams from batch 'b' was typically lower than that of beams from batch 'a'. Dissimilarities were also evidenced in the observed cracking patterns at the end of the test (Fig. 5.9).

In the beams with an ordinary reinforcing bar (FSRB), flexural cracks first formed within the constant-moment region (central span), and progressed to form a dense crack pattern. In beam FSRB-a, cracking localized in a diagonal crack that opened in the shear-span and bent approximately 45º approaching one of the loading points. Judging by the inclination, the crack seemed typical of a shear-flexure failure. In contrast, the decisive crack in beam FSRB-b emerged within the central span and propagated

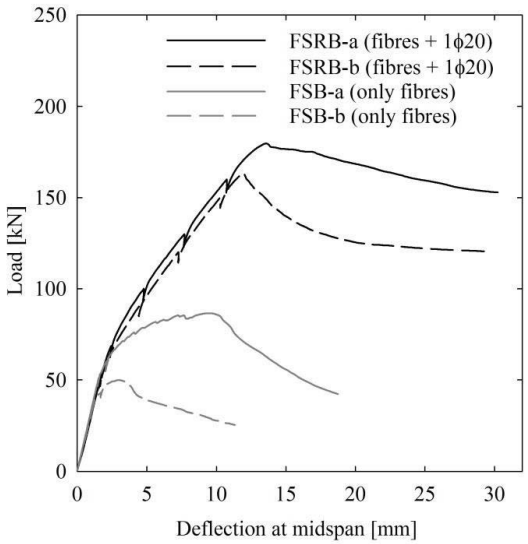

Fig. 5.8. Results of bending tests for the full-scale beams.

approximately vertically. In both cases, localization of the crack led to a reduction in load capacity. While maximum applied loads varied by about 10%, the difference was 27% at a deflection-span ratio (δ/L) of 1/100. The fibres seem therefore to have a different effect on the flexural response of the two specimens.

The deviation in the flexural response was even greater for the beams with only fibres (FSB). In beam FSB-a, several flexural cracks developed, mostly in the central span. Because of the absence of ordinary reinforcement, these cracks were only arrested by the fibres. After cracking, the load still increased 27% up to $\delta/L = 1/280$. From this deflection, damage localized in one crack and the load decreased. During the flexural failure, the beam exhibited a certain ductility; at $\delta/L = 1/150$ the beam was supporting approximately half of its maximum capacity. The critical crack arose within the central span, developed vertically, and merged with multiple inclined cracks resulting in a diffuse and tortuous path. Beam FSB-b had much lower capacity than beam FSB-a. The applied load at the onset of cracking was lower than for all the other beams, and led to a sudden failure along a single crack. This crack started 17 cm from midspan, and grew at an angle of 60º to the longitudinal direction, away from the centre of the beam.

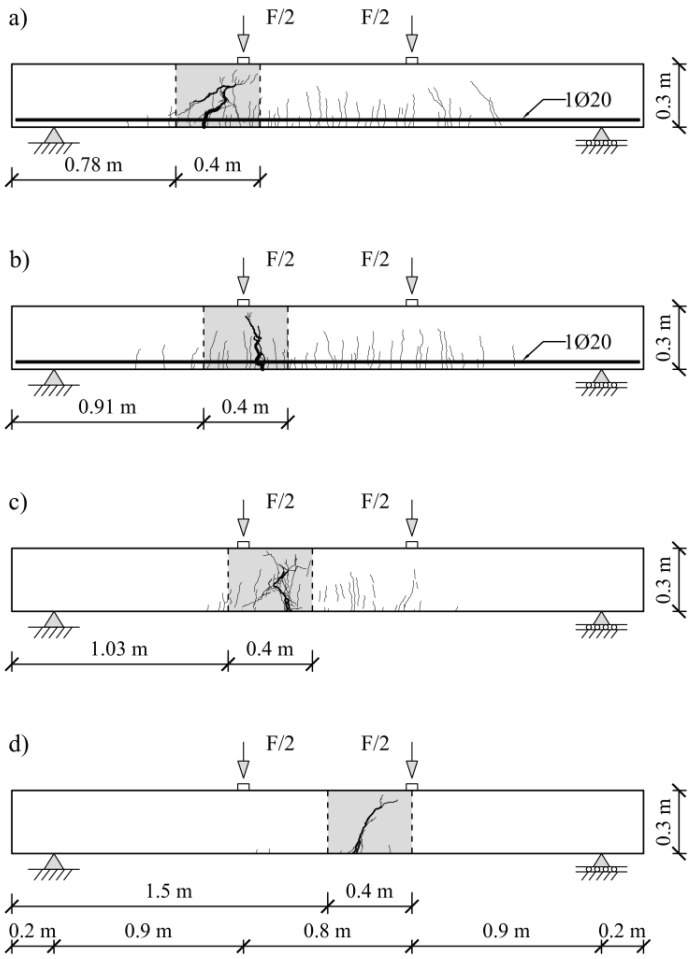

Fig. 5.9. Experimental test setup and crack patterns for the four full-scale beams: a) FSRB-a, b) FSRB-b, c) FSB-a, and d) FSB-b. The shading depicts the region that was CT-scanned.

The specific configuration of the fibres in the beams greatly affected the cracking pattern and loading capacity. To underline this, Fig. 5.10 shows a comparison of the fracture regions near the critical crack for beams reinforced only with fibres. The findings based on beams FSB-a and FSB-b are basically valid and representative for beams FSRB-a and FSRB-b as well.

The fibre skeletons provide a first insight into the inhomogeneity of the fibres, which seem to align in full-scale beams following wavy flow lines. This feature was already anticipated with the sawn beams, but here it was detected for the entire height of the beams.

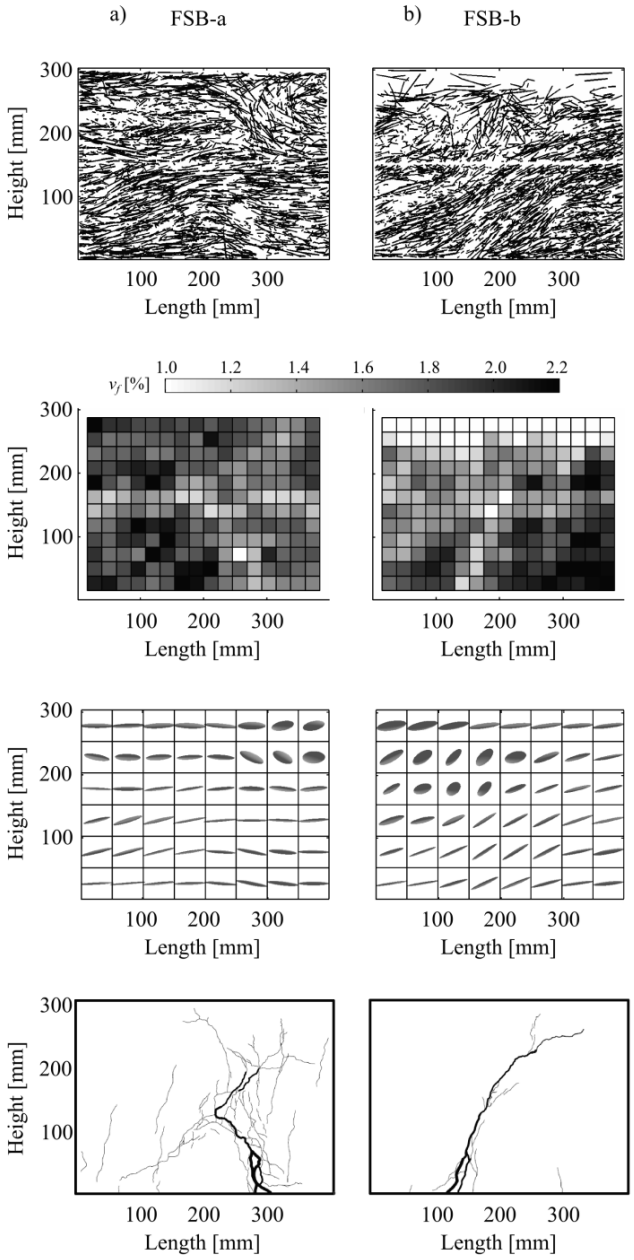

Fig. 5.10. From top to bottom: the skeleton of fibres, fibre volume fraction, orientation ellipsoids, and crack pattern in the critical fracture region of full-scale beams with fibres only: a) FSB-a and b) FSB-b.

In a more descriptive way, the colour maps representing the volume fraction indicate the presence of areas with low fibre content. Both cases show that these areas form bands that might be related to the concrete distributed in plug-flow layers. Moreover, beam FSB-b has a low density of fibres at the top, indicating that segregation of fibres has occurred. The maps of orientation ellipsoids show the same trend as the sawn beams: mainly elongated ellipsoids in the height-length plane and thick in the width-length plane. Fibres are therefore distributed in planes that extend transversal to the beam.

In both examples, the critical crack initiated at the bottom of the beam at a point with low fibre content, and then the crack propagated along a band with low fibre content and parallel to the direction of the fibres. This is clear in FSB-b (Fig. 5.10b), where a well-defined inclination of the ellipsoids coincides with the inclination of a band with low fibre density. This defines a distinctly weak surface and explains why the crack emerged and grew rapidly in that direction.

Unlike FSB-b, beam FSB-a did not present an in-plane weak surface that extended all along the height of the beam. Instead, the crack rotated following a discontinuous band with low fibre content and merged with other inclined cracks that formed parallel to the direction of fibres. This diffuse and tortuous fracture of FSB-a activated a larger number of fibres than the failure of FSB-b. This seems to explain the greater load-carrying capacity and more ductile behaviour of FSB-a compared with FSB-b.

5.3.4 From characterization tests to structural application

Several disadvantages are associated with the uniaxial tension test of cylinders to characterize the material. On the one hand, the fibres in cylinders cast in a mould adopt an unfavourable orientation that is not representative for the orientation in full-scale beams. Moreover, filling small moulds with 60 mm fibres complicates adequate sampling and causes large variations in the fibre content between the cylinders (Table 5.3), and a large scatter in the test results (Fig. 5.2). On the other hand, while fibres in drilled cores are without a doubt representative of the full-scale application, it was observed in this study that the fibre configuration varies greatly within a full-scale beam, so the tensile response of such small cores is very much influenced by their location within the beam, and naturally by the drilling direction. The uniaxial tension test also presents functional difficulties when the crack is localized outside the notched area. For all these reasons, the uniaxial tension test is not recommended as a practical and reliable test method for characterization of flowable FRC with high fibre content.

Three-point bending tests also present difficulties connected with the type of specimen. The constrained casting conditions in standard beams, and the 90º rotation around their longitudinal axis, mean that fibres are not distributed in planes that extend transversal to

the beam, as seen in full-scale beams. Instead, fibres distribute in vertical planes, which contributes to their high residual strength in bending.

Sawn beams naturally have a fibre orientation representative of full-scale beams, but their fibre configuration still depends on the location in which they are sawn. Most importantly, due to the presence of the notch, the critical crack does not emerge in the locally weakest section as it does in a full-scale test. This is of paramount importance for a highly reinforced concrete that exhibits inhomogeneity of fibres at the structural level.

In Fig. 5.11, the results from the three-point bending tests are used in a sectional analysis to model the bending of full-scale beams. The tensile behaviour of FRC is defined with a simplified elasto-plastic model. The residual flexural strength f_{R3} is used to define the uniaxial residual tensile strength (f_{Ftu}) in accordance with the relationship $f_{Ftu} = f_{R3}/3$ (*fib*, 2010). An initial elastic branch with elastic modulus of 30 GPa is considered up to f_{Ftu}, disregarding the effect of cracking. Only the standard beams BF1-BF3 for each batch, six in total, were tested at the same age as the full-scale beams, i.e. at 28 days. Their average f_{R3} was 18 MPa, which was lower than the average for the standard beams BF4-BF6 discussed in Section 5.3.2 (f_{R3} = 21 MPa), most likely due to the age of the latter beams at the moment of testing. The compressive behaviour is defined with a parabola-rectangle model. A compressive strength of 86 MPa was determined experimentally. For the ordinary reinforcement, the yield stress was tested to be 520 MPa, and the elastic modulus was assumed to be 200 GPa.

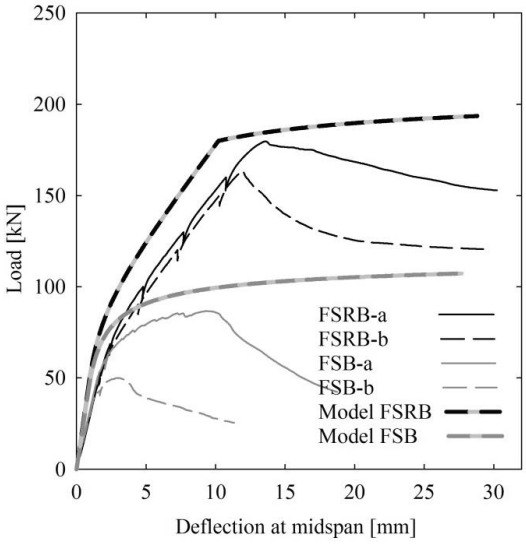

Fig. 5.11. Results of the experimental and modelled bending tests of the full-scale beams.

In Fig. 5.11, the modelled curves overestimate the experimental pre-peak region and maximum load. This is the consequence of f_{Ftu} being too high because it is defined from the results of standard beams, where is it high mainly due to the factors discussed above: an unrepresentative fibre orientation, and the presence of the notch. Moreover, the modelled curves do not capture the reduction of the applied load associated with the crack localization. This is mainly because the models do not take into account the inhomogeneity of the material, which is the actual cause of crack localization and load reduction in the full-scale beams.

5.4 Conclusions

The results presented in this investigation have shed light on the structural performance of flowable FRC with high fibre content. The mix investigated had 2% vol. of 60 mm steel fibres. Full-scale application of the mix exhibited lower capacity and ductility than expected from three-point bending testing.

Analysis of the fibre distribution and orientation confirmed that casting under full-scale conditions induced inhomogeneities: fibres oriented in accordance with flow lines, and some areas had low fibre content. The bending performance of the full-scale beams confirmed that load-carrying capacity and ductility are very sensitive to such inhomogeneities. During loading, the orientation of fibres and areas with low fibre content played an important role in the crack propagation, and the reduction in load-carrying capacity was the result of the activation of cracks following weakness paths.

Small test specimens showed limitations in predicting the mechanical behaviour of the full-scale beams. Uniaxial tension tests of notched cylinders provided results which strongly depended on the fibre configuration in the notched section. Three-point bending tests of notched beams generally gave somewhat better results, but the favourable distribution of fibres in standard beams contributes to the overestimation of the capacity of full-scale beams. Sawing test beams ensures a representative fibre orientation and distribution, but the presence of the notch reduces the dependence of the mechanical response on the fibre configuration, which proved decisive at the structural level.

For the above-mentioned reasons, small-scale tests should only be used to evaluate the potential quality of flowable FRC with high fibre volume. In addition to robust mixes, methods for the detection or prediction of fibre configuration in full-scale applications are needed.

Acknowledgements

The authors wish to acknowledge support from COIN – the Concrete Innovation Centre (www.coinweb.no) – a centre for research-based innovation, which was initiated by the Research Council of Norway (RCN) in 2006 for an eight-year period. The Centre was directed by SINTEF, with NTNU as a research partner, and the most recent industrial partners included Aker Solutions, Norcem, Norwegian Public Roads Administration, Rescon Mapei, Skanska, Unicon, Veidekke, and Weber Saint Gobain.

Chapter 6

Combined effect of fibre orientation and volume fraction

Paper III

Impact of the combined effect of fibre orientation and volume fraction on the mechanical properties of fibre reinforced concrete

E.V. Sarmiento, T. Kanstad, M.R. Geiker & M.A.N. Hendriks
In: *Proceedings of the XXII Nordic Concrete Research Symposium, Reykjavik, Iceland.* Norsk betongforening, Oslo, Norway; 2014. p. 141-144.

Abstract
Variations in the fibre orientation are generally accepted to have great impact on the mechanical performance of fibre-reinforced concrete (FRC), while less or no attention is generally paid to local variations of the fibre volume fraction. The present paper discusses the applicability of a single parameter, the fibre efficiency μ, integrating contributions of both the fibre orientation and the local volume fraction, to be related to the post-cracking response of the material. The formulation of the fibre efficiency parameter allows the evaluation of the impact of the two contributions. The results demonstrate that the volume fraction, and not exclusively the orientation, has a great impact on the mechanical response of FRC.

Key words
Fibres, SCC, Structural design, Fibre efficiency

6.1 Introduction

The heterogeneity of FRC is often accounted for in the prediction of the post-cracking response of the material by evaluating variations in the fibre orientation, see e.g. Ferrara et al. (2011), Grünewald et al. (2012) or Švec et al. (2014). However, less or no attention is paid to the significance of local variations of the fibre volume fraction, assuming that a uniform distribution of fibres is generally achieved. The present paper discusses the need to incorporate the contributions of both the local fibre orientation and the local volume fraction in the relationship with the mechanical performance of FRC.

6.2 Materials and methods

6.2.1 Experimental set

An experimental series is presented to illustrate the relationship between the local performance of fibres and the residual strength. The series includes 18 beams with dimensions 0.6 m × 0.15 m × 0.15 m. The fibre reinforcement corresponded to 40 kg/m^3 (0.5% vol.) of hooked-end steel fibres. The length and diameter of fibres were 60 mm and 0.75 mm, respectively. The beams were sawn at different locations from a total of 6 slabs (1.2 m × 1.2 m × 0.15 m) cast with a fixed discharging point. A radially spread flow, characteristic from casting slabs (Ferrara et al., 2011, Abrishambaf et al., 2012), aligned fibres orthogonally to the flow. As a result, the sawn beams cover a wide range of different fibre distribution and orientation. A description of the mix design, casting process and fresh concrete properties can be found in Švec et al. (2014).

All specimens were scanned by means of a Computed Tomography (CT) scanner. The scanned images were post-processed to compute the position of all fibres. The mechanical response in flexure was studied by performing three-point bending tests according to EN 14651 (European Standard, 2005). In order to capture the structural effect due to differences in the fibre distribution, the beams were tested with the bottom cast surface on the tensile edge. Large variations of the residual flexural strength were registered between the specimens (CV = 41% for the residual flexural strength at 2.5 mm crack width). The basis of this large scatter must be ascribed to variations of the fibre dispersion. Relating the local fibre properties to the residual flexural strength is the main objective of the proposed approach.

6.2.2 The fibre efficiency parameter

The fibre efficiency parameter μ is proposed by the authors in order to link the local fibre properties to the mechanical performance of the material. The parameter incorporates the contributions of both the fibre orientation and the local volume fraction, and is formulated as the linear combination:

$$\mu = w_1(\alpha) + w_2\left(\frac{v_f}{\overline{v_f}}\right) \tag{6.1}$$

where w_1 and w_2 are normalized weights (with $w_1+w_2 = 1$) for the orientation and volume fraction components, respectively; α is the orientation term, v_f is the local volume fraction; and $\overline{v_f}$ is the volume fraction for the concrete batch. In absence of any digital information of the fibres (Žirgulis et al., 2013), fibre orientation can be deduced from the formulation by Soroushian and Lee (1990), which relates orientation to fibre counts over cross-sections. Local volume fraction can be assessed by separating fibres from a crushed concrete slice.

When the locations of the fibres in a specimen are known, as it is after a CT-analysis, local volume fractions can be directly computed and the fibre orientation of a certain volume can be described by the second-order orientation tensor (Advani and Tucker, 1987, Ferrara et al., 2011, Şanal and Özyurt Zihnioğlu, 2013, Švec et al., 2014). The efficiency of fibres on bridging a crack depends on their orientation with respect to the crack plane. This relative orientation refers to the angle between the dominant fibre direction and the direction normal to the crack plane, which is formulated as:

$$\cos\theta = \mathbf{a}_1 \cdot \mathbf{n} \tag{6.2}$$

where $\mathbf{a}_1$ is the eigenvector associated to the largest eigenvalue of the orientation tensor, $\mathbf{n}$ is the vector normal to the crack plane, and θ is the angle between the two vectors. Under these conditions, Eq. 6.1 can be reformulated as:

$$\mu = w_1(\cos\theta) + w_2\left(\frac{v_f}{\overline{v_f}}\right) \tag{6.3}$$

6.3 Results and discussion

In this section a linear relationship between the residual flexural tensile strength f_{R3} and the fibre efficiency parameter μ is proposed for the present series of beams. f_{R3} is the flexural strength at 2.5 mm crack mouth opening displacement obtained during the three-point bending test. The relationship μ - f_{R3} is deduced from the linear regressions of the experimental data set.

Processing the results from CT-scan provides the fibre orientation and volume fraction for any discrete volume of a specimen. Four alternative volumes in the vicinity of the notch (Fig. 6.1) were studied in order to define the relevant volume in which fibre properties and, therefore μ, must be assessed to be related to the mechanical properties of the material. As an example, the results from one of the beams are presented in Table 6.1, where differences between the zones relate mainly to the volume fraction, most likely caused by the downward settlement of fibres.

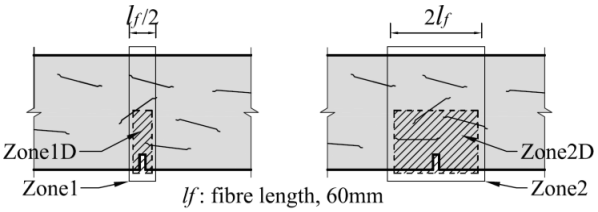

Fig. 6.1. Alternative volumes considered for defining parameter μ. The zones extend over the thickness of the specimen.

Table 6.1. Fibre orientation (cosθ) and volume fraction (v_f) over the different zones.

Zone	cosθ	v_f (%)
Zone 1	0.68	0.40
Zone 1D	0.66	0.53
Zone 2	0.70	0.39
Zone 2D	0.67	0.49

The relative impact of the contribution from orientation and from volume fraction in the relationship with the mechanical properties can be studied during the assessment of the weight parameters w_1 and w_2 (Eq. 6.3). The linear fit of the experimental data has been compared for different combinations of w_1 and w_2. As an example, Fig. 6.2 illustrates the data sets resulting by computing the two extreme combinations: orientation only ($w_1 = 1, w_2 = 0$) and volume fraction only ($w_1 = 0, w_2 = 1$).

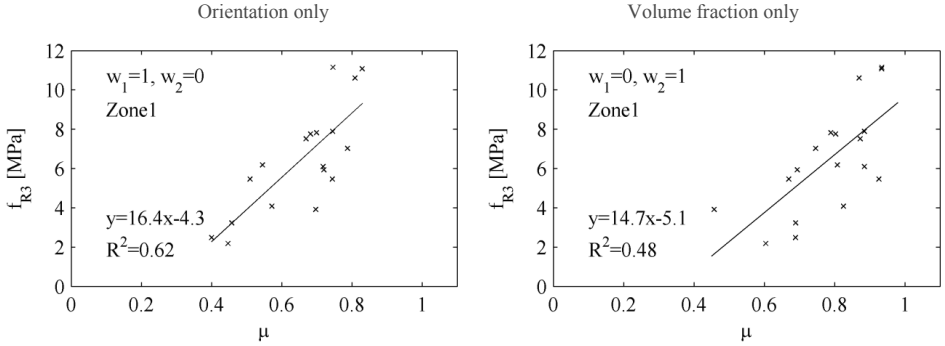

Fig. 6.2. Relationship between the fibre efficiency parameter μ and the residual flexural tensile strength f_{R3} for the two extreme combinations of the normalized weight factors, defined over Zone1.

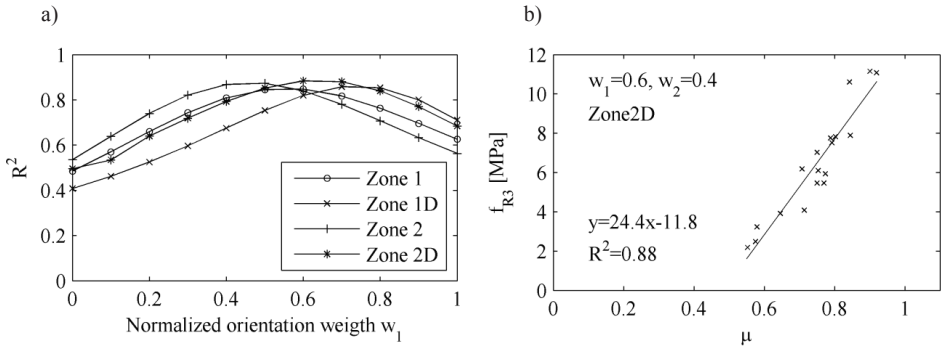

Fig. 6.3. a) Variation of the coefficient of determination R^2 with the normalized weight w_1; b) relationship between the fibre efficiency parameter μ and the residual flexural tensile strength f_{R3}, defined over Zone2D.

The goodness of the linear regressions for the different relevant volumes and combination of weight factors has been evaluated based on the coefficient of determination R^2 (Fig. 6.3a). The relevant volume and w_1,w_2-combination satisfying the criteria of best linear fit (i.e. maximum R^2) are "Zone 2D" and $w_1 = 0.6$, $w_2 = 0.4$, respectively. This result highlights the great impact of variations in the volume fraction, and not exclusively in orientation, when defining the post-cracking response of FRC. Finally, the linear regression from Fig. 6.3b is therefore proposed to relate the residual flexural strength and the fibre efficiency parameter for the present study.

6.4 Conclusions

This paper discusses the need to incorporate the contributions of both the fibre orientation and the local volume fraction in the relationship with the mechanical performance of FRC. The results demonstrate that a poor agreement with the residual flexural strength is obtained when considering only orientation ($w_1 = 1$ and $w_2 = 0$) or only volume fraction ($w_1 = 0$ and $w_2 = 1$). In contrast, a good correlation results from considering a combination of the two aspects. For the present study, it is concluded that the residual flexural strength is for 60% explained by variations in the fibre orientation, and for 40% by variations in the local volume fraction.

Acknowledgements

The paper is based on work performed in COIN - Concrete Innovation Centre (www.coinweb.no) - which is a Centre for Research based Innovation financed by the Research Council of Norway and industrial partners (2007-2014).

Part III

Finite element modelling of FRC as an inhomogeneous and anisotropic material

Chapter 7

Accounting for the influence of the fibre structure

Paper IV

Accounting for the fibre orientation on the structural performance of flowable fibre reinforced concrete

E.V. Sarmiento, M.A.N. Hendriks, T. Kanstad

In: *Computational Modelling of Concrete Structures, Volume 2*. N. Bícanić N, H. Mang, G. Meschke, R. de Borst R, editors. CRC Press, Leiden, The Netherlands; 2014. p. 609-618.

Abstract

Often large scatters are found in test results for fibre-reinforced structural elements caused by a non-homogenous distribution of the fibres. This paper presents a numerical approach where spatial variations of the fibre orientation and relative volume fraction are taken into account by discretizing a specimen into volumes and using volume-wise constant material properties. The approach includes the definition of a constitutive model which takes into account the local fibre orientation and local variation of the relative volume fraction. The applicability of the approach is explored and discussed by a case study, using detailed data of the fibre structure and experimentally observed load–deflection responses.

7.1 Introduction

The overall mechanical behaviour of fibre-reinforced concrete (FRC) elements is often predicted by defining the fracture process based on the stress-strain or stress-crack width relationship. The nature of this relationship can be established by analytical definition (Laranjeira de Oliveira, 2010), derived from the technical recommendations (RILEM, 2003, *fib*, 2010), or based on inverse analysis of test specimens (Tlemat et al., 2006). However, modelling fibre-reinforced concrete as a homogeneous material tends to lead to inaccurate results, especially for flowable FRC where physical phenomena occurring during the fresh state result in an uneven distribution of the constituents. The efficiency of the fibres depends on the fibre structure. That is, the inhomogeneity of the fibres over the length or depth of the specimen and the alignment of the fibres with respect to the principal stress directions.

As an attempt to account for the fibre structure, FRC can be modelled as a two-phase material (Radtke, 2012, Cunha et al., 2012). In this approach, the concrete matrix is described as a homogeneous material, while single fibres are treated explicitly as discrete entities. The approach has the advantage of directly including the effect of fibre location and orientation. However, it requires the definition of the stress transfer between matrix and fibres. This interaction is often based on results obtained from pull-out tests of single fibres and/or analytical expressions that include effects as the fibre embedded length, fibre inclinations, or the anchorage of the fibre end (Laranjeira de Oliveira, 2010, Cunha et al., 2010). For large fibre volumes failure mechanisms can be interacting, creating collective failure that cannot be captured by single fibre failure (Laranjeira de Oliveira, 2010, Sandbakk, 2011).

The current work presents a numerical approach for analysing a FRC structural element, in which the fibre structure is modelled by assuming volume-wise constant material properties. The process consists of: (i) obtaining the fibre structure, (ii) discretizing the structural element in several volumes; and (iii) homogenizing the material properties within each discrete volume (Fig. 7.1). Owing to this, the model uses a single phase material definition for each volume, with the consequent computational advantage for application to structural members. The homogenization is carried out by calibrating the material model against a great number of experimental tests with different fibre orientations and fibre densities. By this practical approach the definition of the matrix-fibre interface behaviour is circumvented.

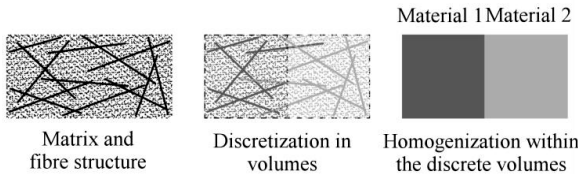

Fig. 7.1. Overview of the process for the numerical approach.

7.2 Numerical approach

The next three sections describe how the fibre structure is represented in each finite volume and how the material model in each volume depends on this representation.

7.2.1 Representing the fibre structure within a discrete volume

A local description of the fibre orientation and volume fraction is proposed in the present work based on a complete characterization of the fibre structure. In such a complete characterization the position and orientation of every single fibre is known. Several methodologies can be utilized for assessing the fibre structure of a FRC member (Žirgulis et al., 2013). Among them, flow simulations (Švec et al., 2011), numerical algorithms based on probabilistic distribution (Cunha et al., 2012), Computed Tomography (CT) analysis (Švec et al., 2014), and visualisation of fibres within a viscous transparent fluid (Zhou and Uchida, 2013). After the characterization of the fibre structure, all fibres are mapped to the concrete volumes in which the structural element is discretized. A fibre can belong to one or intersect several volumes. In the current approach, fibres will exclusively and for the full length contribute to the (cubic) volume in which their centre points are located (Fig. 7.1).

While local variations on the fibre orientation are generally accepted to have great impact on the mechanical performance of FRC, less attention is paid to the significance of local variations of the fibre volume fraction. However, the high demands on flowablity can, in some cases, compromise the stability of the concrete. As a result, considerable variations in the local fibre volume fraction are often found. For this reason, the current model incorporates all the information from the spatial distribution of the fibres which appears to influence the mechanical performance, namely the orientation and the local volume fraction.

The fibre orientation pattern of a certain body can be described by a set of second-order orientation tensors (Švec et al., 2014, Advani and Tucker, 1987, Ferrara et al., 2011, Şanal and Özyurt Zihnioğlu, 2013), defined over discrete volumes of the body. Each

orientation tensor defines the dominant fibre orientation state of the volume and is defined as:

$$\mathbf{A}=\frac{\sum_n L_n \mathbf{p}_n \mathbf{p}_n^{\mathrm{T}}}{\sum_n L_n} \tag{7.1}$$

where **A** is the orientation tensor of a discrete volume. For the number of fibres found in the volume, the unit vector $\mathbf{p}_n$ is the orientation and L_n the length of each single fibre. By definition, the orientation tensor has the properties of being symmetric and having normalized components.

Symmetric second-order tensors can be visualized using 3D ellipsoids, where the eigenvectors and eigenvalues give the direction and half length of the principal axes of the ellipsoids. In this way, ellipsoids are used as a visual tool to identify the dominant direction of the fibres in each discrete volume.

7.2.2 Fibre efficiency

When a crack arises, the efficiency of the fibres on bridging the crack depends on their orientation with respect to the crack plane. This relative orientation refers to the angle between the dominant fibre direction and the direction normal to the crack plane, which is formulated as:

$$\cos\theta=\mathbf{a_1}\cdot\mathbf{n} \tag{7.2}$$

where $\mathbf{a_1}$ is the eigenvector associated to the largest eigenvalue of tensor **A**, **n** is the vector normal to the crack plane, and θ is the angle between the two vectors. Fig. 7.2 exemplifies two fibre orientation states represented by ellipsoids and illustrates the relevance of the value $\cos\theta$ as a measure of the fibre efficiency.

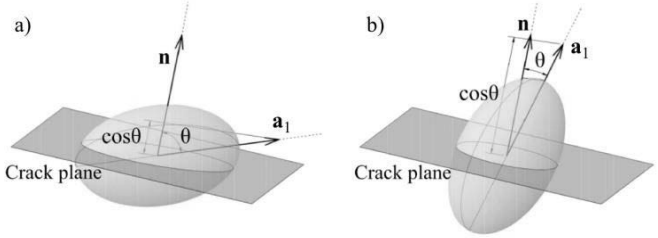

Fig. 7.2. Orientation state of fibres represented by ellipsoids for a predominant a) unfavourable orientation, and b) favourable orientation.

The description of the fibre structure by orientation tensors does not incorporate variations of the fibre volume fraction. For convenience, a single parameter is introduced that integrates the contributions of the local fibre orientation and local volume fraction. This fibre efficiency parameter μ is defined as a linear combination:

$$\mu = w_1(\cos\theta) + w_2\left(\frac{v_f}{\overline{v}_f}\right) \tag{7.3}$$

where w_1 and w_2 are normalized weights, with $w_1+w_2 = 1$, for the orientation and volume fraction components, respectively; v_f is the local volume fraction for the discrete volume; and $\overline{v}_f$ is the volume fraction for the entire specimen. The determination of w_1 and w_2 will be discussed in the case study.

7.2.3 Constitutive model

The volume-wise definition of the fibre structure, as described in the previous section, is used to locally adapt the material model in a numerical analysis. This section describes the constitutive model used and how it depends on the local fibre efficiency parameter μ. For convenience, it is assumed that the finite element mesh exactly matches the used volume discretization for the homogenization. Every single finite element thus has unique material properties.

Because fibres main contribution occurs after the crack initiation, both compressive and pre-cracking response can be assumed to be similar to the one of plain concrete. The local fibre properties are thus incorporated to define the post-cracking tensile behaviour. The tri-linear diagram from Fig. 7.3 is proposed to describe the σ-ε behaviour in tension.

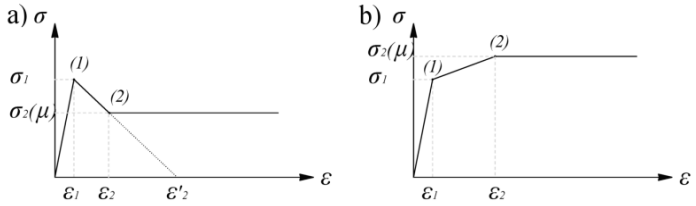

Fig. 7.3. Tensile constitutive model.

Parameters σ_1 and ε_1 can be obtained from three-point bending tests on notched beams according to EN 14651. The residual tensile strength σ_2, which defines an ideal plastic post-cracking behaviour, is defined dependant on the fibre efficiency parameter μ. When the local value of σ_2 results in strain softening, the post-peak drop is assumed to follow the behaviour of plain concrete, until the intersection with the residual post-cracking branch (point *(2)* in Fig. 7.3a). On the contrary, when σ_2 exceeds the tensile strength σ_1, leading to a hardening response, the residual strength is assumed to be reached at a strain corresponding to a crack opening of 0.5 mm.

The relationship between the residual tensile strength σ_2 and the fibre parameter μ needs to be established for the particular material, type and geometry of fibres, as well as for

the concrete properties where fibres are embedded in. A relationship is formulated for the case study presented in the next section.

It is the aim of the present paper to investigate the application of a non-homogeneous material model based on the real fibre structure, rather than to propose a more sophisticated description of the σ-ε behaviour for the numerical implementation. It is therefore worth to mention that the proposed constitutive model (i) allows the definition of the tensile behaviour from three-point bending tests, as advised by some recommendations (RILEM, 2003, *fib*, 2010) and (ii) reduces the number of parameters which depend on the fibre efficiency parameter to one, namely σ_2.

7.3 Case study

In the following, an application of the proposed numerical approach is presented using real fibre structure data. Analysis results are compared with experimental results. Finally, a variation study discusses the sensitivity to the main parameters that define the tensile constitutive model.

7.3.1 Three beams in three-point bending

The case study considers three fibre-reinforced self-compacting concrete beams with dimensions of 0.6 m × 0.15 m × 0.15 m. The three beams, identified as S1, S2 and S3, were sawn from a slab (1.2 m × 1.2 m × 0.15 m) at different locations. The fibre reinforcement includes a volume fraction of 0.5% hooked-end steel fibres. The length and diameter of fibres were 60 mm and 0.75 mm, respectively. A description of the mixture design, casting process and fresh concrete properties can be found in Švec et al. (2014).

The three specimens were scanned by means of a Computed Tomography (CT) scanner. The three-dimensional fibre structure over the structural element was obtained from the digital analysis of the scanned images. Fig. 7.4 is an example of the fibre structure visualization. A skeletonizing technique was implemented in order to register topology, length and direction of all the fibres present in the three specimens.

Fig. 7.4. Visualization of the fibre structure for specimen S1.

The mechanical response in flexure was studied by performing three-point bending tests according to EN 14651 (European Standard, 2005). Under these conditions, the specimens were notched at midspan reducing their cross-section height to 125 mm. Despite the beams were sawn from the same slab, which guarantees comparable mixture and casting conditions, variations of about 40% of the residual flexural strength were observed between the three specimens. The basis of this large scatter must be ascribed to variations of the fibre dispersion. Explaining this difference by a numerical verification is the main purpose of this case study.

7.3.2 Local fibre orientation and volume fraction

The volume of the beams was discretized in right rectangular prismatic volumes. An initial discretization comprised 12 mm × 12.5 mm × 150 mm volumes. These volumes anticipated on structural analyses with plane stress elements of 12 mm × 12.5 mm and a thickness of 150 mm. The results were compared with a second discretization with regions 25 mm × 25 mm × 150 mm and an equivalent finite element model with plane stress elements of 25 mm × 25 mm. The choice of using equivalent discretizations for the homogenization of the fibre structure and for the structural analysis is a pragmatic one. In the current simplified approach, where a single fibre only contributes to a single volume, the sizes of the volumes should not get substantially smaller than the lengths of the fibres (60 mm). On the contrary, from the structural analysis point of view, relative small elements would be preferable.

The set of local fibre orientation tensors and local volume fraction was obtained from the fibre 3D-structure. As an example, Fig. 7.5 illustrates for the coarser volume discretization, the orientation tensors visualized as ellipsoids and the local volume fraction percentage for one of the specimens (beam S1).

7.3.3 Definition of the residual tensile strength σ_2

In this section, a relationship between the residual tensile strength σ_2 and the fibre efficiency parameter μ is established for this particular case study. The relationship is derived from the analysis of an experimental set of 15 specimens, which also includes the three studied beams. Therefore, equivalent mixture and casting conditions apply. The set comprises the results of three-point bending test of a group of notched beams, which were previously CT-scanned, and which cover a wide range of fibre dispersions (Švec et al., 2014).

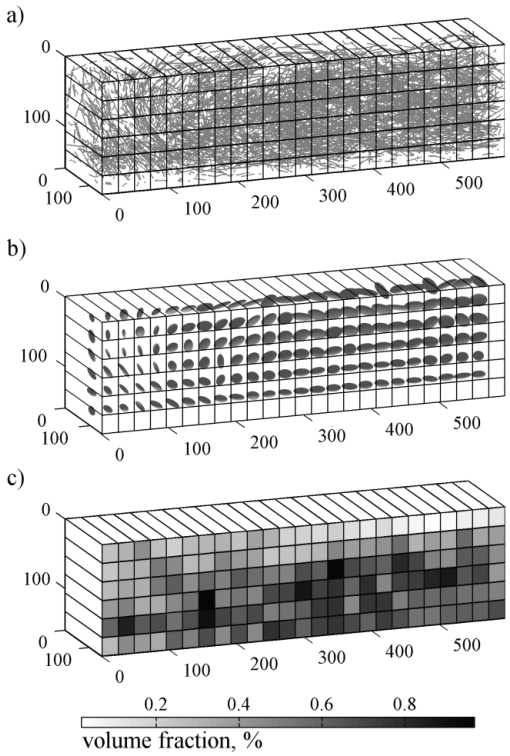

Fig. 7.5. a) Discretization in volumes 25 mm × 25 mm × 150 mm for specimen S1; b) ellipsoids representing the orientation tensor; and c) local variations of the fibre volume fraction. Dimensions in mm.

The residual flexural tensile strength corresponding to 2.5 mm crack width (in codes denoted as f_{R3}), derived from the bending test, is the result used for calibrating σ_2. By assuming the whole compressive force is concentrated in the top edge of the cross-section and that the remaining part of the cross section has reached the residual tensile strength σ_2, rotational equilibrium results in the relationship:

$$\sigma_2 = \frac{f_{R3}}{3} \tag{7.4}$$

The fibre efficiency parameter μ was calculated considering two alternative volumes close by the notch, termed zone 1 and zone 2, with in-plane dimensions of 24 mm × 75 mm and 72 mm × 75 mm, see inset figure in Fig. 7.6. For possible combinations of the normalized weights w_1 and w_2 (Eq. 7.3), the relations between μ and the equivalent residual strength σ_2 were evaluated. Weight parameters of 0.7 and 0.3 for w_1 and w_2, respectively, led to the best linear fit ($R^2 = 0.85$) of the data set (Fig. 7.6). This result highlights the importance of including the variation of the fibre volume fraction, and not

exclusively the orientation, when defining the post-cracking response of FRC: the residual strength is for 70% explained by variations in the fibre orientation and for 30% by variations in the local relative fibre volume fraction.

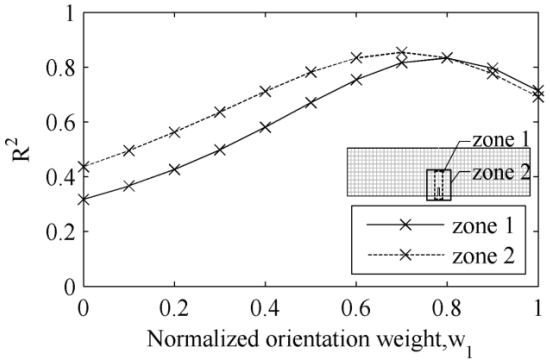

Fig. 7.6. Variation of the coefficient of determination with w_1.

The established relationship between the residual strength σ_2 and the fibre parameter μ is defined by the piecewise function presented in Fig. 7.7. The fibre efficiency parameter was calculated considering zone 2. The linear regression from the data fit is completed with an initial branch, assuming that fibres with a combination of unfavourable orientation and low volume fraction, i.e. with a low μ, are still able to carry a minimum stress.

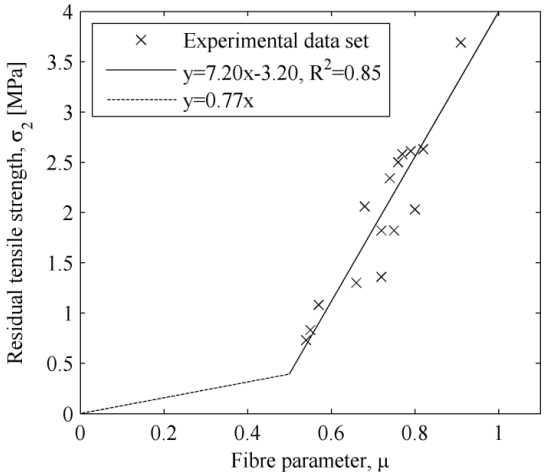

Fig. 7.7. Effect of the fibre parameter μ on the residual strength σ_2.

7.3.4 Numerical model

The finite element mesh used for modelling the three specimens matches the volume discretization for which fibre properties were locally defined. Eight-node quadrilateral plane stress elements were used with 2 × 2 Gauss integration scheme. The nonlinear behaviour of the material was modelled with a rotating smeared crack model. It is envisioned that the cracks will all be nearly vertical and limited rotation is expected. An elastic ideal-plastic behaviour was defined to model the material in compression. The tensile behaviour presented in Section 7.2.3 was differentiated for each element, based on the local fibre properties. Because the crack location and direction was controlled by the notched section, the fibre efficiency parameter μ can be evaluated for each element prior to the numerical analysis. For the general case, where crack directions are not know on beforehand, the fibre efficiency parameter should be calculated during the analysis depending on the crack direction and the material model should be updated accordingly. Fig. 7.8 illustrates the variations of the residual tensile strength σ_2 after applying the formulated relationship with μ.

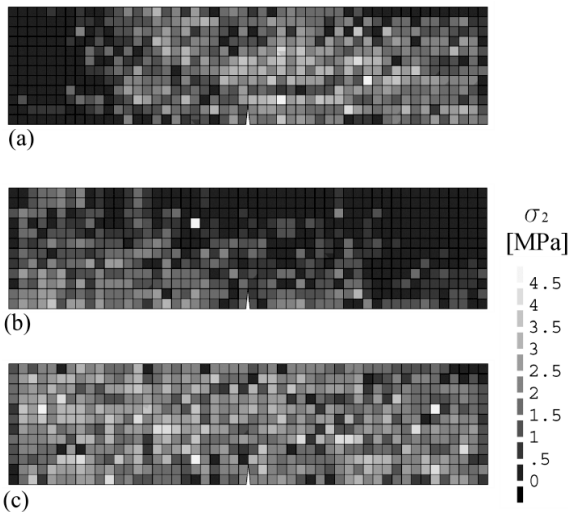

Fig. 7.8. Variations of the residual tensile strength σ_2 over the finite elements, for specimens (a) S1, (b) S2, and (c) S3.

In this regard, the application of this numerical approach results in a non-homogenous model, which is able to incorporate differences in the tensile behaviour, as the ones presented in Fig. 7.8. The remaining input parameters for the definition of the σ-ε relationship are listed in Table 7.1.

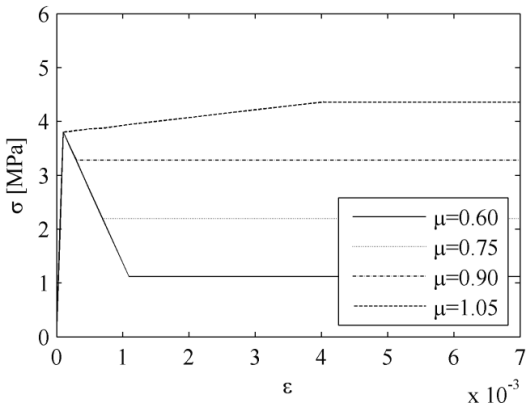

Fig. 7.9. Tensile constitutive model for specimens S1, S2 and S3.

Table 7.1. Input material parameters.

Input parameters		
f_{cm}	[MPa]	65
E_c	[MPa]	38000
σ_1	[MPa]	3.8
ε_1	‰	0.1
ε'_2	‰	1.5

7.3.5 Results

The load-deflection curves obtained from analysis and experiments are shown in Fig. 7.10. The analyses used the discretization with volumes of 12 mm × 12.5 mm × 150 mm and an equivalent plane stress finite element model. The differences between the three numerical curves are exclusively related to the heterogeneities in the material model of the elements. In general terms, a good agreement with the experimental responses was obtained for the three specimens. The favourable fibre distribution in the proximities of the crack, both for specimens S1 and S3, causes the bridging effect of fibres to be sufficient to sustain or even increase the capacity after crack initiation. On the contrary, an unfavourable fibre distribution for specimen S2 results in an abrupt drop of the capacity immediately after cracking. It can be seen from the numerical results that the proposed simplified constitutive model is able to describe the different stages of the fracture process.

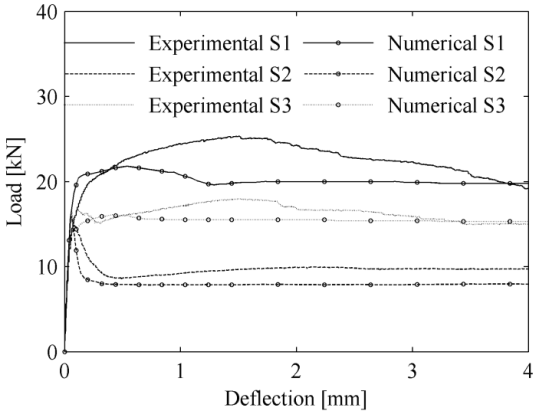

Fig. 7.10. Experimental and numerical load-deflection response for three-point bending test.

The predicted load-deflection curve for specimen S1 slightly decreases after exceeding a deflection of 0.5 mm, diverging from the experimental curve. This descent of the capacity corresponds to the formation of a new macro-crack. The stress redistribution during the loading process leads to a new "weakness path" within the non-homogeneous mesh. Fig. 7.11 illustrates the crack pattern corresponding to a deflection of 3.5 mm.

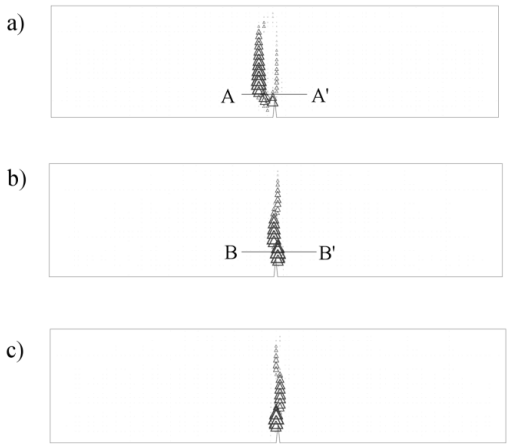

Fig. 7.11. Crack pattern for specimens a) S1, b) S2, and c) S3, corresponding to a deflection of 3.5 mm.

Fig. 7.12 illustrates the principal strains at the integration points for a horizontal line 22 mm above the notch, i.e. lines A-A' and B-B' indicated in Fig. 7.11. It can be seen from Fig. 7.11a and Fig. 7.12a that a second crack arises after a deflection of 0.5 mm for beam S1. The global hardening response of specimen S1 (Fig. 7.10) favours the opening

of new cracks, in similarity with the multiple-crack pattern typical for conventional reinforced concrete. A single crack localizes for specimens S2 and S3, as presented in Fig. 7.11b-c, and Fig. 7.12b. The formation of a second crack highlights the ability of the model to define a crack path through FRC elements based on the specified material inhomogeneity.

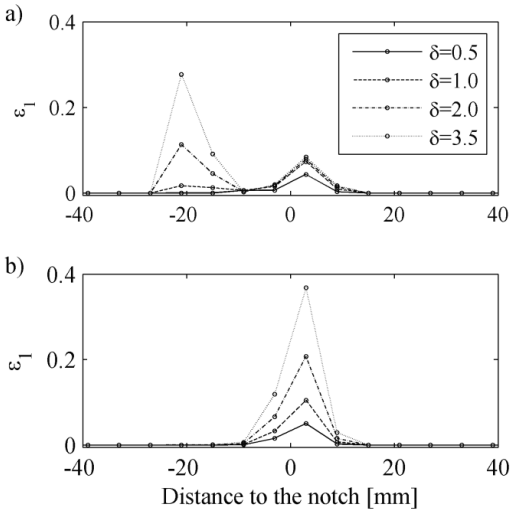

Fig. 7.12. Principal strain at the integration points for lines A-A' and B-B' (Fig. 7.11a and b), for specimens a) S1 and b) S2, respectively.

7.3.6 Variation study

Three sensitivities of the modelling approach will be analysed in the sequel: the (initial) tensile strength, the post-peak softening and the volumes used to discrete the fibre structure.

The relevance of including the initial tensile strength σ_1 for this numerical approach was evaluated by comparing the results with the results of an elasto-perfectly plastic model. Neglecting the initial tensile strength is a common assumption for design of fibre-reinforced concrete (*fib*, 2010).

Fig. 7.13 presents the load-deflection curves for the experimental and numerical analyses for this variation. The numerical curve for specimen S2 indicates the deficiency of the elasto-perfectly plastic model in describing the maximum load capacity and load at low deflections. However, the load at large deflection could still be considered in good agreement with the experimental results for specimens S2 and S3.

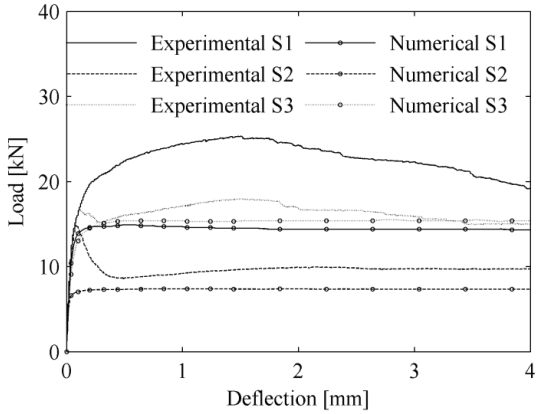

Fig. 7.13. Load-deflection curves using an elasto-perfectly plastic model.

The major drawback of the model refers to specimen S1, for which the load capacity is largely underestimated. For this specimen, the reduction of the section due to the notch appears to be insufficient to guarantee the crack localizes above the notch (Fig. 7.14). Instead, the location of the crack path is now governed by paths with low residual stresses σ_2, resulting from unfavourable fibre dispersions (Fig. 7.8).

Fig. 7.14. Crack pattern for specimen S1, corresponding to a deflection of 3.5 mm.

The post-peak softening is controlled by the parameter ε_2' (Fig. 3). A large sensitivity of the numerical results was observed for this parameter. Assuming the post-peak drop to follow the behaviour of plain concrete, ε_2' refers to its ultimate strain level. When a linear softening behaviour is assumed, the ultimate strain level can be related to the fracture energy by the expression:

$$\frac{G_F}{h} = \frac{1}{2}\sigma_1 \varepsilon_2' \tag{7.5}$$

where G_F and h are the fracture energy and characteristic length, respectively. In absence of experimental tests for plain concrete, G_F is estimated according to *fib* (2010), resulting in 0.154 N/mm. The common assumption that the crack localizes in one element, yields to the value $\varepsilon_2' = 6.7 \cdot 10^{-3}$. From Fig. 7.15 it can be seen that the use of this value leads to a significant overestimation of the capacity after cracking. A possible explanation is that a linear softening underestimates the initial softening behaviour. Alternatively, the σ-ε relationship proposed by RILEM (2003), for the specific case

$\sigma_2 = ½\sigma_1$, leads to $\varepsilon_2' = 0.3 \cdot 10^{-3}$. This value represents an abrupt drop of strain after cracking, which makes that the peak in the load-deflection response disappears, as seen from Fig. 7.15. The local tensile strengths σ_1 are not put in effect since they are not addressed simultaneously. A step size refinement has been carried out to confirm this. The outcome of these two cases leads to the consideration of an intermediate strain value ε_2' of $0.15 \cdot 10^{-3}$ used in the previous section. A more solid definition of the softening part of the curve is recommendable.

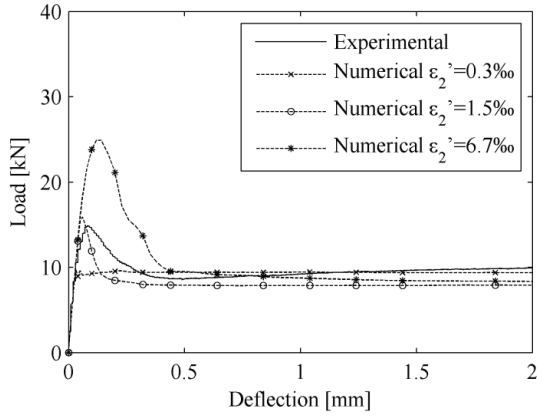

Fig. 7.15. Load-deflection curves for different values of parameter ε_2'.

Finally, the sensitivity to the discretization of the specimens was evaluated by studying a second discretization with volumes of 25 mm × 25 mm × 150 mm, and an equivalent finite element model with plane stress elements of 25 mm × 25 mm. The input tension curve σ-ε from Fig. 7.3a was modified, reducing parameter ε_2' by factor ½ to obtain constant energy dissipation for the plain concrete region of the σ-ε relation. The need of rescaling the post-peak stress-strain relationship when changing the element size has been reported by other authors based on the concept of the characteristic crack band width, which applies to softening materials (Beghini et al., 2007, Tlemat et al., 2006).

The load deflection curves obtained from analysis and experiments are presented in Fig. 7.16. While the load at large deflections does not significantly change for curves S1 and S2, compared with the results from a finer mesh (Fig. 7.10), curve S3 shows a larger capacity. This overestimation is ascribed to variations in the residual tensile strength σ_2, caused by homogenizing the fibre properties in large or small volume regions. These variations are presented in Fig. 7.17. By the relatively large discretization volumes, possible weak residual tensile paths are “averaged away”.

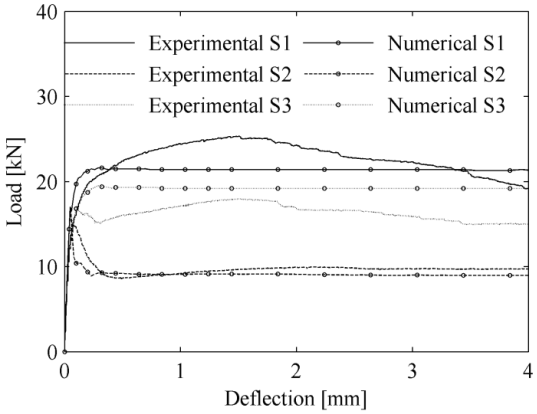

Fig. 7.16. Load-deflection curves for the coarse discretization (25 mm × 25 mm × 150 mm).

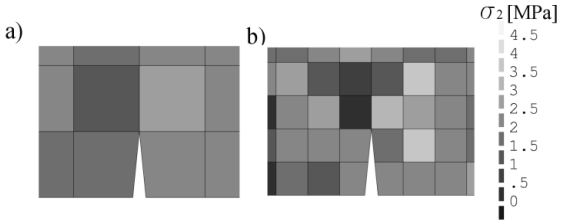

Fig. 7.17. Variation of the residual tensile strength σ_2 over the elements, for discretizations: a) 25 mm × 25 mm × 150 mm, and b) 12 mm × 12.5 mm × 150 mm.

In contrast with the results for a finer mesh, a coarser mesh cannot capture the opening of a second crack for specimen S1 and, therefore, a drop of the load capacity after 1 mm deflection is not observed in this case.

Large differences in the strains are observed between the two meshes. Fig. 7.18 illustrates the principal strains at the integration points for the same horizontal line B-B' (Fig. 7.11b) over the notch, corresponding to a deflection at midspan of 3.5 mm. Despite the differences of the maximum strain, both cases localize the crack within one element, leading to similar energy dissipation over the failure surface.

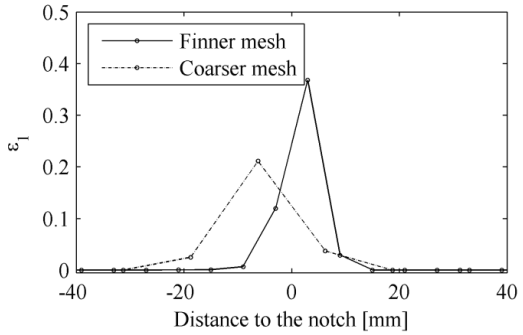

Fig. 7.18. Principal strain at the integration points for line B-B' (Fig. 7.11b).

7.4 Conclusions

In the current work, a numerical approach for analysing FRC structural elements was presented, in which the fibre structure was included assuming volume-wise constant material properties. In this respect, the model used a single phase material definition for each volume. The applicability of the model was described and explored by presenting a case study.

The numerical finite element analysis revealed a good agreement with the experimental observations. The distinct load-deflection responses of the simulations of the three tests could only be attributed to the inclusion of the spatial variations of fibre orientation and fibre dispersion in the model. The main characteristics of the experimentally observed responses were captured, both qualitatively and quantitatively.

The approach is relevant to evaluate to which extent the scatter from standard tests can be ascribed to the fibre dispersion. It should be pointed out that the commonly observed scatter on the residual strength is one of the actual drawbacks for design of FRC structures. Furthermore, the application of this numerical approach is especially relevant to structural elements for which the flow of FRC at the pouring stage and subsequent sedimentation of fibres is expected to lead to uneven distribution of fibres.

Further refinements of the numerical approach should include a more detailed study of the influence of the volume discretization, linked with a possible improvement of the homogenization approach of the fibre distribution. The definition of the used stress-strain relations should be reconsidered, especially for the strain softening part. The numerical model can be extended to structural elements where the fibre dispersion is obtained by flow simulations.

Acknowledgements

The paper is based on work performed in COIN (Concrete Innovation Centre, www.coinweb.no), which is a Centre for Research based Innovation initiated by the Research Council of Norway (RCN) in 2006. COIN is financed by RCN (approx. 40%), industrial partners (approx. 45%), and by SINTEF and NTNU.

Chapter 8

Improved modelling of the influence of the fibre structure

Paper V

Modelling the influence of the fibre structure on the structural behaviour of flowable fibre-reinforced concrete

E.V. Sarmiento, M.A.N. Hendriks, M.R. Geiker & T. Kanstad
Submitted to an international scientific journal in September 2015

Abstract
This paper presents a modelling approach for fibre-reinforced concrete elements in which the fibre structure is taken into account in simulating the mechanical behaviour. The fibre structure is discretized in volumes and two fibre parameters are defined for each discrete volume: the dominant fibre orientation and the fibre volume fraction. These parameters are incorporated in a numerical model that uses a single-phase material definition dependent on the fibre parameters. The first part of this paper describes the methodology and constitutive modelling. The second part addresses the simulation of two beams that exhibited large differences in bending because of uneven fibre distribution. Data on the fibre structure was obtained using Computed Tomography scanning. The modelling approach captured the large difference in the flexural response of the two beams and provided an adequate prediction of the location and propagation of the critical cracks.

Keywords
Fibre reinforced concrete, Inhomogeneity of the fibre structure, Fibre orientation tensor, Fibre volume fraction, Nonlinear finite element modelling

8.1 Introduction

Predicting the overall mechanical behaviour of a fibre-reinforced concrete (FRC) element usually requires the characterization of the post-cracking behaviour of the FRC. This is often determined either directly, in direct tension tests, or indirectly by performing inverse analysis of bending tests, splitting tests, or other indirect tension tests (European Standard, 2005, ASTM International, 2012a, Ozyurt et al., 2007, Löfgren et al., 2008, Di Prisco et al., 2013b). Inverse analysis of the test results makes it possible to determine the material tensile behaviour considering a certain stress-strain or stress-crack width relationship. Bi-, tri- and poly-linear functions are usually proposed in the literature to describe the post-cracking behaviour of FRC (Uchida et al., 1995, Kooiman, 2000, Grünewald, 2004, Meda et al., 2004, Barros et al., 2005, De Oliveira e Sousa and Gettu, 2006, Tlemat et al., 2006, Cominoli et al., 2007, Löfgren et al., 2008, Cunha, 2010). Several technical recommendations (RILEM, 2002a, RILEM, 2003, *fib*, 2010, DAfStb, 2012) also provide simplified formulations of the constitutive behaviour of FRC based on bending tests, which facilitate the material characterization for design purposes.

The post-cracking behaviour of FRC in a structural element, especially if it is flowable or self-compacting FRC, can differ from the post-cracking behaviour of a test specimen. The rheological properties, the casting procedure, and the structural geometry can lead to an uneven fibre structure in the element, meaning inhomogeneity of the fibre volume over the length or depth of the element and a preferred alignment of the fibres (Ferrara and Meda, 2006, Stähli et al., 2008, Vandewalle et al., 2008, Boulekbache et al., 2010, Ferrara et al., 2011, Abrishambaf et al., 2013). In such cases, modelling the FRC as if it were a homogeneous material can lead to inaccurate results.

In an attempt to take into account its fibre structure, FRC can be modelled as a two-phase material (Radtke, 2012, Cunha et al., 2012, Huespe et al., 2013), where the concrete matrix is described as a homogeneous material, while the fibres are treated explicitly as discrete entities. This approach has the advantage of directly including the effect of fibre location and orientation, but requires a definition of the concrete matrix model, the fibre model, and the interface model for the fibre-matrix bond response. This response is often based on results from pull-out tests of single fibres and/or analytical expressions that include effects such as the fibre embedded length, fibre inclination, or the anchorage of the fibre end (Laranjeira de Oliveira, 2010, Cunha et al., 2010). It is commonly assumed that fibres do not interact with neighbouring fibres, but when a large fibre dosage is used, failure mechanisms can be interactive, creating a collective failure that cannot be captured by describing the failures of individual fibres (Laranjeira de Oliveira, 2010, Sandbakk, 2011).

The current paper presents a modelling approach for analysing FRC structural elements in which the fibre structure is modelled by assuming volume-wise constant material properties. Since the material cannot be assumed to be homogeneous on the scale of the structural element, a spatial discretization of the element is defined within which the material can be considered homogeneous. The process consists of (see Fig. 8.1): (i) obtaining the fibre structure, (ii) discretizing the structural element in volumes, (iii) determining the fibre structure properties within each discrete volume, (iv) defining an adequate constitutive model that describes the behaviour of the FRC at the discrete volume level making use of the fibre structure properties, and finally, (v) simulating the structural response using finite element (FE) modelling.

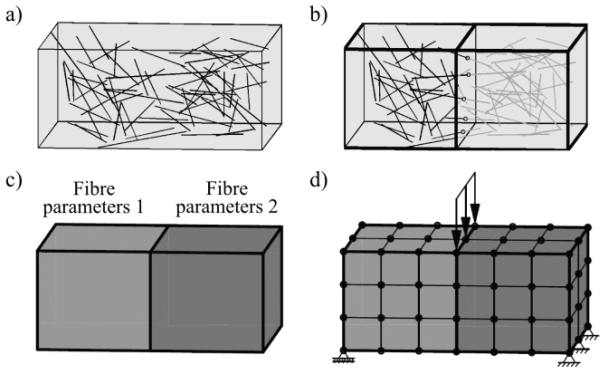

Fig. 8.1. a) Matrix and fibre structure, b) discretization in volumes, c) homogenization within discrete volumes, and d) finite element model.

The constitutive model (iv) is applied at an intermediate level which is between the fibre level and the structural element level. It uses a single-phase material definition, with the consequent computational advantages for application to structural elements. In this way, the definition of the matrix-fibre interface behaviour is circumvented. However, a new issue is raised. As already mentioned, single-phase material models for FRC are commonly calibrated by inverse analysis of test results at the scale of test specimens. Such an approach is not feasible for the intermediate level. Since the focus of this research was on the modelling approach as a whole (i-v) and in the absence of a well-established constitutive modelling technique for this intermediate level, heuristic assumptions were used for the constitutive modelling.

8.2 Modelling approach

Starting from a complete characterization of the fibre structure, this section describes the modelling steps that result in the proposed constitutive model for FRC for use at the discrete volume level. The section ends with an illustration of the constitutive model for various fibre structure parameters.

8.2.1 Fibre parameters within a discrete volume

In the present investigation, fibre structure properties were derived from a complete characterization of the fibre structure in which the precise position of every fibre is known. Several methodologies can be utilized for assessing the fibre structure of an FRC element, including flow simulations (Švec et al., 2011), numerical algorithms based on probabilistic distributions (Cunha et al., 2012), X-ray Computed Tomography (CT) (Stähli et al., 2008), and visualization of fibres within a viscous transparent fluid (Zhou and Uchida, 2013).

To define the local fibre properties, a discretization of the structural element in volumes was considered. The discrete volume size had to take into account criteria related to the size of the fibres and be sufficiently descriptive of the inhomogeneities of the fibre structure. Fibre properties were determined considering the fibres located in each volume. Because fibres can intersect one or several discrete volumes, the intersection points with the boundaries of the volumes needed to be determined. In this way, each segment of a fibre is considered in the volume in which it is located (Fig. 8.1b). Intersection points were obtained by assuming that fibres are perfectly straight.

This model incorporates the information from the spatial distribution of the fibres which can potentially influence the mechanical performance of a flowable FRC element, namely the fibre orientation and the local fibre content. The fibre orientation pattern of a body can be described using a set of second-order orientation tensors (Advani and Tucker, 1987, Ferrara et al., 2011, Şanal and Özyurt Zihnioğlu, 2013, Švec et al., 2014) defined over a set of discrete volumes of the body. Each orientation tensor describes the fibre orientation state within the volume and can be defined as:

$$\mathbf{A} = \frac{\sum_n L_n \mathbf{p}_n \mathbf{p}_n{}^T}{\sum_n L_n} \tag{8.1}$$

where $\mathbf{A}$ is the orientation tensor of a discrete volume. For all the fibres and fibre segments in the volume, $\mathbf{p}_n$ is a unit vector in the fibre direction, and L_n is the length of the fibre or fibre segment. By definition, the orientation tensor has the properties of being symmetric and having normalized components. Symmetric second-order tensors can be visualized using ellipsoids, where the eigenvectors, $\mathbf{a_i}$, and eigenvalues, λ_i, give

the direction and half-length of the principal axes of the ellipsoids. In this way, ellipsoids are used as a visual tool to identify the dominant direction of the fibres in each discrete volume.

The second aspect, the local fibre content, is expressed in terms of volume fraction (v_f) and can be computed for each discrete volume as:

$$v_f = \frac{\sum_n L_n A_f}{V_c} \tag{8.2}$$

where A_f is the fibre cross-section area and V_c the discrete volume. The procedure described here makes it possible to represent the orientation and distribution pattern of a structural element by choosing a certain discretization of the element in volumes and assessing the fibre parameters **A** and v_f within each discrete volume. This is illustrated in Fig. 8.2 for the example shown in Fig. 8.1a.

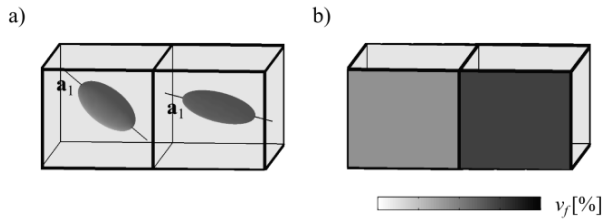

Fig. 8.2. a) Orientation ellipsoids and dominant fibre orientation, and b) fibre volume fraction.

8.2.2 Definition of fibre efficiency

When a crack arises, the efficiency of a fibre that bridges the crack depends on its orientation with respect to the crack plane. This can be expressed by the angle θ between the direction normal to the crack plane (**n**) and the fibre direction. In a similar manner, it can be assumed that the efficiency of a group of fibres depends on the angle between **n** and the dominant fibre direction of the group of fibres. For the group of fibres (or fibre segments) in each discrete volume, the dominant fibre direction is given by the eigenvector associated with the largest eigenvalue of the orientation tensor ($\mathbf{a_1}$). The angle with respect to the crack plane may therefore be formulated as:

$$\cos\theta = \mathbf{a_1} \cdot \mathbf{n} \qquad (\|\mathbf{a_1}\| = \|\mathbf{n}\| = 1) \tag{8.3}$$

Fig. 8.3 depicts two fibre orientation states represented by ellipsoids and illustrates the relevance of the variable $\cos\theta$ as a measure of fibre efficiency.

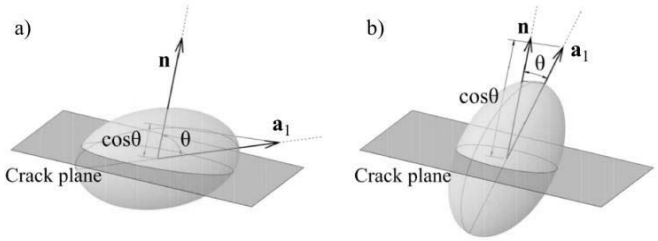

Fig. 8.3. Orientation state of fibres represented by ellipsoids for a) a predominantly unfavourable orientation, and b) a favourable orientation.

For convenience, a single variable is introduced that integrates the local fibre orientation with the local volume fraction. This fibre efficiency variable μ is defined as a linear combination:

$$\mu = w_1(\cos\theta) + w_2 \left(\frac{v_f}{\bar{v}_f}\right) \tag{8.4}$$

where w_1 and w_2 are weightings for the orientation and volume fraction components, respectively (with $w_1+w_2 = 1$), and $\bar{v}_f$ is the nominal fibre volume fraction of the mix.

It is worth noting that $\mathbf{a_1}$ and v_f are material parameters that describe the characteristics of the fibres in each discrete volume of the specimen. In contrast, $\cos\theta$ and therefore also μ are evaluated at each integration point of the FE model, and they are actually variables that depend on the cracking model adopted and the crack plane, so they may change during the simulation. It is worth noting that the FE mesh may not necessarily coincide with the discretization of the fibre structure (as depicted in Fig. 8.1d).

It should also be mentioned that defining the orientation term in Eq. 8.3 entails the simplification of the overall orientation state to the direction $\mathbf{a_1}$. This aspect is illustrated in Fig. 8.4, where the orientation tensors of two groups of fibres are visualized using ellipsoids. In Fig. 8.4a, an elongated ellipsoid represents a markedly unidirectional orientation, while the more spherical ellipsoid in Fig. 8.4b describes a more isotropic orientation. Both groups have the same dominant direction ($\mathbf{a_1}$), but simplifying the orientation state to $\mathbf{a_1}$ seems to be adequate only in the first group. This means that the fibre efficiency variable, here defined based on $\mathbf{a_1}$, requires a certain degree of unidirectionality of fibres within each discrete volume. This is ensured if the eigenvalues of tensor $\mathbf{A}$ satisfy the condition that λ_1 is significantly greater than λ_2 and λ_3.

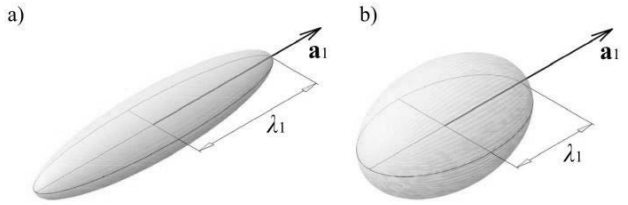

Fig. 8.4. Orientation state of fibres with equal $\mathbf{a}_1$ *for a) a markedly unidirectional orientation, and b) an orientation closer to isotropic.*

8.2.3 Uniaxial stress-strain relationship

It is generally agreed that fibres contribute primarily after crack initiation. For this reason, compressive and pre-cracking responses are assumed to agree with those of plain concrete. The uniaxial stress-strain relationship in tension is assumed to be as depicted in Fig. 8.5, which describes an initial linear-elastic response up to the tensile strength (σ_1), which characterizes the onset of cracking. After this point, the post-cracking behaviour is described with a tri-linear diagram, as used by several other researchers (Barros et al., 2005, Cominoli et al., 2007, Löfgren et al., 2008, Cunha, 2010). The residual tensile strength (σ_2), which defines an ideal plastic post-cracking behaviour, is defined as dependent on the fibre efficiency variable (μ). When the value of σ_2 results in strain softening, $\sigma_2 < \sigma_1$, the post-peak drop is assumed to follow the behaviour of plain concrete until it intersects with the residual post-cracking branch, point (2) in Fig. 8.5a. In contrast, when σ_2 exceeds the tensile strength, a hardening response, the residual strength is assumed to be reached at a strain ε_2 (Fig. 8.5b). Both plateaus end at a strain level ε_3, which activates a softening branch that ends at the ultimate strain ε_{ult}. Only the strain levels ε_2' and ε_{ult}, which are associated with localization of the crack (see Fig. 8.5), are regularized in terms of the finite element size.

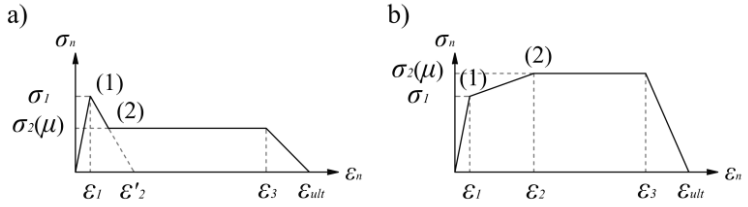

Fig. 8.5. Uniaxial tensile stress-strain relationship for a) strain softening, and b) strain hardening behaviour.

The relationship between the residual tensile strength and the fibre efficiency variable needs to be established based on the type and geometry of the fibres, as well as on the properties of the concrete where the fibres are embedded.

It should be noted that the focus of this paper is on the use of a material model based on actual fibre structure, rather than proposing a more sophisticated description of the stress-strain behaviour for the numerical implementation. With this in mind, it is worth mentioning that the proposed model limits the number of parameters that depend on fibre efficiency to one, namely σ_2, and makes it possible to calibrate the σ_2-μ relationship against data from standard mechanical characterization tests (RILEM, 2003, *fib*, 2010). This is discussed in later sections.

8.2.4 Constitutive modelling

The uniaxial stress-strain behaviour can be generalized to multiaxial stress and strain states by embedding it in a rotating crack model based on a total strain concept, see e.g. Rots (1988). This means that an explicit modelling of the shear retention after cracking is not needed. During an analysis, upon rotation of the principal strains, the (potential) crack orientation rotates and the uniaxial stress-strain behaviour normal to the crack changes too, since it depends on the angle θ with the dominant fibre direction.

The dependence of the uniaxial stress-strain relationship on the fibre parameters and on the crack direction is shown in Fig. 8.6. This figure illustrates an FRC specimen similar to that in Fig. 8.1a-c. For the sake of clarity, the FE mesh coincides with the volume discretization of the fibre structure in this case. The uniaxial tensile stress-strain relationship at the integration point of each element depends on two main aspects: 1) $\mathbf{a_1}$ and v_f as the fibre parameters, and 2) the direction normal to the crack (**n)**, which depends on the current state of stresses. In Fig. 8.6a, the stress-strain relationships of the two elements differ depending on the dominant fibre direction of each element. Similarly, in Fig. 8.6b the stress-strain relationships differ based on a variation in the fibre content. Unlike the two previous cases, the two elements in Fig. 8.6c have the same fibre parameters, but this time different crack directions. Depending on **n**, the variable μ and therefore also σ_2 are different in each element, which leads once again to two different stress-strain relationships.

This modelling approach is therefore able to take into account both the inhomogeneities of the fibre structure and the dependence of the material on the direction of the principal strains, which is related to the anisotropic behaviour of the material.

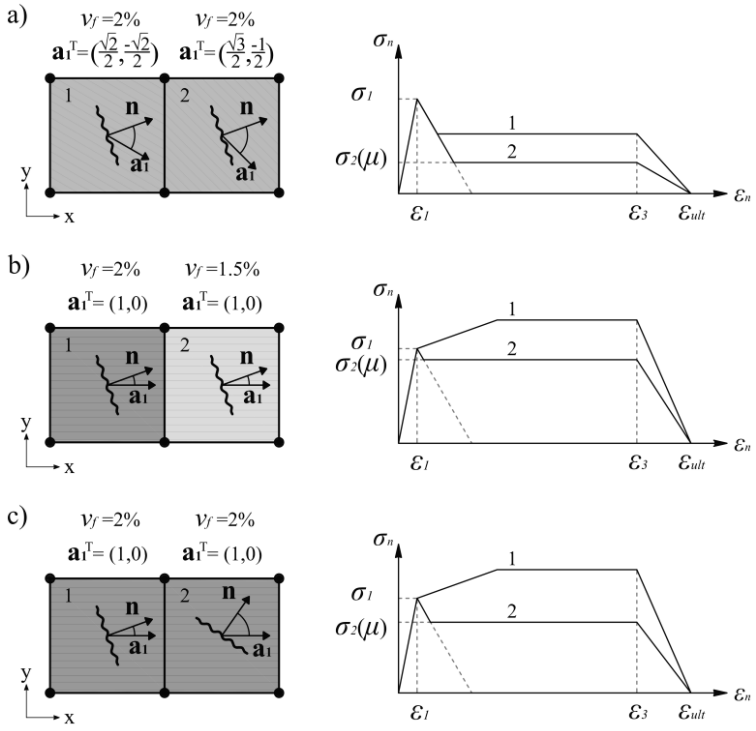

Fig. 8.6. Tensile constitutive model for two elements with differences in a) fibre orientation, b) fibre volume fraction, and c) the direction normal to the crack.

8.3 Two beams in four-point bending tests

The structural performance of a flowable FRC mix with high fibre content was investigated experimentally. In material characterization tests, this mix had previously exhibited high ductility and high residual flexural strength. Two full-scale beams tested in bending showed load-carrying capacity and ductility lower than typically expected, and a significant mutual difference in response.

8.3.1 Materials and specimens

The mix was developed during research work by Kjellmark et al. (Kjellmark et al., 2014) on the optimization of flowable FRC mixes with high ductility. It has reasonably good casting properties, with adequate flowability and compactability, and it does not require vibration. The mix contains 2% vol. hooked-end steel fibres, with a length of 60 mm and an aspect ratio of 67. Table 8.1 gives the mix proportions.

Table 8.1. Mix proportioning.

Component	Dosage
Cement [kg/m^3]	492.2
Silica fume [kg/m^3]	24.6
Total free water [kg/m^3]	197.5
Aggregate 0-8 mm [kg/m^3]	1594
Super-plasticizer [kg/m^3]	7.4-9.8
Stabilizer [kg/m^3]	0.5
Steel fibres [kg/m^3, (% vol.)]	156, (2)
w/b ratio [-]	0.35
Matrix volume (< 0.125 mm) [l/m^3]	400

The two beams with dimensions of 200 mm × 300 mm × 3000 mm were cast with a falling stream of concrete from a single discharge point, which was initially located at one end of the formwork. When approximately 70% of the formwork was filled, the casting point was moved towards the centre of the formwork to complete the filling. The two beams, FSB-a and FSB-b, were cast with concrete from two different batches, for which the same mixing procedure was adopted.

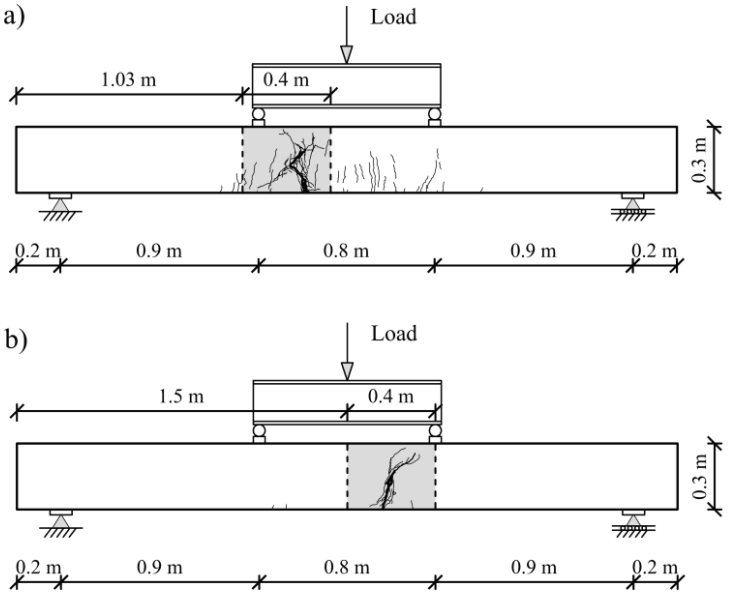

Fig. 8.7. Experimental setup and final crack pattern of a) beam FSB-a, and b) beam FSB-b. The shaded parts were sawn and CT-scanned.

Both beams were tested at the age of 28 days under the bending conditions given in Fig. 8.7. The beams were loaded using a hydraulic jack acting on a steel profile that transferred the load to the loading points. The deflection at midspan was measured with displacement transducers attached to the bottom face of the beams. For more details on the experimental programme, the reader may refer to Sarmiento et al. (2015).

8.3.2 Experimental results

The crack patterns in Fig. 8.7 and the load-deflection curves in Fig. 8.8 show clearly different behaviour in the two beams. In beam FSB-a, several flexural cracks developed, mostly in the central span, after the load reached 50 kN. In the absence of ordinary reinforcement, these cracks were only arrested by the fibres. After cracking, the load applied continued to increase up to 87 kN, when the deflection at midspan was 9.3 mm (deflection-span ratio δ/L of 1/280). From this deflection, damage localized in one crack and the load decreased gradually. The critical crack arose within the central span, developed vertically, and merged with multiple inclined cracks resulting in diffuse and tortuous paths. During the flexural failure, the beam exhibited some ductility; at a deflection of 17 mm ($\delta/L \approx 1/150$), the beam supported approximately half of its maximum load. Beam FSB-b had a much lower capacity than beam FSB-a. The onset of cracking led to sudden failure along a single crack. This crack started 17 cm from midspan, and propagated at an angle of approximately 60º towards the end of the beam.

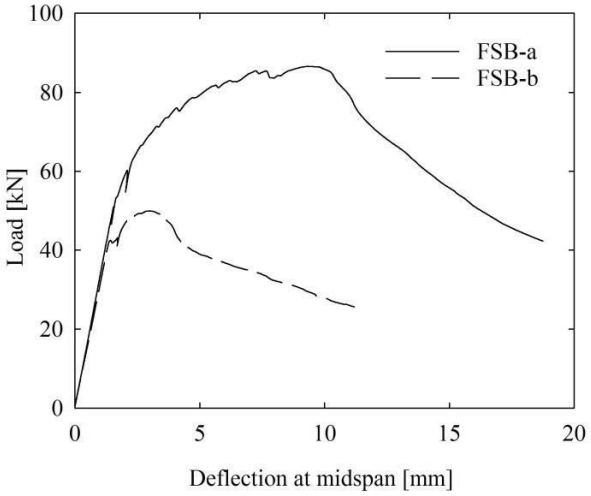

Fig. 8.8. Experimental load-deflection response of full-scale beams FSB-a and FSB-b.

8.4 Modelling and analysis results

The proposed modelling approach was evaluated modelling the beams FSB-a and FSB-b. As a first step to the numerical modelling, the fibre structure had to be obtained and the dependence of the residual strength on the fibre parameters had to be established. Numerical solutions in terms of load-deflection relationships and crack patterns were then compared with the experimental results to validate the approach and determine the predictive ability of the model.

8.4.1 Fibre structure and fibre parameters

CT scanning has been successfully used as a non-destructive method for the qualitative and quantitative evaluation of the orientation and distribution of steel fibres in FRC (Stähli et al., 2008, Suuronen et al., 2013, Švec et al., 2014, Sarmiento et al., 2014a). Scanning of an element produces a large number of radiographic images, and digital analysis of the sequence of images allows 3D visualization of the structure of fibres. Moreover, post-processing the images to a skeleton converts fibres into 3D segments located in the volume from which their topology, length and direction can be extracted.

Pieces 400 mm in length containing the critical cracks (Fig. 8.7) were sawn and examined using a medical CT scanner (Siemens SOMATOM Sensation 4). The fibre skeletons in Fig. 8.9 provide a first insight into the inhomogeneity of the fibre structure. The figure illustrates the skeleton of fibres in a longitudinal slice just 20 mm thick to avoid too dense an accumulation of fibres in the image.

To locally define $\mathbf{a_1}$ and v_f from the fibre structure of the sawn pieces, two discretizations in rectangular prismatic volumes were considered. The first discretization comprised 25 mm × 25 mm × 200 mm volumes. These volumes anticipated structural analysis with plane stress elements of 25 mm × 25 mm and a thickness of 200 mm. The second discretization consisted of 50 mm × 50 mm × 200 mm volumes.

Fig. 8.9 illustrates the sets of orientation ellipsoids and local volume fractions using the fine discretization. The grayscale maps of the volume fractions indicate the presence of areas with low fibre content. Beam FSB-b has a low density of fibres in its upper part, which shows that segregation of fibres has occurred. The orientation ellipsoids look like elongated ellipses in the height-length plane, and the direction of their major axis indicates the dominant fibre orientation ($\mathbf{a_1}$). The orientation tensors of the 48 discrete volumes of beam FSB-a in Fig. 8.9a have average ratios of the eigenvalues $\lambda_2/\lambda_1 = 0.37$

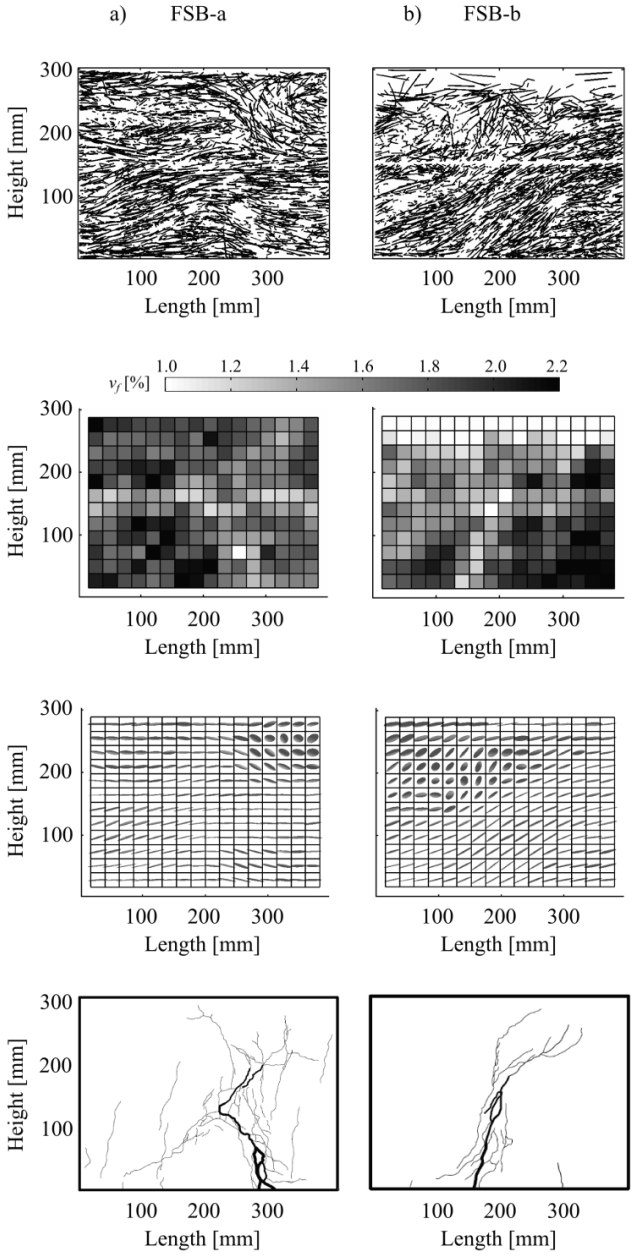

Fig. 8.9. From top to bottom: skeleton of fibres, local fibre volume fractions, orientation ellipsoids, and crack patterns of the scanned parts of a) beam FSB-a, and b) beam FSB-b.

and $\lambda_3/\lambda_1 = 0.17$. Note that in isotropic conditions the ratios would satisfy $\lambda_2/\lambda_1 = \lambda_3/\lambda_1 = 1$ and the orientation ellipsoids would be spheres. This confirms that there is a markedly unidirectional orientation of the fibres within the volumes in the direction $\mathbf{a_1}$, which supports the use of the fibre efficiency variable as described in Eq. 8.4.

8.4.2 Relationship between the residual tensile strength and fibre efficiency

The relationship between the residual tensile strength (σ_2) and the fibre efficiency variable (μ) was established from the experimental results of material characterization tests. The set of test specimens consisted of 12 notched beams (150 mm × 150 mm × 550 mm) and 10 notched cylinders (Ø150 mm × 150 mm) that were either cast in moulds or sawn/drilled from a structural element (Sarmiento et al., 2015). All the specimens were entirely CT scanned before being tested. The beams were put through three-point bending tests in accordance with EN14651 (European Standard, 2005) and the cylinders were tested in uniaxial tension based on RILEM (2001).

For the beams, the residual flexural tensile strength corresponding to 2.5 mm crack opening, often denoted f_{R3}, was used to calibrate the uniaxial residual strength (σ_2) in accordance with the relationship $\sigma_2 = f_{R3}/3$. The principles and assumptions of this relationship can be found elsewhere, e.g. in *fib* (2010). For the cylinders, σ_2 was taken as the tensile stress measured at a crack strain value of 0.02. This choice was based on the need to provide a consistent relationship between the results from bending and uniaxial tension tests (Ferrara et al., 2012b), despite the different strain distribution along the ligament of the respective specimens. Assuming a linear distribution of strains in the beams and the structural characteristic length equal to the ligament depth (125 mm), a crack width opening of 2.5 mm corresponds to a maximum tensile strain of 0.02 (Ferrara et al., 2012b). It is worth mentioning that two of the cylinders did not provide stable measurements at this strain level due to the initially unstable opening of the crack. These two cylinders were therefore excluded from the data set.

To characterize μ (Eq. 8.4), the fibre parameters $\mathbf{a_1}$ and v_f were determined in a slice located in the middle of the specimen with the thickness of the fibre length (60 mm). Because the specimens were notched, $\mathbf{n}$ was assumed perpendicular to the plane that contained the notched section. Normalized weightings w_1 and w_2 of 0.6 and 0.4, respectively, gave the best curve fit of the data set (see Fig. 8.10) with the power law:

$$\sigma_2 = 7.7\,\mu^{3.5} \quad \text{(in MPa)} \tag{8.5}$$

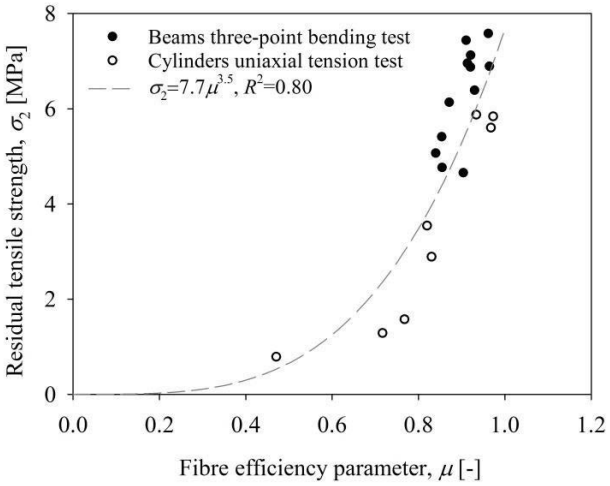

Fig. 8.10. Relationship between fibre efficiency and residual tensile strength derived from test specimens.

The values of w_1 and w_2 highlight the importance of including the variation of the fibre content, and not just the orientation, when defining the post-cracking response of FRC: 60% of the residual strength is explained by variations in the fibre orientation and 40% by variations in the local relative fibre volume fraction. This topic is further discussed in Sarmiento et al. (2014b).

8.4.3 Models with inhomogeneous and homogeneous fibre parameters

Due to the geometry and casting conditions of the beams, inhomogeneities of fibres across the width were negligible. In general, the dominant fibre directions $\mathbf{a_1}$ align parallel to the height-length plane of the beams. For this reason, and without limiting the generality of the foregoing, simulation of the beams FSB-a and FSB-b was addressed as a 2D plane stress problem.

The outline of the model of beam FSB-b is depicted in Fig. 8.11a. The darker shading corresponds to the scanned region where the fibre parameters were determined. For the rest of the beam, it was assumed that fibres oriented and distributed homogeneously, with $\mathbf{a_1}$ aligned with the longitudinal direction and fibre content $v_f = \overline{v}_f$.

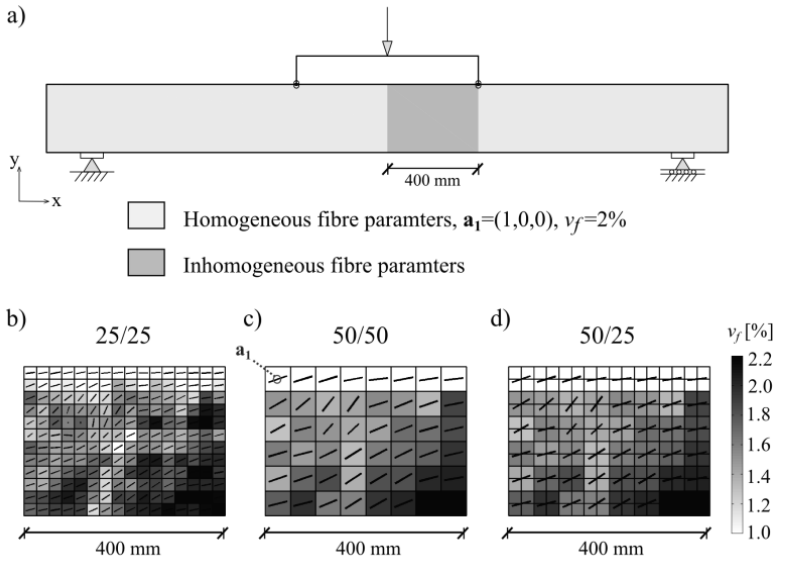

Fig. 8.11. a) Outline of the FE model of beam FSB-b. Variations in the fibre orientation and volume fraction that were considered in the elements of models: b) 25/25, c) 50/50, and d) 50/25.

Eight-node quadrilateral plane stress elements were used with 2 × 2 Gauss integration. Two models were defined with the element size (l_{el} × l_{el} × width of the beam) coinciding with the volume discretization presented in Section 8.4.1. Elements with l_{el} of 25 mm and 50 mm are considered sufficiently fine to allow kinematic modelling of the observed failure patterns and sufficiently coarse to justify a homogenization of the fibre properties within the volumes. A third model combines the coarser discretization of the fibre structure with the finer FE mesh. The models are denoted 25/25, 50/50 and 50/25, where the first term refers to the discretization of the fibre structure, and the second term indicates l_{el} of the finite elements. For example, the fibre parameters assigned to the elements of the inhomogeneous regions of the three models of beam FSB-b are illustrated in Fig. 8.11b-d. For comparison, models denoted hom/25 and hom/50 were analysed with homogeneous fibre parameters along the entire beam.

The steel profile that distributes the load (Fig. 8.7) was modelled with beam elements. Incremental loading was applied using deformation control of the centre of the profile. In this way, the external load was transferred symmetrically to the two loading points. The convergence criterion was set at 5% based on a force norm.

8.4.4 Material parameters for the stress-strain relationship

The material modelling framework presented in Section 8.2.4 was used. The compressive behaviour was defined using an elastic-ideal plastic model. A compressive strength of 86 MPa was determined experimentally, while the elastic modulus was simply assumed to be 30 GPa. The material parameters that define the stress-strain relationship in tension (Fig. 8.5) are discussed in the following.

The uniaxial tensile strength σ_1 was determined as the average tensile strength of the notched beams and cylinders described in Section 8.4.2. For the beams tested in bending, the uniaxial strength was estimated from the flexural strength in accordance with the relationship in *fib* (2010). The strain ε_2' was defined based on an approximation of the ultimate strain of plain concrete. In smeared cracking, such a strain is considered to be an element-related material property, which is usually estimated from the tensile strength, the fracture energy (G_F), and a characteristic length of the element, the equivalent length (h). An ultimate strain determined from a linear softening model could underestimate the steepness of the initial softening behaviour, as discussed in Sarmiento et al. (2014a). Because the initial part of the softening curve is the most decisive in the current model, it was considered more appropriate to define ε_2' in accordance with an exponential softening model (TNO DIANA, 2014). In this case, ε_2' can be expressed as:

$$\varepsilon_2' = \frac{\varepsilon_1}{2} + \frac{G_F}{h\,\sigma_1} \tag{8.6}$$

Due to the absence of experimental data, the fracture energy was determined in accordance with CEB-FIP (1990), and h was assumed to be l_{el} (note that all elements are square). The strain ε_3 was calibrated against the experimental results of the cylinders. In Fig. 8.12, the tensile stress is normalized by the residual stress measured at a crack strain of 0.02 (taken as σ_2 in Section 8.4.2) to make it possible to compare the post-cracking responses, which varied greatly depending on the fibre structure. As shown in the figure, the end of the plateau was assumed at a strain ε_3 of 0.1. The test measurements were unstable at the onset of cracking, even for cylinders with a hardening response. This meant that the hardening strain ε_2 at the initiation of the plateau could not be calibrated against the test results. In the absence of experimental data, ε_2 was estimated to be:

$$\varepsilon_2 = \varepsilon_1 + 1.5\ ‰ \tag{8.7}$$

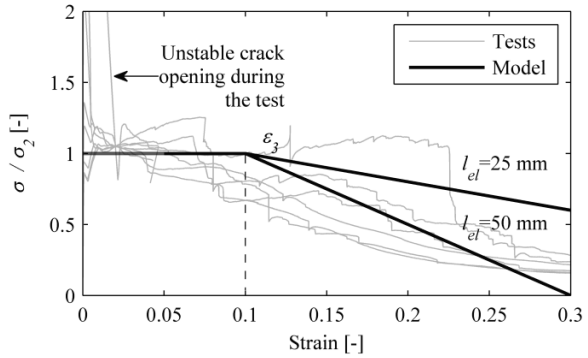

Fig. 8.12. Calibration of the material parameter ε_3 against the experimental uniaxial tension tests of cylinders.

The ultimate strain (ε_{ult}) was defined on the basis of the ultimate crack opening (w_{ult}) and regularized with the size of the finite element in accordance with $\varepsilon_{ult} = w_{ult}/l_{el}$. Some investigations, e.g. Kooiman (2000) and Cunha (2010), have related w_{ult} to the average projected embedded length of the fibres, which in turn can be determined as $l_f/4$, where l_f is the fibre length. In accordance with this, w_{ult} = 15 mm was used in the present work. Lateral contraction effects were neglected because the material was extensively cracked from an early stage of the analysis. The material parameters for this example are summarized in Table 8.2.

Table 8.2. Material input parameters.

Component	
Young modulus [MPa]	30000
Poisson ratio [-]	0
Compressive strength [MPa]	86
Fracture energy of plain concrete, G_F [N/mm]	0.113
Tensile strength, σ_1 [MPa]	5.12
ε_1 [-]	$1.71 \cdot 10^{-4}$
ε_2' [-] for l_{el} = 25 mm / 50 mm	$9.67 \cdot 10^{-4}$ / $5.26 \cdot 10^{-4}$
ε_2 [-]	$1.67 \cdot 10^{-3}$
ε_3 [-]	0.10
ε_{ult} [-] for l_{el} = 25 mm / 50 mm	0.60 / 0.30

8.4.5 Analysis results and discussion

Fig. 8.13a and b compare the experimental load-displacement curves of the beams FSB-a and FSB-b with their respective numerical solutions. The markers indicate the points where the analyses failed to reach full convergence. Non-converged steps were always

alternated with converged steps: within any deflection interval of 1.6 mm, at least one step converged.

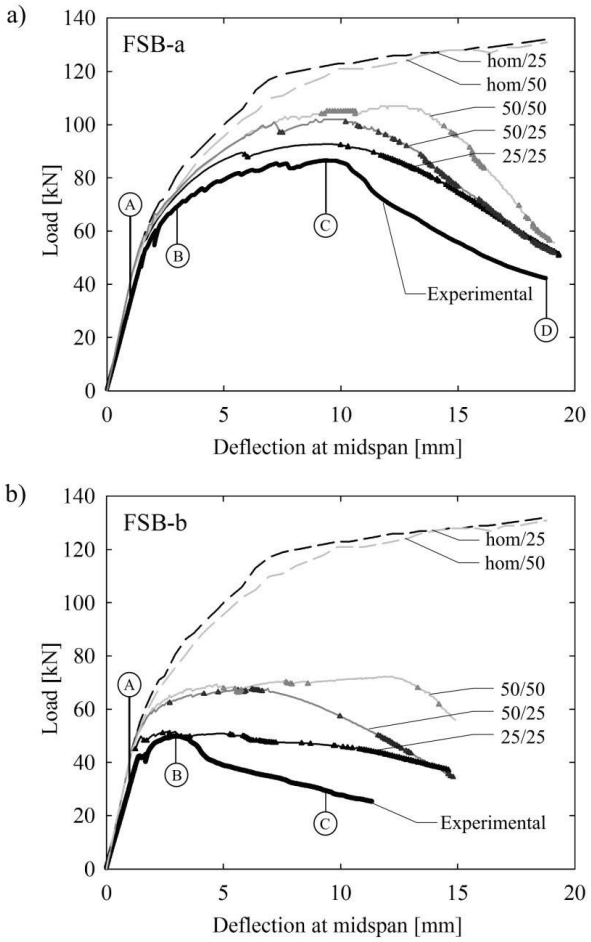

Fig. 8.13. Experimental and modelled load-deflection responses of full-scale beams: a) FSB-a, and b) FSB-b.

As expected, all the models predict exactly the same load-deflection relationship up to the onset of cracking. From that point on, the response depends greatly on the model. The homogeneous models provide a large load increase associated with strain hardening of the tensile stress-strain relationship. Note that for the homogeneous fibre parameters ($\mathbf{a_1}$ = (1,0,0) and v_f = 2%) and a vertical crack plane ($\mathbf{n}$ = (1,0,0)), the residual strength σ_2 in Eq. 8.5 takes the value 7.7 MPa. This value represents a theoretical case and is not intended to correspond to the results of standard beams, for which the average residual

strength was somewhat lower (6.3 MPa). A change of slope in the load-deflection curves of the hom/25 and hom/50 models occurs when the strains in the central span reach the plateau of the σ_n-ε_n diagram. Beyond this point, the load increases due to the spread of the fracture area, which activates an increasing number of fibres.

There are large differences in the load-deflection curves between homogeneous and inhomogeneous models, especially for beam FSB-b, whose fibre properties were particularly unfavourable. Apart from this, the three inhomogeneous models are able to predict the different structural performance between the two beams just by considering the fibre parameters in the inhomogeneous region. Nevertheless, the 50/50 and 50/25 models significantly overestimate the experimental results. Only the 25/25 model offers a realistic prediction up to the peak load; although it still overestimates the post-peak response.

Fig. 8.14 illustrates the crack propagation phenomenon with the 25/25 model. The contour plots depict the maximum principal strain at various deflection stages (A, B, C and D in Fig. 8.13). At stage A, cracking has initiated in the lower part of the beams. With increasing load, the crack localizes in the inhomogeneous region. In beam FSB-a, an inclined crack develops at the same time as the damage zone grows (see stage B in Fig. 8.14a). At stage C, cracking has spread over the inclined crack and in the lower part of the central span. The highly deformed areas sustain a constant stress, because the strains range within the limits of the plateau of the σ_n-ε_n diagram. Globally, the beam has reached the maximum load. Increasing the load causes crack localization in the inhomogeneous region once again. The load decreases gradually due to the unloading of the adjacent regions and the strain softening of the critical crack when reaching the strain level ε_3. Stage D shows the critical crack around a densely fractured area.

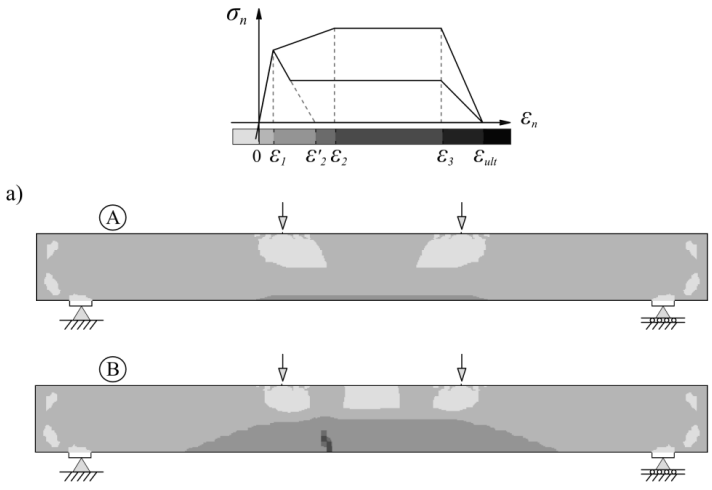

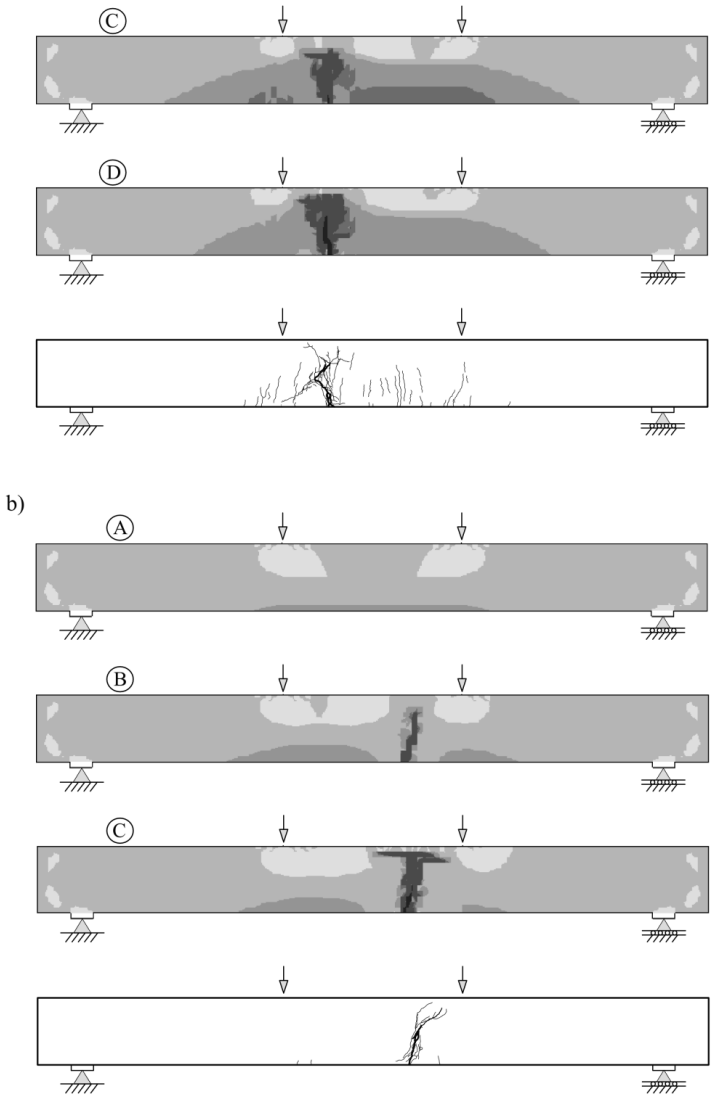

Fig. 8.14. Strain levels of the maximum principal strain for beams: a) FSB-a, and b) FSB-b. The deflection levels A, B, C and D are depicted in Fig. 8.13.

The critical crack of beam FSB-b develops at the onset of cracking (Fig. 8.14b). At stage B, the beam has reached the maximum load, and the critical crack has developed beyond 80% of the height of the beam. Increasing load leads to propagation of the crack towards the compressive zone. The crack path bifurcates in two opposite horizontal directions (see stage C). This splitting crack is the result of the large reduction in the

compressive zone depth above the crack, causing transverse tensile stresses. The crack easily propagates horizontally due to the low residual tensile strength in the vertical direction. This is related to the lack of fibres aligned in this direction and the low fibre content in the upper part of the beam. From a numerical point of view, the bifurcating crack path can also be due to the complex stress fields at the tips of the cracks paths (Jirásek and Bauer, 2012, Slobbe et al., 2014). Experimentally, the crack branched and inclined close to this area, but only in the direction of the end of the beam.

In general, the 25/25 model accurately predicts the location of the critical crack. Limiting the fibre inhomogeneity to a part of the model undoubtedly helped localize the crack in this region, but besides the crack location the model is able to capture adequately its propagation and the overall fracture process as well.

Comparison of the load-deflection results of the 50/25 and 25/25 models provides actual information on the extent to which the inhomogeneity of the fibre structure is well captured. The two models correlate closely only at large deflections. Otherwise, the 50/25 model estimates a greater post-cracking response and peak load. This can be ascribed to variations in the residual strength σ_2 caused by homogenizing the fibre parameters in smaller or larger volume regions. If larger volumes are used, possible weak paths are "averaged away" (see Fig. 8.11b and d), which explains why the load-carrying capacity of the 50/25 model is greater than that of the 25/25 model.

Up to its peak load, the results of the 50/25 model agree with those of the 50/50 model. The 50/50 model, however, reaches its peak load at a considerably greater deflection. Since the load decreases when the maximum strain exceeds ε_3, it seems that this strain level may not have been properly calibrated. This parameter needs further study, especially in terms of its mesh-size dependence.

Fig. 8.15 illustrates the strain contours of the three models of beam FSB-b at the deflection stage B. Only the inhomogeneous region is depicted. The 25/25 model shows the highly concentrated strains that follow the weak path of the fibre parameters (Fig. 8.11a). In the 50/25 and 50/50 models, the location of the critical crack is slightly offset because of the greater homogenization of the fibre structure in coarser volumes. Nevertheless, both models capture a certain inclination of the crack.

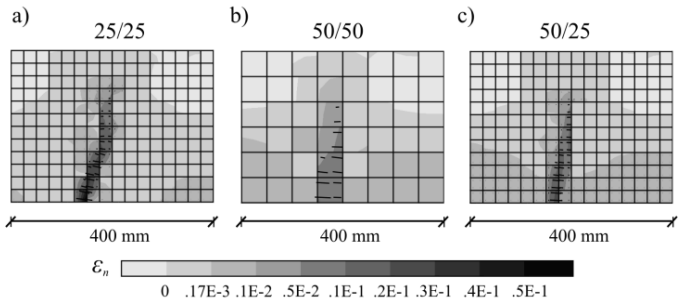

Fig. 8.15. Strain levels of the maximum principal strain and vectors for the inhomogeneous region of beam FSB-b in the three models: a) 25/25, b) 50/50, and c) 50/25.

8.5 Summary and conclusions

The current paper presents a modelling approach for FRC structural elements in which the fibre structure is considered at an intermediate level between the fibre level and the structural element level. The fibre structure is discretized and homogenized in volumes, and incorporated in a numerical model. The model uses a single-phase material definition depending on the local fibre parameters. In the absence of well-established constitutive modelling techniques for this intermediate level, a simplified stress-strain relationship was adopted. Heuristic material parameters were assumed, and a phenomenological relationship to describe the effect of the fibre parameters in the post-cracking response was calibrated. Further refinements should be aimed at establishing a fundamentally-based definition of the material at this level to make it possible to generalize the use of the method.

The modelling approach was implemented to analyse two beams in bending tests. The fibre structures of the beams in their critical region were obtained using CT scanning. The numerical results of the models incorporating these actual fibre structures presented large differences from the models assuming homogeneous fibre properties. The approach was able to capture a large difference in the bending capacity of the two beams, which can only be attributed to the differences in their fibre structures. Furthermore, it provided an adequate prediction of the location and propagation of the critical cracks. The estimated maximum load proved to be sensitive to the volume discretization of the fibre structure. A discretization in the range of half the fibre length led to a good agreement with the experimental maximum loads. In general, the post-peak responses were somewhat overestimated, which might be expected in view of the simplicity of the material model.

The use of this numerical approach is especially relevant to structural elements in which the flow of FRC at the casting stage is expected to lead to an uneven distribution of the fibres. The approach can be applied to structural elements whose fibre structure is obtained using flow simulations. Furthermore, the low computational cost of the numerical analyses makes it possible to study more complex structures.

Acknowledgement

The authors wish to acknowledge support from COIN – the Concrete Innovation Centre (www.coinweb.no) – a centre for research-based innovation, which was initiated by the Research Council of Norway (RCN) in 2006 for an eight-year period. The Centre was directed by SINTEF, with NTNU as a research partner, and the most recent industrial partners included Aker Solutions, Norcem, Norwegian Public Roads Administration, Rescon Mapei, Skanska, Unicon, Veidekke, and Weber Saint Gobain.

Chapter 9

Towards an integrated simulation of casting and structural performance

9.1 Introduction

In the previous chapters, a novel modelling approach was presented in which the fibre structure was taken into account in simulating the mechanical behaviour of FRC elements. The actual fibre structure was experimentally determined using CT scanning. This made it possible to validate the predicting ability of the proposed approach. In practice, though, CT scans will not be available.

In this chapter, the approach is applied to a structural element whose fibre structure is obtained using simulation of the concrete flow during casting. The aim is to demonstrate the coupling between the two simulation approaches. A validation will not be provided.

The demonstration example comprises the analysis of a wall element cast with self-compacting FRC. The investigation by Døssland (2008) revealed large variation in fibre orientation within wall elements using a vertical casting process. Her study served as a precedent for later analysis of these elements at NTNU. The wall element here presented was described in Žirgulis et al. (2015b). The authors performed numerical simulations of the casting process and a comparison of the fibre orientation with experimental results. Standard test elements were sawn from the wall element. For this reason, full-scale testing was not possible and experimental results are not available to validate the results of the present chapter.

The fibre structure from the flow simulation presented in Žirgulis et al. (2015b) is incorporated in the numerical approach to investigate the flexural behaviour of the wall

element in relation to the inhomogeneity of the fibre distribution and orientation. A three-point bending test was modelled for this purpose.

9.2 Materials and casting

The wall element illustrated in Fig. 9.1 was cast from a single point using self-compacting FRC. Four tie bars were used to tie the vertical walls of the formwork. In addition, nine standard beams (150 mm × 150 mm × 550 mm) were cast for three-point bending testing in accordance with EN14651 (European Standard, 2005).

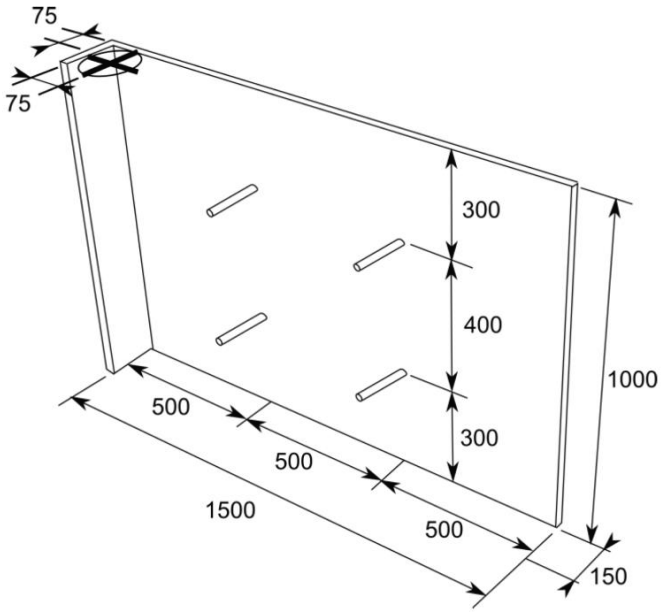

Fig. 9.1. Formwork dimensions, casting point, and position of the four tie bars. Dimensions in mm (Žirgulis et al., 2015b).

The mix design is given in Table 9.1. It contained 0.5% vol. of steel fibres, which had hooked-ends, a length of 60 mm, an aspect ratio of 80, and a minimum tensile strength of 1050 N/mm^2 according to the manufacturer.

The concrete was stable and had a satisfactory workability to fill the formwork by its own weight. The casting point was located close to one edge of the wall, see Fig. 9.1. Mixing procedure, fresh concrete properties and casting process are described in detail in Žirgulis et al. (2015b).

Table 9.1. Mix design for steel FRC with 0.5% vol. fibres.

Component	Dosage
Cement [kg/m^3]	388
Silica fume [kg/m^3]	19.4
Total free water [kg/m^3]	196
Aggregate 0-8 mm [kg/m^3]	1182
Aggregate 8-16 mm [kg/m^3]	570
Super-plasticizer [kg/m^3]	4.7
Air entrainer (1:7) [kg/m^3]	1.0
Steel fibres [kg/m^3, (% vol.)]	40, (0.5)
w/b ratio [-]	0.47
Matrix volume (< 0.125 mm) [l/m^3]	364

9.3 Simulation of vertical wall casting

A numerical framework was recently developed which is capable of predicting the free surface flow of a suspension of rigid particles in a non-Newtonian fluid (Švec and Skoček, 2013, Švec et al., 2012b). The framework is a combination of the lattice-Boltzmann method for fluid flow, a mass tracking algorithm for free surface representation, the immersed boundary method for two-way coupled interactions between fluid and rigid particles, and an algorithm for the dynamics and mutual interactions of rigid particles. The numerical framework models steel fibres as thin rigid cylinders and takes into account features such as the interaction between the fluid and the fibres, collisions between the fibres or between the fibres and the formwork, though unfortunately it does not include the segregation effect.

This numerical framework was used to simulate the vertical casting process of the wall element (Fig. 9.2). In Žirgulis et al. (2015b), the simulated fibre orientation pattern was compared to the actual fibre structure, which was experimentally investigated using CT scanning. The comparison showed reasonably good agreement and validated the use of the numerical simulation tool.

At the end of casting, fibre orientation appeared to be strongly influenced by the casting process. Most of the fibres were horizontally oriented in the area below the casting point and close to the bottom surface of the formwork. Furthermore, the results revealed a great impact of the tie bars on the fibre orientation and distribution.

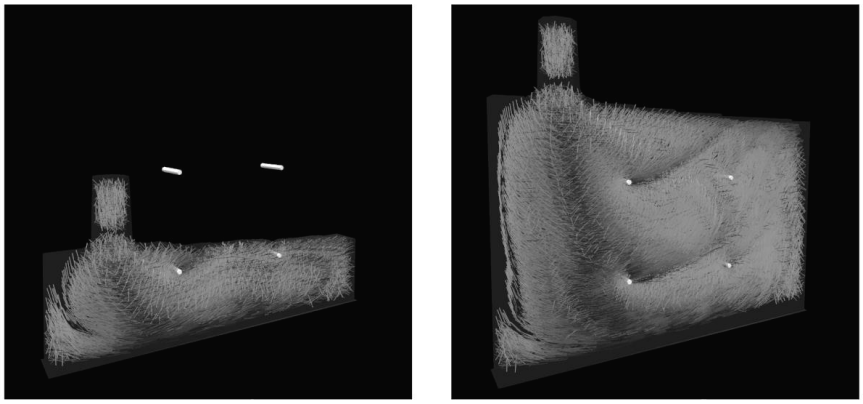

Fig. 9.2. Simulation of fibre orientation during vertical wall casting[5]. The white bars represent the bars used to tie the vertical walls of the formwork.

9.4 Simulation of a bending test

9.4.1 FRC as an inhomogeneous and anisotropic material

The flow simulation presented in Section 0 can fully describe the fibre structure in the investigated wall by providing the location of every fibre at the end of casting. The fibre structure was discretized in volumes with dimensions of 50 mm × 50 mm × 150 mm, in length, height and thickness direction, in order to define the local fibre properties. The variations of the fibre orientation and distribution across the element thickness were negligible, which explains why the wall is not discretised in that direction.

The fibre skeletons in Fig. 9.3a provides a first insight into the inhomogeneous and anisotropic fibre structure. The figure illustrates the skeleton of fibres in a longitudinal slice just 50 mm thick to avoid a too dense image. Fig. 9.3b and c illustrate the set of local volume fractions and orientation ellipsoids obtained from the fibre structure. The grayscale map reveals an uneven fibre distribution within the wall, though the low fibre content along the edges seems unrealistic.

The nonlinear FE simulation of the wall was addressed as a 2D plane stress problem. Eight-node quadrilateral plane stress elements with 2 × 2 Gauss integration were used. The model was defined with the element size (50 mm × 50 mm × thickness of the wall)

[5] www.dti.dk/4c-flow/33808

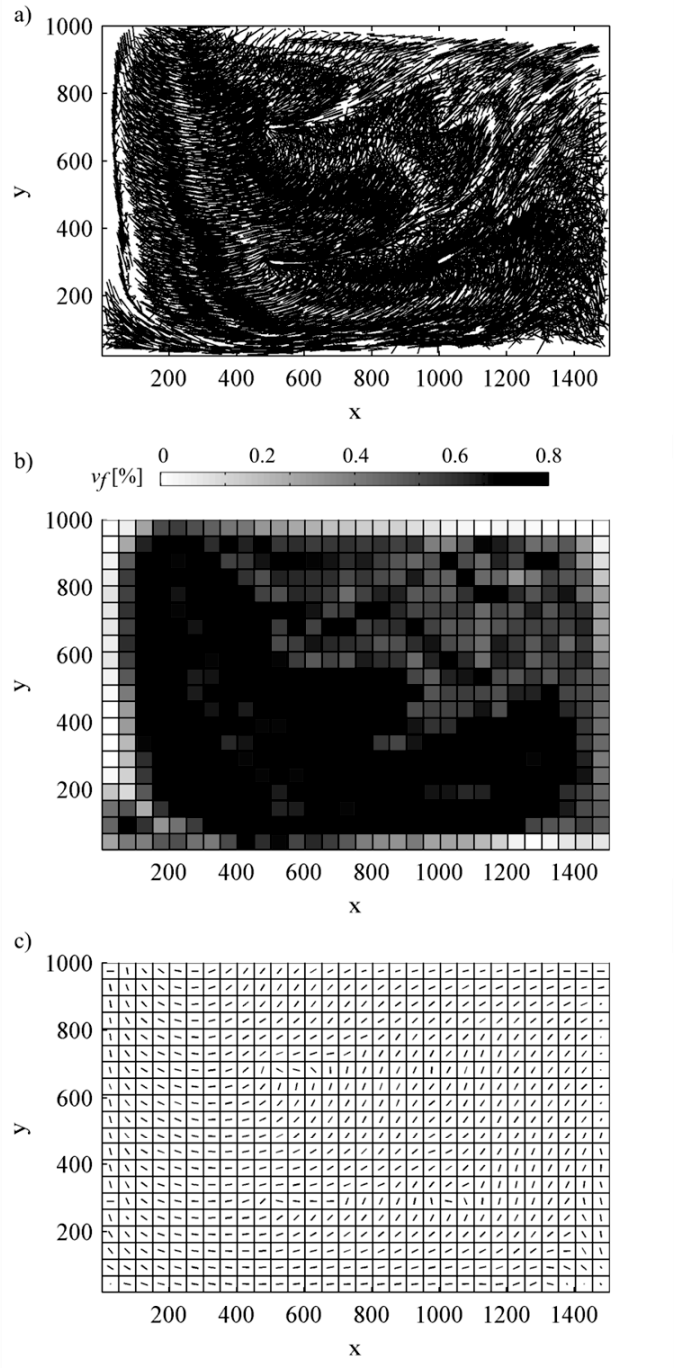

Fig. 9.3. a) Skeleton of fibres, b) local volume fractions and c) dominant fibre directions ($\mathbf{a}_1$).

coinciding with the volume discretization of the fibre structure. The model is denoted 50/50, where the first term refers to the volume discretization and the second term indicates the size of the finite elements.

An imaginary loading was applied at the central point at the topside of the wall. The horizontal displacement of this point was constrained, as well as the vertical displacement of the two supports (Fig. 9.4). The load was applied incrementally using displacement control. A linear elastic behaviour was assumed for the elements adjacent to the supports and loading point. The convergence criterion was set at 5% based on a force norm.

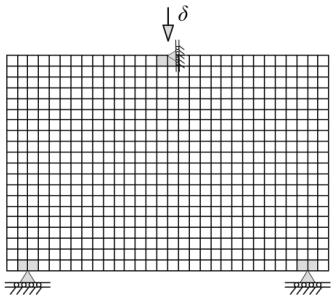

Fig. 9.4. Mesh with 50 mm × 50 mm elements, supports and loading system for a wall element.

The nonlinear behaviour of the material was modelled with a rotating smeared crack model based on a total strain concept. The compressive behaviour was defined using an elastic-ideal plastic stress-strain model. The uniaxial tensile stress-strain model was assumed to be as depicted in Fig. 9.5. Most parameters were derived from experimental data and are related with the composition and characteristics of the FRC under consideration. The calibration of the material parameters was already described in previous sections (Sections 7.2.3 and 8.4.4). Table 9.2 summarizes the material parameters considered in this case study.

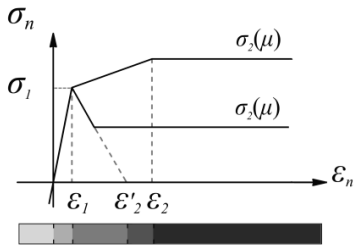

Fig. 9.5. Uniaxial tensile stress-strain relationship.

Table 9.2. Material input parameters.

Material parameter	
Young modulus [MPa]	38000
Compressive strength [MPa]	65
Fracture energy of plain concrete, G_F [N/mm]	0.154
Tensile strength, σ_1 [MPa]	3.8
ε_1 [-]	$1.0 \cdot 10^{-4}$
ε_2' [-] (Eq. 8.6)	$8.6 \cdot 10^{-4}$
ε_2 [-] (Eq. 8.7)	$1.6 \cdot 10^{-3}$

The FE modelling evaluates the fibre efficiency variable μ at each integration point based on the fibre parameter v_f and the angle θ between the fibre dominant orientation ($\mathbf{a_1}$) and the principal strain direction (Eq. 7.4). The model thus assesses the residual tensile strength σ_2 that defines completely the uniaxial stress-strain model. Eq. 9.1 and 9.2 describe the relationship between σ_2 and μ. For the present mix, this relationship was established in Section 7.3.3 from the analysis of an experimental set of 15 specimens which covered a wide range of fibre dispersions (see Fig. 7.7).

$$\sigma_2 = 7.20\,\mu - 3.20\,, \quad \text{if} \quad \mu \geq 0.5 \tag{9.1}$$

$$\sigma_2 = 0.77\,\mu\,, \quad \text{if} \quad \mu < 0.5 \tag{9.2}$$

This model is therefore able to take into account the inhomogeneities of the fibre structure and the anisotropic behaviour of the material.

9.4.2 FRC as a homogeneous and isotropic material (Reference model)

A reference model, denoted Reference/50, was considered for the purpose of comparison. This model did not incorporate the local fibre parameters. The material behaviour was therefore assumed to be isotropic and homogeneous throughout the wall element. The uniaxial tensile behaviour was defined in accordance with Fig. 9.5, but in this case the residual tensile strength σ_2 was fixed as any other parameter of the diagram. Its value was derived from three-point bending tests of the standard beams cast in addition to the wall, and calibrated in accordance with the relationship $\sigma_2 = f_{R3}/3$ (*fib*, 2010). The average residual flexural tensile strength f_{R3} obtained for the nine beams was 8.9 MPa; therefore σ_2 was assumed to be 3.0 MPa.

The material parameters and the FE mesh for this model were the same as those for the 50/50 model (Table 9.2, Fig. 9.4).

9.4.3 Analysis results

Fig. 9.6 compares the load-displacement curves of the 50/50 and Reference/50 models. As expected, the two models predict exactly the same load-deflection relationship up to the onset of cracking. Fig. 9.7-Fig. 9.10 illustrate the crack propagation phenomenon of the two models using contour plots that depict the maximum principal strain at the deflection stages A-D indicated in Fig. 9.6.

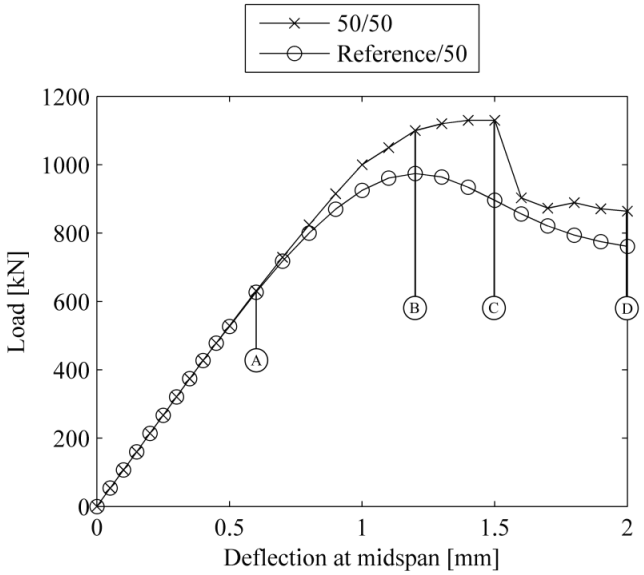

Fig. 9.6. Load-deflection responses of the wall for 50/50 model, and Reference/50 model.

At stage A, cracking has been initiated in the lower part of both models (Fig. 9.7). The Reference/50 model reaches the peak load at the deflection level B. At this stage the damage zone has extended and large strains concentrate at midspan in the lower part of the wall (Fig. 9.8a). From that point on, the damage area grows upwards (Fig. 9.8a-Fig. 9.10a), and the load decreases gradually; at stage D the value is 79% of the peak load.

At stage B, the 50/50 model sustains 13% larger load than the Reference/50 model. Moreover, Fig. 9.8b shows a smaller area of large strains compared to Fig. 9.8a. The load increases up to stage C, at which the value is 26% larger than for the Reference/50 model. Increasing the deflection causes a sudden load reduction. At stage D, the applied load is 76% of the peak load. For the 50/50 model, damage extends over a larger area than for the Reference/50 model, and large strains do not propagate uniformly, but are governed by the local material properties (Fig. 9.9b-Fig. 9.10b).

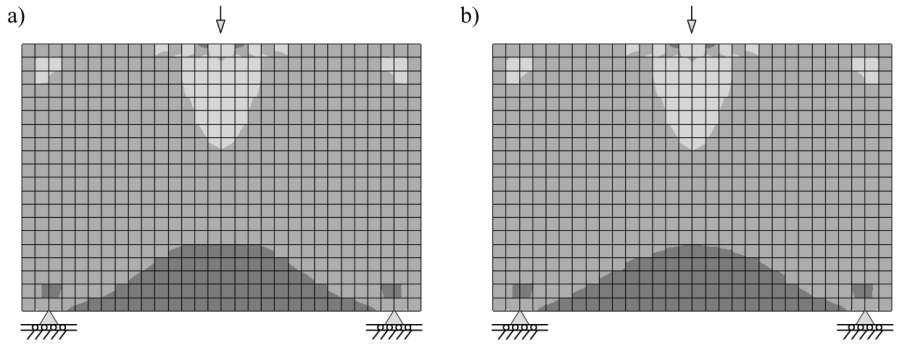

Fig. 9.7. Strain levels of the maximum principal strain of the wall at a deflection level A (Fig. 9.6) for: a) Reference/50 model, and b) 50/50 model (grayscale levels are defined in Fig. 9.5).

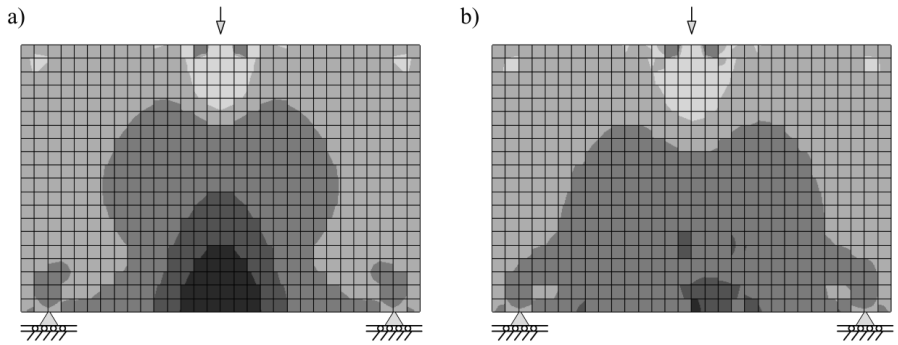

Fig. 9.8. Strain levels of the maximum principal strain of the wall at a deflection level B (Fig. 9.6) for: a) Reference/50 model, and b) 50/50 model (grayscale levels are defined in Fig. 9.5).

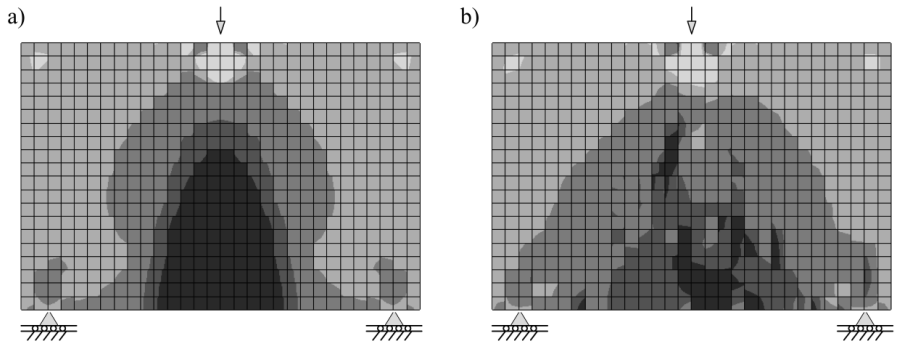

Fig. 9.9. Strain levels of the maximum principal strain of the wall at a deflection level C (Fig. 9.6) for: a) Reference/50 model, and b) 50/50 model (grayscale levels are defined in Fig. 9.5).

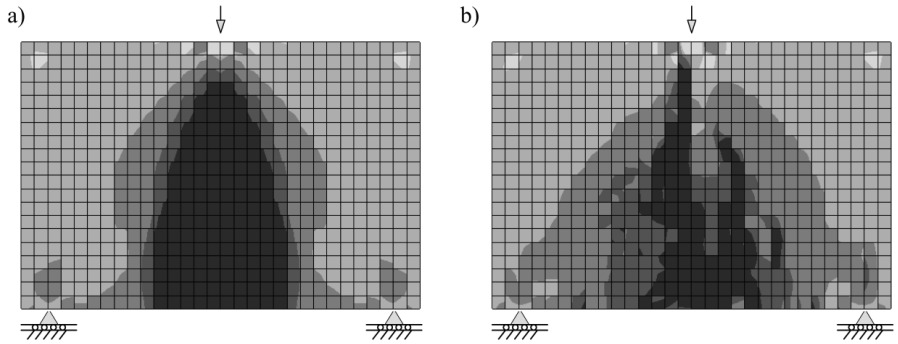

Fig. 9.10. Strain levels of the maximum principal strain of the wall at a deflection level D (Fig. 9.6) for: a) Reference/50 model, and b) 50/50 model (grayscale levels are defined in Fig. 9.5).

The results in Fig. 9.6 indicate that modelling the walls disregarding the inhomogeneous and anisotropic fibre configuration leads, in this case, to an underestimation of the load-carrying capacity.

9.5 Conclusions

In this chapter, the coupling between the simulation of the casting process and the modelling approach presented in Chapters 7 and 8 was demonstrated.

The flexural behaviour of a wall element cast with self-compacting FRC was analysed. The fibre structure simulated in Žirgulis et al. (2015b) was incorporated in a FE model based on the principles of the proposed modelling approach. The analysis was able to take into account the inhomogeneities of the fibre structure and the anistotropic behaviour of the material. This model was compared with a reference model, in which the behaviour of the FRC was assumed to be isotropic and homogeneous throughout the wall element. The comparison of the results revealed significant differences in the load-carrying capacity and in the crack pattern.

This coupling between simulation tools offers a comprehensive framework linking the casting process to the structural response. Simulations integrating casting and testing might contribute to further investigate the limitations and opportunities of the use of flowable FRC in load-carrying structures.

Chapters 4 and 5 had revealed mainly negative effects of the inhomogeneous and anisotropic fibre configuration on the flexural behaviour of full-scale beams cast with flowable FRC. The analysis presented in this chapter suggests, however, that the uneven

fibre distribution and orientation may also have a beneficial effect, especially in elements that can provide high levels of stress redistribution.

Part IV

Concluding remarks

Chapter 10

Conclusions and future perspectives

10.1 Conclusions

This thesis has investigated the application of flowable FRC to structural beams. The research included comparison between the performance of standard specimens and full-scale beams with regard to fibre distribution and orientation, and their influence on design assumptions and structural behaviour. Moreover, the research project involved development of a modelling approach especially devised for structural elements cast with flowable FRC.

The scope of this work aimed at covering the objectives presented in the introduction of the thesis. In the following, the main conclusions of the project are presented in relation to its original aims.

The structural behaviour of full-scale beams cast with flowable FRC

The results from the experimentally tested beams cast with flowable FRC reveal that the increase in the load-carrying capacity provided by the fibres did not correspond to the expected behaviour.

The mix with 2% vol. of steel fibres presented large deviations between the four tested full-scale beams, a significant loss of ductility and atypical crack patterns. Similar deviations were not observed for the hybrid polymer-steel FRC mix, whose fibre dosage was limited to 1% vol. In both cases, however, full-scale beams exhibited considerably less load-carrying capacity than estimated from the results of the standard three-point bending tests.

Fibre distribution and orientation in full-scale beams and their impact on flexural behaviour

The characterization of the fibre configuration revealed that uneven distribution and orientation of fibres can occur in full-scale beams cast with flowable FRC even though inhomogeneity is not detected at the production stage.

The following observations were made for the full-scale beams cast with the hybrid mix with 1% vol. of fibres:

- The polymer fibres distributed uniformly over the height and length of the beams.
- The tendency of the steel fibres to segregate depended on the consistency of the fresh concrete; in any case, a non-uniform distribution was observed after a certain flow length.
- The most pronounced orientation in the length direction occurred in the bottom half of the beams.
- A higher degree of orientation was observed for polymer fibres than for steel fibres.
- These uneven fibre configurations led to varying mechanical properties of the FRC within the beams. As a consequence, the overall structural performance of each beam was most likely governed by a locally unfavourable fibre configuration.

The following observations were made for the full-scale beams cast with the mix with 2% vol. of steel fibres:

- CT scanning revealed that the fibres were oriented in accordance with wavy flow lines.
- The fibre distribution presented an uneven pattern with bands differing in fibre content and signs of segregation for some of the elements.
- The bands with low fibre content and the varying fibre orientation played an important role in crack propagation and triggered early failure and loss of ductility.

Despite the apparently beneficial conditions of beam casting with regard to fibre orientation, the present investigation has highlighted the potential existence of fibre inhomogeneities associated with it. Furthermore, this study has helped disclose the strong connection between variations in fibre configuration and variations in structural behaviour, which might otherwise have been understood as variations intrinsic to the material.

Fibre distribution and orientation in standard test specimens and their impact on the material characterization

Chapters 4 and 5 evaluated the representativeness of small-scale specimens for the characterization of the behaviour of full-scale beams for two types of specimens:

specimens cast in a standard procedure, and specimens sawn or drilled to represent the material in a structural application as closely as possible.

The results show that the fibre configuration in the standard beams differed little from the average fibre configuration in the full-scale beams. This suggests that standard beams can be representative for the material used in full-scale beams. Nonetheless:

- The inhomogeneities observed in the full-scale beams were not present in the standard beams and, as previously mentioned, the presence of weak regions governed the overall structural performance of the full-scale beams.
- CT scanning revealed a preferred orientation of fibres in planes perpendicular to the vertical casting direction. This was observed in both full-scale beams and standard beams, but the 90º rotation of the standard beams means that fibres were distributed in vertical planes during testing.
- The presence of the notch in the standard beams reduced the influence of the fibre configuration on the mechanical response.

The fibre configurations obtained by using CT confirmed that a test beam sawn from a full-scale element and tested in the relevant direction is certainly a more representative specimen than a standard beam. However, if a non-uniform fibre configuration occurs in the full-scale element, the structural behaviour of the sawn beam will depend on its location within the full-scale element.

Cylinders for uniaxial tension test showed large variations in their fibre configurations. For cast cylinders, these variations were the result of constrained casting, while for drilled cores they were related to the location of the cores within the full-scale beams. The test results demonstrated the strong impact of fibre configuration, which indicates the great difficulties associated with the use of this test.

This research project has demonstrated that variations in fibre content may be significant in both test specimens and full-scale beams. If a non-uniform distribution of the fibres occurs in an element, the determination of the orientation factor without considering the actual volume fraction may lead to unsound conclusions. The combined effect of the fibre orientation and the local volume fraction appears to explain the variations in the post-cracking behaviour of FRC. A single parameter that incorporates the contributions of both the fibre orientation and the local volume fraction, denoted the fibre efficiency parameter (μ), has been found to correlate well with the residual tensile strength.

Incorporating the effect of fibre configuration in the prediction of the structural behaviour of flowable FRC

Based on the observations of non-uniform distribution and orientation of the fibres in the full-scale beams studied, procedures for estimating the structural performance of flowable FRC need to include determinations or predictions of the fibre configuration.

From a design-oriented perspective, one possible solution is to use small-scale standard beams to evaluate the quality of the FRC and correct the design material properties derived from this test to include favourable or unfavourable effects of the fibre configuration, as recommended in e.g. the Model Code 2010. However, this correction is based on the fibre orientation alone. In view of the large variations in fibre content that were identified, both in test specimens and in full-scale beams, it is suggested that correction methods should take account of potential variations in the fibre content as well as orientation.

As a more advanced solution, a novel approach for FRC structural elements is proposed, in which the actual fibre configuration is taken into account to simulate the mechanical behaviour using FE modelling. The analyses presented in this thesis demonstrated that this methodology was able to properly predict the large differences in bending capacity of the beams tested, their loss of ductility, and their atypical crack patterns. Further refinements should be aimed at improving the robustness of the simulations and establishing a more fundamental definition of the material.

The application of the proposed approach calls for the use of predictive methods based on flow simulations to determine the fibre configuration in the intended structural application. The example presented in Chapter 9 showed that a coupling of the two simulation approaches is possible and can lead to integrated simulations of casting and structural behaviour. The proposed modelling approach combined with flow simulations could contribute to a more efficient structural use of FRC.

10.2 Future perspectives

The present research project has helped illuminate the significance of fibre configuration for the mechanical behaviour of flowable FRC. However, the correlation of fresh concrete properties with structural design is a topic that deserves much further investigation.

Some of the findings of this thesis suggest that to achieve material development there is a need to characterize the robustness and fresh state performance of flowable FRC under full-scale casting conditions. Both the casting process and the flow length require

consideration. Flow-induced effects on fibre distribution are differentiating features of flowable FRC that should be treated as such already in the material development stage.

Accurate design approaches require characterization of fibre distribution and orientation in the structural application. Further development of detection methods to assess the fibre configuration in multiple structural applications would help. Research in this field is already ongoing, but further investigations should address increasing their availability for industrial use. It is equally important to further develop the numerical tools that simulate the casting process and predict the most likely fibre configuration. Further development is needed to incorporate the fibre segregation effect, and to overcome the limits imposed by computational time on the size of the structures or the number of fibres that can be simulated.

The identification of design material properties based on the assumption of random distribution and orientation of fibres does not seem to be appropriate for flowable FRC. This is already recognized in several design guidelines for FRC; the Model Code 2010, for instance, allows for favourable and unfavourable effects to be considered based on an experimental evaluation of fibre orientation. However, at present there is a lack of specifications for how this favourable or unfavourable fibre orientation can be identified and implemented to correct the design material properties. The present thesis has helped identify that, in addition to fibre orientation, variations in volume fraction should be carefully considered. Further research is needed, however, to help establish a robust methodology for practical applications.

For research and development purposes, the modelling approach presented in this thesis has shown a potential to describe the influence of fibre structure on flexural behaviour. However, there are still a number of possible improvements, for instance with regard to the robustness and definition of the material. The basis for a fundamental definition of the material should be established to enable more general use of the method. An obvious next step is to evaluate the ability of the approach to both describe and predict the structural behaviour for other geometries and/or loading conditions that lead to other failure mechanisms than flexure.

Variations in fibre distribution and fibre orientation have been shown to have a strong impact on the structural performance of the full-scale beams investigated in this project. However, different structural elements have different sensitivity to the effects of fibre configuration. This is related to the stress redistribution ability of the structural element, and further investigations should address the investigation of this topic.

One specific focus area would be the investigation of dapped-end beams. Experimental research at NTNU has confirmed that flowable FRC may efficiently simplify the high

concentration of reinforcement in the discontinuity region. Future work is planned to analyse these elements with the modelling approach proposed in this thesis and some of the elements have already been simulated and CT-scanned.

Bibliography

ABRISHAMBAF, A., BARROS, J. A. O. & CUNHA, V. M. C. F. (2013) Relation between fibre distribution and post-cracking behaviour in steel fibre reinforced self-compacting concrete panels. *Cement and Concrete Research,* 51**,** 57-66.

ABRISHAMBAF, A., BARROS, J. A. O., CUNHA, V. M. C. F. & CUNHA, F. N. M. (2012) Assessment of fibre orientation and distribution in steel fibre reinforced self-compacting concrete panels. In BARROS, J. A. O. (Ed.) *8th RILEM International Symposium on Fiber Reinforced Concrete: challenges and opportunities (BEFIB 2012).* Guimaraes, Portugal, RILEM Publications SARL**,** 100-112.

ACI COMMITTEE 544 (2002) State-of-the-Art Report on Fiber Reinforced Concrete, ACI 544.1R-96 (Reapproved 2002).

ADVANI, S. G. & TUCKER, C. L. (1987) The use of tensors to describe and predict fiber orientation in short fiber composites. *Journal of Rheology,* 31**,** 751-784.

AKCAY, B. & TASDEMIR, M. A. (2012) Mechanical behaviour and fibre dispersion of hybrid steel fibre reinforced self-compacting concrete. *Construction and Building Materials,* 28**,** 287-293.

ALBERTI, M. G., ENFEDAQUE, A. & GÁLVEZ, J. C. (2014a) On the mechanical properties and fracture behavior of polyolefin fiber-reinforced self-compacting concrete. *Construction and Building Materials,* 55**,** 274-288.

ALBERTI, M. G., ENFEDAQUE, A., GÁLVEZ, J. C., CÁNOVAS, M. F. & OSORIO, I. R. (2014b) Polyolefin fiber-reinforced concrete enhanced with steel-hooked fibers in low proportions. *Materials & Design,* 60**,** 57-65.

ARMELIN, H. S. & BANTHIA, N. (1997) Predicting the Flexural Postcracking Performance of Steel Fiber Reinforced Concrete from the Pullout of Single Fibers. *Materials Journal,* 94**,** 18-31.

ASTM INTERNATIONAL (2010) ASTM C1399 / C1399M-10, Standard Test Method for Obtaining Average Residual-Strength of Fiber-Reinforced Concrete. West Conshohocken, PA, USA.

ASTM INTERNATIONAL (2012a) ASTM C1550-12a, Standard Test Method for Flexural Toughness of Fiber Reinforced Concrete (Using Centrally Loaded Round Panel). West Conshohocken, PA, USA.

ASTM INTERNATIONAL (2012b) ASTM C1609 / C1609M-12, Standard Test Method for Flexural Performance of Fiber-Reinforced Concrete (Using Beam With Third-Point Loading). West Conshohocken, PA, USA.

ASTM INTERNATIONAL (2014) ASTM C1611 / C1611M, Standard Test Method for Slump Flow of Self-Consolidating Concrete. West Conshohocken, PA, USA.

AVESTON, J. & KELLY, A. (1973) Theory of multiple fracture of fibrous composites. *Journal of Materials Science,* 8**,** 352-362.

BANTHIA, N. & GUPTA, R. (2004) Hybrid fiber reinforced concrete (HyFRC): fiber synergy in high strength matrices. *Materials and Structures,* 37**,** 707-716.

BARNETT, S., LATASTE, J.-F., PARRY, T., MILLARD, S. & SOUTSOS, M. (2010) Assessment of fibre orientation in ultra high performance fibre reinforced concrete and its effect on flexural strength. *Materials and Structures,* 43**,** 1009-1023.

BARROS, J. A. O., CUNHA, V. M. C. F., RIBEIRO, A. F. & ANTUNES, J. A. B. (2005) Post-cracking behaviour of steel fibre reinforced concrete. *Materials and Structures,* 38**,** 47-56.

BAY, R. S. & TUCKER, C. L. (1992) Stereological measurement and error estimates for three-dimensional fiber orientation. *Polymer Engineering & Science,* 32**,** 240-253.

BAYASI, M. Z. & SOROUSHIAN, P. (1992) Effect of Steel Fiber Reinforcement on Fresh Mix Properties of Concrete. *Materials Journal,* 89**,** 369-374.

BEGHINI, A., BAZANT, Z. P., ZHOU, Y., GOUIRAND, O. & CANER, F. C. (2007) Microplane model M5f for multiaxial behavior and fracture of fiber-reinforced concrete. *Journal of Engineering Mechanics-ASCE,* 133**,** 66-75.

BENTUR, A. & MINDESS, S. (2006) *Fibre reinforced cementitious composites*, CRC Press.

BERG, S. A. & JACOBSEN, S. (2007) Packing of fibres and aggregate reviewed and calculated with Westmans equation. In KANSTAD, T. (Ed.) *International Workshop & Nordic Miniseminar: Fibre Reinforced Concrete.* Trondheim, Norway, The Nordic Concrete Federation**,** 81-93.

BLANCO, A. (2013) Characterization and modelling of SFRC elements. *Departament d'Enginyeria de la Construcció,* Doctoral thesis*,* Universitat Politècnica de Catalunya*.* Barcelona, Spain.

BOLANDER, J., CHOI, S. & DUDDUKURI, S. (2008) Fracture of fiber-reinforced cement composites: effects of fiber dispersion. *International Journal of Fracture,* 154**,** 73-86.

BOULEKBACHE, B., HAMRAT, M., CHEMROUK, M. & AMZIANE, S. (2010) Flowability of fibre-reinforced concrete and its effect on the mechanical properties of the material. *Construction and Building Materials,* 24**,** 1664-1671.

BURATTI, N. & MAZZOTTI, C. (2012a) Effects of different types and dosages of fibres on the long–term behaviour of fibre–reinforced self–compacting concrete. In BARROS, J. A. O. (Ed.) *8th RILEM International Symposium on Fiber Reinforced Concrete: challenges and opportunities (BEFIB 2012).* Guimaraes, Portugal, RILEM Publications SARL**,** 726- 738.

BURATTI, N. & MAZZOTTI, C. (2012b) Temperature effect on the long-term behaviour of macro-synthetic-and steel-fibre reinforced concrete. In BARROS, J. A. O. (Ed.) *8th RILEM International Symposium on Fiber Reinforced Concrete: challenges and opportunities (BEFIB 2012).* Guimaraes, Portugal, RILEM Publications SARL**,** 715- 725.

BURATTI, N., MAZZOTTI, C. & SAVOIA, M. (2011) Post-cracking behaviour of steel and macro-synthetic fibre-reinforced concretes. *Construction and Building Materials,* 25**,** 2713-2722.

CARMONA, S. & AGUADO, A. (2012) New model for the indirect determination of the tensile stress–strain curve of concrete by means of the Brazilian test. *Materials and Structures,* 45**,** 1473-1485.

CASANOVA, P. & ROSSI, P. (1996) Analysis of metallic fibre-reinforced concrete beams submitted to bending. *Materials and Structures,* 29**,** 354-361.

CEB-FIP (1990) Model Code for Concrete Structures 1990, Comité Euro-International du Béton. Lausanne, Switzerland.

CHIACHIO, M., CHIACHIO, J. & RUS, G. (2012) Reliability in composites – A selective review and survey of current development. *Composites Part B: Engineering,* 43**,** 902-913.

COMINOLI, L., MEDA, A. & PLIZZARI, G. A. (2007) Fracture properties of high-strength hybrid fiber-reinforced concrete. In GROSSE, C. U. (Ed.) *Advances in Construction Materials 2007.* Springer Berlin Heidelberg**,** 139-146.

CUNHA, V., BARROS, J. & SENA-CRUZ, J. (2010) Pullout Behavior of Steel Fibers in Self-Compacting Concrete. *Journal of Materials in Civil Engineering,* 22**,** 1-9.

CUNHA, V. M. C. F. (2010) Steel fibre reinforced self-compacting concrete (from micromechanics to composite behavior). *Departamento de Engenharia Civil,* Doctoral thesis*,* Universidade do Minho*.* Braga, Portugal.

CUNHA, V. M. C. F., BARROS, J. A. O. & SENA-CRUZ, J. M. (2011) An integrated approach for modelling the tensile behaviour of steel fibre reinforced self-compacting concrete. *Cement and Concrete Research,* 41**,** 64-76.

CUNHA, V. M. C. F., BARROS, J. A. O. & SENA-CRUZ, J. M. (2012) A finite element model with discrete embedded elements for fibre reinforced composites. *Computers & Structures,* 94–95**,** 22-33.

DAfStb (2012) Steel fibre reinforced concrete. CEN/TC 250/SC 2/WG 1/TG 2 N 66. Berlin, Germany, DAfStb (German Committee for Structural Concrete).

DAWOOD, E. T. & RAMLI, M. (2012) Mechanical properties of high strength flowing concrete with hybrid fibers. *Construction and Building Materials,* 28**,** 193-200.

DE MONTAIGNAC, R., MASSICOTTE, B. & CHARRON, J.-P. (2012) Design of large SFRC member in bending. In BARROS, J. A. O. (Ed.) *8th RILEM International Symposium on Fiber Reinforced Concrete: challenges and opportunities (BEFIB 2012).* Guimaraes, Portugal**,** 176-188.

DE OLIVEIRA E SOUSA, J. & GETTU, R. (2006) Determining the Tensile Stress-Crack Opening Curve of Concrete by Inverse Analysis. *Journal of Engineering Mechanics,* 132**,** 141-148.

DEEB, R., KARIHALOO, B. L. & KULASEGARAM, S. (2014) Reorientation of short steel fibres during the flow of self-compacting concrete mix and determination of the fibre orientation factor. *Cement and Concrete Research,* 56**,** 112-120.

DI PRISCO, M., COLOMBO, M. & DOZIO, D. (2013a) Fibre-reinforced concrete in *fib* Model Code 2010: principles, models and test validation. *Structural Concrete,* 14**,** 342-361.

DI PRISCO, M., FERRARA, L. & LAMPERTI, M. G. L. (2013b) Double edge wedge splitting (DEWS): an indirect tension test to identify post-cracking behaviour of

fibre reinforced cementitious composites. *Materials and Structures,* 46**,** 1893-1918.

DI PRISCO, M., PLIZZARI, G. & VANDEWALLE, L. (2009) Fibre reinforced concrete: new design perspectives. *Materials and Structures,* 42**,** 1261-1281.

DING, Y., LIU, S., ZHANG, Y. & THOMAS, A. (2008) The investigation on the workability of fibre cocktail reinforced self-compacting high performance concrete. *Construction and Building Materials,* 22**,** 1462-1470.

DING, Y., ZHANG, Y. & THOMAS, A. (2009) The investigation on strength and flexural toughness of fibre cocktail reinforced self-compacting high performance concrete. *Construction and Building Materials,* 23**,** 448-452.

DUPONT, D. & VANDEWALLE, L. (2005) Distribution of steel fibres in rectangular sections. *Cement and Concrete Composites,* 27**,** 391-398.

DØSSLAND, Å. L. (2008) Fibre Reinforcement in Load Carrying Concrete Structures. *Department of Structural Engineering,* Doctoral thesis*,* Norwegian University of Science and Technology (NTNU)*.* Trondheim.

EUROPEAN STANDARD (2004) Eurocode 2: Design of concrete structures. Part 1-1: General rules and rules for buildings. EN 1992-1-1:2004. Brussels, Belgium, European Committee for Standardization.

EUROPEAN STANDARD (2005) Test method for metallic fibre concrete - Measuring the flexural tensile strength (limit of proportionality (LOP), residual). EN 14651:2005+A1:2007. Brussels, Belgium, European Committee for Standardization.

EUROPEAN STANDARD (2006) Testing sprayed concrete. Part 7: Fibre content of fibre reinforced concrete. EN 14488-7:2006. Brussels, Belgium, European Committee for Standardization.

EUROPEAN STANDARD (2007) Test method for metallic fibre concrete, measuring the fibre content in fresh and hardened concrete. EN 14721:2005+A1:2007. Brussels, Belgium, European Committee for Standardization.

EUROPEAN STANDARD (2009a) Testing fresh concrete - Part 6: Density. EN 12350-6:2009. Brussels, Belgium, European Committee for Standardization.

EUROPEAN STANDARD (2009b) Testing fresh concrete - Part 7: Air content, pressure methods. EN 12350-7:2009. Brussels, Belgium, European Committee for Standardization.

EUROPEAN STANDARD (2009c) Testing hardened concrete - Part 3: Compressive strength of test specimens. EN 12390-3:2009. Brussels, Belgium, European Committee for Standardization.

EUROPEAN STANDARD (2010a) Testing fresh concrete - Part 8: Self-compacting concrete - Slump-flow test. EN 12350-8:2010. Brussels, Belgium, European Committee for Standardization.

EUROPEAN STANDARD (2010b) Testing fresh concrete - Part 9: Self-compacting concrete - V-funnel test. EN 12350-9:2010. Brussels, Belgium, European Committee for Standardization.

EUROPEAN STANDARD (2010c) Testing fresh concrete - Part 12: Self-compacting concrete - J-ring test. EN 12350-12:2010. Brussels, Belgium, European Committee for Standardization.

EUROPEAN STANDARD (2010d) Testing fresh concrete - Part 10: Self-compacting concrete - L box test. EN 12350-10:2010. Brussels, Belgium, European Committee for Standardization.

EUROPEAN STANDARD (2010e) Testing fresh concrete - Part 11: Self-compacting concrete - Sieve segregation test. EN 12350-11:2010. Brussels, Belgium, European Committee for Standardization.

FAIFER, M., OTTOBONI, R., TOSCANI, S. & FERRARA, L. (2010) Steel fiber reinforced concrete characterization based on a magnetic probe. *Instrumentation and Measurement Technology Conference (I2MTC), 2010 IEEE.* 157-162.

FANELLA, D. A. & NAAMAN, A. E. (1985) Stress-Strain Properties of Fiber Reinforced Mortar in Compression. *Journal Proceedings,* 82**,** 475-483.

FERRARA, L. (2014) Fiber Reinforced SCC, (Chapter 6). In KHAYAT, K. H. & DE SCHUTTER, G. (Eds.) *Mechanical Properties of Self-Compacting Concrete. State-of-the-Art Report of the RILEM Technical Committee 228-MPS.* Springer**,** 161-219.

FERRARA, L., BAMONTE, P., CAVERZAN, A., MUSA, A. & SANAL, I. (2012a) A comprehensive methodology to test the performance of Steel Fibre Reinforced Self-Compacting Concrete (SFR-SCC). *Construction and Building Materials,* 37**,** 406-424.

FERRARA, L., CAVERZAN, A., MUHAXHERI, M. & DI PRISCO, M. (2012b) Identification of tensile behaviour of SFR-SCC: direct vs. indirect tests. In BARROS, J. A. O. (Ed.) *8th RILEM International Symposium on Fiber Reinforced Concrete: challenges and opportunities (BEFIB 2012).* Guimaraes, Portugal, RILEM Publications SARL**,** 209-221.

FERRARA, L., FAIFER, M. & TOSCANI, S. (2012c) A magnetic method for non destructive monitoring of fiber dispersion and orientation in steel fiber reinforced cementitious composites—part 1: method calibration. *Materials and Structures,* 45**,** 575-589.

FERRARA, L. & MEDA, A. (2006) Relationships between fibre distribution, workability and the mechanical properties of SFRC applied to precast roof elements. *Materials and Structures,* 39**,** 411-420.

FERRARA, L., OZYURT, N. & DI PRISCO, M. (2011) High mechanical performance of fibre reinforced cementitious composites: the role of "casting-flow induced" fibre orientation. *Materials and Structures,* 44**,** 109-128.

FERRARA, L., PARK, Y. D. & SHAH, S. P. (2008) Correlation among fresh state behavior, fiber dispersion, and toughness properties of SFRCs. *Journal of Materials in Civil Engineering,* 20**,** 493-501.

FERRARA, L., SHYSHKO, S. & MECHTCHERINE, V. (2012d) Predicting the flow-induced dispersion and orientation of steel fibers in self-consolidating concrete by distinct element method. In BARROS, J. A. O. (Ed.) *8th RILEM International Symposium on Fiber Reinforced Concrete: challenges and opportunities (BEFIB 2012).* Guimaraes, Portugal, RILEM Publication SARL**,** 918-930.

fib (2010) Model Code for Concrete Structures 2010, International Federation for Structural Concrete (*fib*).

FUENTES, R., GEIKER, M. R. & STANG, H. (In press) Assessment of fibre orientation and mechanical properties of fibre reinforced concrete. *Nordic Concrete Research*.

GEIKER, M. R. (2008) Self-compacting concrete (SCC). In MINDESS, S. (Ed.) *Developments in the formulation and reinforcement of concrete.* Cambridge, Woodhead Publishing Limited**,** 187-207.

GETTU, R., GARDNER, D. R., SALDIVAR, H. & BARRAGAN, B. E. (2005) Study of the distribution and orientation of fibers in SFRC specimens. *Materials and Structures,* 38**,** 31-37.

GRAM, A. & SILFWERBRAND, J. (2011) Numerical simulation of fresh SCC flow: applications. *Materials and Structures,* 44**,** 805-813.

GROTH, P. (2000a) Fibre reinforced concrete - Fracture mechanics methods applied on self-compacting concrete and energetically modified binders. *Department of Civil and Mining Engineering,* Doctoral thesis*,* Luleå University of Technology. Luleå, Sweden.

GROTH, P. (2000b) Steel Fibre Reinforced SCC, Final report of task 6, Brite Euram project (BE 96-3801) - Rational production and improved working environment through using SCC. *Doc. No.: RT6-v1.doc*.

GRÜNEWALD, S. (2004) Performance based design of self compacting steel fiber reinforced concrete. *Department of Structural and Building Engineering,* Doctoral thesis*,* Delft University of Technology. Rotterdam, The Netherlands.

GRÜNEWALD, S., BARTOLI, L., FERRARA, L., KANSTAD, T. & DEHN, F. (2014) Translation of test results of small specimens of flowable fibre concrete to structural behaviour, a discussion paper of *fib* TG 8.8. *Joint ACI–fib International Workshop. Fibre Reinforced Concrete: from Design to Structural Applications.* Montreal, Canada.

GRÜNEWALD, S., LARANJEIRA, F., WALRAVEN, J. C., AGUADO DE CEA, A. & MOLINS BORRELL, C. (2012) Influence of fibre orientation on the performance of steel fibre-reinforced concrete. In BARROS, J. A. O. (Ed.) *8th RILEM International Symposium on Fiber Reinforced Concrete: challenges and opportunities (BEFIB 2012).* Guimaraes, Portugal, RILEM Publications SARL**,** 313-325.

GRÜNEWALD, S. & WALRAVEN, J. C. (2002) Sensitivity of the bending behaviour of self-compacting fibre reinforced concrete to the method of casting. *5th International Symposium on Cement and Concrete.* Shanghai, China.

HORDIJK, D. A. (1991) Local approach to fatigue of concrete. Doctoral thesis*,* Delft University of Technology. Rotterdam, The Netherlands.

HUESPE, A. E., OLIVER, J. & MORA, D. F. (2013) Computational modeling of high performance steel fiber reinforced concrete using a micromorphic approach. *Computational Mechanics,* 52**,** 1243-1264.

JEFFERY, G. B. (1922) The motion of ellipsoidal particles immersed in a viscous fluid. *Proceedings of the Royal Society of London. Series A,* 120**,** 161-179.

JIRÁSEK, M. & BAUER, M. (2012) Numerical aspects of the crack band approach. *Computers & Structures,* 110–111**,** 60-78.

JOHNSTON, C. D. (1996) Proportioning, mixing and placement of fibre-reinforced cements and concretes. In BARTOS, P. J. M., MARRS, D. L. & CLELAND, D. J. (Eds.) *Production methods and workability.* London, E & FN Spon**,** 155-179.

JONES, P. A., AUSTIN, S. A. & ROBINS, P. J. (2008) Predicting the flexural load–deflection response of steel fibre reinforced concrete from strain, crack-width, fibre pull-out and distribution data. *Materials and Structures,* 41**,** 449-463.

KANG, S. T., LEE, B. Y., KIM, J.-K. & KIM, Y. Y. (2011) The effect of fibre distribution characteristics on the flexural strength of steel fibre-reinforced ultra high strength concrete. *Construction and Building Materials,* 25**,** 2450-2457.

KANSTAD, T., JUVIK, D. A., VATNAR, A., MATHISEN, A. E., SANDBAKK, S., VIKAN, H., NIKOLAISEN, E., DØSSLAND, Å. L., LEIRUD, N. & OVERREIN, G. O. (2011) Forslag til retningslinjer for dimensjonering, utførelse og kontroll av fiberarmerte betongkonstruksjoner (*in Norwegian*). Proposed guidelines for design, execution and control of fibre reinforced concrete structures (*translated title*). *COIN Project report 29.* Oslo, Norway, SINTEF Building and Infrastructure.

KANSTAD, T. & ŽIRGULIS, G. (2012) Long-time creep testing of pre-cracked fibre reinforced concrete beams. In BARROS, J. A. O. (Ed.) *8th RILEM International Symposium on Fiber Reinforced Concrete: challenges and opportunities (BEFIB 2012).* Guimaraes, Portugal, RILEM Publications SARL**,** 835-847.

KJELLMARK, G., MARTIUS-HAMMER, T. A. & KANSTAD, T. (2014) COIN's 15 MPa target fibre concrete: materials development towards high residual flexural strenght. *Proceedings of the XXII Nordic Concrete Research Symposium.* Reykjavik, Iceland, Norsk Betongforening**,** 215-218.

KOOIMAN, A. G. (2000) Modelling steel fibre reinforced concrete for structural design. Doctoral thesis*,* Delft University of Technology. Rotterdam, The Netherlands.

KRENCHEL, H. (1964) Fibre reinforcement, Theoretical and practical investigations of the elasticity and strength of fibre-reinforced materials. *Laboratory of Structural Research,* Doctoral thesis*,* Technical University of Denmark. Copenhagen, Denmark.

KRENCHEL, H. (1975) Fibre spacing and specific fibre surface. In NEVILLE, A. (Ed.) *Fibre Reinforced Cement and Concrete, Proc. RILEY Conf.* Lancaster, England, Construction Press**,** 69-79.

LARANJEIRA DE OLIVEIRA, F. (2010) Design-oriented constitutive model for steel fibre reinforced concrete. *Departament d'Enginyeria de la Construcció,* Doctoral thesis*,* Universitat Politècnica de Catalunya. Barcelona, Spain.

LARANJEIRA, F., AGUADO, A., MOLINS, C., GRÜNEWALD, S., WALRAVEN, J. & CAVALARO, S. (2012) Framework to predict the orientation of fibers in FRC: A novel philosophy. *Cement and Concrete Research,* 42**,** 752-768.

LI, Z., PEREZ LARA, M. A. & BOLANDER, J. E. (2006) Restraining effects of fibers during non-uniform drying of cement composites. *Cement and Concrete Research,* 36**,** 1643-1652.

LÖFGREN, I. (2005) Fibre-reinforced Concrete for Industrial Construction - a fracture mechanics approach to material testing and structural analysis. *Department of Civil and Environmental Engineering, Structural Engineering,* Doctoral thesis*,* Chalmers University of Technology. Göteborg, Sweden.

LÖFGREN, I., STANG, H. & OLESEN, J. F. (2008) The WST method, a fracture mechanics test method for FRC. *Materials and Structures,* 41**,** 197-211.

MANGAT, P. S. & MOTAMEDI AZARI, M. (1985) A theory for the creep of steel fibre reinforced cement matrices under compression. *Journal of Materials Science,* 20**,** 1119-1133.

MARKOVIC, I. (2006) High-Performance Hybrid-Fibre Concrete - Development and Utilization. Doctoral thesis*,* Delft University of Technology. Delft, The Netherlands.

MARTINIE, L., ROSSI, P. & ROUSSEL, N. (2010) Rheology of fiber reinforced cementitious materials: classification and prediction. *Cement and Concrete Research,* 40**,** 226-234.

MARTINIE, L. & ROUSSEL, N. (2010) Fiber-Reinforced Cementitious Materials: From Intrinsic Isotropic Behavior to Fiber Alignment. In KHAYAT, K. H. & FEYS, D. (Eds.) *Design, Production and Placement of Self-Consolidating Concrete, Proc. of SCC2010.* Montreal, Canada, Springer**,** 407-415.

MARTINIE, L. & ROUSSEL, N. (2011) Simple tools for fiber orientation prediction in industrial practice. *Cement and Concrete Research,* 41**,** 993-1000.

MECHTCHERINE, V. & SHYSHKO, S. (2007) Virtual concrete laboratory — Continuous numerical modelling of concrete from fresh to the hardened state. In GROSSE, C. (Ed.) *Advances in Construction Materials 2007.* Springer Berlin Heidelberg**,** 479-488.

MEDA, A. & PLIZZARI, G. A. (2001) Fracture of fiber reinforced concrete slabs on grade. In DE BORST, R., MAZARS, J., PIJAUDIER-CABOT, G. & VAN MIER, J. G. M. (Eds.) *Proceedings of the Fourth International Conference on Fracture Mechanics of Concrete and Concrete Structures.* Cachan, France**,** 1013-1020.

MEDA, A., PLIZZARI, G. A. & SORELLI, L. (2004) Uni-axial and bending test for the determination of fracture properties of fiber reinforced concrete. In LI, V. C., LEUNG, C. K. Y., WILLAM, K. J. & BILLINGTON, S. L. (Eds.) *Proceedings*

of the Fifth International Conference on Fracture Mechanics of Concrete and Concrete Structures. Vail, USA, 2**,** 1163-1170.

MONTAIGNAC, R., MASSICOTTE, B. & CHARRON, J.-P. (2012) Design of SFRC structural elements: flexural behaviour prediction. *Materials and Structures,* 45**,** 623-636.

MØRTSELL, E. (1996) Modellering av delmaterialenes betydning for betongens konsistens (*in Norwegian*). *Department of structural engineering,* Doctoral thesis*,* Norwegian University of Science and Technology. Trondheim, Norway.

NEDRELID, H. & KANSTAD, T. (2014a) RC beams with dapped ends or openings containing steel fibres. *The 1st Concrete Innovation Conference, CIC 2014*. Oslo, Norway.

NEDRELID, H. & KANSTAD, T. (2014b) Structural fibre-reinforced concrete: design approaches and experimental results. *COIN Project report*. Oslo, Norway, SINTEF Building and Infrastructure.

OLESEN, J. F. (2001) Fictitious crack propagation in fiber-reinforced concrete beams. *Journal of Engineering Mechanics-ASCE,* 127**,** 272-280.

OLIVER, J., MORA, D. F., HUESPE, A. E. & WEYLER, R. (2012) A micromorphic model for steel fiber reinforced concrete. *International Journal of Solids and Structures,* 49**,** 2990-3007.

OZYURT, N., MASON, T. O. & SHAH, S. P. (2006a) Non-destructive monitoring of fiber orientation using AC-IS: An industrial-scale application. *Cement and Concrete Research,* 36**,** 1653-1660.

OZYURT, N., MASON, T. O. & SHAH, S. P. (2007) Correlation of fiber dispersion, rheology and mechanical performance of FRCs. *Cement and Concrete Composites,* 29**,** 70-79.

OZYURT, N., WOO, L. Y., MASON, T. O. & SHAH, S. P. (2006b) Monitoring Fiber Dispersion in Fiber-Reinforced Cementitious Materials: Comparison of AC-Impedance Spectroscopy and Image Analysis. *Materials Journal,* 103**,** 340-347.

PARK, S. H., KIM, D. J., RYU, G. S. & KOH, K. T. (2012) Tensile behavior of Ultra High Performance Hybrid Fiber Reinforced Concrete. *Cement and Concrete Composites,* 34**,** 172-184.

PEDERSEN, C. (1996) New production processes, materials and calculation techniques for fiber reinforced concrete pipes. Technical University of Denmark, Department of Structural Engineering and Materials. Lyngby, Denmark.

PUJADAS, P., BLANCO, A., CAVALARO, S. & AGUADO, A. (2014a) Plastic fibres as the only reinforcement for flat suspended slabs: Experimental investigation and numerical simulation. *Construction and Building Materials,* 57**,** 92-104.

PUJADAS, P., BLANCO, A., CAVALARO, S., DE LA FUENTE, A. & AGUADO, A. (2014b) Fibre distribution in macro-plastic fibre reinforced concrete slab-panels. *Construction and Building Materials,* 64**,** 496-503.

PUJADAS, P., BLANCO, A., CAVALARO, S. H. P., DE LA FUENTE, A. & AGUADO, A. (2014c) Multidirectional double punch test to assess the post-cracking behaviour and fibre orientation of FRC. *Construction and Building Materials,* 58**,** 214-224.

QIAN, C. & STROEVEN, P. (2000a) Fracture properties of concrete reinforced with steel–polypropylene hybrid fibres. *Cement and Concrete Composites,* 22**,** 343-351.

QIAN, C. X. & STROEVEN, P. (2000b) Development of hybrid polypropylene-steel fibre-reinforced concrete. *Cement and Concrete Research,* 30**,** 63-69.

RADTKE, F. K. F. (2012) Computational modelling of fibre-reinforced cementitious composites: An analysis of discrete and mesh-independent techniques. *Faculty of Civil Engineering and Geosciences,* Doctoral thesis*,* Delft University of Technology. Rotterdam, The Netherlands.

RANDL, N. & MÉSZÖLY, T. (2014) The effect of fibers in UHPFRC beams with longitudinal steel reinforcement. *Joint ACI–fib International Workshop. Fibre Reinforced Concrete: from Design to Structural Applications.* Montreal, Canada.

RILEM (2001) RILEM TC 162-TDF: Test and design methods for steel fibre reinforced concrete. Uni-axial tension test for steel fibre reinforced concrete - Recommendations. *Materials and Structures,* 34**,** 3-6.

RILEM (2002a) RILEM TC162-TDF: Test and design methods for steel fibre reinforced concrete. Design of steel fibre reinforced concrete using the σ-w method: principles and applications. *Materials and Structures,* 35**,** 262-278.

RILEM (2002b) RILEM TC 162-TDF: Test and design methods for steel fibre reinforced concrete: Bending test - Final recommendation. *Materials and Structures,* 35**,** 579-582.

RILEM (2003) RILEM TC162-TDF: Test and design methods for steel fibre reinforced concrete. σ-ε-design method - Final recommendation. *Materials and Structures,* 36**,** 560-567.

ROBINS, P. J., AUSTIN, S. A. & JONES, P. A. (2003) Spatial distribution of steel fibres in sprayed and cast concrete. *Magazine of Concrete Research,* 55**,** 225-235.

ROMUALDI, J. P. & MANDEL, J. A. (1964) Tensile Strength of Concrete Affected by Uniformly Distributed and Closely Spaced Short Lengths of Wire Reinforcement. *Journal Proceedings,* 61**,** 657-672.

ROQUETA, G., JOFRE, L., ROMEU, J. & BLANCH, S. (2011) Microwave Time-Domain Reflection Imaging of Steel Fiber Distribution on Reinforced Concrete. *IEEE Transactions on Instrumentation and Measurement,* 60**,** 3913-3922.

ROSSI, P. (1997) High Performance Multimodal Fiber Reinforced Cement Composites (HPMFRCC): the LCPC Experience. *Materials Journal,* 94**,** 478-783.

ROSSI, P., ACKER, P. & MALIER, Y. (1987) Effect of steel fibres at two different stages: The material and the structure. *Materials and Structures,* 20**,** 436-439.

ROSSI, P. & HARROUCHE, N. (1990) Mix design and mechanical behaviour of some steel-fibre-reinforced concretes used in reinforced concrete structures. *Materials and Structures,* 23**,** 256-266.

ROTS, J. G. (1988) Computational modeling of concrete fracture. *Civil Engineering Department,* Doctoral thesis*,* Delft University of Technology. Rotterdam, The Netherlands.

ROUSSEL, N. (2006) A Theoretical Frame to Study Stability of Fresh Concrete. *Materials and Structures,* 39**,** 81-91.

ROUSSEL, N. (2007) The LCPC BOX: a cheap and simple technique for yield stress measurements of SCC. *Materials and Structures,* 40**,** 889-896.

ROUSSEL, N., GEIKER, M. R., DUFOUR, F., THRANE, L. N. & SZABO, P. (2007) Computational modeling of concrete flow: General overview. *Cement and Concrete Research,* 37**,** 1298-1307.

ŞANAL, İ. & ÖZYURT ZIHNIOĞLU, N. (2013) To what extent does the fiber orientation affect mechanical performance? *Construction and Building Materials,* 44**,** 671-681.

SANDBAKK, S. (2011) Fibre Reinforced Concrete. Evaluation of test methods and material development. *Department of Structural Engineering,* Doctoral thesis*,* Norwegian University of Science and Technology. Trondheim, Norway.

SARMIENTO, E. V. (2011) Influence of concrete flow on the mechanical properties of ordinary and fibre reinforced concrete. *Department of Structural Engineering,*

Master thesis*,* Norwegian University of Science and Technology and Universitat Politècnica de Catalunya*.*

SARMIENTO, E. V., GEIKER, M. R. & KANSTAD, T. (2015) Influence of fibre configuration on the mechanical behaviour of standard test specimens and full-scale beams made of flowable FRC. *Submitted to Construction and Building Materials*.

SARMIENTO, E. V., HENDRIKS, M. A. N. & KANSTAD, T. (2014a) Accounting for the fibre orientation on the structural performance of flowable fibre reinforced concrete. In BÍCANIĆ, N., MANG, H., MESCHKE, G. & DE BORST, R. (Eds.) *Computational Modelling of Concrete Structures.* CRC Press, 2**,** 609-618.

SARMIENTO, E. V., KANSTAD, T., GEIKER, M. R. & HENDRIKS, M. (2014b) Impact of the combined effect of fibre orientation and volume fraction on the mechanical properties of fibre reinforced concrete. *Proceedings of the XXII Nordic Concrete Research Symposium, Reykjavik, Iceland 2014.* Norsk betongforening**,** 141-144.

SCHÖNLIN, K. (1988) Ermittlung der Orientierung, Menge und Verteilung der Fasern in faserbewehrtem Beton (*in German*). *Beton- und Stahlbetonbau,* 83**,** 168-171.

SFRC CONSORTIUM (2014) Design guideline for structural applications of steel fibre reinforced concrete. Denmark.

SLOBBE, A. T., HENDRIKS, M. A. N. & ROTS, J. G. (2014) Smoothing the propagation of smeared cracks. *Engineering Fracture Mechanics,* 132**,** 147-168.

SOROUSHIAN, P. & LEE, C.-D. (1990) Distribution and orientation of fibres in steel fiber reinforced concrete. *Materials Journal,* 87**,** 433-439.

SOUTSOS, M. N., LE, T. T. & LAMPROPOULOS, A. P. (2012) Flexural performance of fibre reinforced concrete made with steel and synthetic fibres. *Construction and Building Materials,* 36**,** 704-710.

SPANGENBERG, J., ROUSSEL, N., HATTEL, J. H., SARMIENTO, E. V., ŽIRGULIS, G. & GEIKER, M. R. (2012a) Patterns of gravity induced aggregate migration during casting of fluid concretes. *Cement and Concrete Research,* 42**,** 1571-1578.

SPANGENBERG, J., ROUSSEL, N., HATTEL, J. H., STANG, H., SKOCEK, J. & GEIKER, M. R. (2012b) Flow induced particle migration in fresh concrete: Theoretical frame, numerical simulations and experimental results on model fluids. *Cement and Concrete Research,* 42**,** 633-641.

STROEVEN, P. (1978) Morphometry of fibre reinforced cementitious materials. Part I: Efficiency and spacing in idealized structures. *Matériaux et Construction,* 11**,** 31-38.

STROEVEN, P. (1979) Morphometry of fibre reinforced cementitious materials. Part II: Inhomogeneity, segregation and anisometry of partially oriented fibre structures. *Matériaux et Construction,* 12**,** 9-20.

STÄHLI, P., CUSTER, R. & VAN MIER, J. G. M. (2008) On flow properties, fibre distribution, fibre orientation and flexural behaviour of FRC. *Materials and Structures,* 41**,** 189-196.

STÄHLI, P. & VAN MIER, J. G. M. (2007) Manufacturing, fibre anisotropy and fracture of hybrid fibre concrete. *Engineering Fracture Mechanics,* 74**,** 223-242.

SUURONEN, J.-P., KALLONEN, A., EIK, M., PUTTONEN, J., SERIMAA, R. & HERRMANN, H. (2013) Analysis of short fibres orientation in steel fibre-reinforced concrete (SFRC) by X-ray tomography. *Journal of Materials Science,* 48**,** 1358-1367.

ŠVEC, O. (2013) Flow modelling of steel fibre reinforced self-compacting concrete - Simulating fibre orientation and mechanical properties. . *Department of Civil Engineering,* Doctoral thesis*,* Technical University of Denmark. Lyngby, Denmark.

ŠVEC, O. & SKOČEK, J. (2013) Simple Navier's slip boundary condition for the non-Newtonian Lattice Boltzmann fluid dynamics solver. *Journal of Non-Newtonian Fluid Mechanics,* 199**,** 61-69.

ŠVEC, O., SKOČEK, J., OLESEN, J. F. & STANG, H. (2012a) Fibre reinforced self-compacting concrete flow simulations in comparison with L-Box experiments using Carbopol. In BARROS, J. A. O. (Ed.) *8th RILEM International Symposium on Fiber Reinforced Concrete: challenges and opportunities (BEFIB 2012).* Guimaraes, Portugal, RILEM Publications SARL**,** 897-905.

ŠVEC, O., SKOČEK, J., STANG, H., GEIKER, M. R. & ROUSSEL, N. (2012b) Free surface flow of a suspension of rigid particles in a non-Newtonian fluid: A lattice Boltzmann approach. *Journal of Non-Newtonian Fluid Mechanics,* 179–180**,** 32-42.

ŠVEC, O., SKOČEK, J., STANG, H., OLESEN, J. F. & POULSEN, P. N. (2011) Flow simulation of fiber reinforced self compacting concrete using Lattice Boltzmann method. *13th International Congress on the Chemistry of Cement (ICCC).* Madrid, Spain.

ŠVEC, O., ŽIRGULIS, G., BOLANDER, J. E. & STANG, H. (2014) Influence of formwork surface on the orientation of steel fibres within self-compacting concrete and on the mechanical properties of cast structural elements. *Cement and Concrete Composites,* 50**,** 60-72.

SWAMY, R. N. (1975) Fibre reinforcement of cement and concrete. *Matériaux et Construction,* 8**,** 235-254.

SWAMY, R. N. & MANGAT, P. S. (1974) Influence of fibre-aggregate interaction on some properties of steel fibre reinforced concrete. *Matériaux et Construction,* 7**,** 307-314.

SWEDISH STANDARDS INSTITUTE (2014) Fibre Concrete - Design of Fibre Concrete Structures. SS 812310:2014. Sweden.

TAILHAN, J.-L., ROSSI, P. & BOULAY, C. (2012) Tensile and bending behaviour of a strain hardening cement-based composite: Experimental and numerical analysis. *Cement and Concrete Composites,* 34**,** 166-171.

THORENFELDT, E. (2003) Theoretical tensile strength after cracking. Fibre orientation and average stress in fibres. In KANSTAD, T. (Ed.) *Nordic Miniseminar: Design rules for steel fibre reinforced concrete structures.* Oslo, Norway, The Nordic Concrete Federation**,** 43-60.

TLEMAT, H., PILAKOUTAS, K. & NEOCLEOUS, K. (2006) Modelling of SFRC using inverse finite element analysis. *Materials and Structures,* 39**,** 221-233.

TNO DIANA (2014) Material library. In MANIE, J. & KIKSTRA, W. P. (Eds.) *DIANA Finite Element Analysis User's Manual, release 9.6.* Delft, The Netherlands, TNO DIANA.

TORRENTS, J. M., BLANCO, A., PUJADAS, P., AGUADO, A., JUAN-GARCÍA, P. & SÁNCHEZ-MORAGUES, M. (2012) Inductive method for assessing the amount and orientation of steel fibers in concrete. *Materials and Structures,* 45**,** 1577-1592.

TORRENTS, J. M., JUAN-GARCÍA, P., PATAU, O. & AGUADO, A. (2009) Surveillance of steel fibre reinforced concrete slabs measured with an open-ended coaxial probe. *Proceedings of the XIX IMEKO World Congress: Fundamental and Applied Metrology.* Lisbon, Portugal**,** 2282-2284.

UCHIDA, Y., KURIHARA, N., ROKUGO, K. & KOYANAGI, W. (1995) Determination of tension softening diagrams of various kinds of concrete by means of numerical analysis. In WITTMANN, F. H. (Ed.) *Proceedings of the Second International Conference on Fracture Mechanics of Concrete and Concrete Structures.* Freiburg, Germany, AEDIFICATIO Publishers, 1**,** 17-30.

VAN DAMME, S., FRANCHOIS, A., DE ZUTTER, D. & TAERWE, L. (2004) Nondestructive determination of the steel fiber content in concrete slabs with an open-ended coaxial probe. *IEEE Transactions on Geoscience and Remote Sensing,* 42**,** 2511-2521.

VANDEWALLE, L. (2007) Hybrid fibre concrete: is there a synergetic effect? In GROSSE, C. (Ed.) *Advances in Construction Materials 2007*. Springer Berlin Heidelberg**,** 219-228.

VANDEWALLE, L., HEIRMAN, G. & VAN RICKSTAL, F. (2008) Fibre orientation in self-compacting fibre reinforced concrete. In GETTU, R. (Ed.) *7th RILEM International Symposium on Fibre Reinforced Concrete: Design and Applications - BEFIB 2008*. Chennai, India, RILEM Publications SARL**,** 719-728.

VIKAN, H., SANDBAKK, S. & KANSTAD, T. (2011) Material properties influencing concrete residual bending strength - Experimental study. *COIN Project report 28.* Oslo, Norway, SINTEF Building and Infrastructure.

WILLE, K., TUE, N. V. & PARRA-MONTESINOS, G. J. (2014) Fiber distribution and orientation in UHP-FRC beams and their effect on backward analysis. *Materials and Structures,* 47**,** 1825-1838.

WOO, L. Y., WANSOM, S., OZYURT, N., MU, B., SHAH, S. P. & MASON, T. O. (2005) Characterizing fiber dispersion in cement composites using AC-Impedance Spectroscopy. *Cement and Concrete Composites,* 27**,** 627-636.

WUEST, J., DENARIÉ, E., BRÜHWILER, E., TAMARIT, L., KOCHER, M. & GALLUCCI, E. (2009) Tomography Analysis of Fiber Distribution and Orientation in Ultra High-Performance Fiber-Reinforced Composites with High-Fiber Dosages. *Experimental Techniques,* 33**,** 50-55.

ZHOU, B. & UCHIDA, Y. (2013) Fiber Orientation in Ultra High Performance Fiber Reinforced Concrete and its Visualization. In VAN MIER, J. G. M., RUIZ, G., ANDRADE, C., YU, R. C. & ZHANG, X. X. (Eds.) *Proceedings of the Eighth International Conference on Fracture Mechanics of Concrete and Concrete Structures.* Toledo, Spain, International Center for Numerical Methods in Engineering.

ŽIRGULIS, G. (2015) Fibre Orientation in Steel-Fibre-reinforced concrete, Quantification methods and influence of formwork surface and reinforcement bars in structural elements. *Department of Structural Engineering,* Doctoral thesis*,* Norwegian University of Science and Technology. Trondheim, Norway.

ŽIRGULIS, G., GEIKER, M. R., ŠVEC, O. & KANSTAD, T. (2013) Potential methods for quality control of fibre distribution in FRC SCC. *7th RILEM International Conference on Self-Compacting Concrete.* Paris, France.

ŽIRGULIS, G., ŠVEC, O., GEIKER, M. R., CWIRZEN, A. & KANSTAD, T. (2015a) Influence of reinforcement bar layout on fibre orientation and distribution in slabs cast from fibre-reinforced self-compacting concrete (FRSCC). *Submitted to Structural Concrete*.

ŽIRGULIS, G., ŠVEC, O., GEIKER, M. R., CWIRZEN, A. & KANSTAD, T. (2015b) Variation in fibre orientation and volume in walls: Experimental and numerical investigation. *Submitted to Structural Concrete*.

ŽIRGULIS, G., ŠVEC, O., SARMIENTO, E. V., GEIKER, M. R., CWIRZEN, A. & KANSTAD, T. (2015c) Importance of quantification of steel fibre orientation for residual flexural tensile strength in FRC. *Submitted to Materials and Structures*.

DEPARTMENT OF STRUCTURAL ENGINEERING
NORWEGIAN UNIVERSITY OF SCIENCE AND TECHNOLOGY

N–7491 TRONDHEIM, NORWAY
Telephone: +47 73 59 47 00 Telefax: +47 73 59 47 01

"Reliability Analysis of Structural Systems using Nonlinear Finite Element Methods"
C. A. Holm, 1990:23, ISBN 82-7119-178-0.

"Uniform Stratified Flow Interaction with a Submerged Horizontal Cylinder"
Ø. Arntsen, 1990:32, ISBN 82-7119-188-8.

"Large Displacement Analysis of Flexible and Rigid Systems Considering Displacement-Dependent Loads and Nonlinear Constraints"
K. M. Mathisen, 1990:33, ISBN 82-7119-189-6.

"Solid Mechanics and Material Models including Large Deformations"
E. Levold, 1990:56, ISBN 82-7119-214-0, ISSN 0802-3271.

"Inelastic Deformation Capacity of Flexurally-Loaded Aluminium Alloy Structures"
T. Welo, 1990:62, ISBN 82-7119-220-5, ISSN 0802-3271.

"Visualization of Results from Mechanical Engineering Analysis"
K. Aamnes, 1990:63, ISBN 82-7119-221-3, ISSN 0802-3271.

"Object-Oriented Product Modeling for Structural Design"
S. I. Dale, 1991:6, ISBN 82-7119-258-2, ISSN 0802-3271.

"Parallel Techniques for Solving Finite Element Problems on Transputer Networks"
T. H. Hansen, 1991:19, ISBN 82-7119-273-6, ISSN 0802-3271.

"Statistical Description and Estimation of Ocean Drift Ice Environments"
R. Korsnes, 1991:24, ISBN 82-7119-278-7, ISSN 0802-3271.

"Properties of concrete related to fatigue damage: with emphasis on high strength concrete"
G. Petkovic, 1991:35, ISBN 82-7119-290-6, ISSN 0802-3271.

"Turbidity Current Modelling"
B. Brørs, 1991:38, ISBN 82-7119-293-0, ISSN 0802-3271.

“Zero-Slump Concrete: Rheology, Degree of Compaction and Strength. Effects of Fillers as Part Cement-Replacement”
C. Sørensen, 1992:8, ISBN 82-7119-357-0, ISSN 0802-3271.

“Nonlinear Analysis of Reinforced Concrete Structures Exposed to Transient Loading”
K. V. Høiseth, 1992:15, ISBN 82-7119-364-3, ISSN 0802-3271.

“Finite Element Formulations and Solution Algorithms for Buckling and Collapse Analysis of Thin Shells”
R. O. Bjærum, 1992:30, ISBN 82-7119-380-5, ISSN 0802-3271.

“Response Statistics of Nonlinear Dynamic Systems”
J. M. Johnsen, 1992:42, ISBN 82-7119-393-7, ISSN 0802-3271.

“Digital Models in Engineering. A Study on why and how engineers build and operate digital models for decision support”
J. Høyte, 1992:75, ISBN 82-7119-429-1, ISSN 0802-3271.

“Sparse Solution of Finite Element Equations”
A. C. Damhaug, 1992:76, ISBN 82-7119-430-5, ISSN 0802-3271.

“Some Aspects of Floating Ice Related to Sea Surface Operations in the Barents Sea”
S. Løset, 1992:95, ISBN 82-7119-452-6, ISSN 0802-3271.

“Modelling of Cyclic Plasticity with Application to Steel and Aluminium Structures”
O. S. Hopperstad, 1993:7, ISBN 82-7119-461-5, ISSN 0802-3271.

“The Free Formulation: Linear Theory and Extensions with Applications to Tetrahedral Elements with Rotational Freedoms”
G. Skeie, 1993:17, ISBN 82-7119-472-0, ISSN 0802-3271.

“Høyfast betongs motstand mot piggdekkslitasje. Analyse av resultater fra prøving i Veisliter'n”
T. Tveter, 1993:62, ISBN 82-7119-522-0, ISSN 0802-3271.

“A Nonlinear Finite Element Based on Free Formulation Theory for Analysis of Sandwich Structures”
O. Aamlid, 1993:72, ISBN 82-7119-534-4, ISSN 0802-3271.

“The Effect of Curing Temperature and Silica Fume on Chloride Migration and Pore Structure of High Strength Concrete”
C. J. Hauck, 1993:90, ISBN 82-7119-553-0, ISSN 0802-3271.

“Failure of Concrete under Compressive Strain Gradients”
G. Markeset, 1993:110, ISBN 82-7119-575-1, ISSN 0802-3271.

“An experimental study of internal tidal amphidromes in Vestfjorden”
J. H. Nilsen, 1994:39, ISBN 82-7119-640-5, ISSN 0802-3271.

“Structural analysis of oil wells with emphasis on conductor design”
H. Larsen, 1994:46, ISBN 82-7119-648-0, ISSN 0802-3271.

“Adaptive methods for non-linear finite element analysis of shell structures”
K. M. Okstad, 1994:66, ISBN 82-7119-670-7, ISSN 0802-3271.

“On constitutive modelling in nonlinear analysis of concrete structures”
O. Fyrileiv, 1994:115, ISBN 82-7119-725-8, ISSN 0802-3271.

“Fluctuating wind load and response of a line-like engineering structure with emphasis on motion-induced wind forces”
J. Bogunovic Jakobsen, 1995:62, ISBN 82-7119-809-2, ISSN 0802-3271.

“An experimental study of beam-columns subjected to combined torsion, bending and axial actions”
A. Aalberg, 1995:66, ISBN 82-7119-813-0, ISSN 0802-3271.

“Scaling and cracking in unsealed freeze/thaw testing of Portland cement and silica fume concretes”
S. Jacobsen, 1995:101, ISBN 82-7119-851-3, ISSN 0802-3271.

“Damping of water waves by submerged vegetation. A case study of laminaria hyperborea”
A. M. Dubi, 1995:108, ISBN 82-7119-859-9, ISSN 0802-3271.

“The dynamics of a slope current in the Barents Sea”
Sheng Li, 1995:109, ISBN 82-7119-860-2, ISSN 0802-3271.

“Modellering av delmaterialenes betydning for betongens konsistens”
Ernst Mørtsell, 1996:12, ISBN 82-7119-894-7, ISSN 0802-3271.

“Bending of thin-walled aluminium extrusions”
Birgit Søvik Opheim, 1996:60, ISBN 82-7119-947-1, ISSN 0802-3271.

“Material modelling of aluminium for crashworthiness analysis”
Torodd Berstad, 1996:89, ISBN 82-7119-980-3, ISSN 0802-3271.

"Estimation of structural parameters from response measurements on submerged floating tunnels"
Rolf Magne Larssen, 1996:119, ISBN 82-471-0014-2, ISSN 0802-3271.

"Numerical modelling of plain and reinforced concrete by damage mechanics"
Mario A. Polanco-Loria, 1997:20, ISBN 82-471-0049-5, ISSN 0802-3271.

"Nonlinear random vibrations - numerical analysis by path integration methods"
Vibeke Moe, 1997:26, ISBN 82-471-0056-8, ISSN 0802-3271.

"Numerical prediction of vortex-induced vibration by the finite element method"
Joar Martin Dalheim, 1997:63, ISBN 82-471-0096-7, ISSN 0802-3271.

"Time domain calculations of buffeting response for wind sensitive structures"
Ketil Aas-Jakobsen, 1997:148, ISBN 82-471-0189-0, ISSN 0802-3271.

"A numerical study of flow about fixed and flexibly mounted circular cylinders"
Trond Stokka Meling, 1998:48, ISBN 82-471-0244-7, ISSN 0802-3271.

"Estimation of chloride penetration into concrete bridges in coastal areas"
Per Egil Steen, 1998:89, ISBN 82-471-0290-0, ISSN 0802-3271.

"Stress-resultant material models for reinforced concrete plates and shells"
Jan Arve Øverli, 1998:95, ISBN 82-471-0297-8, ISSN 0802-3271.

"Chloride binding in concrete. Effect of surrounding environment and concrete composition"
Claus Kenneth Larsen, 1998:101, ISBN 82-471-0337-0, ISSN 0802-3271.

"Rotational capacity of aluminium alloy beams"
Lars A. Moen, 1999:1, ISBN 82-471-0365-6, ISSN 0802-3271.

"Stretch Bending of Aluminium Extrusions"
Arild H. Clausen, 1999:29, ISBN 82-471-0396-6, ISSN 0802-3271.

"Aluminium and Steel Beams under Concentrated Loading"
Tore Tryland, 1999:30, ISBN 82-471-0397-4, ISSN 0802-3271.

"Engineering Models of Elastoplasticity and Fracture for Aluminium Alloys"
Odd-Geir Lademo, 1999:39, ISBN 82-471-0406-7, ISSN 0802-3271.

"Kapasitet og duktilitet av dybelforbindelser i trekonstruksjoner"
Jan Siem, 1999:46, ISBN 82-471-0414-8, ISSN 0802-3271.

“Etablering av distribuert ingeniørarbeid; Teknologiske og organisatoriske erfaringer fra en norsk ingeniørbedrift”
Lars Line, 1999:52, ISBN 82-471-0420-2, ISSN 0802-3271.

“Estimation of Earthquake-Induced Response”
Símon Ólafsson, 1999:73, ISBN 82-471-0443-1, ISSN 0802-3271.

“Coastal Concrete Bridges: Moisture State, Chloride Permeability and Aging Effects”
Ragnhild Holen Relling, 1999:74, ISBN 82-471-0445-8, ISSN 0802-3271.

“Capacity Assessment of Titanium Pipes Subjected to Bending and External Pressure”
Arve Bjørset, 1999:100, ISBN 82-471-0473-3, ISSN 0802-3271.

“Validation of Numerical Collapse Behaviour of Thin-Walled Corrugated Panels”
Håvar Ilstad, 1999:101, ISBN 82-471-0474-1, ISSN 0802-3271.

“Strength and Ductility of Welded Structures in Aluminium Alloys”
Miroslaw Matusiak, 1999:113, ISBN 82-471-0487-3, ISSN 0802-3271.

“Thermal Dilation and Autogenous Deformation as Driving Forces to Self-Induced Stresses in High Performance Concrete”
Øyvind Bjøntegaard, 1999:121, ISBN 82-7984-002-8, ISSN 0802-3271.

“Some Aspects of Ski Base Sliding Friction and Ski Base Structure”
Dag Anders Moldestad, 1999:137, ISBN 82-7984-019-2, ISSN 0802-3271.

“Electrode reactions and corrosion resistance for steel in mortar and concrete”
Roy Antonsen, 2000:10, ISBN 82-7984-030-3, ISSN 0802-3271.

“Hydro-Physical Conditions in Kelp Forests and the Effect on Wave Damping and Dune Erosion. A case study on Laminaria Hyperborea”
Stig Magnar Løvås, 2000:28, ISBN 82-7984-050-8, ISSN 0802-3271.

“Random Vibration and the Path Integral Method”
Christian Skaug, 2000:39, ISBN 82-7984-061-3, ISSN 0802-3271.

“Buckling and geometrical nonlinear beam-type analyses of timber structures”
Trond Even Eggen, 2000:56, ISBN 82-7984-081-8, ISSN 0802-3271.

“Structural Crashworthiness of Aluminium Foam-Based Components”
Arve Grønsund Hanssen, 2000:76, ISBN 82-7984-102-4, ISSN 0809-103X.

“Measurements and simulations of the consolidation in first-year sea ice ridges, and some aspects of mechanical behaviour”
Knut V. Høyland, 2000:94, ISBN 82-7984-121-0, ISSN 0809-103X.

"Kinematics in Regular and Irregular Waves based on a Lagrangian Formulation"
Svein Helge Gjøsund, 2000-86, ISBN 82-7984-112-1, ISSN 0809-103X.

"Self-Induced Cracking Problems in Hardening Concrete Structures"
Daniela Bosnjak, 2000-121, ISBN 82-7984-151-2, ISSN 0809-103X.

"Ballistic Penetration and Perforation of Steel Plates"
Tore Børvik, 2000:124, ISBN 82-7984-154-7, ISSN 0809-103X.

"Freeze-Thaw resistance of Concrete. Effect of: Curing Conditions, Moisture Exchange and Materials"
Terje Finnerup Rønning, 2001:14, ISBN 82-7984-165-2, ISSN 0809-103X

"Structural behaviour of post tensioned concrete structures. Flat slab. Slabs on ground"
Steinar Trygstad, 2001:52, ISBN 82-471-5314-9, ISSN 0809-103X.

"Slipforming of Vertical Concrete Structures. Friction between concrete and slipform panel"
Kjell Tore Fosså, 2001:61, ISBN 82-471-5325-4, ISSN 0809-103X.

"Some numerical methods for the simulation of laminar and turbulent incompressible flows"
Jens Holmen, 2002:6, ISBN 82-471-5396-3, ISSN 0809-103X.

"Improved Fatigue Performance of Threaded Drillstring Connections by Cold Rolling"
Steinar Kristoffersen, 2002:11, ISBN: 82-421-5402-1, ISSN 0809-103X.

"Deformations in Concrete Cantilever Bridges: Observations and Theoretical Modelling"
Peter F. Takâcs, 2002:23, ISBN 82-471-5415-3, ISSN 0809-103X.

"Stiffened aluminium plates subjected to impact loading"
Hilde Giæver Hildrum, 2002:69, ISBN 82-471-5467-6, ISSN 0809-103X.

"Full- and model scale study of wind effects on a medium-rise building in a built up area"
Jónas Thór Snæbjørnsson, 2002:95, ISBN82-471-5495-1, ISSN 0809-103X.

"Evaluation of Concepts for Loading of Hydrocarbons in Ice-infested water"
Arnor Jensen, 2002:114, ISBN 82-417-5506-0, ISSN 0809-103X.

"Numerical and Physical Modelling of Oil Spreading in Broken Ice"
Janne K. Økland Gjøsteen, 2002:130, ISBN 82-471-5523-0, ISSN 0809-103X.

"Diagnosis and protection of corroding steel in concrete"
Franz Pruckner, 20002:140, ISBN 82-471-5555-4, ISSN 0809-103X.

"Tensile and Compressive Creep of Young Concrete: Testing and Modelling"
Dawood Atrushi, 2003:17, ISBN 82-471-5565-6, ISSN 0809-103X.

"Rheology of Particle Suspensions. Fresh Concrete, Mortar and Cement Paste with Various Types of Lignosulfonates"
Jon Elvar Wallevik, 2003:18, ISBN 82-471-5566-4, ISSN 0809-103X.

"Oblique Loading of Aluminium Crash Components"
Aase Reyes, 2003:15, ISBN 82-471-5562-1, ISSN 0809-103X.

"Utilization of Ethiopian Natural Pozzolans"
Surafel Ketema Desta, 2003:26, ISSN 82-471-5574-5, ISSN:0809-103X.

"Behaviour and strength prediction of reinforced concrete structures with discontinuity regions"
Helge Brå, 2004:11, ISBN 82-471-6222-9, ISSN 1503-8181.

"High-strength steel plates subjected to projectile impact. An experimental and numerical study"
Sumita Dey, 2004:38, ISBN 82-471-6282-2 (printed version), ISBN 82-471-6281-4 (electronic version), ISSN 1503-8181.

"Alkali-reactive and inert fillers in concrete. Rheology of fresh mixtures and expansive reactions"
Bård M. Pedersen, 2004:92, ISBN 82-471-6401-9 (printed version), ISBN 82-471-6400-0 (electronic version), ISSN 1503-8181.

"On the Shear Capacity of Steel Girders with Large Web Openings"
Nils Christian Hagen, 2005:9 ISBN 82-471-6878-2 (printed version), ISBN 82-471-6877-4 (electronic version), ISSN 1503-8181.

"Behaviour of aluminium extrusions subjected to axial loading"
Østen Jensen, 2005:7, ISBN 82-471-6873-1 (printed version), ISBN 82-471-6872-3 (electronic version), ISSN 1503-8181.

"Thermal Aspects of corrosion of Steel in Concrete"
Jan-Magnus Østvik, 2005:5, ISBN 82-471-6869-3 (printed version), ISBN 82-471-6868 (electronic version), ISSN 1503-8181.

"Mechanical and adaptive behaviour of bone in relation to hip replacement. A study of bone remodelling and bone grafting"
Sébastien Muller, 2005:34, ISBN 82-471-6933-9 (printed version), ISBN 82-471-6932-0 (electronic version), ISSN 1503-8181.

"Analysis of geometrical nonlinearities with applications to timber structures"
Lars Wollebæk, 2005:74, ISBN 82-471-7050-5 (printed version), ISBN 82-471-7019-1 (electronic version), ISSN 1503-8181.

"Pedestrian induced lateral vibrations of slender footbridges"
Anders Rönnquist, 2005:102, ISBN 82-471-7082-5 (printed version), ISBN 82-471-7081-7 (electronic version), ISSN 1503-8181.

"Initial Strength Development of Fly Ash and Limestone Blended Cements at Various Temperatures Predicted by Ultrasonic Pulse Velocity"
Tom Ivar Fredvik, 2005:112, ISBN 82-471-7105-8 (printed version), ISBN 82-471-7103-1 (electronic version), ISSN 1503-8181.

"Behaviour and modelling of thin-walled cast components"
Cato Dørum, 2005:128, ISBN 82-471-7140-6 (printed version), ISBN 82-471-7139-2 (electronic version), ISSN 1503-8181.

"Behaviour and modelling of selfpiercing riveted connections"
Raffaele Porcaro, 2005:165, ISBN 82-471-7219-4 (printed version), ISBN 82-471-7218-6 (electronic version), ISSN 1503-8181.

"Behaviour and Modelling og Aluminium Plates subjected to Compressive Load"
Lars Rønning, 2005:154, ISBN 82-471-7169-1 (printed version), ISBN 82-471-7195-3 (electronic version), ISSN 1503-8181.

"Bumper beam-longitudinal system subjected to offset impact loading"
Satyanarayana Kokkula, 2005:193, ISBN 82-471-7280-1 (printed version), ISBN 82-471-7279-8 (electronic version), ISSN 1503-8181.

"Control of Chloride Penetration into Concrete Structures at Early Age"
Guofei Liu, 2006:46, ISBN 82-471-7838-9 (printed version), ISBN 82-471-7837-0 (electronic version), ISSN 1503-8181.

"Modelling of Welded Thin-Walled Aluminium Structures"
Ting Wang, 2006:78, ISBN 82-471-7907-5 (printed version), ISBN 82-471-7906-7 (electronic version), ISSN 1503-8181.

"Time-variant reliability of dynamic systems by importance sampling and probabilistic analysis of ice loads"
Anna Ivanova Olsen, 2006:139, ISBN 82-471-8041-3 (printed version), ISBN 82-471-8040-5 (electronic version), ISSN 1503-8181.

"Fatigue life prediction of an aluminium alloy automotive component using finite element analysis of surface topography"
Sigmund Kyrre Ås, 2006:25, ISBN 82-471-7791-9 (printed version), ISBN 82-471-7791-9 (electronic version), ISSN 1503-8181.

"Constitutive models of elastoplasticity and fracture for aluminium alloys under strain path change"
Dasharatha Achani, 2006:76, ISBN 82-471-7903-2 (printed version), ISBN 82-471-7902-4 (electronic version), ISSN 1503-8181.

"Simulations of 2D dynamic brittle fracture by the Element-free Galerkin method and linear fracture mechanics"
Tommy Karlsson, 2006:125, ISBN 82-471-8011-1 (printed version), ISBN 82-471-8010-3 (electronic version), ISSN 1503-8181.

"Penetration and Perforation of Granite Targets by Hard Projectiles"
Chong Chiang Seah, 2006:188, ISBN 82-471-8150-9 (printed version), ISBN 82-471-8149-5 (electronic version), ISSN 1503-8181.

"Deformations, strain capacity and cracking of concrete in plastic and early hardening phases"
Tor Arne Hammer, 2007:234, ISBN 978-82-471-5191-4 (printed version), ISBN 978-82-471-5207-2 (electronic version), ISSN 1503-8181.

"Crashworthiness of dual-phase high-strength steel: Material and Component behaviour"
Venkatapathi Tarigopula, 2007:230, ISBN 82-471-5076-4 (printed version), ISBN 82-471-5093-1 (electronic version), ISSN 1503-8181.

"Fibre reinforcement in load carrying concrete structures"
Åse Lyslo Døssland, 2008:50, ISBN 978-82-471-6910-0 (printed version), ISBN 978-82-471-6924-7 (electronic version), ISSN 1503-8181.

"Low-velocity penetration of aluminium plates"
Frode Grytten, 2008:46, ISBN 978-82-471-6826-4 (printed version), ISBN 978-82-471-6843-1 (electronic version), ISSN 1503-8181.

"Robustness studies of structures subjected to large deformations"
Ørjan Fyllingen, 2008:24, ISBN 978-82-471-6339-9 (printed version), ISBN 978-82-471-6342-9 (electronic version), ISSN 1503-8181.

"Constitutive modelling of morsellised bone"
Knut Birger Lunde, 2008:92, ISBN 978-82-471-7829-4 (printed version), ISBN 978-82-471-7832-4 (electronic version), ISSN 1503-8181.

"Experimental Investigations of Wind Loading on a Suspension Bridge Girder"
Bjørn Isaksen, 2008:131, ISBN 978-82-471-8656-5 (printed version), ISBN 978-82-471-8673-2 (electronic version), ISSN 1503-8181.

"Cracking Risk of Concrete Structures in The Hardening Phase"
Guomin Ji, 2008:198, ISBN 978-82-471-1079-9 (printed version), ISBN 978-82-471-1080-5 (electronic version), ISSN 1503-8181.

"Modelling and numerical analysis of the porcine and human mitral apparatus"
Victorien Emile Prot, 2008:249, ISBN 978-82-471-1192-5 (printed version), ISBN 978-82-471-1193-2 (electronic version), ISSN 1503-8181.

"Strength analysis of net structures"
Heidi Moe, 2009:48, ISBN 978-82-471-1468-1 (printed version), ISBN 978-82-471-1469-8 (electronic version), ISSN1503-8181.

"Numerical analysis of ductile fracture in surface cracked shells"
Espen Berg, 2009:80, ISBN 978-82-471-1537-4 (printed version), ISBN 978-82-471-1538-1 (electronic version), ISSN 1503-8181.

"Subject specific finite element analysis of bone – for evaluation of the healing of a leg lengthening and evaluation of femoral stem design"
Sune Hansborg Pettersen, 2009:99, ISBN 978-82-471-1579-4 (printed version), ISBN 978-82-471-1580-0 (electronic version), ISSN 1503-8181.

"Evaluation of fracture parameters for notched multi-layered structures"
Lingyun Shang, 2009:137, ISBN 978-82-471-1662-3 (printed version), ISBN 978-82-471-1663-0 (electronic version), ISSN 1503-8181.

"Modelling of Dynamic Material Behaviour and Fracture of Aluminium Alloys for Structural Applications"
Yan Chen, 2009:69, ISBN 978-82-471-1515-2 (printed version), ISBN 978-82 471-1516-9 (electronic version), ISSN 1503-8181.

"Nanomechanics of polymer and composite particles"
Jianying He 2009:213, ISBN 978-82-471-1828-3 (printed version), ISBN 978-82-471-1829-0 (electronic version), ISSN 1503-8181.

"Mechanical properties of clear wood from Norway spruce"
Kristian Berbom Dahl 2009:250, ISBN 978-82-471-1911-2 (printed version) ISBN 978-82-471-1912-9 (electronic version), ISSN 1503-8181.

"Modeling of the degradation of TiB_2 mechanical properties by residual stresses and liquid Al penetration along grain boundaries"
Micol Pezzotta 2009:254, ISBN 978-82-471-1923-5 (printed version) ISBN 978-82-471-1924-2 (electronic version) ISSN 1503-8181.

"Effect of welding residual stress on fracture"
Xiabo Ren 2010:77, ISBN 978-82-471-2115-3 (printed version) ISBN 978-82-471-2116-0 (electronic version), ISSN 1503-8181.

"Pan-based carbon fiber as anode material in cathodic protection system for concrete structures"
Mahdi Chini 2010:122, ISBN 978-82-471-2210-5 (printed version) ISBN 978-82-471-2213-6 (electronic version), ISSN 1503-8181.

"Structural Behaviour of deteriorated and retrofitted concrete structures"
Irina Vasililjeva Sæther 2010:171, ISBN 978-82-471-2315-7 (printed version) ISBN 978-82-471-2316-4 (electronic version) ISSN 1503-8181.

"Prediction of local snow loads on roofs"
Vivian Meløysund 2010:247, ISBN 978-82-471-2490-1 (printed version) ISBN 978-82-471-2491-8 (electronic version) ISSN 1503-8181.

"Behaviour and modelling of polymers for crash applications"
Virgile Delhaye 2010:251, ISBN 978-82-471-2501-4 (printed version) ISBN 978-82-471-2502-1 (electronic version) ISSN 1503-8181.

"Blended cement with reducted CO_2 emission – Utilizing the Fly Ash-Limestone Synergy"
Klaartje De Weerdt 2011:32, ISBN 978-82-471-2584-7 (printed version) ISBN 978-82-471-2584-4 (electronic version) ISSN 1503-8181.

"Chloride induced reinforcement corrosion in concrete. Concept of critical chloride content – methods and mechanisms"
Ueli Angst 2011:113, ISBN 978-82-471-2769-9 (printed version) ISBN 978-82-471-2763-6 (electronic version) ISSN 1503-8181.

"A thermo-electric-Mechanical study of the carbon anode and contact interface for Energy savings in the production of aluminium"
Dag Herman Andersen 2011:157, ISBN 978-82-471-2859-6 (printed version) ISBN 978-82-471-2860-2 (electronic version) ISSN 1503-8181.

"Structural Capacity of Anchorage Ties in Masonry Veneer Walls Subjected to Earthquake. The implications of Eurocode 8 and Eurocode 6 on a typical Norwegain veneer wall"
Ahmed Mohamed Yousry Hamed 2011:181, ISBN 978-82-471-2911-1 (printed version) ISBN 978-82-471-2912-8 (electronic ver.) ISSN 1503-8181.

"Work-hardening behaviour in age-hardenable Al-Zn-Mg(-Cu) alloys"
Ida Westermann , 2011:247, ISBN 978-82-471-3056-8 (printed ver.) ISBN 978-82-471-3057-5 (electronic ver.) ISSN 1503-8181.

"Behaviour and modelling of selfpiercing riveted connections using aluminium rivets"
Nguyen-Hieu Hoang, 2011:266, ISBN 978-82-471-3097-1 (printed ver.) ISBN 978-82-471-3099-5 (electronic ver.) ISSN 1503-8181.

"Fibre reinforced concrete. Evaluation of test methods and material development"
Sindre Sandbakk, 2011:297, ISBN 978-82-471-3167-1 (printed ver.) ISBN 978-82-471-3168-8 (electronic ver) ISSN 1503:8181.

"Dynamic behaviour of cablesupported bridges subjected to strong natural wind"
Ole Andre Øiseth, 2011:315, ISBN 978-82-471-3209-8 (printed ver.) ISBN 978-82-471-3210-4 (electronic ver.) ISSN 1503-8181.

"Constitutive modeling of solargrade silicon materials"
Julien Cochard, 2011:307, ISBN 978-82-471-3189-3 (printed ver). ISBN 978-82-471-3190-9 (electronic ver.) ISSN 1503-8181.

"Constitutive behavior and fracture of shape memory alloys"
Jim Stian Olsen, 2012:57, ISBN 978-82-471-3382-8 (printed ver.) ISBN 978-82-471-3383-5 (electronic ver.) ISSN 1503-8181.

"Field measurements in mechanical testing using close-range photogrammetry and digital image analysis"
Egil Fagerholt, 2012:95, ISBN 978-82-471-3466-5 (printed ver.) ISBN 978-82-471-3467-2 (electronic ver.) ISSN 1503-8181.

"Towards a better understanding of the ultimate behaviour of lightweight aggregate concrete in compression and bending"
Håvard Nedrelid, 2012:123, ISBN 978-82-471-3527-3 (printed ver.) ISBN 978-82-471-3528-0 (electronic ver.) ISSN 1503-8181.

"Numerical simulations of blood flow in the left side of the heart"
Sigrid Kaarstad Dahl, 2012:135, ISBN 978-82-471-3553-2 (printed ver.) ISBN 978-82-471-3555-6 (electronic ver.) ISSN 1503-8181.

"Moisture induced stresses in glulam"
Vanessa Angst-Nicollier, 2012:139, ISBN 978-82-471-3562-4 (printed ver.) ISBN 978-82-471-3563-1 (electronic ver.) ISSN 1503-8181.

"Biomechanical aspects of distraction osteogensis"
Valentina La Russa, 2012:250, ISBN 978-82-471-3807-6 (printed ver.) ISBN 978-82-471-3808-3 (electronic ver.) ISSN 1503-8181.

"Ductile fracture in dual-phase steel. Theoretical, experimental and numerical study"
Gaute Gruben, 2012:257, ISBN 978-82-471-3822-9 (printed ver.) ISBN 978-82-471-3823-6 (electronic ver.) ISSN 1503-8181.

"Damping in Timber Structures"
Nathalie Labonnote, 2012:263, ISBN 978-82-471-3836-6 (printed ver.) ISBN 978-82-471-3837-3 (electronic ver.) ISSN 1503-8181.

"Biomechanical modeling of fetal veins: The umbilical vein and ductus venosus bifurcation"
Paul Roger Leinan, 2012:299, ISBN 978-82-471-3915-8 (printed ver.) ISBN 978-82-471-3916-5 (electronic ver.) ISSN 1503-8181.

"Large-Deformation behaviour of thermoplastics at various stress states"
Anne Serine Ognedal, 2012:298, ISBN 978-82-471-3913-4 (printed ver.) ISBN 978-82-471-3914-1 (electronic ver.) ISSN 1503-8181.

"Hardening accelerator for fly ash blended cement"
Kien Dinh Hoang, 2012:366, ISBN 978-82-471-4063-5 (printed ver.) ISBN 978-82-471-4064-2 (electronic ver.) ISSN 1503-8181.

"From molecular structure to mechanical properties"
Jianyang Wu, 2013:186, ISBN 978-82-471-4485-5 (printed ver.) ISBN 978-82-471-4486-2 (electronic ver.) ISSN 1503-8181.

“Experimental and numerical study of hybrid concrete structures”
Linn Grepstad Nes, 2013:259, ISBN 978-82-471-4644-6 (printed ver.) ISBN 978-82-471-4645-3 (electronic ver.) ISSN 1503-8181.

“Mechanics of ultra-thin multi crystalline silicon wafers”
Saber Saffar, 2013:199, ISBN 978-82-471-4511-1 (printed ver.) ISBN 978-82-471-4513-5 (electronic ver). ISSN 1503-8181.

“Through process modelling of welded aluminium structures”
Anizahyati Alisibramulisi, 2013:325, ISBN 978-82-471-4788-7 (printed ver.) ISBN 978-82-471-4789-4 (electronic ver.) ISSN 1503-8181.

“Combined blast and fragment loading on steel plates”
Knut Gaarder Rakvåg, 2013:361, ISBN978-82-471-4872-3 (printed ver.) ISBN 978-82-4873-0 (electronic ver.) ISSN 1503-8181.

“Characterization and modelling of the anisotropic behaviour of high-strength aluminium alloy”
Marion Fourmeau, 2014:37, ISBN 978-82-326-0008-3 (printed ver.) ISBN 978-82-326-0009-0 (electronic ver.) ISSN 1503-8181.

“Behaviour of threated steel fasteners at elevated deformation rates”
Henning Fransplass, 2014:65, ISBN 978-82-326-0054-0 (printed ver.) ISBN 978-82-326-0055-7 (electronic ver.) ISSN 1503-8181.

“Sedimentation and Bleeding”
Ya Peng, 2014:89, ISBN 978-82-326-0102-8 (printed ver.) ISBN 978-82-326-0103-5 (electric ver.) ISSN 1503-8181.

“Impact against X65 offshore pipelines”
Martin Kristoffersen, 2014:362, ISBN 978-82-326-0636-8 (printed ver.) ISBN 978-82-326-0637-5 (electronic ver.) ISSN 1503-8181.

“Formability of aluminium alloy subjected to prestrain by rolling”
Dmitry Vysochinskiy, 2014:363,, ISBN 978-82-326-0638-2 (printed ver.) ISBN 978-82-326-0639-9 (electronic ver.) ISSN 1503-8181.

“Experimental and numerical study of Yielding, Work-Hardening and anisotropy in textured AA6xxx alloys using crystal plasticity models”
Mikhail Khadyko, 2015:28, ISBN 978-82-326-0724-2 (printed ver.) ISBN 978-82-326-0725-9 (electronic ver.) ISSN 1503-8181.

"Behaviour and Modelling of AA6xxx Aluminium Alloys Under a Wide Range of Temperatures and Strain Rates"
Vincent Vilamosa, 2015:63, ISBN 978-82-326-0786-0 (printed ver.) ISBN 978-82-326-0787-7 (electronic ver.) ISSN 1503-8181.

"A Probabilistic Approach in Failure Modelling of Aluminium High Pressure Die-Castings"
Octavian Knoll, 2015:137, ISBN 978-82-326-0930-7 (printed ver.) ISBN 978-82-326-0931-4 (electronic ver.) ISSN 1503-8181.

"Ice Abrasion on Marine Concrete Structures"
Egil Møen, 2015:189, ISBN 978-82-326-1034-1 (printed ver.) ISBN 978-82-326-1035-8 (electronic ver.) ISSN 1503-8181.

"Fibre Orientation in Steel-Fibre-Reinforced Concrete"
Giedrius Zirgulis, 2015:229, ISBN 978-82-326-1114-0 (printed ver.) ISBN 978-82-326-1115-7 (electronic ver.) ISSN 1503-8181.

"Effect of spatial variation and possible interference of localised corrosion on the residual capacity of a reinforced concrete beam"
Mohammad Mahdi Kioumarsi, 2015:282, ISBN 978-82-326-1220-8 (printed ver.) ISBN 978-82-1221-5 (electronic ver.) ISSN 1503-8181.